Michel O. Deville

An Introduction to the Mechanics of Incompressible Fluids

OPEN ACCESS

Springer

An Introduction to the Mechanics of Incompressible Fluids

Michel O. Deville

An Introduction to the Mechanics of Incompressible Fluids

Springer

Michel O. Deville
School of Engineering
Swiss Federal Institute of Technology
École Polytechnique Fédérale de Lausanne
Lausanne, Vaud, Switzerland

ISBN 978-3-031-04682-7 ISBN 978-3-031-04683-4 (eBook)
https://doi.org/10.1007/978-3-031-04683-4

This Springer imprint is published by the registered company Springer Nature Switzerland AG
The registered company address is: Gewerbestrasse 11, 6330 Cham, Switzerland

Not all equations tell the whole story
To Christina with love and passion

Foreword

The book: An Introduction to the Mechanics of Incompressible Fluids by Prof. Michel Deville is another feather in the cap of the author, who is extremely prolific in writing books on multiple aspects of continuum mechanics (with emphasis on fluid mechanics), high accuracy scientific computing by high order methods and topics of applied mathematics. The present book is a fine addition to this list. Even though the book is titled as an introduction to the subject of incompressible flow, the author has covered extensively from topics on potential flow theory to direct numerical simulation of fluid flow. Apart from teaching the subject to his students for a long time, he has also performed extensive research on many topics in the book. He has brought a good balance with early exposition on the topics, while covering the most recent developments in some other topics. One of the most distinguishing features of the book is that the author has introduced the essentials of the topics, while he has cited enough references to augment the details which the reader can consult. This has kept the book quite concise, while the topics covered are quite wide. I am very happy to see that the book covers many useful topics of classical field like conformal mapping that influenced early developments in aerodynamics; to applications in applied mathematics; to contemporary topics in bio-fluid mechanics. A special feature is the introduction to direct numerical simulation and large eddy simulation of incompressible flows. The book is very well organized, written in a lucid style, which the students will find very easy to follow. This will be an ideal book written with information and reference very up-to-date. I find the third chapter to be very interesting containing many equilibrium unsteady flows, which can be of immense value to researchers who would like to read the receptivity and instability of such flows. The instability of flow has been introduced with the Taylor-Couette flow as an apt example, which is known to suffer modal instability. Inclusion of the topic of Reynolds averaged Navier-Stokes equation to explain turbulent flow is perhaps the easy and correct approach to introduce readers to this topic. The author is a widely acclaimed expert in the theoretical and computational aspects of incompressible fluid flow, specifically on spectral and higher order methods. He and his group of researchers are well-known for scholarly contributions which have been pursued

over more than five decades. He has authored many books on various aspects of fluid flow and its computing and the present book will be a nice addition to that.

October 2021

Tapan K. Sengupta
IIT Dhanbad
Jharkhand, India

Preface

Fluid Mechanics is a fascinating subject in science and engineering because fluids are everywhere in nature, technology and in facts of every day life. The water for the shower, the air we breathe, the blood in our cardiovascular system. From the technological point of view, water is a source of energy in turbines, pumps, and hydraulic systems. Without air we could hardly fly or use a boomerang for fun. In summary, fluids occupy a central place in humanity reflected in the popular saying "Water is life". Therefore, the investigation of fluid behavior has been a central theme in research for many centuries. Recall Archimedes running in the streets of Syracuse with joy "Eureka". In the following centuries, many great minds tackled the study of the fluid flows. The Swiss mathematician Leonhard Euler (1707–1783) brought significant developments and conceived the "Euler" equations that describe the mechanics of inviscid (non-viscous) fluids. This was a major breakthrough that impacted the fluid dynamics science. In the following century, Claude Louis Marie Henri Navier (1785–1836) and George Gabriel Stokes (1819–1903) wrote the celebrated "Navier–Stokes" equations that form the basis for viscous fluid mechanics. In this monograph, we will restrict our attention to incompressible fluids. Therefore, we will avoid all physical phenomena associated with compressibility like sound waves or shocks that appear as soon as we deal with air flows at finite values of the Mach number.

Writing a book on fluid mechanics constitutes a real challenge. The topic is broad and incorporates a lot of experimental results, theoretical considerations and modeling aspects. The mathematical core of fluid mechanics rests upon applied mathematics tools like the solution of ordinary and partial differential equations making it less tasty in an era where everything is available through the Internet. However, my teaching practice to mechanical engineering and physics students at the Catholic University of Louvain in Belgium and at the Swiss Federal Institute of Technology in Lausanne over more than three decades led me to three choices while writing these lecture notes. First of all, the contents of this book is what I consider as unmissable knowledge to start afresh with fluid mechanics problems. Secondly, with the invasion of computers and omnipresent softwares to facilitate mathematical developments, I have decided to go through every step in detail to show that as soon we master the

main mathematical tools, we are able to carry through any major chunk of fluid mechanics problem. Thirdly, some topics like the flow around an airfoil in Chap. 6 or the stability of the circular Couette flow in Chap. 8 come from my professional life as a consultant at ONERA (Office National d'Études et de Recherches Aérospatiales, the French Aerospace Lab) and my postdoc years at the MIT Department of Mathematics with Steve A. Orszag. Steve had a deep influence on my career and my research as he educated me with spectral methods which became the central theme of my work. The application of the Fourier–Chebyshev spectral method to the Couette flow stability led to a joint IUTAM symposium communication that was published later.

The course I taught to the Physics students was named Hydrodynamics, a decision that pertained to the EPFL (École Polytechnique Fédérale de Lausanne) Physics Department. Therefore, I was tempted to title the monograph with the same headline. However, comparing my contribution to the renowned book by Sir Horace Lamb refrained my enthusiasm and this is the reason of the present title. As I am not an experimentalist the flavor of the book comes from mathematical developments and the conclusions we can draw from them.

Let us consider the red thread that goes through the text. We start focusing on basic fluid mechanics from the general principles of continuum mechanics in Chap. 1. Governing equations are presented together with the boundary and initial conditions. Special attention is devoted to the meaning and differences between incompressible and compressible fluids. This chapter is a very abridged presentation of the necessary concepts of continuum mechanics. The reader who wants to get a longer and deeper understanding of these topics is referred to the monograph that my EPFL colleague John Botsis and myself published with the EPFL Press [16].

Chapter 2 develops the principles of dimensional analysis allowing the definition of the Reynolds number, a dimensionless number characterizing the flow properties. The application of the Vaschy-Buckingham theorem sheds some light on the benefits of dealing with dimensionless equations. The analysis of the compressible Navier–Stokes equations shows how the incompressible equations are recovered when the Mach number goes to zero. The nature of pressure is also discussed.

Chapter 3 covers extensively various exact solutions of the Navier–Stokes equations for steady-state and transient cases. Of particular interest are the pulsating flows in a channel and in a circular pipe as these solutions are relevant for blood flow analysis, a field of bioengineering that has grown at an extremely rapid pace over the last decade.

Chapter 4 introduces the concepts of vorticity and circulation. This leads to the famous Bernoulli equation that is taught in every physics course. A detailed study of the vorticity production on a solid wall is undertaken. The flow behind a grid solved by Kovasznay provides a benchmark solution for the eager numericist. The chapter ends with the Taylor-Green vortex where the Clebsch potentials are introduced to compute the vorticity lines.

Then in Chap. 5 Stokes flows, also called creeping flows because the viscous effects are dominant, are considered. The Moffatt eddies in a corner are described. The flow around a sphere is detailed and leads to the Stokes formula. Stokes eigenmodes

are analyzed and a three-dimensional Stokes solution is given. The flow around a circular cylinder leads to the Stokes' paradox.

Chapter 6 describes the mechanics of inviscid fluids through the use of complex variables and potentials. The flow around a circular cylinder is detailed. Then using conformal mapping and especially the Joukowski transformation, it is possible to consider an aerodynamics application, namely the flow around an airfoil. The Blasius theorem allows for the computation of the forces and moment generated by flow around an immersed body. It is applied to the case of the cylinder and Joukowski profile.

The boundary layer theory is the subject of Chap. 7. The Prandtl's equations are obtained via dimensional analysis considerations. The case of the flat plate is treated as a suitable example for the development of the boundary layer on simple geometry. The von Kármán integral equation allows the elaboration of the approximate von Kármán–Pohlausen method where the velocity profile is given as a polynomial. This leads to the calculation of the various thicknesses.

Chapter 8 treats flow instabilities. The stability of plane parallel channel flow leads to the well-known Orr-Sommerfeld equation which is solved by a Chebyshev spectral method. The associated Fortran program is given in the appendix. Then the stability of the circular Couette flow between two concentric cylinders is carried out first by an inviscid approach that yields the Rayleigh stability criterion. The incorporation of the viscous and pressure terms generates through a linearization process a set of differential equations again solved by high-order discretization methods through a generalized eigenvalue problem. The chapter ends with the case of the non-linear axisymmetric Taylor vortices.

The penultimate chapter deals with turbulence which is a physical phenomenon present in nature like rivers and ocean currents, waves on a beach, storms, tsunamis, etc., and in technological applications like the air turbulence in a rough flight. Turbulence is still a phenomenon that is far from being completely understood. Reynolds averaged Navier–Stokes (RANS) equations are obtained. Several linear turbulence models are presented in the RANS framework: $K-\varepsilon$, $K-\omega$. Non-linear models are built on the anisotropy tensor and the incorporation of the concept of integrity bases. The chapter ends with the theory of large eddy simulations with a few up-to-date models: dynamic model, approximate deconvolution method.

Each chapter proposes a few exercises that come from the large set used for the EPFL recitation classes. The solutions are given in Chap. 10.

Chapter 6 on the theory of complex variables and potentials is based on mathematics that goes back mainly to the first half of the twentieth century. I have long debated to decide if I would skip this matter or leave it as a nice piece of theory that generates deep insight into important fluid flows. This is especially crucial when we all know that it is so easy to compute the flow around an airfoil using numerical methods like finite volumes or finite elements. The final decision was based on the fact that this theory is a cornerstone of fluid mechanics which nobody escapes.

The monograph comes from my own lecture notes. In its present form it is intended to be the support for a one-semester course with three lectures of 1 hour a week. The teacher should choose the topics at his/her own taste.

Despite careful checks, some errors might have sneaked in the text. They are my own responsibility and for that, I beat myself up saying “mea culpa, ...”.

Rules for the notations In this book, the scalar quantities are in Roman or italic characters such as p, T. Vectors and tensors are in bold characters like $\boldsymbol{v}, \boldsymbol{\sigma}, \boldsymbol{L}$. When vectors and tensors are written in index notation, the indices are chosen in most cases from the letters i, j, k, l, m, n. Therefore, the vectors will have components v_i and the tensors components σ_{ij}.

Lausanne, Switzerland Michel O. Deville
February 2022

Acknowledgments

My sincere and grateful thanks go to the School of Engineering (SE) and the Section of Mechanical Engineering (SME) of the École Polytechnique Fédérale de Lausanne (Swiss Federal Institute Lausanne) that funded the editorial costs for this Open Access book with Springer Nature. This magnificent opportunity demonstrates the suitability of the EPFL policy to help and propagate the scientific knowledge to a vast majority of interested readers. More specifically I am indebted to the SE Dean, Professor Ali H. Sayed, and the SME Director, François Gallaire, and their staff who supported the initiative of this fluid mechanics book.

Several key persons influenced deeply the contents of the book: my former Ph.D. advisor, Professor Marcel Crochet, and my UCLouvain colleagues (now deceased), Professors François Dupret and Pierre Wauters, who taught the Fluid Mechanics course with me at the Ecole Polytechnique de Louvain. They brought their enthusiasm and knowledge to choose the best presentation of the subject making it digest and fully interesting. Pierre Monkewitz, my EPFL colleague, introduced me to experiments and to his major contributions to the theory of instability.

Marc Brachet drew my attention to the Physics of Fluids paper where he and his co-authors use Clebsch potentials to compute vorticity lines.

Marc-Antoine Habisreutinger provided me with his program to compute and draw the resulting streamlines around an airfoil using the Joukovski transformation. My co-author Paul Fischer [23] helped me to restore the Orr-Sommerfeld Fortran program with the Lapack software to solve the complex eigenvalue problem.

My former Ph.D. students participated to the pedagogical supervision of the Fluid Mechanics tutorials: Nicolas Bodard, Christoph Bosshard, Roland Bouffanais, Peter Corbett, Wouter Couzy, Nicolas Fiétier, Marc-Antoine Habisreutinger, Azadeh Jafari, Thibauld Jongen, Vincent Keller, Emmanuel Leriche, Célestin Leupi, Luc Machiels, Eric Magère, Orestis Malaspinas, Michele Mossi, Riccardo Puragliesi, Theo Randriarifara, and Daniel Weill. They all conceived exercises and solved them to promote the fluid mechanics classes.

Contents

Chapter 1
Incompressible Newtonian Fluid Mechanics

We present the properties of incompressible Newtonian viscous fluids and their modelling based on the Navier–Stokes equations. At constant ambient temperature, incompressible fluids are characterized by their invariable density. They are present in nature as well as in many technical applications. Incompressible flows offer very rich and very complex physical phenomena and therefore, their study is appealing and exciting.

Many books are devoted to incompressible fluid mechanics as well as to hydrodynamics. Without wishing to be exhaustive, we can cite the books of Batchelor [10], Guyon, Hulin, Petit and Mitescu [37], Lamb [47], Landau and Lifschitz [48], Meyer [57], Ockendon and Ockendon [64], Panton [71], Rieutord [79], Ryhming [83], Tritton [108], Truesdell and Rajagopal [111], and Yih [125]. The review article of synthesis by Serrin [90] is also a source of information and inspiration.

In this chapter, we will write the fundamental governing relations obtained from the principles of Continuum Mechanics. The reader who wishes to go through all the needed developments is referred to the monograph by Botsis and Deville [16] where full details are provided.

1.1 Introduction

Incompressible viscous fluids are part of our daily lives without our clear consciousness. The most obvious example is that of water, which accompanies our most ordinary actions: coffee or tea we drink, the baths, the wetting rain, etc. Then, we understand that water is ubiquitous, both in nature: oceans, rivers, lakes, waves as well as in technical applications: hydraulic turbines, forced ducts, boat design, canals, etc. Water, in the eyes of the fluid mechanicist, is a typical example of Newtonian viscous incompressible fluid. The Newtonian qualification will be explained in the sequel.

M. O. Deville, *An Introduction to the Mechanics of Incompressible Fluids*,
https://doi.org/10.1007/978-3-031-04683-4_1

Some incompressible fluids have rheological behaviors different from that of water, such as, for example, blood, molten polymers, mud, agro-alimentary fluids, ... In the case of blood, it contains the formed elements: platelets, white and red cells. Their presence within the flow modifies the mechanical behavior of the fluid. As part of the microcirculation, blood is a non-Newtonian shear-thinning fluid with a viscosity decreasing when the shear stress increases.

For polymer melts, it is the long chains of molecules that affect the rheology which also depends on the concentration of the polymer in the solvent. Finally, agro-alimentary fluids have a range of features, such as stress thresholds, viscosity depending on the local shear rate, etc. All these fluids form the class of non-Newtonian fluids; some of them, for example polymers, are viscoelastic and exhibit memory effects such as creep and stress relaxation, which take into account the history of their deformation. However, we will not examine them in this monograph. The interested reader is referred to the book of Deville and Gatski [24] to discover the foundations of complex fluids and flows.

Fluid constitutive models and basic equations are derived from the mechanics of continuous media [5, 16]. We will use the Eulerian description which is the representation where the fluids are generally studied. We place ourselves in a fixed spatial position and observe the flow from this point.

We will use a system of rectangular Cartesian coordinates that is the set formed by point 0 taken as the origin and three orthonormal basis vectors $(\boldsymbol{e}_1, \boldsymbol{e}_2, \boldsymbol{e}_3)$ at this origin. Therefore the Cartesian coordinates of a point P in the system is given by the associated vector position of a fluid particle with respect to $(\boldsymbol{e}_1, \boldsymbol{e}_2, \boldsymbol{e}_3)$ such that $\boldsymbol{x} = (x_1, x_2, x_3)$ (this particle is understood at the macroscopic scale, but being small enough to carry out infinitesimal analysis). The position will also depend on time t. The velocity vector has three components that in this system, we note classically $\boldsymbol{v} = (v_1, v_2, v_3)$. In some cases, we will use cylindrical coordinates with $\boldsymbol{v} = (v_r, v_\theta, v_z)$ or spherical coordinates with $\boldsymbol{v} = (v_r, v_\varphi, v_\theta)$.

The flow behavior is characterized by a dimensionless number, the Reynolds number defined by the relation

$$Re = \frac{UL}{\nu}\,, \tag{1.1}$$

where U and L are a reference velocity and length of the problem at hand, respectively, while ν is the kinematic viscosity of the fluid expressed in SI (Système International in French; International System of Units) units, i.e. $\mathrm{m}^2\,\mathrm{s}^{-1}$. Let us recall that for water, $\nu_{water} = 10^{-6}\,\mathrm{m}^2\,\mathrm{s}^{-1}$. In this last case, one concludes that the ν presence in the denominator of Eq. (1.1) produces immediately a high Re value. In reality, Re is comprised between values close to zero for slow or creeping flows that are laminar to values of $10^6 \ldots 10^7$ for turbulent flows. For these high Re values, we are in the case of developed turbulence whose space-time dynamics is very fluctuating. Between these two extreme values, flows are subject to instabilities and bifurcations that are the features of transition phenomena. Recently, chaos theory allowed to penetrate more deeply in the concept of weak turbulence where Re presents moderate values going from a few hundreds to a few (dozens of) thousands.

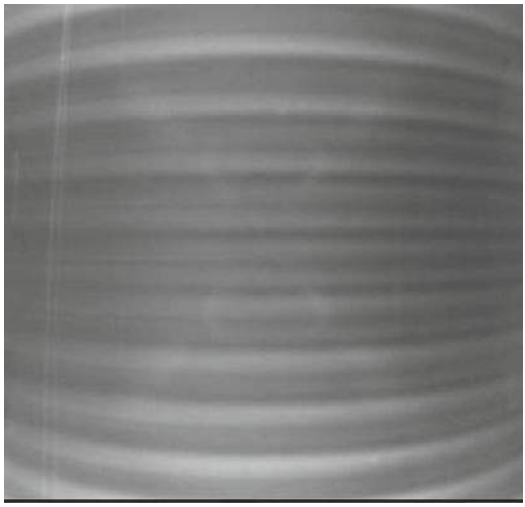

Fig. 1.1 Symmetric Taylor vortices. Courtesy of N. Borhani with permission

1.1.1 Circular Couette Flow

The so-called spectral transition is well illustrated by the circular Couette flow between two concentric vertical cylinders. Let us examine the particular case where the inner cylinder of radius R_1 is rotating with a constant angular velocity ω and the outer cylinder of radius R_2 is fixed.

The Reynolds number is now defined as

$$Re = \frac{\omega R_1 (R_2 - R_1)}{\nu} , \tag{1.2}$$

where $(R_2 - R_1)$ is the gap dimension. For small Re values, the steady-state laminar flow is described by the azimuthal velocity

$$v_\theta = Ar + B/r , \tag{1.3}$$

with $A = -\omega R_1^2/(R_2^2 - R_1^2)$ and $B = \omega R_1^2 R_2^2/(R_2^2 - R_1^2)$.

If the angular velocity of the inner cylinder is increased, the flow goes through a first transition towards the Taylor vortices [103]. This discovery impacted deeply the study of fluid dynamics so much so that this flow is now named the Taylor–Couette flow. Figure 1.1 shows these vortices for an experimental set-up with $R_1 = 8$ cm and a gap $R_2 - R_1 = 0.5$ cm. The rotation velocity is such that the Reynolds number is $Re = 150$ and the Taylor vortices are axisymmetric and steady-state. In a meridian plane, they appear in counter rotating pairs. A fluid particle follows an helical path placed on the surface of a torus centered on the rotation axis. Increasing the inner cylinder rotation, a second transition occurs and the Taylor toruses are deformed in

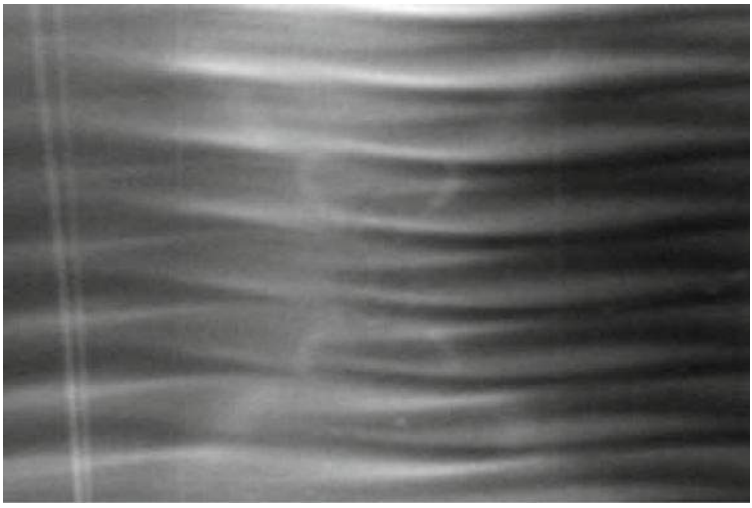

Fig. 1.2 Wavy Taylor vortices. Courtesy of N. Borhani with permission

the azimuthal direction. Figure 1.2 displays the steady-state wavy Taylor vortices pattern for $Re = 200$.

Subsequent transitions modify the number of vortices pairs in the vertical direction and the wavenumber of the azimuthal deformations in direction θ. At some value of the Reynolds number, the flow becomes unsteady. This physical phenomenon is a Hopf bifurcation giving in phase space a limit cycle with a clearly identified time period. Donald Coles [20] has shown experimentally that by increasing the inner cylinder rotation the route to turbulence is not the same as by decreasing the rotation velocity. Typically the flow presents a hysteresis.

1.1.2 Flow Around a Cylinder

The uniform, parallel flow upstream of a horizontal circular cylinder is of paramount importance in hydrodynamics. As we will note in the sequel, this flow can be transformed in the flow around an airfoil through the Joukowski transformation. The Reynolds number is defined by U, the uniform upstream velocity, $L = D$, the diameter of the cylinder, and ν, the kinematic viscosity of the fluid. Figure 1.3[1] shows the flow at $Re \simeq 0$ for which the streamlines are symmetric with respect to the horizontal, vertical, and diagonal directions. The streamlines follow closely the shape of the obstacle.

[1] Figures 1.1–1.7 are taken from text [114]. Attempts to identify the copyright owner have not as yet succeeded, and he or she is invited to contact the publisher.

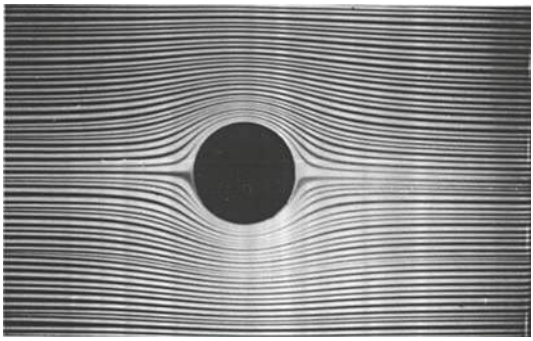

Fig. 1.3 Flow around a cylinder at $Re \simeq 0$

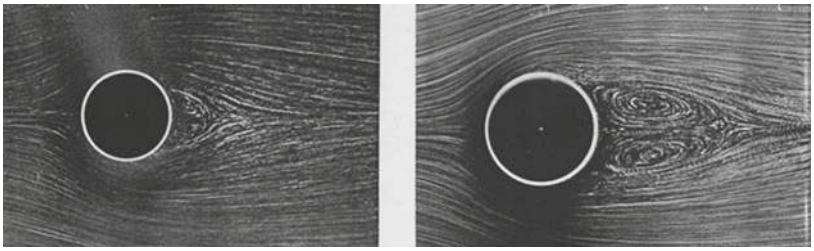

Fig. 1.4 Flow around a cylinder for (left) $Re = 13.1$ and (right) 26

As Re grows, for the values 13.1 and 26 shown in Fig. 1.4, it is seen that the flow is stationary and symmetric with respect to the horizontal axis. However, two counter-rotating recirculation zones appear behind the cylinder. The length of the recirculation zone increases linearly with Re while the distance separating the centers of the vortices grows as $\sqrt{Re}$.

At $Re = 47.5$, the first critical Reynolds number is reached, at which point the physical phenomena become unstable. Results over the last decade have shown that this is truly not a fixed number. The associated Hopf bifurcation can be multiple in number. Please note the experimental observations of Homann in [89]. A von Kármán vortex street is produced behind the cylinder with vortices alternately shed above and below. A similar vortex street is shown in Fig. 1.5 for $Re = 140$, taken from [114]. The shed vortices are regularly produced at a frequency corresponding to a limit cycle in phase space: a Hopf bifurcation. This frequency, denoted f, leads to the definition of the Strouhal number, St

$$St = \frac{f D}{U} \,. \tag{1.4}$$

For values of Re around one hundred, St is 0.13.

Stability analyses are based on the Ginzburg–Landau equation [26] which determines the non-linear development of perturbations superimposed on an underlying

Fig. 1.5 von Kármán vortex street for $Re = 140$

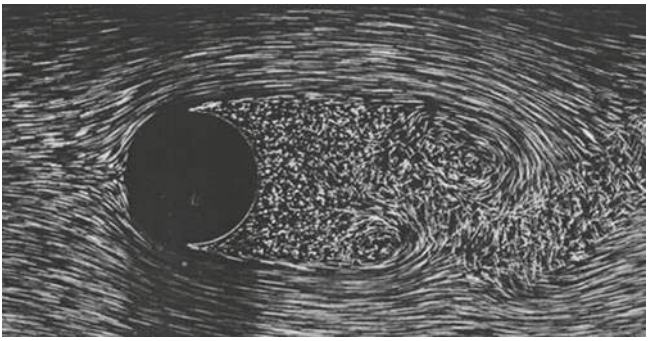

Fig. 1.6 von Kármán vortex street for $Re = 2000$

flow. This theory extends over a vast domain that this book cannot cover. We refer the reader to specialized texts, for example, [18, 27, 86]. If the Reynolds number is again increased, the flow passes through transitional regimes before finally attaining the turbulent state. An excellent synthesis of the dynamics of the wakes of circular cylinders is that of Williamson [121].

Figure 1.6 shows the flow pattern for weak turbulence. The boundary layer, where viscous effects are of the same order of magnitude as inertial effects, is laminar in front of the cylinder, develops around it, undergoes a separation, and produces a turbulent wake. It is still possible to observe two vortices resulting from the nonlinear dynamics.

At $Re = 10^4$ as in Fig. 1.7, the flow has roughly the same form, with two identifiable vortices.

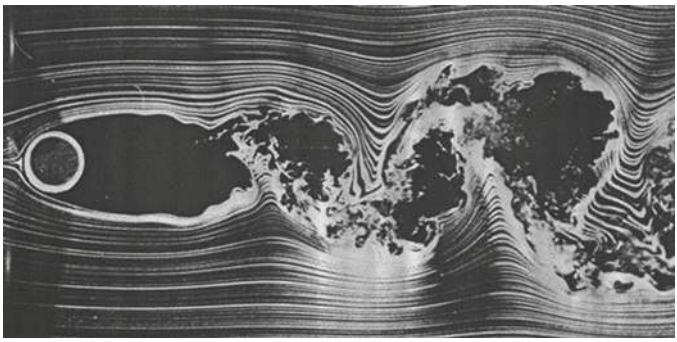

Fig. 1.7 von Kármán vortex street for $Re = 10^4$

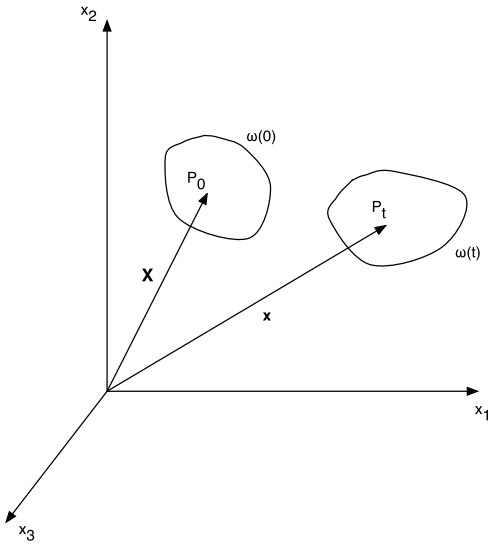

Fig. 1.8 Representation of the fluid deformation configurations

1.2 Fluid Kinematics

Fluid flows in a three-dimensional Euclidean space. In order to describe its deformation, the concept of motion is needed. For the sake of simplicity, a system of Cartesian rectangular orthonormal coordinates is chosen. Let $\boldsymbol{X}$ be the initial position vector of a fluid particle P_0 in a material volume $\omega(0)$ at time $= 0$ (cf. Fig. 1.8). At the present time $t \geq 0$, the position of this particle P_t is located by the actual position vector $\boldsymbol{x}$ in the volume $\omega(t)$. The particle motion is described by a vector function $\boldsymbol{\chi}$ defined over time t that depends on $\boldsymbol{X}$:

$$\boldsymbol{x} = \boldsymbol{\chi}(\boldsymbol{X}, t)\,. \tag{1.5}$$

If the initial reference position ($t = 0$) coincides with the current position, the function $\boldsymbol{\chi}$ must satisfy the condition

$$\boldsymbol{X} = \boldsymbol{\chi}(\boldsymbol{X}, 0)\,. \tag{1.6}$$

The motion $\boldsymbol{\chi}$ is a bijection ensuring a one-to-one correspondence between the initial and current positions of the fluid particles. The existence of the function $\boldsymbol{\chi}$ and its inverse $\boldsymbol{\chi}^{-1}$

$$\boldsymbol{X} = \boldsymbol{\chi}^{-1}(\boldsymbol{x}, t) \tag{1.7}$$

with

$$\boldsymbol{X} = \boldsymbol{\chi}^{-1}(\boldsymbol{X}, 0) \tag{1.8}$$

guarantees the integrality and the unity of the fluid body as a whole.

1.2.1 Material and Spatial Descriptions

The material description, also called the Lagrangian description, of fluid mechanics signifies the study of physical phenomena under consideration by observing what happens to a fluid particle or in its neighborhood. Alternatively the spatial description, known as the Eulerian description, consists of observing the events occurring at a fixed point in space. Uppercase letters for the material representation and lowercase letters for the spatial representation will be used to distinguish them clearly without any ambiguity.

Hydrodynamics problems are most of the time expressed in spatial description as fluids undergo huge deformations (let us think about the river flowing from its source till the sea or the ocean). The spatial description will use $\boldsymbol{x}, t$ as independent variables.

1.2.2 Velocity, Material Derivative and Acceleration

1.2.2.1 Velocity

The velocity of a material particle at time t is the derivative of the motion function in (1.5) with respect to time. By definition, in the material description, we have

$$\boldsymbol{V}(\boldsymbol{X}, t) = \frac{\partial \boldsymbol{\chi}(\boldsymbol{X}, t)}{\partial t} \tag{1.9}$$

$$V_i(\boldsymbol{X}, t) = \frac{\partial \chi_i(\boldsymbol{X}, t)}{\partial t}\,. \tag{1.10}$$

The vector $\boldsymbol{V}(\boldsymbol{X}, t)$ expresses the velocity at time t of the particle that initially was at $\boldsymbol{X}$. Note that (1.9) is obtained using (1.5), taking into account that $\boldsymbol{X}$ is one of the independent variables.

The spatial description of velocity, written as $\boldsymbol{v}$ according to our convention, is obtained by

$$\boldsymbol{v}(\boldsymbol{x}, t) = \boldsymbol{V}\left(\boldsymbol{\chi}^{-1}(\boldsymbol{x}, t), t\right) = \boldsymbol{V}(\boldsymbol{X}, t)\,. \tag{1.11}$$

The vector $\boldsymbol{v}(\boldsymbol{x}, t)$ expresses the velocity at an instant t of the particle that, at that time, passes through the position $\boldsymbol{x}$.

1.2.2.2 Material Derivative

Let us introduce the notion of material derivative. Let φ be a scalar field. During a motion $\boldsymbol{\chi}$, the material derivative of $\varphi(\boldsymbol{x}, t)$, written $\dot{\varphi}$ or $D\varphi/Dt$, is the rate of change of $\varphi(\boldsymbol{x}, t)$ with time (the derivative with respect to time) for a single particle in a fixed space position. In the material description, that is $\varphi\left(\boldsymbol{\chi}(\boldsymbol{X}, t), t\right) = \Phi(\boldsymbol{X}, t)$, we simply have

$$\frac{D\varphi(\boldsymbol{x}, t)}{Dt} = \dot{\varphi} = \left.\frac{\partial \Phi(\boldsymbol{X}, t)}{\partial t}\right|_{\boldsymbol{X}=\boldsymbol{\chi}^{-1}(\boldsymbol{x}, t)}\,. \tag{1.12}$$

The last equation shows that the material derivative is applied to the same particle. For that reason, some authors call it the particle derivative. Since we can write $\Phi(\boldsymbol{X}, t) = \Phi\left(\boldsymbol{\chi}^{-1}(\boldsymbol{x}, t), t\right) = \varphi(\boldsymbol{x}, t)$, we obtain

$$\frac{\partial \Phi(\boldsymbol{X}, t)}{\partial t} = \frac{\partial \varphi}{\partial x_1}\frac{\partial \chi_1}{\partial t} + \frac{\partial \varphi}{\partial x_2}\frac{\partial \chi_2}{\partial t} + \frac{\partial \varphi}{\partial x_3}\frac{\partial \chi_3}{\partial t} + \left.\frac{\partial \varphi}{\partial t}\right|_{\boldsymbol{x}=\boldsymbol{\chi}(\boldsymbol{X}, t)}\,. \tag{1.13}$$

Using the definition of the velocity (1.9), the preceding equation takes the following form:

$$\frac{\partial \Phi(\boldsymbol{X}, t)}{\partial t} = \left.\frac{\partial \varphi}{\partial t}\right|_{\boldsymbol{x}=\boldsymbol{\chi}(\boldsymbol{X}, t)} + V_i(\boldsymbol{X}, t)\left.\frac{\partial \varphi}{\partial x_i}\right|_{\boldsymbol{x}=\boldsymbol{\chi}(\boldsymbol{X}, t)}, i = 1, 2, 3\,, \tag{1.14}$$

where the Einstein convention of summation on repeated indices holds. The notation $\partial\varphi/\partial x_i$ designates the Cartesian components of the gradient of the scalar field φ, namely $\nabla\varphi$, which is a vector field.

Since the goal is to express the rightmost term of (1.14) in spatial coordinates, we make the substitution $\boldsymbol{X} = \boldsymbol{\chi}^{-1}(\boldsymbol{x}, t)$ in the last equation which gives

$$\left.\frac{\partial \Phi(\boldsymbol{X}, t)}{\partial t}\right|_{\boldsymbol{X}=\boldsymbol{\chi}^{-1}(\boldsymbol{x}, t)} = \frac{\partial \varphi}{\partial t} + v_i(\boldsymbol{x}, t)\frac{\partial \varphi}{\partial x_i}\,, \tag{1.15}$$

where we used

$$V_i(\boldsymbol{X},t)\Big|_{\boldsymbol{X}=\boldsymbol{\chi}^{-1}(\boldsymbol{x},t)} = v_i(\boldsymbol{x},t)\,. \tag{1.16}$$

Now we can define the following derivative:

$$\dot{\varphi}(\boldsymbol{x},t) = \frac{D\varphi(\boldsymbol{x},t)}{Dt} \equiv \left.\frac{\partial \Phi(\boldsymbol{X},t)}{\partial t}\right|_{\boldsymbol{X}=\boldsymbol{\chi}^{-1}(\boldsymbol{x},t)}, \tag{1.17}$$

where, from (1.15),

$$\frac{D\varphi(\boldsymbol{x},t)}{Dt} = \frac{\partial\varphi(\boldsymbol{x},t)}{\partial t} + \boldsymbol{v}(\boldsymbol{x},t)\cdot\nabla\varphi(\boldsymbol{x},t)\,, \tag{1.18}$$

$$= \frac{\partial\varphi(\boldsymbol{x},t)}{\partial t} + v_j\frac{\partial\varphi(\boldsymbol{x},t)}{\partial x_j}\,. \tag{1.19}$$

The dot in Eq. (1.18) represents the scalar product of two vectors. The derivative $D\varphi(\boldsymbol{x},t)/Dt$ is called the ***material derivative*** and represents the rate of change of the function φ following the same particle whose velocity is $\boldsymbol{v}(\boldsymbol{x},t)$. Alternatively, this derivative can be considered as giving the change of φ over time, as seen by an observer moving with the particle that is at $\boldsymbol{x}$.

For a vector field $\boldsymbol{w}$, we have a similar formula for its material derivatives:

$$\frac{D\boldsymbol{w}}{Dt} = \dot{\boldsymbol{w}} = \left.\frac{\partial \boldsymbol{W}(\boldsymbol{X},t)}{\partial t}\right|_{\boldsymbol{X}=\boldsymbol{\chi}^{-1}(\boldsymbol{x},t)} \tag{1.20}$$

$$\frac{Dw_i}{Dt} = \dot{w}_i = \left.\frac{\partial W_i(\boldsymbol{X},t)}{\partial t}\right|_{\boldsymbol{X}=\boldsymbol{\chi}^{-1}(\boldsymbol{x},t)}$$

$$\dot{\boldsymbol{w}} = \frac{\partial\boldsymbol{w}(\boldsymbol{x},t)}{\partial t} + \big(\nabla\boldsymbol{w}(\boldsymbol{x},t)\big)\left.\frac{\partial\boldsymbol{\chi}(\boldsymbol{X},t)}{\partial t}\right|_{\boldsymbol{X}=\boldsymbol{\chi}^{-1}(\boldsymbol{x},t)} \tag{1.21}$$

$$\dot{w}_i = \frac{\partial w_i(\boldsymbol{x},t)}{\partial t} + \frac{\partial w_i(\boldsymbol{x},t)}{\partial x_j}\,v_j\,.$$

1.2.2.3 Acceleration

The acceleration $\boldsymbol{A}$ of a material particle at time t is the derivative of its velocity $\boldsymbol{V}$ with respect to time, that is, the material derivative of $\boldsymbol{V}$. In the material description, we have

$$\boldsymbol{A}(\boldsymbol{X},t) = \frac{\partial\,\boldsymbol{V}(\boldsymbol{X},t)}{\partial t} = \frac{\partial^2\boldsymbol{\chi}(\boldsymbol{X},t)}{\partial t^2} \tag{1.22}$$

$$A_i = \dot{V}_i = \frac{\partial^2\chi_i(\boldsymbol{X},t)}{\partial t^2}\,,$$

and in the spatial description, we have

$$\boldsymbol{a} = \dot{\boldsymbol{v}} = \frac{\partial \boldsymbol{v}(\boldsymbol{x}, t)}{\partial t} + \big(\nabla \boldsymbol{v}(\boldsymbol{x}, t)\big)\boldsymbol{v}(\boldsymbol{x}, t) \tag{1.23}$$
$$a_i = \dot{v}_i = \frac{\partial v_i(\boldsymbol{x}, t)}{\partial t} + \frac{\partial v_i(\boldsymbol{x}, t)}{\partial x_j}\, v_j(\boldsymbol{x}, t)\,.$$

The notation $\nabla \boldsymbol{v}$ represents the velocity gradient, a second-order tensor that has the components $\partial v_i / \partial x_j$. The first term on the right-hand side of (1.23) can be considered as the acceleration due to the time dependence of the velocity at a fixed point in space. The second term can be interpreted as the contribution to the acceleration of the material particle due to the heterogeneity of the velocity field. These terms are sometimes called the local and convective (or advective) parts, respectively, of the acceleration. The advection corresponds to the transport of the velocity field by itself.

1.2.3 Jacobian

The Jacobian of the transformation (1.5), i.e.

$$J = \det\left(\frac{\partial \chi_i}{\partial X_j}\right) \tag{1.24}$$

represents the dilatation of an infinitesimal volume during the motion. For the inverse function $\boldsymbol{\chi}^{-1}$ to be differentiable, we have the condition

$$0 < J < \infty\,. \tag{1.25}$$

An elegant relationship due to L. Euler reads

$$\dot{J} = J \operatorname{div} \boldsymbol{v}\,. \tag{1.26}$$

1.2.4 Reynolds Transport Theorem

Theorem 1.1 (Reynolds theorem) *If the current time t value of the integral $I(t)$ of property $f(\boldsymbol{x}, t)$ over a fluid volume $\omega(t)$ is defined by the equation*

$$I(t) = \int_{\omega(t)} f(\boldsymbol{x}, t)\, dV\,, \tag{1.27}$$

the time derivative of I is given by

$$\mathrm{d}I(t) = \int_{\omega(t)} \left[\frac{Df}{Dt} + f\, div\, \boldsymbol{v} \right] dV \ , \tag{1.28}$$

where $\frac{D}{Dt}$ *is the material derivative defined by (1.18) such that*

$$\frac{Df}{Dt} = \frac{\partial f}{\partial t} + v_j \frac{\partial f}{\partial x_j} = \frac{\partial f}{\partial t} + \boldsymbol{v} \cdot \boldsymbol{\nabla} f \ . \tag{1.29}$$

We can consider that Reynolds theorem is somehow the generalization to a fluid material of the one-dimensional Leibnitz' integral whose integration limits are also function of the integration variable. In (1.27), the function f may be a scalar, vector or tensor function.

1.3 Velocity Gradient and Associated Tensors

In numerous problems of fluid mechanics, an interesting kinematic quantity is not the change in the shape of the material volume, but the rate at which this change is produced.

Let $\mathcal{V}$ be the neighborhood of the point P with coordinates x_i, and Q an arbitrary point belonging to $\mathcal{V}$ with coordinates $x_i + dx_i$. The spatial velocity of Q is given by

$$v_i(x_j + dx_j, t) = v_i(x_j, t) + \frac{\partial v_i(x_j, t)}{\partial x_j} dx_j + \cdots \ . \tag{1.30}$$

The tensor $\boldsymbol{L}$ whose components are

$$L_{ij} = \frac{\partial v_i}{\partial x_j} = \left(\boldsymbol{\nabla v}\right)_{ij} \tag{1.31}$$

is the ***velocity gradient*** that already appeared in Eq. (1.23). The symmetric part of $\boldsymbol{L}$, that is,

$$d_{ij} = \frac{1}{2}\left(\frac{\partial v_i}{\partial x_j} + \frac{\partial v_j}{\partial x_i} \right) \tag{1.32}$$

$$\boldsymbol{d} = \frac{1}{2}\left(\boldsymbol{\nabla v} + (\boldsymbol{\nabla v})^T \right) \tag{1.33}$$

is called the ***rate of deformation tensor***, and the antisymmetric part of $\boldsymbol{L}$, that is,

$$\dot{\omega}_{ij} = \frac{1}{2}\left(\frac{\partial v_i}{\partial x_j} - \frac{\partial v_j}{\partial x_i} \right) \tag{1.34}$$

$$\dot{\boldsymbol{\omega}} = \frac{1}{2}\left(\boldsymbol{\nabla v} - (\boldsymbol{\nabla v})^T \right) \tag{1.35}$$

is called the ***rotation rate tensor*** or ***vorticity tensor***. The upper index T in (1.33) and (1.35) denotes the transpose. Thus we can write

$$\boldsymbol{L} = \boldsymbol{d} + \dot{\boldsymbol{\omega}} \,. \tag{1.36}$$

As an antisymmetric tensor has only three independent components, they can form the dual or axial vector $\dot{\Omega}_i$ associated with the rotation rate tensor, that is,

$$\dot{\Omega}_i = \frac{1}{2}\varepsilon_{ikj}\dot{\omega}_{jk} = -\frac{1}{2}\varepsilon_{ijk}\dot{\omega}_{jk} = \frac{1}{2}\varepsilon_{ijk}\dot{\omega}_{kj} \quad , \tag{1.37}$$

is called the ***rotation rate vector***. The permutation symbol ε_{ijk} is a third order tensor defined as follows

$$\varepsilon_{ijk} = \begin{cases} 1 \text{ if } ijk \text{ is an even permutation of } 123 \\ -1 \text{ if } ijk \text{is an odd permutation of } 123 \\ 0 \text{ all other cases,} \end{cases} \tag{1.38}$$

or as

$$\varepsilon_{ijk} = \frac{1}{2}(i-j)(j-k)(k-i) \,. \tag{1.39}$$

Note that in fluid mechanics, one typically introduces the vorticity vector $\boldsymbol{\omega}$ with the definition as the curl of the velocity. Then

$$\boldsymbol{\omega} = \mathbf{curl}\, \boldsymbol{v} = \boldsymbol{\nabla} \times \boldsymbol{v} \tag{1.40}$$

or

$$\omega_i = \varepsilon_{ijk}\frac{\partial v_k}{\partial x_j} \,. \tag{1.41}$$

And we easily deduce that

$$\boldsymbol{\omega} = 2\dot{\boldsymbol{\Omega}}. \tag{1.42}$$

To better understand the vorticity vector, consider the decomposition of a local motion of a fluid. Let P be a point at position $\boldsymbol{x}$ and P′ a neighboring point as shown in Fig. 1.9.

The vector position of P′ relative to P is $d\boldsymbol{x}$. After an infinitesimal lapse of time, P and P′ occupy new positions. P moves with the local velocity $\boldsymbol{v}$ and P′ with the velocity $\boldsymbol{v} + d\boldsymbol{v}$. We consider P to be the principal fluid particle and, subtracting its translational velocity, we describe the motion of P′ as observed from this principal particle. This reasoning is valid only when the distance $d\boldsymbol{x}$ is very small. We can decompose the motion of P and P′ into three distinct parts: a translation, a rigid body rotation, and a strain. The translational motion is given by the velocity $\boldsymbol{v}$ of P. All the other motions, taken together, are given by $d\boldsymbol{v}$, the velocity of P′ with respect to P. We then have

$$d\boldsymbol{v} = \frac{\partial \boldsymbol{v}}{\partial \boldsymbol{x}} d\boldsymbol{x} = \boldsymbol{L}\, d\boldsymbol{x} \,. \tag{1.43}$$

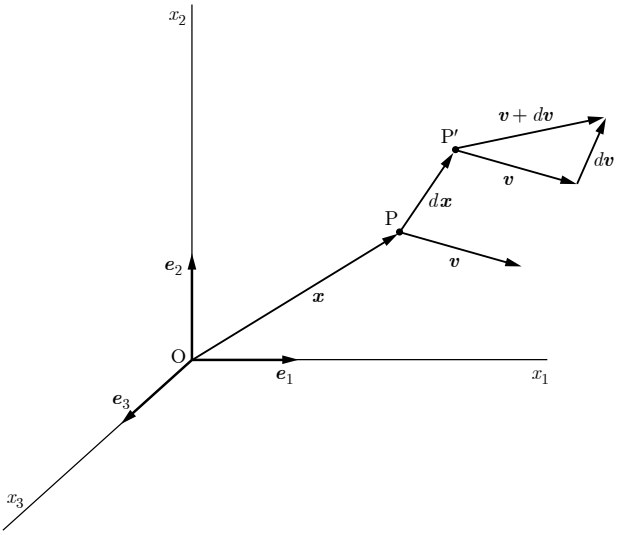

Fig. 1.9 Relative motion of two fluid particles

By (1.36), the strain motions (stretching, shortening, ...) of P′ with respect to P are described by $\boldsymbol{d}$. Consequently the rotational motion of P′ with respect to P is taken into account by $\dot{\boldsymbol{\omega}}$. We can write

$$d\boldsymbol{v}^{(r)} = \dot{\boldsymbol{\omega}}\, d\boldsymbol{x} \ , \tag{1.44}$$

where the superscript r refers to rotation.

The rigid body rotational motion of P′ with respect to P must have the form of the equation $\boldsymbol{v} = \boldsymbol{\Omega} \times \boldsymbol{x}$, where $\boldsymbol{\Omega}$ is the rate of angular rotation (a vector). By (1.37) and (1.42), we have $-\dot{\omega}_{ij} = \frac{1}{2}\varepsilon_{ijk}\omega_k = \dot{\omega}_{ji}$. Thus the rotational component of motion is given by

$$\begin{aligned} dv_j^{(r)} &= \dot{\omega}_{ji}\, dx_i = \frac{1}{2}\varepsilon_{ijk}\omega_k\, dx_i \\ &= \frac{1}{2}\varepsilon_{jki}\,(\omega_k)\; dx_i \ . \end{aligned} \tag{1.45}$$

This last equation is of the form $d\boldsymbol{v} = \boldsymbol{\Omega} \times d\boldsymbol{x}$. The vorticity vector $\boldsymbol{\omega}$ corresponds to an angular velocity such that the vorticity $\boldsymbol{\omega}$ is equal to $2\boldsymbol{\Omega}$, that is two times the vector rate of rigid body rotation of P′ with respect to P.

Note that in the case of rotation of a rigid body, one can show that $\boldsymbol{d} = 0$ and $\boldsymbol{L} = \dot{\boldsymbol{\omega}}$. The rotation rate tensor is thus entirely determined by the instantaneous rotation of the body.

1.4 Mass Conservation

The principle of mass conservation reads as follows: *For the same material volume* $\omega(t)$, *the mass* $M(t)$ *remains constant in time.*

One has:

$$\mathrm{d}M(t) = 0\ . \tag{1.46}$$

In order to write the local form of the principle of mass conservation, the Reynolds transport theorem is needed. Indeed, the mass $M(t)$ can be expressed by the definition

$$M(t) = \int_{\omega(t)} \rho\, dV\ , \tag{1.47}$$

where ρ is the mass density of the fluid. It has for SI[2] units kg/m^3 or dimensions ML^{-3} where M is the mass and L a length. For water, at standard sea level temperature, ρ is 1,000 kg/m^3. Fluid mechanicists name incorrectly ρ density. Strictly speaking, density is defined as the ratio of the volumic mass of the fluid (or the material) at hand to that of water. Therefore water density (specific gravity) is equal to 1.

As ρ can in general depend on position and time, the Eqs. (1.28) and (1.47) yield in local form:

$$\frac{D\rho}{Dt} + \rho\ \mathrm{div}\ \boldsymbol{v} = 0\ , \tag{1.48}$$

or

$$\frac{\partial \rho}{\partial t} + \mathrm{div}\ (\rho\, \boldsymbol{v}) = 0\ . \tag{1.49}$$

A fluid is considered as incompressible when the density $\rho(\boldsymbol{x}, t)$ is constant and $D\rho(\boldsymbol{x}, t)/Dt = 0$. It also follows from (1.49) that the ***incompressibility condition*** can be expressed by the following relationship:

$$\mathrm{div}\ \boldsymbol{v} = \frac{\partial v_i}{\partial x_i} = 0\,. \tag{1.50}$$

Note that the velocity field that satisfies (1.50) is solenoidal. As div $\boldsymbol{v} = 0$, it follows from (1.26) that $\dot{J} = 0$, so J remains constant over time. Since $J(\boldsymbol{X}, 0) = 1$, the motion of an incompressible material takes place with constant volume and is often called isochoric.

The incompressibility condition (1.50) can be satisfied by the vector potential $\boldsymbol{\Psi}$ such that

$$\boldsymbol{v} = \mathbf{curl}\, \boldsymbol{\Psi}\ , \tag{1.51}$$

as this verifies the vector identity div **curl** $= 0$.

[2] International System of Units, Système International d'Unités, designated SI in all languages.

1.5 Equation of Motion

In a fluid, the applied forces on the volume $\omega(t)$ are of two types

1. volume or body forces (acting at a distance) by unit volume such as gravity $\boldsymbol{g}$ or electromagnetic forces, including the Lorentz force, defined by $\rho \boldsymbol{b}(\boldsymbol{x}, t)$
2. contact forces by unit surface $\boldsymbol{t}(\boldsymbol{x}, t, \boldsymbol{n})$.

In the contact forces, appears $\boldsymbol{n}$ the unit normal vector to the surface $\partial\omega(t)$ where the force is exerted.

The principle of conservation of momentum which is the generalization of Newton's law, reads: *The rate of change of the momentum of an arbitrary volume of a fluid at time t is equal to the sum of the forces applied to $\omega(t)$ at that instant.*

The principle states

$$\frac{d}{dt}\int_{\omega(t)} \rho(\boldsymbol{x}, t)\boldsymbol{v}(\boldsymbol{x}, t)\, dV = \int_{\omega(t)} \rho(\boldsymbol{x}, t)\boldsymbol{b}(\boldsymbol{x}, t)\, dV + \int_{\partial\omega(t)} \boldsymbol{t}(\boldsymbol{x}, t, \boldsymbol{n})\, dS\,. \tag{1.52}$$

Theorem 1.2 (Cauchy theorem) *The stress vector $\boldsymbol{t}$ is linked to the outward unit normal $\boldsymbol{n}$ of the closed material surface $\partial\omega(t)$ via the stress tensor $\boldsymbol{\sigma}$.*

$$\boldsymbol{t}(\boldsymbol{x}, t, \boldsymbol{n}) = \boldsymbol{\sigma}(\boldsymbol{x}, t)\,\boldsymbol{n} \quad \text{or} \quad t_i(\boldsymbol{x}, t, \boldsymbol{n}) = \sigma_{ij}(\boldsymbol{x}, t)n_j\,. \tag{1.53}$$

The symbol σ_{ij} is the stress component in direction i of the Cartesian rectangular coordinate system acting on a surface element with a unit normal oriented in the direction of the basis vector $\boldsymbol{e}_j$. Taking mass conservation into account, the left hand side of (1.52) becomes

$$\frac{d}{dt}\int_{\omega(t)} \rho\, \boldsymbol{v}\, dV = \int_{\omega(t)} \rho\, \frac{D\boldsymbol{v}}{Dt}\, dV\,. \tag{1.54}$$

Let us introduce the Gauss theorem that will be useful for many developments.

Theorem 1.3 (Gauss theorem) *Gauss theorem, also known as the divergence theorem, transforms the volume integral of the divergence of a continuous media property into a surface integral*

$$\int_{\omega(t)} \boldsymbol{div}\, \boldsymbol{L}\, dV = \int_{\partial\omega(t)} \boldsymbol{L}\,\boldsymbol{n}\, dS\,. \tag{1.55}$$

With Eq. (1.53) and the divergence theorem for a second-order tensor $\boldsymbol{L}$ the contact force term yields

$$\int_{\partial\omega(t)} \sigma_{ij}\, n_j\, dS = \int_{\omega(t)} \frac{\partial\sigma_{ij}}{\partial x_j}\, dV \quad \text{or} \quad \int_{\partial\omega(t)} \boldsymbol{\sigma}\boldsymbol{n}\, dS = \int_{\omega(t)} \boldsymbol{div}\, \boldsymbol{\sigma}\, dV. \tag{1.56}$$

Equation (1.52) now reads

$$\int_{\omega(t)} \left[\rho \frac{D\boldsymbol{v}}{Dt} - \boldsymbol{div}\,\boldsymbol{\sigma} - \rho \boldsymbol{b} \right] dV = 0 \,. \tag{1.57}$$

Invoking the localization theorem

Theorem 1.4 *For an arbitrary material volume, the integral equation is identically satisfied when the integrand vanishes,*
Eq. (1.57) gives

$$\rho \frac{D\boldsymbol{v}}{Dt} = \boldsymbol{div}\,\boldsymbol{\sigma} + \rho \boldsymbol{b} \,. \tag{1.58}$$

In absence of volume torque, the principle of conservation of angular momentum implies the symmetry of the Cauchy stress tensor

$$\boldsymbol{\sigma} = \boldsymbol{\sigma}^T \,. \tag{1.59}$$

This reduces the number of unknown stress components from 9 to 6.

1.6 Equation of Energy

The principle of conservation of energy is expressed as:
For the same material volume $\omega(t)$, the time derivative of the total energy is equal to the sum of the power of the volume and contact forces and the rate of heat received by the material.

The total energy is the sum of the kinetic energy defined by

$$\int_{\omega(t)} \frac{1}{2} \rho \, \boldsymbol{v} \cdot \boldsymbol{v} \, dV \tag{1.60}$$

and the internal energy

$$\int_{\omega(t)} \rho \, u \, dV, \tag{1.61}$$

where u is the internal energy density per unit mass. One gets

$$\frac{d}{dt} \int_{\omega(t)} \left[\frac{1}{2} (\boldsymbol{v} \cdot \boldsymbol{v}) + u \right] \rho \, dV = \int_{\partial\omega(t)} \boldsymbol{t} \cdot \boldsymbol{v} \, dS + \int_{\omega(t)} \rho \boldsymbol{b} \cdot \boldsymbol{v} \, dV + \int_{\partial\omega(t)} (-\boldsymbol{q} \cdot \boldsymbol{n}) dS + \int_{\omega(t)} r \, dV \,. \tag{1.62}$$

In Eq. (1.62), $\boldsymbol{q}$ represents the heat flux vector across the surface $\partial\omega(t)$, while r designates the heat produced or received per unit time and volume. For example, r

could be the heat produced or consumed by a chemical reaction in the material or heating by the Joule effect.

By the application of the conservation of mass (1.48), of Cauchy principle (1.53) and divergence and localization theorems to the relation (1.62), we obtain:

$$\rho \frac{D}{Dt}\left(\frac{1}{2}(\boldsymbol{v}\cdot\boldsymbol{v})+u\right) = \operatorname{div}(\boldsymbol{\sigma}\,\boldsymbol{v}) + \rho\boldsymbol{b}\cdot\boldsymbol{v} - \operatorname{div}\boldsymbol{q} + r\ . \tag{1.63}$$

The first term on the right hand side of Eq. (1.63) can be written as

$$\operatorname{div}(\boldsymbol{\sigma}\,\boldsymbol{v}) = \operatorname{div}(\boldsymbol{\sigma})\cdot\boldsymbol{v} + \boldsymbol{\sigma} : \nabla\boldsymbol{v}\ . \tag{1.64}$$

Subtracting from (1.63) the equation of motion (1.58) multiplied by $\boldsymbol{v}$, we have:

$$\rho\frac{Du}{Dt} = \boldsymbol{\sigma} : \nabla\boldsymbol{v} - \operatorname{div}\boldsymbol{q} + r\ . \tag{1.65}$$

The product $\boldsymbol{\sigma} : \nabla\boldsymbol{v}$ is the scalar product of two tensors such that in indexed form, one has

$$(\boldsymbol{\sigma} : \nabla\boldsymbol{v}) = \sigma_{ij}\frac{\partial v_i}{\partial x_j}\ . \tag{1.66}$$

1.7 Constitutive and State Equations

The elaboration of the constitutive equation for a viscous Newtonian fluid is based on the following assumptions:

i. For a fluid at rest, the viscous fluid behaves as a perfect (without viscosity) or inviscid fluid.

ii. For a moving fluid, the stress tensor depends through a linear relation on the strain rate tensor or the rate of deformation tensor. This hypothesis is characteristic of the Newtonian behavior of the fluid. The necessity of a quantitative relation between the internal forces in a moving fluid and the kinematical quantities describing the motion is due to Newton. Langlois and Deville [49] extract from his famous book *Philosophiae Naturalis Principia Mathematica* the following excerpt.

Resistentiam quae oritur ex defectu lubricitatis partium fluidi, caeteris paribus, proportionatem esse velocitati, qua partes fluidi separantur ab invicem[3].

iii. The fluid is isotropic.

These hypotheses allow writing the general constitutive equation of a viscous incompressible fluid in the form

$$\boldsymbol{\sigma} = -p\,\boldsymbol{I} + 2\,\mu\,\boldsymbol{d}\ . \tag{1.67}$$

[3] The resistance arising from imperfect slipping between fluid particles to be proportional to the velocity with which the particles are moving apart, other things being equal.

The symbol p represents the pressure. The strain rate tensor $\boldsymbol{d}$, which is the symmetric part of the velocity gradient tensor $\boldsymbol{\nabla v}$, has for components:

$$d_{ij} = \frac{1}{2}\left(\frac{\partial v_i}{\partial x_j} + \frac{\partial v_j}{\partial x_i}\right) . \tag{1.68}$$

The factor μ is the dynamic viscosity coefficient of dimension $ML^{-1}T^{-1}$ expressed in Pa.s. The tensor $\boldsymbol{I}$ is the unit tensor; using indices, it corresponds to the Kronecker symbol δ_{ij} defined by the relation

$$\delta_{ij} = \begin{cases} 1 \text{ if } i = j, \\ 0 \text{ if } i \neq j. \end{cases} \tag{1.69}$$

In an incompressible fluid, pressure is the scalar field resulting from the imposition of the continuity constraint. For the incompressible viscous fluid, the continuity Eq. (1.50) is equivalent to $tr(\boldsymbol{d}) = 0$, with tr being the trace operator of a tensor defined as the sum of its diagonal elements. The incompressible perfect fluid is obtained for a vanishing viscosity in (1.67):

$$\boldsymbol{\sigma} = -p\,\boldsymbol{I}. \tag{1.70}$$

In this last case, the stress tensor is spherical, because only its diagonal elements are non zero.

The incompressible fluid is a particular case from the thermodynamics point of view, as ρ is supposed to be a constant. The specific heat capacity is therefore unique and will be denoted by c. Furthermore we assume that the relation between the internal energy u and c is

$$\frac{du}{dT} = c(T) .$$

This relation can be integrated if the heat capacity is considered as a constant, and with an appropriate choice of the integration constants, we get

$$u = c\,T. \tag{1.71}$$

A last constitutive equation is still to be considered to close the system of equations to be solved, namely the heat flux. For the vast majority of Newtonian fluids, experimental data show that there exists a linear relation between the heat flux and the temperature gradient. This is given by Fourier's law

$$\boldsymbol{q} = -k(T)\ \boldsymbol{grad}\ T\ , \tag{1.72}$$

k being the coefficient of thermal conductivity, which is, most often, only a function of temperature. Its SI units are W m^{-1} K^{-1}. For air considered as an ideal gas, $k = 0.0262$ W $m^{-1}K^{-1}$.

1.8 Incompressible Navier–Stokes Equations

We suppose that the flow is isothermal with $T = cnst$. The principle of conservation of energy is satisfied. Inserting the constitutive equation (1.67) in the Eq. (1.58), we generate the incompressible Navier–Stokes equations or more precisely the Navier–Stokes equations for the incompressible fluid

$$\operatorname{div} \boldsymbol{v} = 0 \tag{1.73}$$

$$\rho \frac{D\boldsymbol{v}}{Dt} = -\nabla p + \mu \triangle \boldsymbol{v} + \rho \boldsymbol{b} \,. \tag{1.74}$$

Equation (1.74) is a non-linear second-order partial differential equation. It states that acceleration is produced by the actions of the pressure gradient, the viscous forces, and the body forces. Note that the presence of the non-linearity in the acceleration term, namely the advective acceleration, renders the search for closed form or analytical solutions extremely dreadful. This partial differential equation requires initial and boundary conditions to be integrated and solved.

1.9 Boundary and Initial Conditions

1.9.1 No Slip Wall

A viscous fluid in contact with a rigid wall will adhere to the wall due to the effects of viscosity. The no-slip condition can therefore be written as

$$\boldsymbol{v}_{fluid} = \boldsymbol{v}_{wall} \,. \tag{1.75}$$

1.9.2 Interface

An interface occurs when two immiscible fluids are in direct contact. For a two-dimensional flow, the interface is a planar curvy line, while in the three-dimensional case, the interface is a surface. Examples are provided by coating flows where multi-layer materials are produced in the polymeric industrial applications.

Consider Fig. 1.10. The interface condition expresses the mechanical equilibrium of the contact forces applied by fluids I and II on either side of the interface. We have

$$\boldsymbol{t}_{\mathrm{I}} + \boldsymbol{t}_{\mathrm{II}} = \boldsymbol{0} \,, \tag{1.76}$$

with definition (1.53) for $\boldsymbol{t}$. Taking the equality $\boldsymbol{n}_{\mathrm{I}} = -\boldsymbol{n}_{\mathrm{II}}$ into account, one obtains

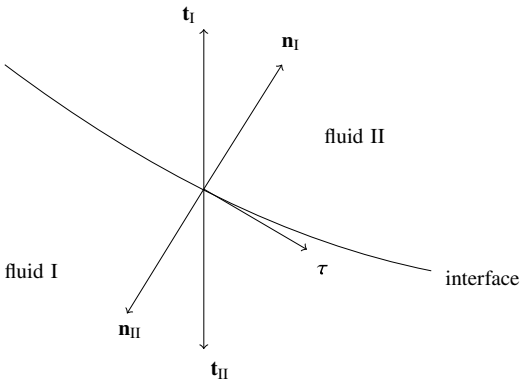

Fig. 1.10 Interface description

$$\boldsymbol{\sigma}_{\mathrm{I}}\boldsymbol{n}_{\mathrm{I}} = \boldsymbol{\sigma}_{\mathrm{II}}\boldsymbol{n}_{\mathrm{I}} \,. \tag{1.77}$$

The interface conditions are obtained by projecting Eq. (1.77) onto the normal $\boldsymbol{n}_{\mathrm{I}}$ and the tangent vector $\boldsymbol{\tau}$ giving

$$\boldsymbol{\sigma}_{\mathrm{I}}\boldsymbol{n}_{\mathrm{I}} \cdot \boldsymbol{n}_{\mathrm{I}} = \boldsymbol{\sigma}_{\mathrm{II}}\boldsymbol{n}_{\mathrm{I}} \cdot \boldsymbol{n}_{\mathrm{I}} \,, \tag{1.78}$$

$$\boldsymbol{\sigma}_{\mathrm{I}}\boldsymbol{n}_{\mathrm{I}} \cdot \boldsymbol{\tau} = \boldsymbol{\sigma}_{\mathrm{II}}\boldsymbol{n}_{\mathrm{I}} \cdot \boldsymbol{\tau} \,. \tag{1.79}$$

1.9.3 Laminar Free Surface

An interesting particular case of an interface is that of a free surface (cf. Fig. 1.11) where a laminar viscous fluid is in contact with an inviscid fluid: e.g. air, assumed to be at rest. Taking $\boldsymbol{n}$, the outgoing normal vector from the viscous fluid, as a reference, we have here $\boldsymbol{\sigma}_{\mathrm{II}} = -p_{invis}\boldsymbol{I}$, where p_{invis} is the pressure in the perfect (inviscid) fluid. The fluid index I is omitted for simplicity. Conditions (1.78) and (1.79) are now written as

$$\boldsymbol{\sigma}\boldsymbol{n} \cdot \boldsymbol{n} = -p_{invis}(\boldsymbol{n} \cdot \boldsymbol{n}) = -p_{invis} \,, \tag{1.80}$$

$$\boldsymbol{\sigma}\boldsymbol{n} \cdot \boldsymbol{\tau} = \boldsymbol{0} \,. \tag{1.81}$$

The latter relation is consistent with the fact that an inviscid fluid is incapable to sustain a shear force.

Free surface conditions imply that we know the form of the surface for their application. However, the form of the surface is itself part of the solution of the problem at hand. We find that free surface problems constitute one of the major difficulties in fluid mechanics as they are intrinsically non-linear. In some cases,

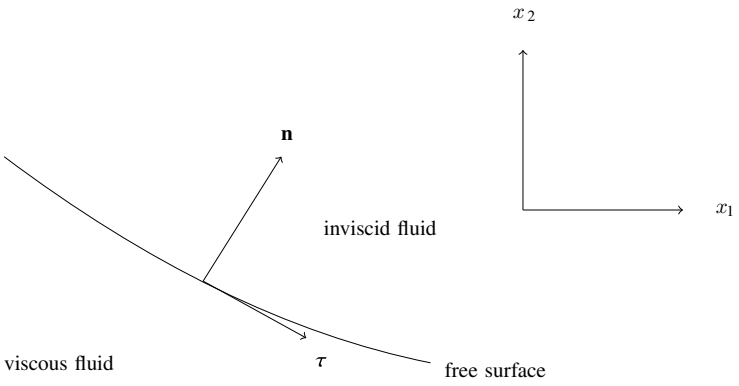

Fig. 1.11 Free surface

closed form solutions are sought in Lagrangian formulation. The initial geometrical domain is prescribed and the solution method tracks the trajectories of fluid particles. This procedure is carried out in the breaking of a dam problem as described in Chap. 12 of the monograph by Stoker [100].

For certain fluids, condition (1.80) needs to be extended to take into account surface tension. Then we have

$$\boldsymbol{\sigma n} \cdot \boldsymbol{n} = -p_{invis} + \gamma \left(\frac{1}{R_1} + \frac{1}{R_2} \right) , \tag{1.82}$$

in which R_1 and R_2 are the principal radii of curvature of the surface, and γ is the viscous-inviscid surface tension coefficient expressed in N/m. The newton N is the force that gives to a mass of 1 kg an acceleration of 1 m/s. For example, for the water-air interface, we have $\gamma = 0.072$ N/m. The quantity inside the parentheses multiplying the surface tension coefficient in Eq. (1.82) is equal to 2Ξ, where Ξ is the average curvature of the surface. Its sign depends on the concavity $(-)$ or the convexity $(+)$ of the surface.

In practice, we generally limit the study to a part of the space occupied by the fluid. In this case, it is necessary to add the conditions on the entry section, where the velocity vector is typically prescribed, and the exit surface, where contact forces are usually imposed. The latter are most often taken to be zero, which corresponds to a situation where the fluid is allowed to exit at its own speed.

For the case of a transient problem, the initial conditions are the velocities, which are often zero at the start.

1.9.4 Perfect Fluid

As viscosity plays no role here, the fluid can slip along a wall. The adherence condition no longer applies. We impose that the normal component of the fluid velocity be zero with respect to the wall with which it is in contact. The slip condition is written as

$$\boldsymbol{v}_{fluid} \cdot \boldsymbol{n} = \boldsymbol{v}_{wall} \cdot \boldsymbol{n} \ . \tag{1.83}$$

Similarly, we impose the value of the normal component of the fluid velocity for the entry section and the pressure on the exit section. For transient flows, we proceed as for viscous flows.

Finally, in aerodynamics (external flows, for example, the flow around a wing profile or an airfoil), we very often find conditions to impose on an immaterial boundary (which may be at infinity). The typical example is that of a finite obstacle (like a slender body) placed in an unconfined flow. In this case we impose the condition that the flow is uniform at infinity.

1.10 Thermodynamics Considerations and Incompressibility

The speed of sound in ambient air at temperature 293 K is of the order of $340\,\mathrm{ms}^{-1}$, whereas in water, it is $1500\,\mathrm{ms}^{-1}$. By definition, the speed of sound is the variation of pressure with respect to density at fixed entropy s

$$a^2 = \left.\frac{\partial p}{\partial \rho}\right|_s \ . \tag{1.84}$$

As a^2 is obtained by the limit

$$a^2 = \lim_{\Delta\rho \to 0} \frac{\Delta p}{\Delta \rho} \ , \tag{1.85}$$

for an incompressible fluid, $\Delta\rho = 0$ and then the speed of sound is infinite. Therefore the question is raised: "How do we define the concept of an incompressible fluid?".

1.10.1 Compressible Fluid and Compressible Navier–Stokes Equations

To examine this matter, let us consider the Navier–Stokes equations for the compressible fluid in detail. The mass conservation equation is given by (1.48). To produce the

Navier–Stokes equations, we need the constitutive equation for compressible viscous fluids

$$\boldsymbol{\sigma} = -p\,\boldsymbol{I} + \lambda(\rho, T)\, tr(\boldsymbol{d})\boldsymbol{I} + 2\,\mu(\rho, T)\,\boldsymbol{d}\ , \tag{1.86}$$

where λ is the volume viscosity. The coefficients λ and μ depend on the density ρ and the temperature T. In the compressible case, the pressure is a thermodynamic variable such that $p = p(\rho, T)$. If we assume that the fluid internal energy does not depend on density, but only on temperature, we are in the framework of the ideal gas that satisfies the Boyle–Mariotte law "at constant temperature, the product of the pressure p and the volume V is constant". This law allows us to write the pressure state equation

$$p = \rho R T\ , \tag{1.87}$$

that is a scalar constitutive equation for the pressure. R is the ideal gas constant expressed in J kg^{-1}K^{-1}. For ambient air, $R = 287$ J kg^{-1}K^{-1}.

Introducing the constitutive equation (1.86) in the momentum equation (1.58), we obtain the Navier–Stokes equations for the compressible fluid

$$\rho\frac{D\boldsymbol{v}}{Dt} = -\boldsymbol{\nabla}\, p + \boldsymbol{\nabla}\,(\lambda\, tr\boldsymbol{d}) + \mathrm{div}\,(\boldsymbol{2}\mu\,\boldsymbol{d}) + \rho\boldsymbol{b}\ . \tag{1.88}$$

The treatment of the energy equation (1.65) requires a few more concepts. Assuming that the fluid is an ideal gas, its internal energy u and its mass enthalpy h are defined as

$$h = u + \frac{p}{\rho}\ . \tag{1.89}$$

The variables h and u depend only on the temperature. The specific heat capacities at constant volume and pressure are such that

$$du = c_v(T)dT\ ,\quad dh = c_p(T)dT\ , \tag{1.90}$$

where c_v and c_p are the specific heat capacities at constant volume and constant pressure, respectively. Taking into account the state equations (1.87) and (1.89), one gets

$$dh = du + R\,dT\ , \tag{1.91}$$

from which we obtain

$$R = c_p(T) - c_v(T)\ . \tag{1.92}$$

For air considered as an ideal gas, $c_p = 1006$ J kg^{-1} K^{-1}. If we assume that the heat capacities are constant in the considered temperature range, we can write, within an additive constant,

$$u = c_v\, T\ , \tag{1.93}$$
$$h = c_p\, T\ , \tag{1.94}$$
$$s = c_v \log p - c_p \log \rho\ , \tag{1.95}$$

where s is the entropy. If the flow is isentropic (same entropy), we have

$$\frac{p}{\rho^\gamma} = \text{cnst}\ , \tag{1.96}$$

with the definition of the heat capacity ratio:

$$\gamma = \frac{c_p}{c_v}\,. \tag{1.97}$$

In the special case of an ideal gas, (1.84) takes the form, with the use of (1.96)

$$a^2 = \gamma \frac{p}{\rho} = \gamma RT\ . \tag{1.98}$$

With the help of (1.93), the energy equation (1.65) becomes

$$\rho\, c_v \frac{DT}{Dt} = \boldsymbol{\sigma} : \boldsymbol{\nabla v} - \text{div}\, \boldsymbol{q} + r\ . \tag{1.99}$$

The expression $\boldsymbol{\sigma} : \boldsymbol{\nabla v}$ may be written successively

$$\begin{aligned}\sigma_{ij} \frac{\partial v_i}{\partial x_j} &= \sigma_{ij}\, d_{ij} = -p\, \delta_{ij}\, d_{ij} + \lambda\, d_{kk}\, d_{ij}\, \delta_{ij} + 2\mu (d_{ij})^2 \\ &= -p\, d_{ii} + \lambda (d_{ii})^2 + 2\mu (d_{ij})^2\end{aligned}$$

or

$$\boldsymbol{\sigma} : \boldsymbol{d} = -p\, \text{tr}\, \boldsymbol{d} + \lambda (\text{tr}\, \boldsymbol{d})^2 + 2\mu (\boldsymbol{d} : \boldsymbol{d})\,. \tag{1.100}$$

To obtain the left hand side of Eq. (1.100), we have used the property stating that the trace of the inner product of a symmetric tensor $\boldsymbol{\sigma}^T$ with the antisymmetric part of the tensor $\boldsymbol{\nabla v}$, which is the rotation rate tensor, vanishes. From the mass conservation equation (1.48), we have

$$\text{tr}\, \boldsymbol{d} = -\frac{1}{\rho} \frac{D\rho}{Dt}\,.$$

Therefore Eq. (1.99) yields

$$\rho c_v \frac{DT}{Dt} = \frac{p}{\rho} \frac{D\rho}{Dt} + \lambda\, (\text{tr}\, \boldsymbol{d})^2 + 2\mu\, \boldsymbol{d} : \boldsymbol{d} - \text{div} \boldsymbol{q} + \text{r}\,. \tag{1.101}$$

Using the state equation (1.87), (1.101) is transformed as

$$\rho c_v \frac{DT}{Dt} = \frac{Dp}{Dt} - \rho R \frac{DT}{Dt} + \lambda (\mathrm{tr}\, \boldsymbol{d})^2 + 2\mu\, \boldsymbol{d} : \boldsymbol{d} - \mathrm{div} \boldsymbol{q} + \mathrm{r}\,. \tag{1.102}$$

Let us now modify the energy equation (1.102) by taking the Fourier law (1.72) and the relation (1.92) into account

$$\rho c_p \frac{DT}{Dt} = \frac{Dp}{Dt} + \lambda (\mathrm{tr}\, \boldsymbol{d})^2 + 2\mu\, \boldsymbol{d} : \boldsymbol{d} + \mathrm{div}(\mathrm{k} \boldsymbol{\nabla} \mathrm{T}) + \mathrm{r}\,. \tag{1.103}$$

The compressible Navier–Stokes equations comprise the mass conservation equation (1.48), the momentum equations (1.88), the energy equation (1.103) and the state equation (1.87). To investigate the limit case of the compressible set of equations to the incompressible formulation, we need to write the dimensionless form of the Navier–Stokes equations and let the Mach number go to zero. This analysis is deferred till the next chapter.

1.10.2 Incompressibility

From the mass conservation equation (1.48), we deduce

$$\mathrm{div}\, \boldsymbol{v} = -\frac{1}{\rho} \frac{D\rho}{Dt}\,, \tag{1.104}$$

from which one concludes that incompressibility is obtained when the density does not vary with time along a trajectory, i.e.

$$\frac{d\rho}{dt} = 0\,. \tag{1.105}$$

Let us consider a compressible fluid whose pressure depends on the density and the temperature or whose density is a function of the pressure and the temperature. It is possible to expand the previous relationship

$$\frac{d\rho}{dt} = \left(\frac{\partial \rho}{\partial p}\right)_T \frac{dp}{dt} + \left(\frac{\partial \rho}{\partial T}\right)_p \frac{dT}{dt}\,, \tag{1.106}$$

giving via (1.104)

$$\mathrm{div}\, \boldsymbol{v} + \frac{1}{\rho} \left(\frac{\partial \rho}{\partial p}\right)_T \frac{dp}{dt} + \frac{1}{\rho} \left(\frac{\partial \rho}{\partial T}\right)_p \frac{dT}{dt} = 0\,. \tag{1.107}$$

The coefficient of isothermal compressibility χ_T is defined by

$$\chi_T = \frac{1}{\rho}\left(\frac{\partial \rho}{\partial p}\right)_T . \tag{1.108}$$

For water, one has $\chi_T = 5.10^{-10}$ Pa^{-1}. For air, $\chi_T = 10^{-5}$ Pa^{-1}. The other coefficient is the isobaric expansion

$$\alpha = \frac{1}{\rho}\left(\frac{\partial \rho}{\partial T}\right)_p . \tag{1.109}$$

The compressibility coefficient for liquids is very small. Batchelor [10] notices that water density increases by $\frac{1}{2}\%$ when the pressure augments from 1 to 100 bars, at constant ambient temperature (1 bar $= 10^5$ Pa). This large strength to compression of liquids is one of its main characteristics and from the viewpoint of fluid dynamics, it is a reason why we can consider them as incompressible with a great precision.

1.10.3 Boussinesq Approximation for Weakly Dilatable Fluids

Let us examine the non isothermal flow of a weakly compressible fluid. We are able to consider thermal effects for an incompressible fluid, like e.g. in the case of natural convection. This is achieved by Boussinesq approximation [17] that assumes a constant density in the full set of equations except in the body force term, where temperature differences in the fluid induce an Archimedes' thrust generated by density differences. This modeling is used in materials science, for example to study the convection currents in molten metal (Czochralski process for silicium production), im molten glass (floated glass process), etc. It is also widely used in geophysical flows and in meteorology.

Introducing the inner product

$$\boldsymbol{d} : \boldsymbol{d} = d_{ij} d_{ij}, \tag{1.110}$$

equation (1.99) becomes

$$\rho c \frac{DT}{Dt} = 2\mu\, \boldsymbol{d} : \boldsymbol{d} - \operatorname{div} \boldsymbol{q} + r . \tag{1.111}$$

Using the state equation (1.72), Eq. (1.111) is transformed

$$\rho c \frac{DT}{Dt} = 2\mu\, \boldsymbol{d} : \boldsymbol{d} + \operatorname{div} (k\, \boldsymbol{\nabla} T) + r . \tag{1.112}$$

We notice that the first term in the right hand side is the power dissipated by the viscous effects that in most cases, are negligible. However for very viscous fluids like molten glass or the terrestrial magma, these effects must be taken care of. The

temperature equation (1.112) is simplified for constant k. We have

$$\rho c \frac{DT}{Dt} = 2\mu \, \boldsymbol{d} : \boldsymbol{d} + k \triangle T + r \, . \tag{1.113}$$

In the Boussinesq approximation the body force is gravity and hence $\boldsymbol{b} = \boldsymbol{g}$. Furthermore for the weakly dilatable fluid, the state equation for density is linearized

$$\rho = \rho_0(1 - \alpha(T - T_0)), \tag{1.114}$$

with α the coefficient of volumic expansion expressed in K^{-1}. The quantity ρ_0 is the density at the reference temperature T_0. One observes that when the fluid gets hotter, it is lighter as ρ decreases; when it is cooling, it is heavier as ρ increases. Eventually, the Boussinesq approximation supposes that the fluid is incompressible with all its material characteristics constant, except in the gravity term. The set of Boussinesq equations reads

$$\operatorname{div} \boldsymbol{v} = 0, \tag{1.115}$$

$$\rho_0 \frac{D\boldsymbol{v}}{Dt} = -\boldsymbol{\nabla} p \, + \, \mu \triangle \boldsymbol{v} + \rho_0((1 - \alpha(T - T_0))\boldsymbol{g}, \tag{1.116}$$

$$\rho_0 c \frac{DT}{Dt} = 2\mu \, \boldsymbol{d} : \boldsymbol{d} + k \triangle T + r. \tag{1.117}$$

In this system of equations, the velocity-temperature coupling is obtained by the Archimedes' thrust in the body force term, also called the buoyancy term.

It is customary to modify the pressure term in (1.116) with the following expression

$$\tilde{p} = p + \rho_0 \boldsymbol{g} \cdot \boldsymbol{x} \, , \tag{1.118}$$

where the hydrostatic pressure is incorporated. The corresponding Navier–Stokes equation is

$$\rho_0 \frac{D\boldsymbol{v}}{Dt} = -\boldsymbol{\nabla} \tilde{p} \, + \, \mu \triangle \boldsymbol{v} - \rho_0 \alpha (T - T_0) \boldsymbol{g} \, . \tag{1.119}$$

1.11 The Method of Control Volume

Instead of tackling the fluid mechanics partial differential equations, as will be the usual approach in this monograph, a large number of fluid problems can be solved using the integral formulation of mass and momentum conservation laws expressed on control volumes. The control volume is denoted V with surface S.

The mass conservation law (1.50) yields

$$\int_V \operatorname{div} \boldsymbol{v} \, dV = \int_S \boldsymbol{v} \cdot \boldsymbol{n} \, dS \, . \tag{1.120}$$

The momentum conservation equation (1.52) reads

$$\frac{d}{dt}\int_V \rho(\boldsymbol{x},t)\boldsymbol{v}(\boldsymbol{x},t)\,dV = \int_V \rho(\boldsymbol{x},t)\boldsymbol{b}(\boldsymbol{x},t)\,dV + \int_S \boldsymbol{t}(\boldsymbol{x},t,\boldsymbol{n})\,dS\,. \tag{1.121}$$

For an incompressible fluid we have

$$\frac{d}{dt}\int_V \rho(\boldsymbol{x},t)\boldsymbol{v}(\boldsymbol{x},t)\,dV = \rho\int_V \frac{D\boldsymbol{v}}{Dt}\,dV\,. \tag{1.122}$$

The material derivative (1.23) can be recast in the following form

$$\frac{\partial v_i}{\partial t} + \frac{\partial v_i}{\partial x_j}\,v_j = \frac{\partial v_i}{\partial t} + \frac{\partial v_i v_j}{\partial x_j}\,. \tag{1.123}$$

The second term in the right-hand side of (1.123) is the divergence of the tensor $\boldsymbol{V} = \boldsymbol{v}\otimes\boldsymbol{v}$. Using the divergence theorem one obtains

$$\int_V \boldsymbol{div}\,\boldsymbol{V}\,dV = \int_S \boldsymbol{V}\boldsymbol{n}\,dS = \int_S (\boldsymbol{v}\cdot\boldsymbol{n})\boldsymbol{v}\,dS\,. \tag{1.124}$$

Finally, the relevant equation for the control volume method is

$$\rho\int_V \frac{\partial \boldsymbol{v}}{\partial t}dV + \rho\int_S (\boldsymbol{v}\cdot\boldsymbol{n})\boldsymbol{v}\,dS = \int_V \rho\boldsymbol{b}dV + \int_S \boldsymbol{t}dS\,. \tag{1.125}$$

Exercises

1.1 Evaluate by the method of control volume the shearing force $\boldsymbol{F}$ exerted by the viscous fluid on the plate of length L shown in Fig. 1.12 using the velocity profiles given in the inflow and outflow sections. It is assumed that

- the inflow velocity is uniform of value U and the outflow profile is linear over the height h
- the pressure is uniform in the fluid
- the body force is neglected.

The control volume $ABCD$ in dashed lines has height H.

1.2 Show that the velocity field $v_i = Ax_i/r^3$, where $x_i x_i = r^2$ and A is an arbitrary constant, satisfies the conservation of mass equation for an incompressible fluid.

1.3 Show that the flow given by the velocity field

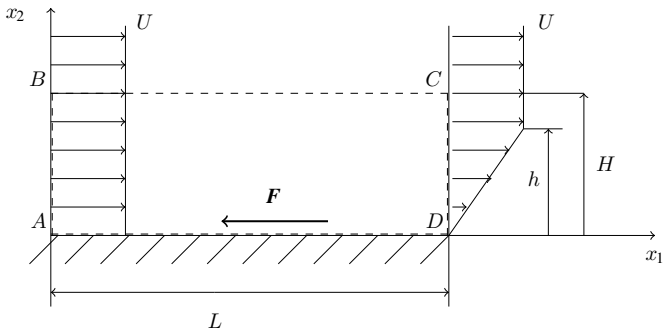

Fig. 1.12 Simplified flow on a flat plate

$$v_r = \frac{(1-r^2)\cos\theta}{r^2}$$
$$v_\theta = \frac{(1+r^2)\sin\theta}{r^2}$$
$$v_z = 0$$

satisfies the incompressibility equation.

1.4 Natural Convection Between Two Differentially Heated Vertical Parallel Walls

Let us consider the steady state, two-dimensional slow flow of a viscous incompressible fluid subjected to a variable temperature field. The fluid flows between two infinite parallel walls at different temperatures, cf. Fig. 1.13, such that $T_2 > T_1$. The heat transfer is by conduction only.

The problem is solved with the Boussinesq approximation. The viscous dissipation and the volume heat production are neglected.

Obtain the simplified temperature and momentum equations and compute the temperature and velocity fields.

1.5 Free Jet

A viscous fluid in laminar flow exits from the cylindrical pipe of a die as it is shown in Fig. 1.14. In the circular pipe the fluid velocity is that of a Poiseuille flow

$$v_z = v_{max}\left(1 - \frac{r^2}{R_0^2}\right) . \tag{1.126}$$

This relation will be demonstrated in Sect. 3.2.2. The maximum velocity v_{max} is reached on the pipe symmetry axis.

The problem is solved in two stages.

- After extrusion, the velocity profile is homogeneous. This means that it is assumed there is no diffusion with the exterior air at the pipe exit and no mixing. Compute

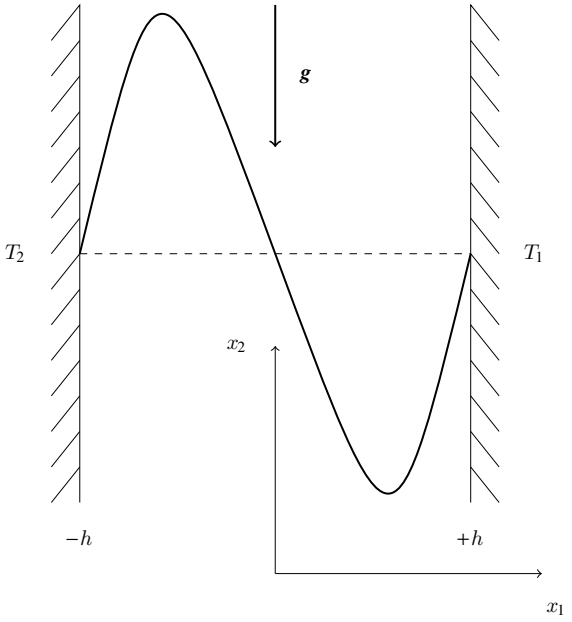

Fig. 1.13 Natural convection in an infinite plane channel. The solid line is the velocity profile

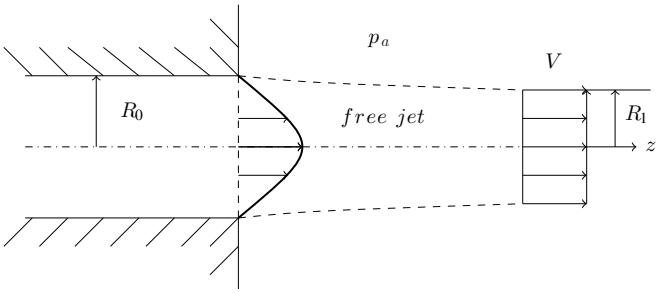

Fig. 1.14 Free jet

the velocity ratio V/v_{max} where V is the flat velocity profile after extrusion. The control volume method is needed in this step.

- Evaluate the contraction coefficient

$$\beta = \frac{R_1^2}{R_0^2}\,, \tag{1.127}$$

where R_1 is the jet radius after extrusion.

Chapter 2
Dimensional Analysis

2.1 Principles and General Concepts

For a deep and thorough presentation of dimensional analysis we refer the reader to the monograph by Barenblatt [9] that covers amply the noticeable properties produced by adequately chosen scalings. Fluid mechanics is very much based on experiments to ascertain the relevant physical phenomena, to watch them and to give them a quantitative approach. The goal of dimensional analysis consists in providing the similarity conditions between the observed phenomena in the physical reality or on a prototype and those yielded on a reduced model or a mock-up.

Let us start by noticing that in dimensional analysis, there is no basic or natural measurement unit for the physical variables. Several universal physical constants are available like the charge of the electron, Planck's constant, the speed of light, etc. But these constants are not characteristic of all physical phenomena. The electron charge is not a fundamental unit to measure the current intensity in an electrical engine. Likewise the flow velocity around an airfoil or the ocean wave velocity are not measured with the light speed as the basic unit. Therefore we may conclude that the measurement scales are arbitrary conventions that are playing no essential role in the physical processes. If we change the size of the length unit, all variables implying a length are rescaled in an appropriate manner.

When considering the dimensional aspect of a problem, it can always be simplified and highlight interesting informations. This is all the more true as dimensional analysis rests on the principle of dimensional invariance that states "the structure of the equations remains unchanged if one performs a modification in size of the system's units".

The aim of dimensional analysis consists in searching the relevant dimensionless numbers that characterize the fluid flow phenomenon. In some cases the values of these numbers offer the possibility of simplifying the mathematical model of the problem at hand. Another benefit of dimensional analysis is the collapse of all experimental data on a single curve that alleviates the burden of various sources of observations, like the drag curve versus the Reynolds number for the flow around

M. O. Deville, *An Introduction to the Mechanics of Incompressible Fluids*,
https://doi.org/10.1007/978-3-031-04683-4_2

a circular cylinder. Please see different vortex shedding for the same $Re = 53$ in the same wind tunnel with two different diameters circular cylinder experimented at different free stream speed in [89].

Suppose the physical problem depends on n variables $v_1, v_2, \ldots, v_n$. Each variable v_i has a dimension denoted by $[v_i]$ such that one writes

$$v_i = u\,[v_i]\,. \tag{2.1}$$

Here u expresses the size of the variable in the chosen system of units. For example if it is the length of a rope, we will write $l = 5[l]$. Defining the dimension of length as $[l] = L$, one has $l = 5L$. Referring to the International System of Units (SI) the dimension L is given in meters (m) and thus $l = 5[l] = 5\,\mathrm{m}$. Besides L, the dimensions M and T are introduced for mass and time, respectively.

The SI system is composed of the meter (m), kilogram (kg), second (s), ampere (A), kelvin (K), candela (cd) and mole (mol). These are the primary units. All other units are secondary and derived from the primary units. As an example of a secondary unit, the definition of the newton (N) reads "The newton is that force which gives to a mass of 1 kg an acceleration of 1 meter per second per second".

2.2 The Vaschy–Buckingham Theorem

From the viewpoint of dimensions, the force F in rational mechanics is defined by the product of the mass m and the acceleration $\ddot{x}$ and leads to the relation

$$[F] = MLT^{-2}\,, \tag{2.2}$$

where M, L, T are the fundamental dimensions of mass, length and time, respectively and $[F]$ is the dimension of F. We notice that in order to express the dimension of a variable, one writes a monomial of powers of the basic quantities. More generally, a physical problem will deal with a model that is the representation of intrinsic relationships between the various variables. We will have

$$f(v_1, v_2, \ldots, v_N) = 0\,, \tag{2.3}$$

or

$$v = g(v_1, v_2, \ldots, v_{N-1})\,. \tag{2.4}$$

As an example, let us consider the stationary flow of a viscous incompressible fluid in a Couette apparatus with the exterior cylinder of radius R_2 fixed and the interior cylinder of radius R_1 rotating with the angular velocity ω. The pressure p in every point of the flow with position $\boldsymbol{x}$ is a dependent variable that involves other quantities describing the problem. One writes

$$f(p, R_1, R_2, \omega, \rho, \mu, \boldsymbol{x}) = 0\,. \tag{2.5}$$

The aim of dimensional analysis is to collect several variables to elaborate a reduced or dimensionless variable. Here we have the group

$$\Pi = \frac{p}{\rho(\omega R_1)^2}\,. \tag{2.6}$$

In this case, the dynamic pressure $\rho(\omega R_1)^2$ is considered as a natural measuring scale for the pressure p. Using this information, one obtains by (2.5)

$$\Pi = \frac{p}{\rho(\omega R_1)^2} = \frac{1}{\rho(\omega R_1)^2}\, g(R_1, R_2, \omega, \rho, \mu, \boldsymbol{x})\,. \tag{2.7}$$

The relation (2.4) is independent of the chosen units' system as a result of the principle of dimensional invariance. This implies that the relation be homogeneous from the dimensional point of view. In other words, the dimension of each variable can be written as

$$[v_i] = P_1^{a_i} P_2^{b_i} P_3^{c_i} \dots\,, \tag{2.8}$$

with P_i denoting a fundamental (primary) quantity (M, L, T).

Let us introduce the concept of dimensional matrix. This matrix is composed by the list of the exponents $a_i, b_i, c_i, \dots$ of the fundamental quantities of each variable or parameter of the problem. It allows to control the linear independence of the variables in terms of the chosen primary quantities. For the Couette problem, the dimensional matrix is the following

	p	$\boldsymbol{x}$	R_1	R_2	μ	ρ	ω
M	1	0	0	0	1	1	0
L	−1	1	1	1	−1	−3	0
T	−2	0	0	0	−1	0	−1

Via the principle of dimensional homogeneity and since each dimension can be written as a monomial of powers, one can demonstrate the following theorem

Theorem 2.1 (Vaschy–Buckingham) *If a physical problem is described by N variables and parameters in r dimensions, i.e. in r independent variables, then it is possible to organise the original variables in dimensionless groups such that*

$$\Pi = v_1^{\alpha_1} v_2^{\alpha_2} \dots v_N^{\alpha_N}\,. \tag{2.9}$$

The function (2.3) may be written in a simpler manner because it does contain only $M = N - r$ variables

$$\Phi(\Pi_1, \Pi_2, \dots, \Pi_M) = 0\,, \tag{2.10}$$

with r the rank of the dimensional matrix.

We will not prove the theorem and for this purpose the reader is referred to Barenblatt [9] or to Panton [71]. In the field of isothermal fluid mechanics, we will suppose that $r = 3$, which corresponds to the choice $P_1 = M$, $P_2 = L$, $P_3 = T$.

2.3 Application of Vaschy–Buckingham Theorem

2.3.1 Circular Couette Flow

Let us choose three independent primary variables R_1, ρ, ω, whose minor of order three in the previous dimensional matrix is different from zero. Let us examine the pressure p and let us construct the first group that is denoted by Π_1. We have with $\alpha_1 = \alpha, \alpha_2 = \beta, \alpha_3 = \gamma$, etc.,

$$\Pi_1 = p R_1^{\alpha} \rho^{\beta} \omega^{\gamma} \ , \tag{2.11}$$

or

$$[\Pi_1] = M^0 L^0 T^0 = M L^{-1} T^{-2} L^{\alpha} (M L^{-3})^{\beta} (T^{-1})^{\gamma} \ . \tag{2.12}$$

Equating the exponents of the fundamental quantities M, L, T of the two sides of Eq. (2.12), one has

$$\begin{aligned} 1 + \beta &= 0 \\ -1 + \alpha - 3\beta &= 0 \\ -2 - \gamma &= 0 \end{aligned} \tag{2.13}$$

Solving system (2.13) one obtains $\alpha = -2, \beta = -1, \gamma = -2$ and the group Π_1 is such that $\Pi_1 = p/(\rho\, \omega^2 R_1^2)$. Afterwards we compute $\Pi_2 = \boldsymbol{x}/R_1$, $\Pi_3 = R_2/R_1$, $\Pi_4 = \mu/(\rho \omega R_1^2)$. Therefore

$$\Pi_1 = \frac{p}{\rho(\omega R_1)^2} = \frac{1}{\rho(\omega R_1)^2}\, h\left(\frac{\boldsymbol{x}}{R_1}, \frac{R_2}{R_1}, \frac{\mu}{\rho \omega R_1^2}\right) . \tag{2.14}$$

The group Π_4 is the inverse of the Reynolds number that in this case reads

$$(\Pi_4)^{-1} = Re = \frac{\omega R_1^2}{\nu} \ , \tag{2.15}$$

where one finds ωR_1 the characteristic velocity, R_1 the geometrical reference length, $\nu = \mu/\rho$.

Choosing now R_1, μ, ω as basic variables, one generates the Π groups: $\Pi_1 = \frac{p}{\mu\omega}$, $\Pi_2 = \frac{\boldsymbol{x}}{R_1}$, $\Pi_3 = \frac{R_2}{R_1}$, $\Pi_4 = \frac{\omega R_1^2}{\nu}$.

We observe that there is no unique way to set up a problem in reduced form, since the rank of the dimensional matrix allows selecting the basic variables very differently.

2.3.2 Flow in a Pump

We consider the flow of an incompressible fluid with density ρ and dynamic viscosity μ in a pump whose rotor rotates at constant angular velocity ω. The respective pressures at suction and discharge sections of the pump are denoted by p_1 and p_2. A choice must be made between several homothetic pumps. According to this homothety, it suffices to fix a characteristic dimension D of the pump, inasmuch that the other dimensions are proportional to it, including the diameters of the input and output sections where the pressure are measured as p_1 and p_2. It is obvious that the flow rate Q is a function of the quantities already introduced ρ, D, μ, ω as well as the pressure increase created by the pump. We have the relationship

$$Q = f(p_2 - p_1, \rho, \mu, D, \omega) \; . \tag{2.16}$$

It is asked to write a dimensionless relation for the cases when the fluid is perfect (without viscosity) and a real viscous fluid.

For the perfect fluid, the dimensional matrix is

	$p_2 - p_1$	Q	D	ρ	ω
M	1	0	0	1	0
L	−1	3	1	−3	0
T	−2	−1	0	0	−1

Choosing ρ, D, ω as basic variables, one obtains

$$\frac{Q}{D^3\omega} = f\left(\frac{p_2 - p_1}{\rho D^2\omega^2}\right) \; . \tag{2.17}$$

This is nothing else than the characteristic curve of the pump, Fig. 2.1.

For the Newtonian viscous fluid, one has

$$\frac{Q}{D^3\omega} = f\left(\frac{p_2 - p_1}{\rho D^2\omega^2}, Re\right) \; . \tag{2.18}$$

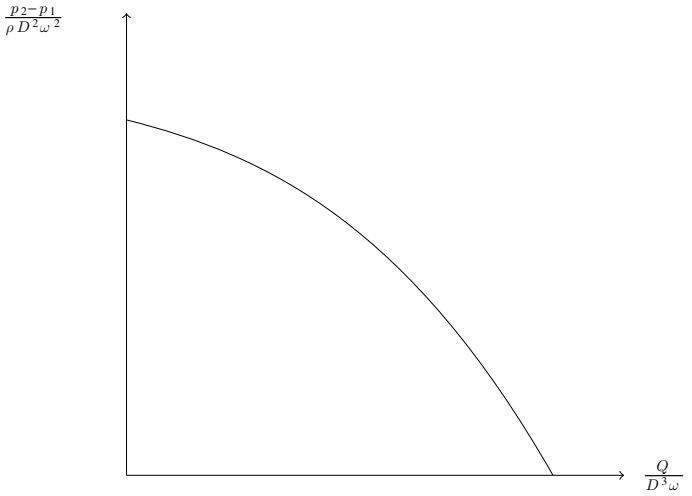

Fig. 2.1 Characteristic of a hydraulic pump

2.4 Dynamic Similarity

Two physical phenomena are said similar if the variables describing them can be matched. Let us suppose that the physical phenomenon of interest is described by the relation

$$\Pi_1 = f(\Pi_2, \ldots, \Pi_n) \, . \tag{2.19}$$

If two flows are such that the dimensionless groups $\Pi_2, \ldots, \Pi_n$ are given the same values, the dependent variables are also identical. If the first flow is the one of the reduced scale model and the second one of reality (the prototype), we have

$$(\Pi_i)_m = (\Pi_i)_p, \quad i = 1, \ldots, n \, . \tag{2.20}$$

This amounts to imposing the equality of the Reynolds numbers if we want to study the flow around an airfoil on a mock-up to draw operational conclusions for the real profile. However the geometrical similarity resting on the Π theorem is sometimes not feasible. Indeed the boundary conditions of an experimental set-up may also affect the similarity rules.

In certain cases, it is impossible to apply strictly the similarity laws because dimensional constants such as gravity step in. As an example, let us study the drag on a boat that is given by the force in direction x_1 of the main flow with velocity U_∞. Building up the dimensional matrix and generating the variables $F_{x_1}, \rho, \mu, U_\infty, g, d$, with d the boat length overall, one obtains

$$C_{x_1} = \frac{F_{x_1}}{\rho d^2 U_\infty^2} = C_{x_1}(Re, Fr) \ , \tag{2.21}$$

with the Froude number defined by the relationship

$$Fr = \left(\frac{U_\infty^2}{gd} \right) \ . \tag{2.22}$$

To fix the ideas, let us work with a ratio of scales between mock-up and prototype equal to 1/20. The similarity rules impose the equality of the Reynolds and Froude numbers. The equality of the Froude numbers leads to

$$\left(\frac{U_\infty^2}{gd} \right)_m = \left(\frac{U_\infty^2}{gd} \right)_p \tag{2.23}$$

or dropping the ∞ subscript

$$\left(\frac{U_m}{U_p} \right)^2 = \frac{d_m}{d_p} = S_d \ , \tag{2.24}$$

with S_d the ratio of the dimensions scales (S). We deduce the ratio of the velocity scales S_U

$$S_U = \frac{U_m}{U_p} = S_d^{1/2} \ . \tag{2.25}$$

The equality of the Reynolds numbers produces the relation

$$\left(\frac{Ud}{\nu} \right)_m = \left(\frac{Ud}{\nu} \right)_p \ , \tag{2.26}$$

and consequently

$$S_\nu = \frac{\nu_m}{\nu_p} = \frac{U_m}{U_p} \frac{d_m}{d_p} = S_U S_d = S_d^{3/2} \ . \tag{2.27}$$

As $S_d = 1/20$, one obtains

$$S_\nu = (\frac{1}{20})^{3/2} = 0.011 \ . \tag{2.28}$$

This last equation means that the model should use a fluid of kinematic viscosity a hundred times less than that of water. Such a fluid is impossible to find. In this case, we will have to use approximate methods in which we have different Reynolds numbers for the model and the prototype, with the hope that the change in Reynolds number will have little effect on the drag measured with the model.

2.5 Self-similarity

Consider the flow generated by the instantaneous motion of a wall in its own plane. As we will note in Sect. 3.3.1, the governing equation reads

$$\frac{\partial v_1}{\partial t} = \nu \frac{\partial^2 v_1}{\partial x_2^2} \, . \tag{2.29}$$

The boundary conditions are

$$t < 0, \quad v_1 = 0, \quad \forall x_1 \, , \tag{2.30}$$

$$t \geq 0, \quad v_1 = U, \text{ for } x_2 = 0, \tag{2.31}$$

$$v_1 = 0, \text{ for } x_2 \to \infty. \tag{2.32}$$

The dimensional matrix is as follows

	v_1	U	x_2	t	ν
M	0	0	0	0	0
L	1	1	1	0	2
T	−1	−1	0	1	−1

As the first line of the matrix is zero, its rank is equal to two. Let us choose as basic variables U and ν. One compute the next three dimensionless groups

$$\Pi_1 = \frac{v_1}{U}, \; \Pi_2 = \frac{x_2 U}{\nu} = \xi, \; \Pi_3 = \frac{t U^2}{\nu} = \zeta \, . \tag{2.33}$$

Therefore we write

$$\frac{v_1}{U} = f(\xi, \zeta) \, . \tag{2.34}$$

However, this relation is too general. We simplify it by noting that the Eqs. (2.29) and (2.31) are always satisfied if we apply a scaling factor α to x_2 and a factor α^2 to time t. As we desire to obtain self-similar solutions by enforcing the condition

$$v_1(t_1, \frac{x_2}{g(t_1)}) = v_1(t_2, \frac{x_2}{g(t_2)}) \, , \tag{2.35}$$

where the function g constitutes a scaling factor for the space, we replace the dimensionless group Π_2 by

$$\Pi_2^* = \frac{\Pi_2}{\sqrt{\Pi_3}} = \frac{x_2}{\sqrt{\nu t}} = \eta \, . \tag{2.36}$$

The relation (2.34) becomes

$$\frac{v_1}{U} = f^*(\eta, \zeta) \, . \tag{2.37}$$

Eq. (2.29) is now written

$$2\frac{\partial^2 f^*}{\partial \eta^2} + \eta \frac{\partial f^*}{\partial \eta} = 0 \,, \tag{2.38}$$

while the conditions (2.30)–(2.32) are

$$\frac{v_1}{U} = 0 \text{ for } \eta \to \infty \,, \tag{2.39}$$

$$\frac{v_1}{U} = 1 \text{ for } \eta = 0 \,. \tag{2.40}$$

Inspecting (2.38)–(2.40), one observes that the function f^* depends only on η and thus eventually

$$\frac{v_1}{U} = f^*(\eta) \,. \tag{2.41}$$

Thanks to (2.41), the partial derivatives problem is reduced to an ordinary differential equation. Relation (2.38) is a self-similar relation.

2.6 Dimensionless Form of the Navier–Stokes Equations

The dimensionless presentation of the Navier–Stokes equations for the incompressible fluid is essential for the understanding of the flow physics. Indeed, by this analysis, we may distinguish the dominating phenomenon and simplify the equations to be tackled that will be more amenable to closed-form solutions.

The dimensional matrix reads

	t	$\boldsymbol{x}$	$\boldsymbol{v}$	p	μ	ρ	L	U	$\boldsymbol{b}$
M	0	0	0	1	1	1	0	0	0
L	0	1	1	−1	−1	−3	1	1	1
T	1	0	−1	−2	−1	0	0	−1	−2

Choosing as basic variables L, ρ, U, with a minor equal to -1, we generate the dimensionless groups

$$\Pi_1 = \frac{tU}{L}, \quad \Pi_2 = \frac{\boldsymbol{x}}{L}, \quad \Pi_3 = \frac{\boldsymbol{v}}{U}, \quad \Pi_4 = \frac{p}{\rho U^2}, \quad \Pi_5 = \frac{\mu}{\rho U L}, \quad \Pi_6 = \frac{\boldsymbol{b}L}{U^2} \,. \tag{2.42}$$

These Π groups allow the introduction of dimensionless variables and functions (denoted with primes) by the relations:

$$x_i = L x_i' \,, \; t = \frac{L}{U} t' \,, \; v_i = U v_i' \,, \; p' = \frac{p - p_0}{\rho U^2} \,, b_i = U^2 \frac{b_i'}{L} \,.$$

We rewrite Eqs. (1.73) and (1.74) with dimensionless quantities

$$\frac{\partial v_i'}{\partial t'} + v_k' \frac{\partial v_i'}{\partial x_k'} = -\frac{\partial p'}{\partial x_i'} + \frac{\mu}{UL\rho} \frac{\partial^2 v_i'}{\partial {x_j'}^2} + b_i' \,, \tag{2.43}$$

$$\frac{\partial v_j'}{\partial x_j'} = 0 \,. \tag{2.44}$$

In Eq. (2.43) appears the dimensionless Reynolds number,

$$Re = \frac{\rho U L}{\mu} = \frac{UL}{\nu} \,.$$

The symbol ν represents the kinematic viscosity defined by the relation

$$\nu = \frac{\mu}{\rho} \,. \tag{2.45}$$

It is expressed in $\mathrm{m^2 s^{-1}}$. Its value for water at ambiant temperature is $\nu_{water} = 1.138\,10^{-6}\,\mathrm{m^2\,s^{-1}}$. The Reynolds number expresses the relative importance of the inertia forces with respect to the viscous forces. It takes values close to 0 for creeping flows dominated by viscous effects up to values of the order of $10^6 \ldots 10^8$ where inertia is the main driving force. In this last case, the flow is turbulent. An example of creeping flow is that of thermal convection in the earth's mantle or the convective currents in a bath of molten glass. The turbulent flows are widespread in nature or in technological applications: the water flow on a boat hull, the aerodynamics design of a car, meteorology, etc.

The Reynolds number can still be interpreted as the ratio of the characteristic time of viscous fluid flows. If we introduce the inertial time $t_{inert} = L/U$ and the viscous time $t_{vis} = L^2/\nu$, the Reynolds number becomes

$$Re = \frac{t_{vis}}{t_{inert}} \,. \tag{2.46}$$

We note that for high values of the Reynolds number, the time scale significant for the fluid inertia is much shorter than the time scale for the action of the viscous effects. This situation explains the stiff character of the numerical integration of the Navier–Stokes equations at high values of the Reynolds number, given the disparity of inertial and viscous time scales. Indeed the numerical integration will march in time with a time step imposed by the inertial dynamical behavior over time ranges long enough to take the viscous effects into account.

The Navier–Stokes equations in dimensionless form read:

$$\frac{D\boldsymbol{v}'}{Dt'} = -\boldsymbol{\nabla}\, p' + \frac{1}{Re}\Delta \boldsymbol{v}' + \boldsymbol{b}'. \tag{2.47}$$

$$\boldsymbol{\nabla}\cdot\boldsymbol{v}' = 0\ , \tag{2.48}$$

If we fix the coordinates x_i and time t and we let the Reynolds number go to infinity, $Re \to \infty$, the system (2.47)–(2.48) leads to the Euler equation for perfect fluids. Note that if $Re \to 0$, we face an inconsistency for (2.47).

When the body force is gravity, with $\boldsymbol{b}' = \boldsymbol{g}' = \boldsymbol{g}/g$ and $g = \| \boldsymbol{g} \|$ is the gravity acceleration, Eq. (2.47) becomes

$$\frac{D\boldsymbol{v}'}{Dt'} = -\boldsymbol{\nabla}\, p' + \frac{1}{Re}\Delta \boldsymbol{v}' + \frac{1}{Fr}\boldsymbol{g}'\ . \tag{2.49}$$

Here we have the Froude number (2.22)

$$Fr = \frac{U^2}{Lg}\ .$$

This number compares inertia forces to gravity forces.

The limit form of the Navier–Stokes equations is obtained by (2.49) when $Re \to \infty$,

$$\frac{D\boldsymbol{v}'}{Dt'} = -\boldsymbol{\nabla}\, p' + \frac{1}{Fr}\boldsymbol{g}'\ . \tag{2.50}$$

These are the Euler equations. If we come back to dimensional variables, we have

$$\rho\frac{D\boldsymbol{v}}{Dt} = -\boldsymbol{\nabla}\, p + \rho\boldsymbol{g}\ . \tag{2.51}$$

Let us consider again Eq. (1.74) and normalize the reduced form of time and pressure by the viscous effects (this is the viewpoint adopted by rheologists):

$$t' = \frac{\nu t}{L^2} \quad \text{and} \quad p' = \frac{(p - p_0)}{(\frac{\mu U}{L})}\ ,$$

the dimensionless form of the Navier–Stokes equations for an incompressible fluid reads

$$\frac{\partial v_i'}{\partial t'} + Re\left(v_k'\frac{\partial v_i'}{\partial x_k'}\right) = -\frac{\partial p'}{\partial x_i'} + \Delta v_i' + \frac{Re}{Fr}g_i'\ . \tag{2.52}$$

Equations (2.49) and (2.52) are different because the time normalization is made on the one hand by the time linked to advection (inertial term) t_{inert}, and on the other hand by the characteristic time of molecular diffusion t_{vis}.

If we now let $Re \to 0$, Eq. (2.52) is simplified and yields:

$$\frac{\partial \boldsymbol{v}'}{\partial t'} = -\nabla\, p' + \Delta \boldsymbol{v}'. \tag{2.53}$$

These are the linear Stokes equations. In dimensional variables, they read

$$\rho \frac{\partial \boldsymbol{v}}{\partial t} = -\nabla\, p + \mu\, \Delta \boldsymbol{v}. \tag{2.54}$$

2.7 Dimensional Analysis of the Compressible Navier–Stokes Equations

The set of the Navier–Stokes equations for the compressible fluid reads

$$\frac{D\rho}{Dt} + \rho \,\mathrm{div}\, \boldsymbol{v} = 0\,, \tag{2.55}$$

$$\rho \frac{D\boldsymbol{v}}{Dt} = -\nabla\, p + \nabla\,(\lambda\, tr \boldsymbol{d}) + \mathrm{div}\,(\boldsymbol{2}\mu\, \boldsymbol{d}) + \rho \boldsymbol{b}\ \ , \tag{2.56}$$

$$\rho c_p \frac{DT}{Dt} = \frac{Dp}{Dt} + \lambda(\mathrm{tr}\, \boldsymbol{d})^2 + 2\mu\, \boldsymbol{d} : \boldsymbol{d} + \mathrm{div}(\mathrm{k}\nabla \mathrm{T}) + \mathrm{r}\,, \tag{2.57}$$

$$p = \rho R T\ . \tag{2.58}$$

We will simplify these relations with the assumptions $r = 0$ and λ, μ, k constants. In addition, we use Stokes' hypothesis

$$3\lambda + 2\mu = 0\,. \tag{2.59}$$

The Stokes relation has been established based on reasoning from the kinetic theory of gases. Although this hypothesis is valid for monatomic gases, it is not valid for polyatomic gases. Nonetheless it is widely used in aerodynamics applications. From the monograph by Langlois and Deville [49] we quote "Neither the theoretical foundation nor the experimental verification of the Stokes relation is especially convincing. Also, Truesdell [109] remarked on p. 229 that "The Stokes relation implies the anomalous result that a spherical mass of fluid may perform symmetrical oscillations in perpetuity, without frictional loss". Stokes himself never took the relation very seriously, and it is now generally conceded to be invalid, except for monatomic gases, with the hard-to-obtain experimental data leniently interpreted."

Table 2.1 Dimensional matrix of the compressible Navier–Stokes variables

	t	$\boldsymbol{x}$	$\boldsymbol{v}$	p	μ	ρ	L	U	$\boldsymbol{b}$	c_p	k	T
M	0	0	0	1	1	1	0	0	0	0	1	0
L	0	1	1	−1	−1	−3	1	1	1	2	1	0
T	1	0	−1	−2	−1	0	0	−1	−2	−2	−3	0
Θ	0	0	0	0	0	0	0	0	0	−1	−1	1

Equations (2.56) and (2.57) become

$$\rho \frac{Dv_i}{Dt} = -\frac{\partial p}{\partial x_i} + \mu \frac{\partial^2 v_i}{\partial x_j \partial x_j} + \frac{\mu}{3} \frac{\partial}{\partial x_i}(d_{kk}) + \rho b_i \tag{2.60}$$

$$\rho c_p \frac{DT}{Dt} = \frac{Dp}{Dt} + k \frac{\partial^2 T}{\partial x_j \partial x_j} - \frac{2}{3} \mu (d_{kk})^2 + 2\mu \, d_{ij} \, d_{ij} \, . \tag{2.61}$$

The fundamental variables to build the dimensional matrix are as usual M, L, T plus the thermodynamic temperature Θ. Recall that the SI units for c_p and k are J kg^{-1} K^{-1} and W m^{-1} k^{-1} respectively, where J is kg m^2 s^{-2}. The dimensional matrix reads (Table 2.1).

Choosing as primary variables ρ, U, L, T, the associated minor is different from zero. The dimensional matrix has rank 4 and we are left with eight dimensionless groups

$$\Pi_1 = \frac{tU}{L}, \quad \Pi_2 = \frac{\boldsymbol{x}}{L}, \quad \Pi_3 = \frac{\boldsymbol{v}}{U}, \quad \Pi_4 = \frac{p}{\rho U^2} \tag{2.62}$$

$$\Pi_5 = \frac{\mu}{\rho U L}, \quad \Pi_6 = \frac{\boldsymbol{b} L}{U^2}, \quad \Pi_7 = \frac{c_p T}{U^2}, \quad \Pi_8 = \frac{kT}{\rho L U^3} \, . \tag{2.63}$$

In Π_5 we recognize the inverse of the Reynolds number and Π_6 is the inverse of the Froude number. The combination $\Pi_5 \Pi_7 / \Pi_8$ yields $Pr = \mu c_p / k$ which is the definition of the Prandtl number.

The careful aerodynamicist is still puzzled by the absence of the Mach number. In fact this number is hidden in Π_4. Using (1.98) we have

$$\frac{p}{\rho U^2} = \frac{RT}{U^2} = \frac{a^2}{\gamma U^2} = \frac{1}{\gamma M^2} \tag{2.64}$$

with the definition of the Mach number

$$M = \frac{U}{a} \, . \tag{2.65}$$

Let us now investigate the set of dimensionless Navier–Stokes equations for the ideal gas with constant heat capacity. Denote the reference values of length, speed, pressure, density, and temperature that characterize the flow under consideration by L, U, p_0, ρ_0, and T_0. The variables p_0, ρ_0, and T_0 designate a thermodynamic reference state. The time scale is L/U and the scale for inertial forces is U^2/L. Now we introduce non-dimensional variables and functions (denoted with primes) with relations

$$x_i = L x_i' \qquad t = \frac{L}{U}\, t' \qquad v_i = U v_i' \qquad p = p_0 p'$$
$$\rho = \rho_0 \rho' \qquad T = T_0 T' \qquad b_i = U^2 \frac{b_i'}{L}\,.$$

We reformulate Eqs. (2.55), (2.56), (2.60), and (2.61) with non-dimensional values, including constant characteristic values μ_0 and k_0 estimated at the temperature T_0, as well as c_p, γ, and R:

$$\frac{\partial \rho'}{\partial t'} + v_j' \frac{\partial \rho'}{\partial x_j'} + \rho' \frac{\partial v_j'}{\partial x_j'} = 0 \tag{2.66}$$

$$\frac{\partial v_i'}{\partial t'} + v_k' \frac{\partial v_i'}{\partial x_k'} = -\frac{p_0}{\rho_0 U^2}\, \frac{1}{\rho'}\, \frac{\partial p'}{\partial x_i'}$$
$$+ \frac{\mu_0}{U L \rho_0}\, \frac{1}{\rho'} \left(\frac{\partial^2 v_i'}{\partial {x_j'}^2} + \frac{1}{3}\, \frac{\partial}{\partial x_i'} (d_{kk}') \right) + b_i' \tag{2.67}$$

$$\rho' \frac{DT'}{Dt'} = \frac{Dp'}{Dt'} + \frac{k_0}{\mu_0 c_p}\, \frac{\mu_0}{\rho_0 U L}\, \frac{\partial^2 T'}{\partial {x_j'}^2}$$
$$- \frac{\mu_0}{\rho_0 U L}\, \frac{U^2}{c_p T_0} \left(\frac{2}{3}\, (d_{kk}')^2 - \frac{1}{2} \left(\frac{\partial v_i'}{\partial x_j'} + \frac{\partial v_j'}{\partial x_i'} \right)^2 \right) \tag{2.68}$$

$$p' = \rho'\, T'\,, \tag{2.69}$$

if we set $p_0 = \rho_0\, R\, T_0$.

In relations (2.66)–(2.68) three non-dimensional numbers appear:

- the ***Reynolds number***

$$Re = \rho_0 \frac{UL}{\mu_0} = \frac{UL}{\nu_0}\;;$$

- the ***Prandtl number***

$$Pr = \frac{c_p \mu_0}{k_0} = \frac{\nu_0}{\Lambda}\;;$$

- the ***Mach number***

$$M = \frac{U}{a_0}\,,$$

which appear also in the group

$$\frac{p_0}{\rho_0 U^2} = \frac{RT_0}{U^2} = \frac{a_0^2}{\gamma U^2} = \frac{1}{\gamma M^2} .$$

The denominator of the Mach number a_0 is the characteristic speed of sound (1.98). The coefficient Λ defined by relation

$$\Lambda = \frac{k_0}{\rho_0 c_p} \tag{2.70}$$

appearing in the Prandtl number is called the ***thermal diffusivity***. The product of the Reynolds and Prandtl numbers yields the Péclet number

$$Pe = \frac{UL}{\Lambda} , \tag{2.71}$$

which is for the heat transfer equation, the counterpart of the Reynolds number for the Navier–Stokes equation.

The Reynolds number expresses the relative importance of the inertial forces with respect to the viscous forces. It takes values from zero up to several million. For $Re = 0$, the Navier–Stokes equations reduce to the Stokes equation. They govern the dynamics of slow or creeping laminar flows. For $Re \geq 10^6$, the flow is turbulent. The Prandtl number estimates the relative importance of the viscous and thermal diffusion phenomena ($Pr = 0.71$ for room temperature air).

The Mach number characterizes the compressibility effects. Its value is $M = 0$ for incompressible fluids. It is between zero and one, $0 < M < 1$ for subsonic flows and $M > 1$ for supersonic flows.

The Navier–Stokes equations take the non-dimensional form

$$\frac{D\rho'}{Dt'} + \rho' \operatorname{div} \boldsymbol{v}' = \mathbf{0} \tag{2.72}$$

$$\rho' \frac{D\boldsymbol{v}'}{Dt'} = -\frac{1}{\gamma M^2} \nabla p' + \frac{1}{Re} \left(\nabla^2 \boldsymbol{v}' + \frac{1}{3} \nabla \left(\operatorname{div} \boldsymbol{v}' \right) \right) + \rho' \boldsymbol{b}' \tag{2.73}$$

$$\rho' \frac{DT'}{Dt'} = \frac{Dp'}{Dt'} + \frac{1}{Pr\, Re} \nabla^2 T' - (\gamma - 1) \frac{M^2}{Re} \left(\frac{2}{3} \left(\operatorname{div} \boldsymbol{v}' \right)^2 - \frac{\mathbf{1}}{\mathbf{2}} \left(\frac{\partial \mathbf{v}_\mathbf{i}'}{\partial \mathbf{x}_\mathbf{j}} + \frac{\partial \mathbf{v}_\mathbf{j}'}{\partial \mathbf{x}_\mathbf{i}} \right)^\mathbf{2} \right) \tag{2.74}$$

$$p' = \rho' T' . \tag{2.75}$$

If we fix the coordinates x_i, time t, and all the parameters M, Pr, γ, and take $Re \to \infty$, then the system (2.72)–(2.75) leads to the Euler system of equations for perfect (inviscid) fluids. Taking the limit where the Mach number goes to zero, with

all the other parameters fixed, should lead to the Navier–Stokes equations for an incompressible fluid.

However, examination of the system (2.72)–(2.75) shows that this is not so, and that the term $-(1/\gamma M^2)\nabla p$ becomes dominant. This behavior is due to the choice of the non-dimensional pressure $p' = p/p_0$, which was made by considering pressure to be a thermodynamic variable. The momentum equation reveals that pressure is also a dynamic variable. It is more natural to choose

$$p^* = \frac{p - p_0}{\rho_0 U^2}$$

for the non-dimensional pressure.

In this case, Eq. (2.73) becomes

$$\rho' \frac{D\boldsymbol{v}'}{Dt'} = -\nabla p^* + \frac{1}{Re}\left(\nabla^2 \boldsymbol{v}' + \frac{1}{3}\nabla\big(\mathrm{div}\boldsymbol{v}'\big)\right) + \rho' \boldsymbol{b}' \,. \tag{2.76}$$

The limiting case of Eqs. (2.66), (2.76), (2.68), and (2.69) when the Mach number goes to zero, yields the relations

$$\frac{D\rho'}{Dt'} + \rho' \mathrm{div}\boldsymbol{v}' = \boldsymbol{0} \tag{2.77}$$

$$\rho' \frac{D\boldsymbol{v}'}{Dt'} = -\nabla p^* + \frac{1}{Re}\left(\nabla^2 \boldsymbol{v}' + \frac{1}{3}\nabla(\mathrm{div}\boldsymbol{v}')\right) + \rho' \boldsymbol{b}' \tag{2.78}$$

$$\rho' \frac{DT'}{Dt'} = \frac{1}{Pr\, Re}\nabla^2 T' \tag{2.79}$$

$$\rho' T' = 1 \,, \tag{2.80}$$

valid for an ***incompressible fluid***, but which still may experience thermal expansion.

To obtain (2.79), we calculate

$$\frac{Dp'}{Dt'} = \frac{1}{p_0}\frac{Dp}{Dt'} = \frac{\rho_0 U^2}{p_0}\frac{Dp^*}{Dt'} = \frac{U^2}{RT_0}\frac{Dp^*}{Dt'} = \gamma M^2 \frac{Dp^*}{Dt'} \,.$$

Equation (2.80) comes from the following evaluation:

$$p' = \rho' T' = \frac{p}{p_0} = 1 + p^* \frac{U^2}{RT_0} = 1 + \gamma M^2 p^* \,.$$

If, in addition, we assume that at the domain wall $T' = 1$, then Eqs. (2.79) and (2.80) as well as the boundary conditions on T' are satisfied by

$$\rho' = 1 \tag{2.81}$$

$$T' = 1 \,. \tag{2.82}$$

Consequently, in this case, Eqs. (2.77) and (2.78) reduce to the equations of an isothermal, incompressible flow.

In this section we may notice the different nature of pressure for compressible versus incompressible fluids. In the compressible case pressure is a thermodynamic variable that is computed through the equation of state as soon as we know ρ from mass conservation and T from energy governing equation. For the incompressible fluid there is no equation of state and the pressure scalar field is the variable that ensures a divergence free velocity field. In finite element theory for incompressible flows, pressure is the Lagrange variable associated with the constraint div $\boldsymbol{v} = 0$ in the weak formulation of the Navier–Stokes equation. A possible way to compute the pressure consists in generating a Poisson pressure equation by taking the divergence of the momentum equation. The difficulty is then to set up the correct boundary condition for the normal component of the pressure gradient at the wall. The reader is referred to the paper by Orszag et al. [69] that proposes several methods to solve this difficulty. A possible solution of the pressure Poisson equation can be obtained with Neumann boundary condition from wall-normal component of Navier–Stokes equation along with no-slip boundary condition. This is routinely done in aerodynamics to calculate lift and drag.

Exercises

2.1 Write the dimensionless Navier–Stokes equations in the framework of the Boussinesq approximation. To obtain a tractable heat equation we neglect in (1.112) the power dissipation and the volume heat production.

We defined the coefficient of thermal diffusivity expressed in $\mathrm{m}^2\,\mathrm{s}^{-1}$ by the relation (2.70). It is possible to obtain three different sets of dimensionless equations according to the choice of the reference velocity: $U = \nu/L$; $U = \Lambda/L$; $U = (g\alpha(T - T_0)L)^{1/2}$. This produces the following dimensionless numbers : Prandtl, Rayleigh, Péclet, Grashof, denoted Pr, Ra, Pe, Gr, respectively, such that

$$Pr = \frac{\nu}{\Lambda},\ Ra = \frac{\alpha g(T - T_0)L^3}{\nu\Lambda},\ Pe = \frac{UL}{\Lambda},\ Gr = \frac{\alpha g(T - T_0)L^3}{\nu^2}\ . \tag{2.83}$$

2.2 Write the velocity profile of Exercise 1.4 in dimensionless form. Which dimensionless number is involved in the solution?

Chapter 3
Exact Solutions of the Navier–Stokes Equations

In this chapter, we solve a few simple problems of fluid mechanics in order to illustrate the fundamental concepts related to the flow of viscous incompressible fluids. All solutions presented in this chapter are exact solutions of the full Navier Stokes equations. The review article by Ratip Berker [14] constitutes an inexhaustible source of these solutions that cover a wide spectrum of incompressible flows. Another compilation of exact solutions is provided in the book by Drazin and Riley [28].

We first consider steady state plane flows: Couette, Poiseuille and the free surface flow over an inclined plane. Further we treat steady state flows in cylindrical geometry: Couette, Poiseuille and their combination in the helical flow between two circular cylinders in relative rotation. Finally we solve unsteady plane and axisymmetric problems, plane periodic flows and various pipe flows.

3.1 Plane Stationary Flows

Here, we examine some exact solutions of the Navier–Stokes equations for plane stationary flows.

3.1.1 Plane Couette Flow

We consider the two-dimensional stationary flow of an incompressible viscous fluid between parallel plates.

Figure 3.1 shows the flow domain. The lower boundary is fixed while the upper boundary moves in its own plane at a given constant velocity U in the x_1 direction.

M. O. Deville, *An Introduction to the Mechanics of Incompressible Fluids*,
https://doi.org/10.1007/978-3-031-04683-4_3

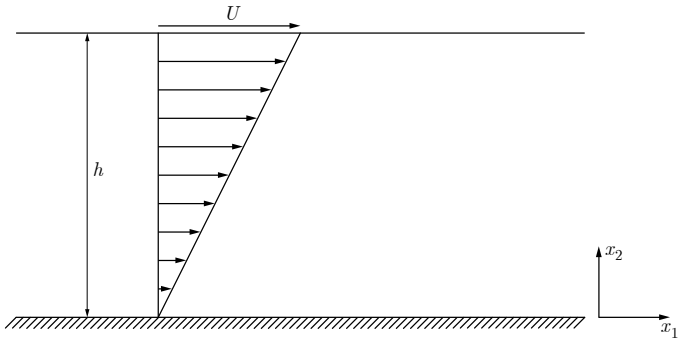

Fig. 3.1 Plane Couette flow

Since the flow is two-dimensional, the vector $\boldsymbol{v}$ reduces to two components, $\boldsymbol{v} = (v_1, v_2, 0)$. We assume that the flow is developed, that is, the transient effects and those from the upstream edges of the plates are negligible. This is a very strong assumption and the subsequent solution is only due to this simplification. In reality a uniform flow impinging on the plates will generate boundary layers where the viscous effects are dominant and after some distance, the layers will merge into the fully viscous solution.

With the previous hypotheses, we can have v_1 as a function only of x_2. The incompressibility condition (1.73) becomes

$$\frac{\partial v_2}{\partial x_2} = 0 \tag{3.1}$$

indicating that v_2 is not a function of x_2; it is thus a function of x_1. However, since at the two boundaries v_2 is zero for all x_1, we conclude that $v_2 = 0$ everywhere. We write the two-dimensional Navier–Stokes equation (1.74) for the velocity component v_1 as

$$\rho\left(\frac{\partial v_1}{\partial t} + v_1\frac{\partial v_1}{\partial x_1} + v_2\frac{\partial v_1}{\partial x_2}\right) = -\frac{\partial p}{\partial x_1} + \mu\triangle v_1 + \rho b_1. \tag{3.2}$$

As the gravitational force is oriented along the negative direction of the axis x_2, $b_1 = 0$. In addition, the problem is stationary, thus $\partial v_1/\partial t = 0$. The term $v_1\partial v_1/\partial x_1$ is zero as $v_1 = v_1(x_2)$. Finally $v_2\partial v_1/\partial x_2$ is also zero since $v_2 = 0$. We can assume that the horizontal component of the pressure gradient is zero as the flow is forced kinematically by the motion of the upper plate. We are left with

$$\mu\frac{d^2 v_1}{dx_2^2} = 0\,. \tag{3.3}$$

Integrating (3.3) once, we obtain

$$\mu \frac{dv_1}{dx_2} = C \ . \tag{3.4}$$

This relation shows that the shear stress is constant across the height of the channel. Integrating again leads to

$$v_1 = Ax_2 + B. \tag{3.5}$$

The adherence boundary conditions

$$v_1(x_2 = 0) = 0, \ v_1(x_2 = h) = U \tag{3.6}$$

permit us to determine the integration constants; we obtain a linear velocity profile

$$v_1 = \frac{Ux_2}{h}. \tag{3.7}$$

The shear stress component (1.67) obtained with (3.7) is a constant

$$\sigma_{12} = \mu \frac{dv_1}{dx_2} = \mu \frac{U}{h} \ . \tag{3.8}$$

If we examine the second Navier–Stokes equation, in direction x_2, we have

$$0 = -\frac{\partial p}{\partial x_2} - \rho g, \tag{3.9}$$

with g the gravitational acceleration. Integrating this relation and taking into account the independence of p with respect to x_1, leads to

$$p = -\rho g x_2 + C. \tag{3.10}$$

As the pressure in an incompressible fluid is only known to an arbitrary constant, we choose it by imposing $p(x_2 = h) = 0$ which yields $C = \rho g h$. The pressure is in hydrostatic equilibrium

$$p = \rho g(h - x_2) \ . \tag{3.11}$$

3.1.2 Plane Poiseuille Flow

Consider the two-dimensional stationary flow of a viscous incompressible fluid in a channel formed by two fixed walls. Figure 3.2 shows the geometric configuration of the domain. In this case, a longitudinal pressure gradient, along direction x_1, is established. We assume that the flow is developed and that the fluid particles move on paths parallel to the walls. Reasoning as for Couette flow, we can write $v_1 = v_1(x_2), \ v_2 = 0$.

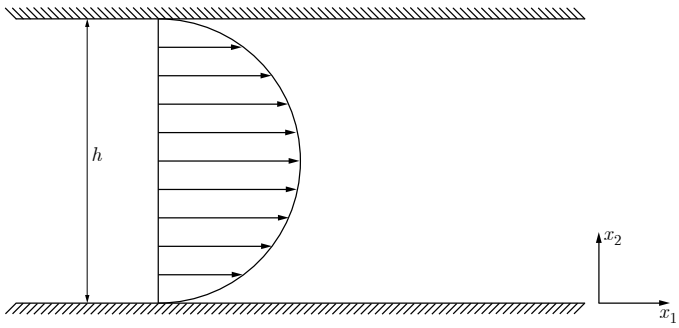

Fig. 3.2 Plane Poiseuille flow

The dynamic equation for velocity v_1 is relation (1.74), which for Poiseuille flow reduces to

$$0 = -\frac{\partial p}{\partial x_1} + \mu \frac{\partial^2 v_1}{\partial x_2^2} \,. \tag{3.12}$$

As for Couette flow, the pressure in the vertical direction is in hydrostatic equilibrium

$$0 = -\frac{\partial p}{\partial x_2} - \rho g \,. \tag{3.13}$$

Integrating this relation, we obtain

$$p = -\rho g x_2 + P(x_1) \,. \tag{3.14}$$

The integration factor, $P(x_1)$, is the pressure on the lower wall, for $x_2 = 0$. The pressure gradient in direction x_1 can be written as

$$\frac{\partial p}{\partial x_1} = \frac{dP}{dx_1} \,, \tag{3.15}$$

as it is a function only of x_1. Equation (3.12) yields

$$\frac{d^2 v_1}{dx_2^2} = \frac{1}{\mu} \frac{dP}{dx_1} = C. \tag{3.16}$$

We note that the first term is a function of x_2 while the second is a function of x_1. It follows that these two terms must be equal to the same constant C. The integration of (3.16) gives us

$$v_1 = \frac{1}{\mu} \frac{dP}{dx_1} \frac{x_2^2}{2} + A x_2 + B. \tag{3.17}$$

Imposing the boundary conditions

$$v_1(x_2 = 0) = v_1(x_2 = h) = 0, \tag{3.18}$$

yields the parabolic Poiseuille velocity profile

$$v_1 = -\frac{h^2}{2\mu}\frac{dP}{dx_1}\frac{x_2}{h}(1 - \frac{x_2}{h}). \tag{3.19}$$

As the pressure in the channel diminishes linearly with distance x_1, $dP/dx_1 < 0$, and the flow is in the positive x_1 direction.

The shear stress component obtained from (3.19) is

$$\sigma_{12} = \mu\frac{dv_1}{dx_2} = -\frac{h}{2}\frac{dP}{dx_1}(1 - \frac{2x_2}{h}) \,. \tag{3.20}$$

We note that the shear (3.20) is zero on the symmetry axis of the channel, $x_2 = h/2$, and the absolute value is at a maximum on both walls.

We can calculate the volume flux or flow rate through the section S of the channel. The general definition of the volume flux is given by the relation

$$Q = \int_S \boldsymbol{v} \cdot \boldsymbol{n}\, dS \,. \tag{3.21}$$

Considering a unit surface in direction x_3, the flow rate in the two-dimensional channel is written

$$Q = \int_0^h v_1\, dx_2 = -\frac{h^3}{12\mu}\frac{dP}{dx_1} = \frac{h^3}{12\mu}\frac{\triangle p}{L}, \tag{3.22}$$

with $\triangle P$ the pressure difference observed at two points with the same ordinate, x_2, separated by a distance L in direction x_1. We define the average velocity by $Q = v_{avg}\, h$, from which we have

$$v_{avg} = \frac{h^2}{12\mu}\frac{\triangle P}{L}. \tag{3.23}$$

As the maximum velocity, v_{max}, is attained on the axis of symmetry of the channel, at $x_2/h = 1/2$, it follows that

$$v_{max} = \frac{h^2}{8\mu}\frac{\triangle P}{L} \tag{3.24}$$

and, consequently

$$v_{avg} = \frac{2}{3}v_{max}. \tag{3.25}$$

In the case where the two-dimensional channel is replaced by a pipe with circular section (see Sect. 3.2.2), we obtain the average velocity equal to half the maximum velocity. This shows that the zone of high velocity constitutes a smaller fraction of the section.

Another way of solving the plane Poiseuille flow consists in moving the origin of the coordinate axes to mid-channel height and locate the two channel planes at $x_2 = \pm h$. The governing equation is still (3.12) with the solution given by (3.17). Now the boundary conditions are

$$v_1(x_2 = \pm h) = 0 \,. \tag{3.26}$$

It is left as an exercise to the reader to perform the algebra. Setting $-dP/dx_1 = G$, one gets the parabolic profile

$$v_1 = \frac{G}{2\mu}\left(h^2 - x_2^2\right) = \frac{Gh^2}{2\mu}\left(1 - \frac{x_2^2}{h^2}\right) \,, \tag{3.27}$$

which will be useful in the pipe flow section.

3.1.3 *Flow of an Incompressible Fluid on an Inclined Plane*

We have a stationary, two-dimensional flow of a viscous Newtonian fluid on a plane inclined at angle α to the vertical (Fig. 3.3). The thickness of the fluid layer is uniform and equal to h. At the free surface, the fluid is in contact with ambient air which we consider to be a perfect fluid at atmospheric pressure p_a. We assume that the flow in the air does not affect the flow of the viscous fluid. The flow is parallel because the trajectories of the fluid particles are parallel to the inclined plane. Then, $\boldsymbol{v} = (v_1, 0, 0)$. From incompressibility we obtain

$$\frac{\partial v_1}{\partial x_1} = 0, \tag{3.28}$$

therefore we deduce that $v_1 = v_1(x_2)$. The only components of the stress tensor are σ_{12} or σ_{21}. As the pressure is uniform at the free surface, the pressure in the viscous fluid can not depend on direction x_1, but only on x_2.

From the motion equation (1.58), written in direction x_1, it follows that

$$\frac{\partial \sigma_{12}}{\partial x_2} + \rho b_1 = \frac{\partial \sigma_{12}}{\partial x_2} + \rho g \cos\alpha = 0 \,. \tag{3.29}$$

Integrating this relation, we have

$$\sigma_{12} = -\rho g \, x_2 \cos\alpha + C \,. \tag{3.30}$$

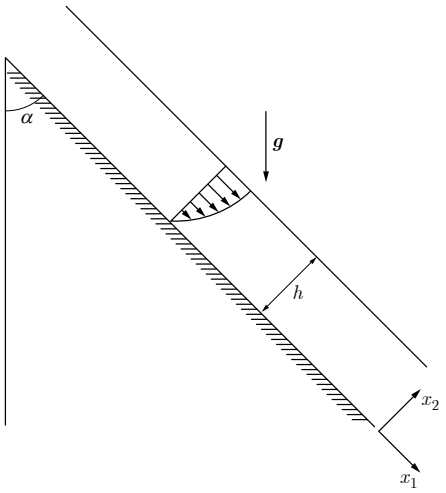

Fig. 3.3 Flow on an inclined plane

At the free surface, $x_2 = h$, the shear stress should be zero. We obtain

$$\sigma_{12} = \rho g \cos\alpha (h - x_2) \; . \tag{3.31}$$

As $\sigma_{12} = \mu \, dv_1/dx_2$, we can evaluate the component v_1 by integrating with respect to x_2, taking into account the boundary condition $v_1(x_2 = 0) = 0$. The velocity profile is given by the relation

$$v_1 = \frac{\rho g \cos\alpha}{2\mu} x_2 (2h - x_2) \; . \tag{3.32}$$

The Navier–Stokes equation for direction x_2 yields the relation

$$-\frac{\partial p}{\partial x_2} + \rho b_2 = -\frac{\partial p}{\partial x_2} - \rho g \sin\alpha = 0 \; . \tag{3.33}$$

Integrating with respect to x_2 and taking into account the condition on the free surface $p(x_2 = h) = p_a$, we can write

$$p = p_a - (\rho \, g \sin\alpha)(x_2 - h) \; . \tag{3.34}$$

The flow rate per unit length in direction x_3 is obtained from

$$Q = \int_0^h v_1 \, dx_2 = \frac{\rho g \cos\alpha \, h^3}{2\mu} . \tag{3.35}$$

3.2 Axisymmetric Stationary Flows

In this section, we consider exact solutions of the Navier–Stokes equations for stationary flows in axisymmetric geometries of revolution. We integrate the Navier–Stokes equations expressed in a cylindrical coordinate system. The vector velocity has components v_r, v_θ, and v_z which we call the radial, azimuthal, and axial velocities, respectively.

3.2.1 Circular Couette Flow

Consider the stationary flow of an incompressible viscous Newtonian fluid between two concentric cylinders supposed to be of infinite axial length. We denote by R_1 and R_2 the radii of the internal and external cylinders, respectively, and ω_1 and ω_2 their respective rates of angular rotation, as shown in Fig. 3.4. We want to calculate the azimuthal velocity v_θ. This flow is known by the name of circular Couette flow. We neglect the effects of the volume forces. The flow has no axial velocity since there is no pressure gradient in that direction. In addition, due to the symmetry of revolution, it also does not depend on the azimuthal coordinate, thus $\partial(\bullet)/\partial\theta = 0$. The two velocity components v_r and v_θ, stationary, thus independent of time, are functions uniquely of the radial coordinate, r, so $v_r = v_r(r)$ and $v_\theta = v_\theta(r)$. Applying adherence to the wall, the boundary conditions are

$$v_r(R_1) = v_r(R_2) = 0, \quad v_\theta(R_1) = \omega_1 R_1, \; v_\theta(R_2) = \omega_2 R_2 \; . \tag{3.36}$$

With these assumptions about the velocity profile, the continuity Eq. (A.20) becomes

$$\frac{1}{r}\frac{d}{dr}(r\, v_r) = 0 \; . \tag{3.37}$$

Taking into account the condition (3.36) that v_r is zero at the boundaries, the solution is

$$v_r = 0 \; . \tag{3.38}$$

In this case the Navier–Stokes equations (A.21)–(A.22) reduce to

$$\frac{\partial p}{\partial r} = \rho \, \frac{v_\theta^2}{r} \; , \tag{3.39}$$

$$\frac{1}{r}\frac{\partial}{\partial r}\left(r \frac{\partial v_\theta}{\partial r}\right) - \frac{v_\theta}{r^2} = 0 \; . \tag{3.40}$$

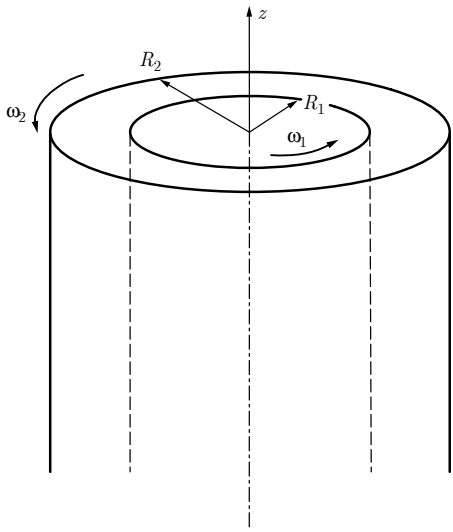

Fig. 3.4 Circular Couette flow

The solution for the component v_θ is in the form

$$v_\theta = \sum_{n=-\infty}^{n=+\infty} a_n r^n \, .$$

Plugging this series into (3.40), we easily find that $n = \pm 1$. Imposing the boundary conditions leads to

$$v_\theta = Ar + \frac{B}{r} = \frac{\omega_2 R_2^2 - \omega_1 R_1^2}{R_2^2 - R_1^2} r - \frac{(\omega_2 - \omega_1) R_1^2 R_2^2}{R_2^2 - R_1^2} \frac{1}{r} \tag{3.41}$$

after solving for the constants A and B. The first term on the right-hand side corresponds to rotation of all the fluid around the central axis. If $\omega_1 = \omega_2 = \omega$, the velocity becomes $v_\theta = \omega r$, which shows that the fluid rotates as a rigid body around the axis. The second term on the right-hand side corresponds to a deformation of the particles over time. If $R_2 \to \infty$ and $\omega_2 = 0$, then we have the case of a cylinder in an infinite fluid. The velocity $v_\theta = \omega_1 R_1^2 / r$ gives circular streamlines around the cylinder, and the velocity distribution is irrotational, that is, $\mathbf{curl}\ \boldsymbol{v} = \mathbf{0}$.

The pressure in the Couette flow is computed from Eq. (3.39). After integration, we obtain

$$\frac{p(r)}{\rho} = \frac{p(R_1)}{\rho} + \frac{(R_2^2\omega_2 - R_1^2\omega_1)^2}{(R_2^2 - R_1^2)^2} \frac{r^2 - R_1^2}{2} - \frac{R_1^4 R_2^4 (\omega_2 - \omega_1)^2}{2(R_2^2 - R_1^2)^2} \left(\frac{1}{r^2} - \frac{1}{R_1^2} \right)$$
$$+ \frac{2(R_2^2\omega_2 - R_1^2\omega_1) R_1^2 R_2^2 (\omega_1 - \omega_2)}{(R_2^2 - R_1^2)^2} \ln \left(\frac{r}{R_1} \right) \, . \tag{3.42}$$

A tangential shear stress $\sigma_{\theta r}$ acts on a surface element with a radial normal, which is expressed by (A.5)

$$\sigma_{\theta r} = \mu \left(\frac{\partial v_\theta}{\partial r} - \frac{v_\theta}{r} + \frac{1}{r} \frac{\partial v_r}{\partial \theta} \right) = \mu \left(\frac{\partial v_\theta}{\partial r} - \frac{v_\theta}{r} \right) = \mu \, r \frac{\partial}{\partial r} \left(\frac{v_\theta}{r} \right) . \tag{3.43}$$

Combining (3.41) and (3.43), we obtain

$$\sigma_{\theta r} = -\frac{2B\mu}{r^2} . \tag{3.44}$$

Next we calculate the viscous moment, M, that acts on the interior cylinder per unit axial length. This moment is equal to the component $\sigma_{\theta r}$ evaluated at $r = R_1$ and the area, $2\pi R_1$, on which this stress acts, multiplied by the lever arm, R_1, the distance between the axis and the point where the force acts. We have

$$M = -2\pi R_1^2 \frac{2B\mu}{R_1^2} = 4\pi\mu \frac{(\omega_2 - \omega_1) R_1^2 R_2^2}{R_2^2 - R_1^2} . \tag{3.45}$$

This last relation indicates that we can measure the viscosity μ of a fluid in a Couette viscometer where the drive motor imposes a torque on one of the cylinders and we measure the resulting rotation speed of the other one.

3.2.2 *Circular Poiseuille Flow in a Cylindrical Pipe*

Poiseuille flow in a circular pipe with radius R is subject to the action of an imposed pressure gradient in direction z (Fig. 3.5). The flow is stationary. From the Navier–Stokes equations in cylindrical coordinates, we show first that the only non-zero component of the velocity is v_z.

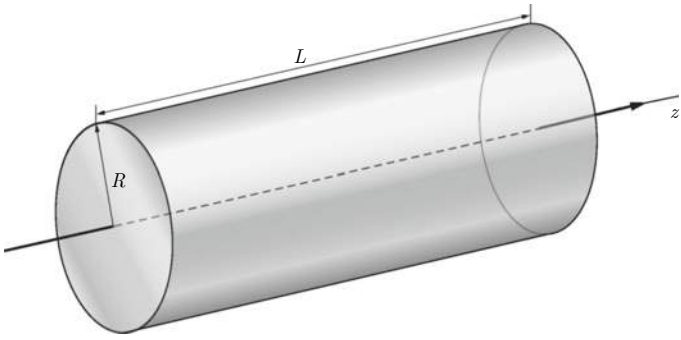

Fig. 3.5 Circular Poiseuille flow in a cylindrical pipe

Given the hypotheses of axial symmetry and stationary flow, $v_\theta = 0$ and the only two components of velocity, v_r and v_z, are functions only of r. The continuity Eq. (A.20) is then

$$\frac{1}{r}\frac{\partial}{\partial r}(r\, v_r) = 0\ . \tag{3.46}$$

Integration yields

$$r v_r = f(z)\ .$$

But, since $v_r = 0$ at the wall, $r = R$, we conclude that $f(z) = 0$ and thus that v_r is zero everywhere in the flow. The Navier–Stokes equation for the radial component of velocity (A.21) reduces to $\partial p/\partial r = 0$. The pressure depends only on z and not on r. The equation for the velocity component v_z (A.23) yields

$$-\frac{dp}{dz} + \mu\left(\frac{\partial^2 v_z}{\partial r^2} + \frac{1}{r}\frac{\partial v_z}{\partial r}\right) = 0$$

or

$$\frac{dp}{dz} = \frac{\mu}{r}\frac{d}{dr}\left(r\,\frac{dv_z}{dr}\right)\ .$$

The left-hand side term only depends on z; on the right-hand side there is only dependence on r. Thus the two terms must be equal to a constant. Integrating, we obtain

$$v_z = \left(\frac{dp}{dz}\right)\frac{1}{\mu}\left(\frac{r^2}{4} + A\ln r + B\right)\ .$$

The velocity must be finite on the axis $r = 0$. This leads to $A \equiv 0$. Taking into account the condition $v_z(R) = 0$, we have

$$v_z = -\left(\frac{dp}{dz}\right)\frac{R^2}{4\mu}\left(1 - \left(\frac{r}{R}\right)^2\right) = \frac{GR^2}{4\mu}\left(1 - \frac{r^2}{R^2}\right)\ , \tag{3.47}$$

with the definition $dp/dz = -G$. In Poiseuille flow, the velocity profile is parabolic. The maximum velocity at the center is

$$v_{max} = -\left(\frac{dp}{dz}\right)\frac{R^2}{4\mu}\ . \tag{3.48}$$

Therefore the parabolic profile may be written

$$v_z = v_{max}\left(1 - \frac{r^2}{R^2}\right) . \tag{3.49}$$

The flow rate is obtained by integration over the section of the pipe. We have

$$Q = 2\pi \int_0^R v_z(r)\, r\, dr = -\left(\frac{dp}{dz}\right)\frac{\pi R^4}{8\mu} = \frac{\pi R^2 v_{max}}{2} . \tag{3.50}$$

The average, or flux, velocity obtained from the flux divided by the area of the section S is

$$v_{avg} = \frac{Q}{S} = \frac{v_{max}}{2} . \tag{3.51}$$

The maximum velocity is thus equal to twice the average velocity. The shear stress at the cylinder wall, which we denote τ_w, is given by the component σ_{zr} evaluated at $r = R$

$$\tau_w = -\mu \frac{dv_z}{dr} \mid_{r=R} = -\left(\frac{dp}{dz}\right)\frac{R}{2} = \frac{2\mu v_{max}}{R} = \frac{4\mu v_{avg}}{R} . \tag{3.52}$$

The sign change between τ_w and σ_{zr} comes from the fact that τ_w represents the shear force exercised on the wall by the fluid. The friction coefficient is defined by the ratio of the stress at the wall to the average dynamic pressure

$$C_f = \frac{\tau_w}{\frac{\rho v_{avg}^2}{2}} = \frac{8\mu}{\rho R v_{avg}} = \frac{8\nu}{R v_{avg}} = \frac{16}{Re_D} , \tag{3.53}$$

with Re_D being the Reynolds number based on the average velocity and the diameter of the section. It is common to define the head loss coefficient λ by the relation

$$-\left(\frac{dp}{dz}\right) = \frac{\rho v_{avg}^2}{2}\frac{\lambda}{D} . \tag{3.54}$$

Thus it follows that

$$\lambda = 4C_f = \frac{64}{Re_D} . \tag{3.55}$$

3.2.3 *Helical Flow Between Two Circular Cylinders in Relative Motion*

From the geometry point of view, this flow occurs in a configuration similar to the circular Couette flow in Fig. 3.4, with the same notation R_1 and R_2 for the radii and ω_1, ω_2 for the angular rates of rotation. Furthermore the viscous fluid between the cylinders is subjected to an axial pressure gradient. As the flow is steady-state,

$\partial/\partial t = 0$, and axisymmetric, $\partial/\partial\theta = 0$, the velocity profile is a function of r only. One has

$$v_r = v_r(r),\ v_\theta = v_\theta(r),\ v_z = v_z(r),\ p = p(r,z)\ . \tag{3.56}$$

With the fluid adherence to the wall, the boundary conditions are

$$\begin{aligned} &v_r(R_1) = v_r(R_2) = 0, \qquad v_\theta(R_1) = \omega_1 R_1,\ v_\theta(R_2) = \omega_2 R_2, \\ &v_z(R_1) = v_z(R_2) = 0\ . \end{aligned} \tag{3.57}$$

Similarly to the Couette flow solution, it is easy to show that the v_r component is zero everywhere. The Navier–Stokes equations (A.21)–(A.23) become

$$\frac{1}{\rho}\frac{\partial p}{\partial r} = \frac{v_\theta^2}{r}\ , \tag{3.58}$$

$$\frac{1}{r}\frac{\partial}{\partial r}\left(r\frac{\partial v_\theta}{\partial r}\right) - \frac{v_\theta^2}{r} = 0\ , \tag{3.59}$$

$$-\frac{\partial p}{\partial z} + \mu\left(\frac{\partial^2 v_z}{\partial r^2} + \frac{1}{r}\frac{\partial v_z}{\partial r}\right) = 0. \tag{3.60}$$

The Couette solution (3.41) remains valid. Equation (3.58) yields

$$p = \rho\int_{R_1}^{r}\frac{v_\theta^2}{r'}dr' + f(z)\ , \tag{3.61}$$

where v_θ is the Couette profile and $f(z)$ is an indeterminate function of z. Introducing (3.61) in (3.60), one gets

$$-\frac{df}{dz} + \mu\frac{1}{r}\frac{d}{dr}\left(r\frac{dv_z}{dr}\right) = 0\ . \tag{3.62}$$

The solutions are obtained taking the boundary conditions (3.57) into account

$$f(z) = -Az + B\ , \tag{3.63}$$

$$v_z(r) = \frac{A}{4\mu}\left[-r^2 + \frac{R_2^2 - R_1^2}{\ln(R_2/R_1)}\ln r + \frac{R_1^2\ln R_2 - R_2^2\ln R_1}{\ln(R_2/R_1)}\right]\ . \tag{3.64}$$

The pressure field is given by

$$p(r,z) = \rho\int_{R_1}^{r}\frac{v_\theta^2}{r'}dr' - Az + B. \tag{3.65}$$

The pressure is known up to a constant B, which will give the reference pressure; the pressure gradient $-A$ acts in the direction of the axis and finally, the first term

of the right hand side member of (3.65) equilibrates the centrifugal forces of the rotating fluid. Note that the axial velocity is independent of the rotation speed of the cylinders, while the azimuthal velocity v_θ is independent of the pressure gradient.

3.3 Plane Transient Flows

Let us now turn our attention to plane flows that depend on time. This situation leads to partial differential equations with independent variables of space and time. In order to arrive at an analytic solution of the problem, we use a change of variables to obtain an ordinary differential equation that is easier to solve.

3.3.1 Transient Flow in a Semi-infinite Space

An incompressible Newtonian viscous fluid occupies a half space ($x_2 \geq 0$), and is at rest for $t < 0$ (Fig. 3.6). At time $t = 0$, the rigid plane which limits the half space is instantaneously set into motion at the constant velocity U in the positive direction of axis x_1. The motion is two-dimensional such that $v_3 = 0$.

The boundary and initial conditions are given by

$$t < 0, \quad v_1 = v_2 = 0, \quad \forall x_1, x_2 \tag{3.66}$$

$$t \geq 0, \quad v_1 = U, v_2 = 0, \text{ for } x_2 = 0, \tag{3.67}$$

$$v_1 = v_2 = 0, \text{ for } x_2 \to \infty. \tag{3.68}$$

We assume that v_1 and v_2 are functions of x_2 and t

$$v_1 = v_1(x_2, t), \; v_2 = v_2(x_2, t) \; , \tag{3.69}$$

and that the pressure p is a function only of x_2 (there is no horizontal pressure gradient; the flow is generated entirely by the motion of the moving wall). The conservation of mass becomes

$$\frac{\partial v_2(x_2, t)}{\partial x_2} = 0 \; . \tag{3.70}$$

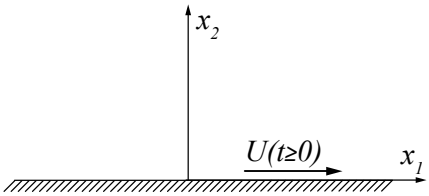

Fig. 3.6 Unsteady flow in an infinite half space

The component v_2 only depends on time, and with conditions (3.67) and (3.68), it is identically zero for all t. The Navier–Stokes equations become

$$\rho \frac{\partial v_1}{\partial t} = \mu \frac{\partial^2 v_1}{\partial x_2^2} , \tag{3.71}$$

$$\frac{\partial p}{\partial x_2} = 0 . \tag{3.72}$$

The pressure p is constant.

We can, if we wish, include the effect of gravity in the pressure calculation, by writing

$$\frac{\partial p}{\partial x_2} = -\rho g x_2 . \tag{3.73}$$

Integration of this relation leads to the calculation of the hydrostatic pressure, where the pressure at a point is equal to the weight of the column of fluid located above that position. The hydrostatic pressure, as its name suggests, does not participate in the dynamics of the flow.

The motion equation (3.71) is a diffusion equation, of the same type as the "heat equation". We can transform this partial differential equation into an ordinary differential equation with a variable change that we obtain from dimensional analysis (cf. Sect. 2.5). Since the problem has no spatial scale other than the variable x_2 nor time scale other than that of t itself, we combine them to form the non-dimensional group (compare with Eq. (2.36))

$$\eta = \frac{x_2}{2\sqrt{\nu t}} . \tag{3.74}$$

This permits us to obtain an ordinary differential equation for which the solution is a function of η. It is called a self-similar solution because the velocity profile with respect to the variable x_2 is similar for all times t.

Setting

$$v_1 = U\, f(\eta) , \tag{3.75}$$

relation (3.71) becomes

$$f'' + 2\eta f' = 0 , \tag{3.76}$$

with conditions

$$\eta = 0,\ f = 1; \quad \eta \to \infty,\ f = 0 . \tag{3.77}$$

Integrating (3.76), we obtain

$$f = A \int_0^\eta e^{-\eta'^2} d\eta' + B . \tag{3.78}$$

Taking into account conditions (3.77), we have for $\eta = 0$, $B = 1$ and for $\eta = \infty$, $A = -2/\sqrt{\pi}$ where we introduced the error function erf(x) defined by Abramowitz and Stegun [1]

$$\text{erf}\,(x) = \frac{2}{\sqrt{\pi}} \int_0^x e^{-\tau^2} d\tau \,, \tag{3.79}$$

such that erf$(\infty) = 1$. Then

$$f = 1 - \text{erf}\,\eta \,, \tag{3.80}$$

and from (3.75) the velocity of the fluid for $t > 0$ is

$$v_1 = U[1 - \text{erf}(\frac{x_2}{2\sqrt{\nu t}})] \,. \tag{3.81}$$

The velocity profile v_1/U as a function of η is shown in Fig. 3.7. For a fixed value of t, the variable η is proportional to x_2. Then, we can deduce the velocity profile at every instant as a function of the distance from the wall. An interesting question is to know the depth of penetration of the wall motion into the semi-infinite space. More precisely, for a given t, what is the distance at which the velocity attains, for example, one per cent of the value of U? Examining the function erf, $1 - \text{erf}$ has the value 0.01 for $\eta \sim 2$. Defined as such, the penetration depth δ is given by

$$\eta_\delta = \frac{\delta}{2\sqrt{\nu t}} \simeq 2, \quad \delta \simeq 4\sqrt{\nu t} \,, \tag{3.82}$$

which is proportional to the square root of the kinematic viscosity and time. If the viscosity is very small, the fluid "sticks" less to the wall and it has a weak effect. If t tends to infinity, the velocity at every point in the half space goes to U.

3.3.2 *Flow on an Oscillating Plane*

Consider the flow produced by the periodic horizontal oscillation of a plate in its own plane (Fig. 3.8).

Equation (3.71) still applies, and we must solve it with the boundary conditions

$$v_1 = U \cos \omega t \quad \text{for} \quad x_2 = 0 \,. \tag{3.83}$$

After the initial transient phenomena, the fluid velocity gradually becomes a periodic function of time at the same frequency as the plate oscillation. Here we examine this periodic regime. Assume that solution v_1 is of the form

$$v_1 = \Re \left(e^{i\omega t} f(x_2) \right) \,, \tag{3.84}$$

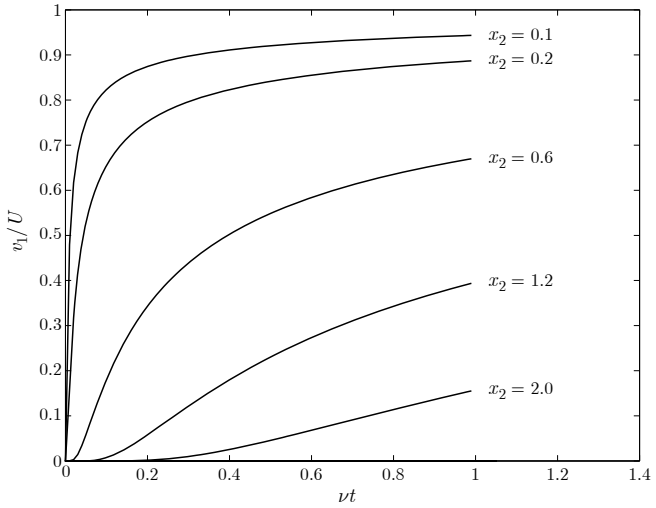

Fig. 3.7 Transient flow in an infinite half space

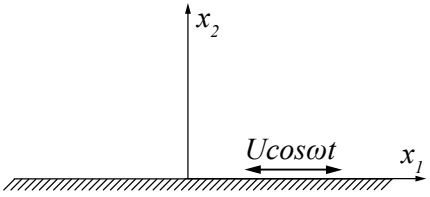

Fig. 3.8 Unsteady flow on an oscillating plane

where $\Re$ means the real part of a complex expression. The combination of (3.71) and (3.84) yields

$$i\omega f = \nu \frac{d^2 f}{dx_2^2} \, .$$

Recall that $i^{1/2} = e^{i\pi/4}$; then the only solution that remains finite as $x_2 \to \infty$ is

$$f = A \exp\left(-(1+i)(\omega/2\nu)^{1/2} x_2\right) \, .$$

The imposition of the boundary condition (3.83) leads to $A = U$ and the solution becomes

$$v_1 = U \exp\left(-(\omega/2\nu)^{1/2} x_2\right) \cos\left(\omega t - (\omega/2\nu)^{1/2} x_2\right) \, . \tag{3.85}$$

The velocity profile is a damped harmonic oscillation of amplitude $U e^{-x_2\sqrt{\omega/2\nu}}$ in a fluid where a layer at distance x_2 has a phase lag of $x_2\sqrt{\omega/2\nu}$ with respect to the motion at the wall. Two layers of fluid separated by the distance $2\pi(2\nu/\omega)^{1/2}$

oscillate in phase. This distance constitutes an estimation of the length of the motion and is called the viscous wave penetration depth. That it increases with viscosity and decreases with frequency is not surprising: if we slowly oscillate a flat plate in a sticky fluid, we expect to drag large masses of fluid along with the plate; on the other hand, if we move the plate rapidly in a fluid of low viscosity, we expect the fluid essentially to ignore the plate, except in a thin boundary layer.

3.3.3 Channel Flow with a Pulsatile Pressure Gradient

Blood flow in the vascular tree is driven by the pulsating pressure gradient produced by the heart that is acting as a pump. In order to avoid (temporarily) the geometrical complexity of cylindrical coordinates of blood flow in the arteries, we will tackle a simplified version of the problem, namely the plane channel flow under an oscillating pressure gradient.

Recall that the standard plane Poiseuille flow as shown in Fig. 3.2 with a steady constant pressure gradient denoted by G gives rise to a parabolic velocity profile. Let us add now an oscillating component characterized by the pulsation ω such that

$$-\frac{1}{\rho}\frac{\partial p}{\partial x_1} = -G - C\cos\omega t \ , \tag{3.86}$$

with C a constant obtained from experimental data, for example. For the sake of simplicity in the analytical treatment, it is customary to resort to Fourier representation and use the relation

$$-\frac{1}{\rho}\frac{\partial p}{\partial x_1} = -G - \Re(Ce^{i\omega t}) \ . \tag{3.87}$$

As the steady state oscillating solution is sought for the velocity field, the solution is written as a complex function

$$v_1 = v_P + \Re\left(u(\omega, x_2)e^{i\omega t}\right) \ . \tag{3.88}$$

where the Poiseuille solution v_P given by Eq. (3.27) corresponds to the constant pressure gradient.

The Navier–Stokes equations lead to the relation

$$\frac{\partial v_1}{\partial t} = -\frac{1}{\rho}\frac{\partial p}{\partial x_1} + \nu\frac{\partial^2 v_1}{\partial x_2^2} \ . \tag{3.89}$$

With Eqs. (3.87) and (3.88), Eq. (3.89) gives

$$i\omega u = -C + \nu\frac{\partial^2 u}{\partial x_2^2} \ . \tag{3.90}$$

The boundary conditions are

$$u(h) = 0, \quad \frac{\partial u}{\partial x_2}(0) = 0 \,. \tag{3.91}$$

The solution of (3.90) is

$$u = \Re\left[\frac{iC}{\omega}\left(1 - \frac{\cosh\sqrt{\frac{i\omega}{\nu}}x_2}{\cosh\sqrt{\frac{i\omega}{\nu}}h}\right)\right] . \tag{3.92}$$

Taking the relation $i^{1/2} = (1+i)/\sqrt{2}$ into account, the real part of (3.92) yields the velocity field

$$v_1 = v_P - \frac{C}{\omega}\left[\left(1 - \frac{f_1(\omega, x_2)}{f_3(kh)}\right)\sin\omega t - \frac{f_2(\omega, x_2)}{f_3(kh)}\cos\omega t\right] , \tag{3.93}$$

where the various notations are defined as follows

$$\begin{aligned} k &= \sqrt{\frac{\omega}{2\nu}} \,, \\ cc(x) &= \cos(x)\cosh(x) \,, \\ ss(x) &= \sin(x)\sinh(x) \,, \\ f_1(\omega, x_2) &= cc(kx_2)cc(kh) + ss(kx_2)ss(kh) \,, \\ f_2(\omega, x_2) &= cc(kx_2)ss(kh) - ss(kx_2)cc(kh) \,, \\ f_3(\omega) &= cc^2(x) + ss^2(x) \,. \end{aligned} \tag{3.94}$$

With $\omega = 1$, in Fig. 3.9, the left part represents the flow for a low frequency case or when the viscous forces are important, i.e. $hk \ll 1$, whereas the right part corresponds to high frequency forcing or to a fluid with very low viscosity. The low frequency solution may be obtained by taking the limit of Eq. (3.93) when $k \to 0$. In that limit, $cc(x) \to 1$, $ss(x) \to x^2$ and therefore, one has

$$v_1 = v_P + \frac{Ch^2}{2\nu}\cos\omega t\left(1 - (\frac{x_2}{h})^2\right) , \tag{3.95}$$

such that the pulsating term is still a parabola with a modified amplitude. The high frequency case or the equivalent inviscid fluid may be treated with the limit $hk \gg 1$. Then $cc(x) \to \frac{1}{2}e^x\cos x$ and $ss(x) \to \frac{1}{2}e^x\sin x$. The limit solution reads

$$v_1 = v_P - \frac{C}{\omega}\left(\sin\omega t - \sin(\omega t - \eta)e^{-\eta}\right) , \tag{3.96}$$

where the new variable η is defined as

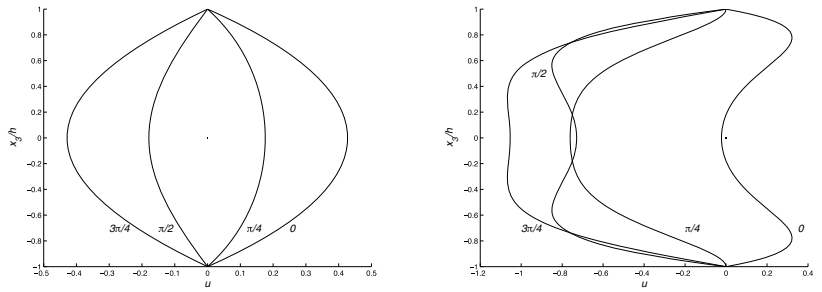

Fig. 3.9 Pulsating velocity field with $\omega = 1$; *left*: $k = 1/\sqrt{2}$; *right*: $k = 5/\sqrt{2}$

$$\eta = k(h - x_2) = \frac{h - x_2}{\sqrt{2\nu/\omega}} \,. \tag{3.97}$$

Note that the first term of the oscillating part is the response of the inviscid fluid ($\nu = 0$) to the pressure gradient.

3.4 Axisymmetric Transient Flows

This section treats time dependent flows. The first case is the starting process from rest in a circular Poiseuille flow when the pressure gradient is applied at the initial time. The second example is the pulsating flow in a circular rigid pipe which is somehow connected to blood flow simulation.

3.4.1 Starting Transient Poiseuille Flow

We examine the transient flow in a circular pipe where the fluid starts from rest to reach the Poiseuille steady parabolic profile (3.47). The only non vanishing velocity component is v_z and the pressure gradient goes instantaneously at $t = 0$ from zero to the value $-G$ everywhere. The dynamic equation is from (A.23)

$$G + \mu \left(\frac{\partial^2 v_z}{\partial r^2} + \frac{1}{r} \frac{\partial v_z}{\partial r} \right) = \rho \frac{\partial v_z}{\partial t} \,, \tag{3.98}$$

with the initial condition

$$v_z(r, 0) = 0, \quad 0 \le r \le R \,, \tag{3.99}$$

and the boundary condition

$$v_z(R,t) = 0, \forall t \ . \tag{3.100}$$

In order to render (3.98) homogeneous, let us change variables

$$w(r,t) = \frac{G}{4\mu}\left(R^2 - r^2\right) - v_z(r,t) \ . \tag{3.101}$$

The new variable will be solution of the equation

$$\frac{\partial^2 w}{\partial r^2} + \frac{1}{r}\frac{\partial w}{\partial r} = \frac{1}{\nu}\frac{\partial w}{\partial t} \ , \tag{3.102}$$

with the initial condition

$$w(r,0) = \frac{G}{4\mu}\left(R^2 - r^2\right), \tag{3.103}$$

and the boundary condition

$$w(R,t) = 0, \quad \forall t \ . \tag{3.104}$$

Through the transient phase, the velocity v_z will increase till the steady state (3.47) is reached, whereas the transient perturbation $w(r,t)$ will decay to zero. To solve (3.102), we proceed by separation of variables

$$w(r,t) = f(r)g(t) \ . \tag{3.105}$$

Substituting in (3.102), one gets

$$\frac{dg(t)}{dt} + C\nu\, g(t) = 0 \ , \tag{3.106}$$

$$\frac{d^2 f}{dr^2} + \frac{1}{r}\frac{df}{dr} + C\, f = 0 \ , \tag{3.107}$$

where C is an arbitrary constant. The solution of (3.106) reads

$$g(t) = B\exp(-C\nu t) \ . \tag{3.108}$$

As $w(r,t)$ decreases with respect to time, we assume that C will involve only positive values so that C can be written λ^2/R^2. This notation will ease the next computations, as we will observe. Equation (3.107) then becomes

$$\frac{d^2 f}{dr^2} + \frac{1}{r}\frac{df}{dr} + \frac{\lambda^2}{R^2}\, f = 0 \ . \tag{3.109}$$

The change of variable $\lambda r/R = z$ leads (3.109) to the canonical form of the Bessel equation (C.1) whose general solution is given by Eq. (C.2) with the Bessel functions J_k and Y_k. Consequently, the solution of (3.109) is

$$f = C_1 J_0(\frac{\lambda r}{R}) + C_2 Y_0(\frac{\lambda r}{R}) \,. \tag{3.110}$$

As Y_0 goes to $-\infty$ when $r \to 0$, one concludes that $C_2 \equiv 0$ for w to remain finite on the axis. The general solution of (3.102) becomes

$$w(r,t) = C_3 J_0(\frac{\lambda r}{R}) \exp(-\frac{\lambda^2}{R^2}\nu t) \,. \tag{3.111}$$

The solution (3.111) verifies condition (3.104) for λ values, denoted λ_n, given by the zeroes of the Bessel function J_0

$$J_0(\lambda_n) = 0 \,. \tag{3.112}$$

The solution is obtained as

$$w(r,t) = \frac{G}{4\mu} \sum_{n=1}^{\infty} c_n \, J_0(\frac{\lambda_n r}{R}) \exp(-\frac{\lambda_n^2}{R^2}\nu t), \tag{3.113}$$

and the coefficients c_n are determined by (3.103):

$$R^2 - r^2 = \sum_{n=1}^{\infty} c_n \, J_0(\frac{\lambda_n r}{R}) \,. \tag{3.114}$$

To solve Eq. (3.114), let us recall the orthogonality properties of Bessel functions as expressed by Lommel integrals

$$\int_0^1 z \, J_n(\lambda_i z) J_n(\lambda_j z) dz = 0, \quad \lambda_i \neq \lambda_j \,, \tag{3.115}$$

$$\int_0^1 z \, J_n^2(\lambda_i z) dz = \frac{1}{2}[J_n'(\lambda_i)]^2 \,. \tag{3.116}$$

Solution of (3.114) is obtained with $z = r/R$ as

$$c_n = \frac{2R^2}{[J_0'(\lambda_n)]^2} \int_0^1 (1 - z^2) z \, J_0(\lambda_n z) dz \,. \tag{3.117}$$

The evaluation of the two integrals in (3.117) is carried out using successively the recurrence relationships (C.4) and then (C.3) with $\ell = 2, m = 0$. This yields

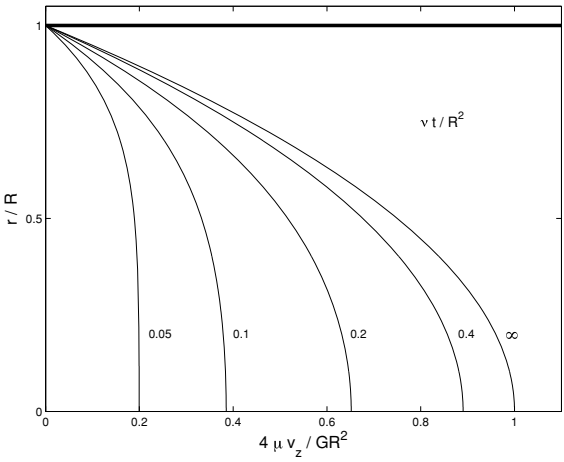

Fig. 3.10 Transient Poiseuille flow in a circular pipe

$$\int_0^1 z\, J_0(\lambda_n z) dz = \frac{1}{\lambda_n} J_1(\lambda_n)\ , \tag{3.118}$$

$$\begin{aligned}\int_0^1 z^3\, J_0(\lambda_n z) dz &= \frac{1}{\lambda_n^4}\left[\lambda_n^3 J_1(\lambda_n) + 2\lambda_n^2 J_0(\lambda_n) - 4\lambda_n J_1(\lambda_n)\right]\ , \\ &= \frac{1}{\lambda_n} J_1(\lambda_n) - \frac{4}{\lambda_n^3} J_1(\lambda_n)\ .\end{aligned} \tag{3.119}$$

One finds with the help of the relation $[J_0'(\lambda_n)]^2 = [J_1(\lambda_n)]^2$: (cf. (C.5) for $m = 0$)

$$c_n = \frac{8R^2}{\lambda_n^3 J_1(\lambda_n)}\ . \tag{3.120}$$

Taking Eqs. (3.101), (3.113) and (3.120) into account, the velocity profile is

$$v_z(r,t) = \frac{G}{4\mu}\left(R^2 - r^2\right) - \frac{2GR^2}{\mu}\sum_{n=1}^{\infty} \frac{J_0(\frac{\lambda_n r}{R})}{\lambda_n^3 J_1(\lambda_n)} \exp(-\frac{\lambda_n^2}{R^2}\nu t)\ . \tag{3.121}$$

Figure 3.10 shows the velocity variation with respect to time.

3.4.2 Pulsating Flow in a Circular Pipe

Let us consider the Poiseuille flow in a circular pipe subject to the action of an oscillating pressure gradient. This problem has been analyzed by Uchida [112] and Womersley [122] and constitutes a modeling of the blood flow in a rigid artery, an assumption far from physiological phenomena as arterial walls deform and move

under pressure waves [6, 127]. As the cardiac cycle is time-periodic, the pressure gradient can be represented by a Fourier series (a dozen of modes are sufficient)

$$\frac{\partial p}{\partial z} = \sum_{k=0}^{\infty} c_k e^{ik\omega t} \,. \tag{3.122}$$

The continuous component c_0 corresponds to the time average of the pressure gradient and produces the Poiseuille profile (3.47). In (3.122), ω is the signal frequency such that $\omega = 2\pi/T$, with T the period of the phenomenon. The pressure gradient corresponds to the real part of the complex representation. The flow governing equation is obtained from (A.23)

$$-\frac{\partial p}{\partial z} + \mu\left(\frac{\partial^2 v_z}{\partial r^2} + \frac{1}{r}\frac{\partial v_z}{\partial r}\right) = \rho\frac{\partial v_z}{\partial t} \,, \tag{3.123}$$

and the solution is sought in terms of the Fourier series

$$v_z(r,t) = \sum_{k=0}^{\infty} \hat{w}_k(r)\, e^{ik\omega t} \,. \tag{3.124}$$

Inserting (3.124) in (3.123), one gets

$$\frac{d^2\hat{w}_k}{dr^2} + \frac{1}{r}\frac{d\hat{w}_k}{dr} - \frac{i\omega k}{\nu}\hat{w}_k = \frac{c_k}{\mu} \,. \tag{3.125}$$

The boundary conditions are

$$\frac{d\hat{w}_k}{dr}\,|_{r=0} = 0, \quad \hat{w}_k\,|_{r=R} = 0 \,. \tag{3.126}$$

The particular solution of (3.125) is quickly found as $-\frac{i\omega k}{\nu}\hat{w}_k = \frac{c_k}{\mu}$.

Introducing the dimensionless variable $z = r/R$, the homogeneous equation becomes

$$\frac{d^2\hat{w}_k}{dz^2} + \frac{1}{z}\frac{d\hat{w}_k}{dz} - \frac{iR^2\omega k}{\nu}\hat{w}_k = 0 \,, \tag{3.127}$$

whose solution is given by

$$\hat{w}_{kh} = C_1 J_0(\alpha\sqrt{k}z\, i^{3/2}) + C_2 Y_0(\alpha\sqrt{k}z\, i^{3/2}) \,, \tag{3.128}$$

where the quantity α is the dimensionless Womersley number

$$\alpha = R\sqrt{\frac{\omega}{\nu}} \,. \tag{3.129}$$

The Womersley number is the ratio of the radius to the penetration depth and is a characteristic feature of pulsatile blood flow. Typical values of α in the aorta range from 20 for a human in good health to 8 for a cat. Another way of interpreting the Womersley number consists in estimating the distance from the rigid wall, say δ, where the viscous forces and the inertia are of equal magnitude. Near the wall, viscosity is dominant and a rough estimate of the viscous forces is $\mu U/\delta^2$. Near the symmetry axis, inertia dominates and yields the estimate $\rho\omega U$. Equating the two forces leads to the definition

$$\delta^2 = \frac{\nu}{\omega} \,. \tag{3.130}$$

Therefore

$$\alpha = \frac{R}{\delta} \,. \tag{3.131}$$

If α is large, the viscous effects are confined to a region very close to the wall. In the centre of the flow, the dynamics will be driven by the equilibrium of inertia and pressure forces, resulting in a velocity profile that will be more blunt than the parabolic profile that comes from the balance of viscous and pressure forces.

The functions J_0 and K_0 with the complex argument are Kelvin functions of order zero [1]. As the boundary conditions impose a finite velocity on the axis, it follows that $C_2 \equiv 0$ because Y_0 and $Y_0' \to \infty$ when $r \to 0$. The velocity profile is

$$\begin{aligned} v_z(r,t) = &-\frac{c_0}{4\mu} R^2 \left(1 - (\frac{r}{R})^2\right) \\ &+ \frac{R^2}{\mu} \sum_{k=1}^{\infty} \Re \left(\frac{i c_k}{\alpha_k^2} \left[1 - \frac{J_0(\alpha_k \frac{r}{R} i^{3/2})}{J_0(\alpha_k i^{3/2})} \right] e^{ik\omega t} \right) \,. \end{aligned} \tag{3.132}$$

In this last relation, we have set $\alpha_k = \alpha\sqrt{k}$. The complex function $J_0(z\, i^{3/2})$ with z real ≥ 0 is decomposed in a real part $Ber(z)$ (real Bessel) and an imaginary part $Bei(z)$ (imaginary Bessel) such that

$$J_0(z\, i^{3/2}) = Ber(z) + i\ Bei(z) \,, \tag{3.133}$$

and the final velocity profile reads

$$\begin{aligned} v_z(r,t) = &-\frac{c_0}{4\mu} R^2 \left(1 - (\frac{r}{R})^2\right) \\ &+ \frac{R^2}{\mu} \sum_{k=1}^{\infty} \Re \left(\frac{i c_k}{\alpha_k^2} \left[1 - \frac{Ber(\alpha_k \frac{r}{R}) + i\, Bei(\alpha_k \frac{r}{R})}{Ber(\alpha_k) + i\, Bei(\alpha_k)} \right] e^{ik\omega t} \right) \,. \end{aligned} \tag{3.134}$$

The velocity profile for mode $k = 1$ is shown in Fig. 3.11 for Womersley numbers between 3.34 and 6.67.

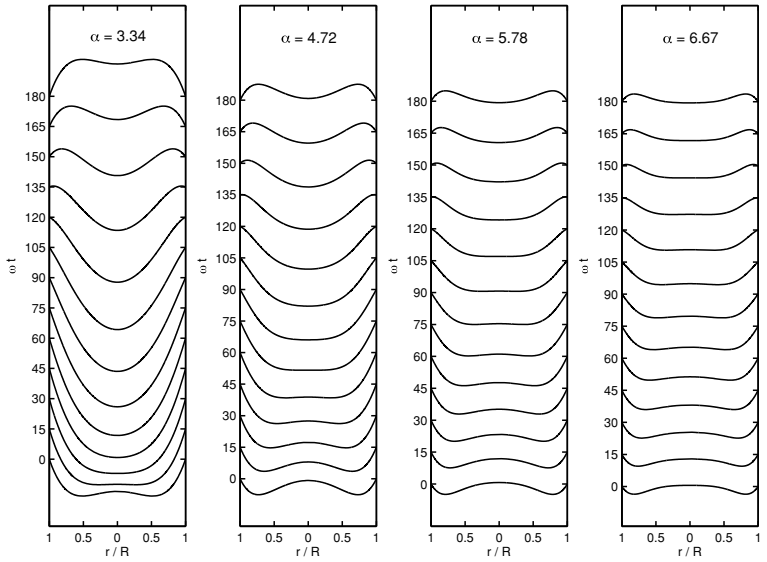

Fig. 3.11 Pulsatile velocity profile for various values of the Womersley number

The flow rate across the pipe section is given by

$$Q = 2\pi \int_0^R v_z(r,t)\, r\, dr$$
$$= -\frac{c_0}{8\mu}\pi R^4 + \frac{\pi R^4}{\mu} \sum_{n=1}^{\infty} \Re\left(\frac{i c_k}{\alpha_k^2} F(\alpha_k) e^{ik\omega t}\right) , \tag{3.135}$$
$$F(\alpha_k) = 1 - 2J_1(\alpha_k\, i^{3/2}) / \left[\alpha_k\, i^{3/2} J_0(\alpha_k\, i^{3/2})\right] . \tag{3.136}$$

The cases of slow and rapid pulsation are interesting limit cases.

3.4.2.1 Slow Pulsation

In this case, α is supposed to be small. The Taylor series of (3.133) (cf. [1]) is

$$J_0(z\, i^{3/2}) = 1 - \frac{(z/2)^4}{(2!)^2} + \frac{(z/2)^8}{(4!)^2} - \frac{(z/2)^{12}}{(6!)^2} \cdots$$
$$+ i \left(\frac{(z/2)^2}{(1!)^2} - \frac{(z/2)^6}{(3!)^2} - \frac{(z/2)^{10}}{(5!)^2} - \cdots\right) . \tag{3.137}$$

Taking the dominant terms into account, one obtains successively

$$\frac{J_0(\alpha_k \frac{r}{R} i^{3/2})}{J_0(\alpha_k i^{3/2})} = \frac{1 + i\frac{(\alpha_k \frac{r}{R})^2}{4} - \frac{(\alpha_k \frac{r}{R})^4}{64} + \cdots}{1 + i\frac{\alpha_k^2}{4} - \frac{\alpha_k^4}{64}} . \tag{3.138}$$

Developing the inverse of the denominator, one has

$$\begin{aligned}(1 + i\frac{\alpha_k^2}{4} - \frac{\alpha_k^4}{64})^{-1} &= 1 - i\frac{\alpha_k^2}{4} - \frac{\alpha_k^4}{16} + \frac{\alpha_k^4}{64} + \cdots \\ &\simeq 1 - \frac{i\alpha_k^2}{4} - \frac{3\alpha_k^4}{64} .\end{aligned} \tag{3.139}$$

Eventually we write

$$\frac{J_0(\alpha_k \frac{r}{R} i^{3/2})}{J_0(\alpha_k i^{3/2})} = 1 - i\frac{\alpha_k^2}{4}\left(1 - (\frac{r}{R})^2\right) - \frac{\alpha_k^4}{64}\left((\frac{r}{R})^4 - 4(\frac{r}{R})^2 + 3\right) + O(\alpha_k^6) . \tag{3.140}$$

The velocity is now

$$\begin{aligned}v_z(r,t) = &-\frac{c_0}{4\mu} R^2 \left(1 - (\frac{r}{R})^2\right) - \frac{R^2}{\mu} \sum_{k=1}^{\infty} \frac{c_k}{4} \left(1 - (\frac{r}{R})^2\right) \cos(k\omega t) \\ &+ \frac{c_k \alpha_k^2}{64} \left((\frac{r}{R})^4 - 4(\frac{r}{R})^2 + 3\right) \sin(k\omega t) .\end{aligned} \tag{3.141}$$

If the continuous Poiseuille component of the velocity is neglected and if we set $v_{z,c} = -c_1 R^2/(4\mu)$ and $\alpha_1 = \alpha$, the first mode $k = 1$ becomes

$$\frac{v_z}{v_{z,c}} = \left(1 - (\frac{r}{R})^2\right) \cos(\omega t) + \frac{\alpha^2}{16} \left((\frac{r}{R})^4 - 4(\frac{r}{R})^2 + 3\right) \sin(\omega t) . \tag{3.142}$$

The flow comprises a Poiseuille part in phase with the imposed pressure gradient and this is perfectly logical as the pulsation is slow and therefore, the flow has time to adjust itself to that variation. The additional term presents a phase shift of $\pi/2$. Figure 3.12 shows the velocity profile for values of $\alpha = 1/\sqrt{2}$ and $\omega t = 0, \pi/4, \pi/2, 3\pi/4$. Starting from the Poiseuille flow at time $\omega t = 0$, at mid period ($\omega = \pi/2$), the profile is still positive while the corresponding pressure gradient vanishes. The phase difference disappears at mid cycle ($\omega t = \pi$) and the Poiseuille flow is recovered.

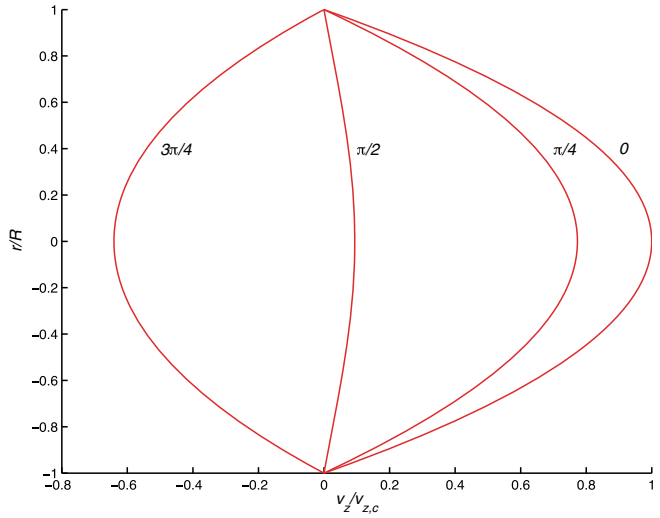

Fig. 3.12 Slow pulsatile flow with $\alpha^2 = 1/2$

3.4.2.2 Rapid Pulsation

The parameter $\alpha r/R$ takes large values and the axis ($r = 0$) is excluded from the analysis. For high values of its argument, the asymptotic development of $J_0(z)$ (cf. Eq. (14.144) of Arfken et al. [3]) is such that

$$J_0(z) = \sqrt{\frac{2}{\pi z}} \cos\left(z - \frac{\pi}{4}\right) + O(|z|^{-1}), \quad \text{with} \quad |arg(z)| < 2\pi \ . \tag{3.143}$$

Using the relation $i^{3/2} = e^{i3\pi/4}$ and $s = \alpha_k r/R$, we perform the next algebraic calculation

$$\begin{aligned}
J_0(e^{i3\pi/4}s) &= e^{-i3\pi/8}\sqrt{\frac{2}{\pi s}} \cos\left(e^{i3\pi/4}s - \frac{\pi}{4}\right) \\
&= e^{-i3\pi/8}\sqrt{\frac{2}{\pi s}} \left(\cos\left(i\frac{s}{\sqrt{2}}\right) - \left(\frac{s}{\sqrt{2}} + \frac{\pi}{4}\right)\right) \\
&= e^{-i3\pi/8}\sqrt{\frac{2}{\pi s}} \left(\cos\left(i\frac{s}{\sqrt{2}}\right)\cos\left(\frac{s}{\sqrt{2}} + \frac{\pi}{4}\right) + \sin\left(i\frac{s}{\sqrt{2}}\right)\sin\left(\frac{s}{\sqrt{2}} + \frac{\pi}{4}\right)\right) \\
&= e^{-i3\pi/8}\sqrt{\frac{2}{\pi s}} \left(\cosh\left(\frac{s}{\sqrt{2}}\right)\cos\left(\frac{s}{\sqrt{2}} + \frac{\pi}{4}\right) + i\sinh\left(\frac{s}{\sqrt{2}}\right)\sin\left(\frac{s}{\sqrt{2}} + \frac{\pi}{4}\right)\right) \\
&= e^{-i3\pi/8}\sqrt{\frac{2}{\pi s}} \cosh\left(\frac{s}{\sqrt{2}} + i\left(\frac{s}{\sqrt{2}} + \frac{\pi}{4}\right)\right) \ .
\end{aligned}$$

Neglecting the decaying exponential in cosh as we deal with large values of the argument, we obtain

$$J_0(e^{i3\pi/4}s) = e^{-i3\pi/8}\sqrt{\frac{1}{2\pi s}}e^{\frac{s}{\sqrt{2}}}e^{i\left(\frac{s}{\sqrt{2}}+\frac{\pi}{4}\right)}\,. \tag{3.144}$$

Consequently one finds

$$\frac{J_0(\alpha_k \frac{r}{R} i^{3/2})}{J_0(\alpha_k i^{3/2})} \approx \frac{1}{\sqrt{r/R}} e^{-(1+i)\frac{\alpha_k}{\sqrt{2}}(1-\frac{r}{R})}\,. \tag{3.145}$$

The first mode of the velocity profile in absence of the continuous Poiseuille component yields

$$\frac{v_z}{v_{z,c}} = \frac{4}{\alpha^2}\left[\sin(\omega t) - \frac{1}{\sqrt{r/R}} e^{-\frac{\alpha}{\sqrt{2}}(1-\frac{r}{R})} \sin\left(\omega t - \frac{\alpha}{\sqrt{2}}(1-\frac{r}{R})\right)\right] + O\left(\frac{1}{\alpha^4}\right)\,. \tag{3.146}$$

We observe that the resulting flow is in complete phase shift by a factor of $\pi/2$ with respect to the pressure gradient. We must again draw the attention of the reader to the assumptions of this approximation which bans the presence of the axis.

3.5 Plane Periodic Solutions

Many exact solutions of the Navier–Stokes equations are obtained for spatial periodic conditions. In this section we consider a two-dimensional (2D) solution due to Walsh [117].

Let us first proof the following theorem.

Theorem 3.1 (Walsh) *Let us consider a vector field* $\boldsymbol{u}$ *in the domain* Ω *that satisfies*

$$\nabla^2 \boldsymbol{u} = \lambda\, \boldsymbol{u}, \tag{3.147}$$

$$\text{div}\ \boldsymbol{u} = 0\,. \tag{3.148}$$

Then the velocity $\boldsymbol{v} = e^{\nu\lambda t}\boldsymbol{u}$ *satisfies the Navier–Stokes equations (1.73)–(1.74) with a pressure* p *such that*

$$\boldsymbol{\nabla}\, p = -\boldsymbol{v}\cdot\boldsymbol{\nabla}\boldsymbol{v}\,. \tag{3.149}$$

The vector $\boldsymbol{v}$ is divergence free as is also $\boldsymbol{u}$. Furthermore,

$$\frac{\partial \boldsymbol{v}}{\partial t} = \nu\lambda\boldsymbol{v} = \nu\Delta\boldsymbol{v}\,. \tag{3.150}$$

It remains to prove that the nonlinear term is a gradient, i.e. that $\nabla \times (\boldsymbol{v} \cdot \nabla \boldsymbol{v}) = 0$. This amounts to showing that

$$\frac{\partial}{\partial x_2}\left(v_1 \frac{\partial v_1}{\partial x_1} + v_2 \frac{\partial v_1}{\partial x_2}\right) = \frac{\partial}{\partial x_1}\left(v_1 \frac{\partial v_2}{\partial x_1} + v_2 \frac{\partial v_2}{\partial x_2}\right) , \tag{3.151}$$

as $\mathbf{curl}\, \nabla = \mathbf{0}$. This is evident by incompressibility and relation (3.150).

In the 2D case, we resort to the streamfunction ψ, assuming that it is an eigenfunction of the Laplacian with eigenvalue λ. Consequently, $\boldsymbol{u} = (\partial\psi/\partial x_2, -\partial\psi/\partial x_1)$ satisfies (3.147)–(3.148) with the same λ. Therefore, $e^{\nu\lambda t}\psi$ is the streamfunction of the associated Navier–Stokes flow. If we have a periodic domain of size 2π, then the eigenvalues λ are of the form $\lambda = -(k_{x_1}^2 + k_{x_2}^2)$, with k_{x_1} and k_{x_2} positive integers. For given k_{x_1}, k_{x_2}, the linearly independent eigenfunctions are

$$\cos(k_{x_1}x_1)\cos(k_{x_2}x_2),\ \sin(k_{x_1}x_1)\sin(k_{x_2}x_2)\ ,$$
$$\cos(k_{x_1}x_1)\sin(k_{x_2}x_2),\ \sin(k_{x_1}x_1)\cos(k_{x_2}x_2)\ .$$

It is possible to build up complicated geometrical patterns by combination of the eigenfunctions named n, m eigenfunction by Walsh, with $\lambda = -(n^2 + m^2)$. A theorem in number theory shows that integers of the form p^{2i} and p^{2i+1}, where p is an integer prime number such that $p \equiv 1 \pmod 4$, may be written as sums of squares in exactly $i + 1$ manners. For example, $625 = 5^4 = 25^2 = 24^2 + 7^2 = 20^2 + 15^2$. Figure 3.13 displays the streamlines corresponding to $\psi = \sin(25x_1) + \cos(25x_2) - \sin(24x_1)\cos(7x_2) + \cos(15x_1)\cos(20x_2) - \cos(7x_1)\sin(24x_2)$.

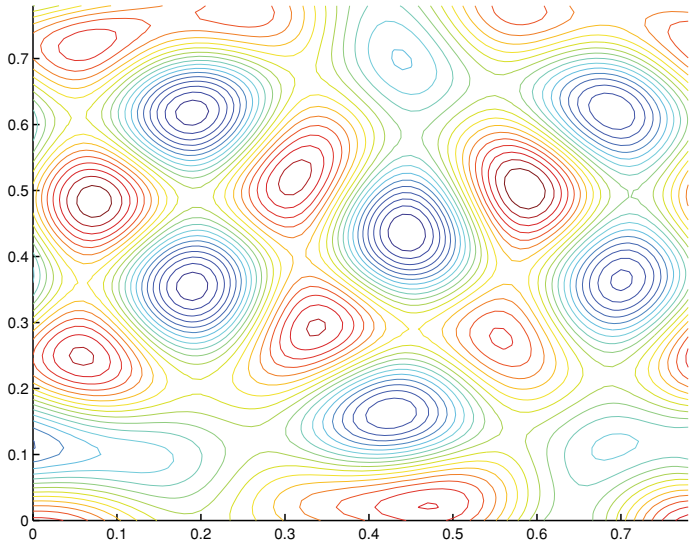

Fig. 3.13 ψ isocontours in the square $(0, \pi/4)^2$

3.6 Pipe Flow

Engineering and industrial applications require very often to move various fluids flowing through pipes: oil, water, grain, etc. To model that situation, we will consider a steady state laminar longitudinal flow in a pipe of arbitrary section in order to obtain afterwards the optimal shape of the pipe. The material presented in this section is much influenced by the book by Langlois and Deville [49].

Let x_3 be the axis of the Cartesian coordinate system parallel to the pipe generatrix. Let us assume that a mechanical device like a pump generates a constant pressure gradient G such that $-\partial p/\partial x_3 = G$. This pressure gradient gives rise to a rectilinear laminar flow along the pipe. Therefore, the velocity profile is

$$v_1 = v_2 = 0, \quad v_3 = v_3(x_1, x_2) \, . \tag{3.152}$$

It is easily verified that the continuity Eq. (1.73) is satisfied and also the Navier–Stokes equations (1.74) in directions x_1 and x_2. If the body force is constant, the third Navier–Stokes equation yields

$$\Delta v_3 + \frac{G}{\mu} = 0 \, , \tag{3.153}$$

where $G = G' + \rho b_3$ with the assumption that $p = C - G' x_3$, $C = cnst$ and Δ is the two-dimensional Laplacian, i.e.

$$\Delta = \frac{\partial^2}{\partial x_1^2} + \frac{\partial^2}{\partial x_2^2} \, . \tag{3.154}$$

Equation (3.153) is a special case of Poisson's equation, a linear, second-order partial differential equation of the elliptic type. We shall look for solutions which satisfy the boundary condition

$$v_3(x_1, x_2) = 0 \quad \text{on } \Gamma \, , \tag{3.155}$$

where Γ is the periphery of the pipe cross section.

The boundary value problem represented by (3.153) and (3.155) is equivalent to the Dirichlet problem

$$\nabla^2 u = 0 \, , \tag{3.156}$$

$$u = f(x_1, x_2) \quad \text{on } \Gamma \, . \tag{3.157}$$

To show the equivalence, we need only set

$$v_3(x_1, x_2) = \frac{G}{2\mu} \left[u(x_1, x_2) - f(x_1, x_2) \right] \, , \tag{3.158}$$

where f is *any* function satisfying

$$\Delta f = 2 \,. \tag{3.159}$$

3.6.1 Polynomial solutions

Many polynomials have constant Laplacian; some of these, when equated to zero, yield the equation of a closed contour. Thus setting $v_3(x_1, x_2)$ equal to such a polynomial, multiplied by an appropriate constant, will satisfy (3.153) and (3.155), with Γ the contour on which the polynomial vanishes. We reject immediately all linear polynomials for two reasons: they vanish only on straight lines, not on closed contours; their Laplacians are not only constant, they vanish. Consideration of quadratic polynomials, however, bears fruit.

3.6.1.1 The Elliptical Pipe

We note first that the Laplacian of any quadratic polynomial is constant. We next recall that equating any quadratic polynomial to zero yields the equation of a conic section. Only the ellipses are of interest to us, for circles were treated in the Sect. 3.2.2 and none of the other conic sections are closed contours. The algebra is simplified by placing the centroid of the ellipse on the x_3-axis, and orienting the x_1- and x_2-axes along the axes of the ellipse as shown in Fig. 3.14. Thus the most general ellipse can be represented by

$$\left(\frac{x_1}{a}\right)^2 + \left(\frac{x_2}{b}\right)^2 = 1 \,. \tag{3.160}$$

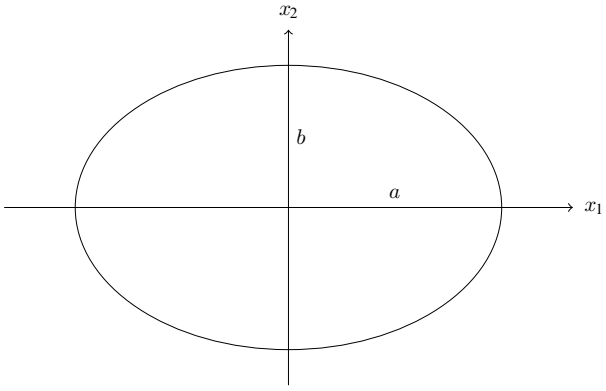

Fig. 3.14 Elliptic pipe

We find by inspection that a solution to (3.153) which vanishes on the ellipse (3.160) is provided by

$$v_3 = \frac{G}{2\mu}\frac{a^2b^2}{a^2+b^2}\left(1-\frac{x_1^2}{a^2}-\frac{x_2^2}{b^2}\right) . \tag{3.161}$$

The volume flow rate is easily calculated. We have

$$Q = \int\int v_3\, dx_1 dx_2 , \tag{3.162}$$

where the integration is carried out over the ellipse. With (3.161),

$$Q = \frac{\pi G}{4\mu}\frac{a^3b^3}{a^2+b^2} . \tag{3.163}$$

This result may be rewritten

$$Q = \frac{GA^2}{4\pi\mu}\frac{R}{1+R^2} , \tag{3.164}$$

where $A = \pi ab$ is the area of the ellipse and $R = a/b$ is the ratio of the semi-axes. We then obtain

$$\frac{\partial Q}{\partial R} = \frac{GA^2}{4\pi\mu}\frac{1-R^2}{(1+R^2)^2} . \tag{3.165}$$

Hence, for μ, G, A all fixed, Q has an extremum at $R = 1$, which is easily shown to be a maximum. We thus find that the circular pipe is more efficient than any elliptical pipe, in the sense that the circular pipe produces a greater volume flow for a given pressure gradient than does an elliptical pipe of the same cross-sectional area.

3.6.1.2 The Triangular Pipe

It seems surprising that we can express in closed form the flow through so unlikely a cross section as an equilateral triangle, but such is the way of polynomial methods. If we place the origin at the intersection of the medians and let the negative x_1-axis pass through one vertex as in Fig. 3.15, the equation of an equilateral triangle with height $3a$ becomes

$$(x_1 - a)(x_1 - \sqrt{3}\,x_2 + 2a)(x_1 + \sqrt{3}\,x_2 + 2a) = 0 . \tag{3.166}$$

Note that the two last parentheses in (3.166) are the equations for the two slanted sides of the triangle. Since

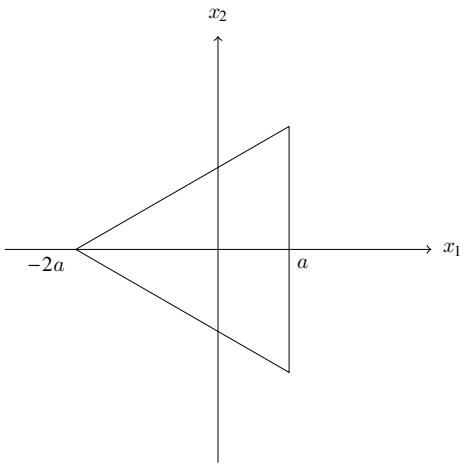

Fig. 3.15 Triangular pipe

$$\Delta\left[(x_1 - a)(x_1 - \sqrt{3}\,x_2 + 2a)(x_1 + \sqrt{3}\,x_2 + 2a)\right] = 12a\ , \tag{3.167}$$

we have

$$v_3 = \left(\frac{G}{12a\mu}\right)(a - x_1)(x_1 - \sqrt{3}\,x_2 + 2a)(x_1 + \sqrt{3}\,x_2 + 2a)\ . \tag{3.168}$$

It is readily verified that the maximum velocity occurs at the origin, and that its value there is $Ga^2/3\mu$.

3.6.2 The Rectangular Pipe

The flow in a rectangular pipe cannot be solved using the previous approach of polynomial solutions as the equation of a rectangle does not have constant Laplacian. Here we resort to the method of separation of variables.

The rectangular section of the pipe has sides $2a$ and $2b$ and is depicted in Fig. 3.16.

The governing equation (3.153) is subjected to the boundary condition

$$v_3 = 0 \quad \text{on} \quad x_1 = \pm a \quad \text{and} \quad x_2 = \pm b\ . \tag{3.169}$$

The solution of (3.153) is decomposed in a particular solution v_{3p} taking the constant term into account and a homogeneous periodic solution v_{3h} of the equation

$$\Delta v_{3h} = 0\ . \tag{3.170}$$

Fig. 3.16 Rectangular pipe

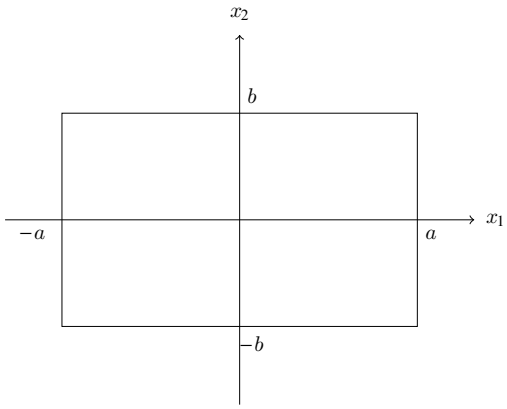

The particular solution is provided by the plane Poiseuille problem (3.27) written as

$$v_{3p} = \frac{G}{2\mu}\left(b^2 - x_2^2\right) \ . \tag{3.171}$$

Consequently the homogeneous solution must satisfy the boundary conditions

$$v_{3h} = \frac{G}{2\mu}(x_2^2 - b^2) \quad \text{on } x_1 = \pm a \ , \tag{3.172}$$

$$v_{3h} = 0 \quad \text{on } x_2 = \pm b \ . \tag{3.173}$$

The homogeneous solution of (3.170) is obtained by separation of variables such that

$$v_{3h} = \sum_{n=0}^{\infty} X_n(x_1) Y_n(x_2) \ . \tag{3.174}$$

One has

$$\frac{X_n''}{X_n} = -\frac{Y_n''}{Y_n} = k_n^2 \ . \tag{3.175}$$

The Y_n solution reads

$$Y_n(x_2) = \cos k_n x_2 \ . \tag{3.176}$$

With the boundary condition (3.173), the coefficient k_n is obtained as $k_n = (2n + 1)\pi/(2b)$. The corresponding $X_n(x_1)$ is determined from

$$\frac{X_n''}{X_n} = k_n^2 \ , \tag{3.177}$$

i.e.,

$$X_n = A_n \cosh k_n x_1 + B_n \sinh k_n x_1 \ . \tag{3.178}$$

Because of the symmetry of the problem, we have $B_n = 0$. Thus we let

$$v_{3h}(x_1, x_2) = \sum_{n=0}^{\infty} A_n \cosh k_n x_1 \cos k_n x_2 \ , \tag{3.179}$$

and set about determining the coefficients A_n so as to satisfy the boundary conditions (3.172). With the symmetry of the hyperbolic cosine, we need

$$\sum_{n=0}^{\infty} A_n \cosh[(n + \frac{1}{2})\frac{\pi a}{b}] \cos k_n x_2 = \frac{G}{2\mu}(x_2^2 - b^2) \ . \tag{3.180}$$

The cosine functions are orthogonal in Fourier analysis. They satisfy the relation

$$\frac{1}{b}\int_{-b}^{b} \cos k_n x_2 \ \cos k_m x_2 \, dx_2 = \delta_{mn} \ . \tag{3.181}$$

Multiplying the two sides of (3.180) by $\cos k_m x_2$ and integrating, we have

$$A_m \cosh[(m + \frac{1}{2})\frac{\pi a}{b}] = \frac{G}{2\mu b}\int_{-b}^{b} (x_2^2 - b^2) \ \cos k_m x_2 \, dx_2 \ . \tag{3.182}$$

Utilizing the relation

$$\int x_2^2 \cos x_2 \, dx_2 = 2x_2 \cos x_2 + (x_2^2 - 2) \sin x_2 \ , \tag{3.183}$$

one gets

$$A_m \cosh[(m + \frac{1}{2})\frac{\pi a}{b}] = \frac{G}{2\mu}\frac{4(-1)^{m+1}}{bk_m^3} = \frac{G}{2\mu}\frac{32(-1)^{m+1}b^2}{(2m+1)^3\pi^3} \ . \tag{3.184}$$

The final solution reads

$$v_3 = \frac{G}{2\mu}\left[b^2 - x_2^2 + \frac{32b^2}{\pi^3}\sum_{n=0}^{\infty} \frac{(-1)^{n+1}\cosh(2n+1)\frac{\pi x_1}{2b} \ \cos(2n+1)\frac{\pi x_2}{2b}}{(2n+1)^3 \cosh(2n+1)\frac{\pi a}{2b}}\right] . \tag{3.185}$$

Figure 3.17 shows isocontour lines for $v_3/v_{max} = cst$ in a channel of rectangular section with $a = 2b = 4$.

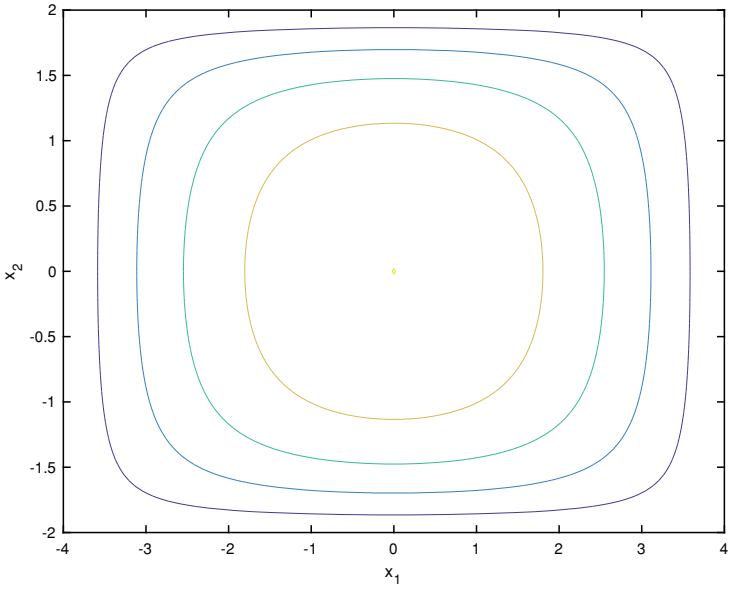

Fig. 3.17 $v_3/v_{max} = 0.2, 0.4, 0.6, 0.8, 1.0$ isocontours for a rectangular section with $a = 2b = 4$

Exercises

3.1 Consider the two-dimensional Couette–Poiseuille flow obtained by superimposing Couette flow induced by the constant velocity motion U of the upper wall and Poiseuille flow resulting from a pressure gradient in direction x_1. Calculate the velocity profile, the shear stress, and the flow rate.

3.2 A solid sphere of radius R is immersed in an incompressible viscous Newtonian fluid that fills the space and is at rest at infinity. The sphere rotates about its diameter at a constant angular velocity Ω. Assume that the Reynolds number is less than one and neglect the volume forces. The streamlines are circles centered on the rotation axis in planes perpendicular to this axis. Working in spherical coordinates, calculate the velocity profile.

3.3 With the same hypotheses as in the preceding exercise, examine the flow of a fluid between two spheres of radii R_1 and R_2 such that $R_1 < R_2$, which rotate at the angular velocities Ω_1 and Ω_2 about a common, fixed axis. Calculate the velocity profile. This solution is called the spherical Couette flow.

3.4 A cylinder of radius R_1 moves parallel to its axis with a constant velocity U inside a fixed, coaxial cylinder of radius R_2.

Calculate the velocity field of a viscous fluid which fills the space between the two cylinders. Find the friction force per unit length that acts on the moving cylinder.

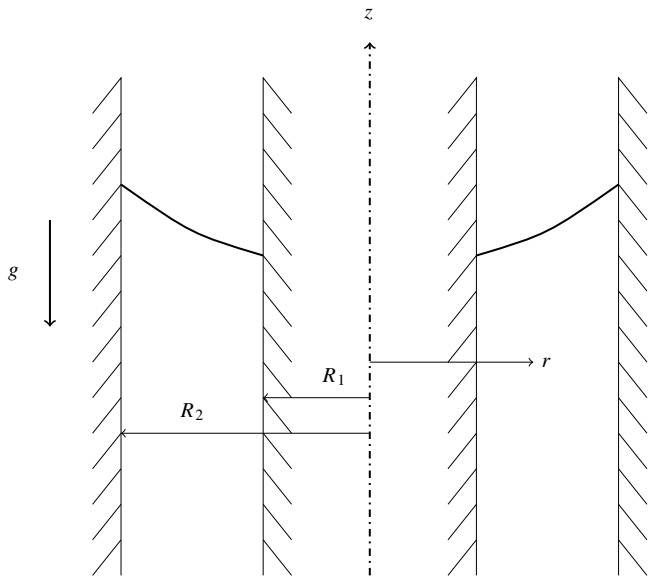

Fig. 3.18 Couette flow with free surface

3.5 Couette flow with a free surface

Consider the circular Couette flow between two cylinders. The viscous fluid fills the annular space under a free surface that is in contact with the ambient air assumed to behave as an inviscid fluid. Figure 3.18 shows the Couette device.

The outer cylinder rotates with the velocity $v_\theta(R_2) = \omega_2 R_2$, while the inner cylinder rotates at velocity $v_\theta(R_1) = \omega_2 R_1$.

- Compute the fluid velocity.
- Compute the shape of the free surface $z = z(r)$. The free surface is an isobar where the pressure is equal to the atmospheric pressure p_a. The fluid height on the inner cylinder is given by $z(R_1) = z_1$.

3.6 Plane Couette flow with two layers

We consider the plane Couette flow of two incompressible fluids of different viscosities and densities as shown in Fig. 3.19. The steady flow is oriented in direction x_1 and is generated by the upper wall moving with constant velocity U. The two layers of height h_1 and h_2, respectively, do not mix and the interface is positioned at $x_2 = 0$. The bottom wall is fixed. It is assumed that no pressure gradient influences the flow.

Evaluate the velocity field and the resulting vorticity.

3.7 Bubble dynamics

A spherical bubble of inviscid gas is contained in an infinite volume of viscous fluid. We suppose that the pressure p_g of the gas inside the bubble varies with time. As a consequence the radius R of the bubble will also vary with time. The varying

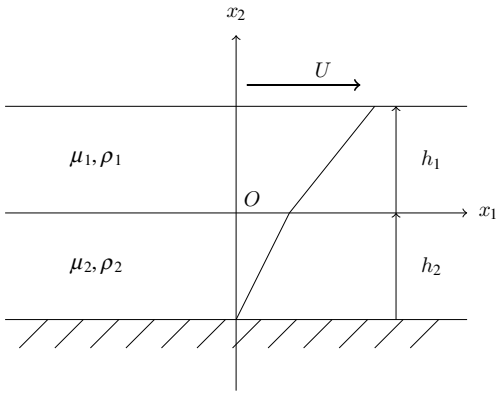

Fig. 3.19 Plane Couette flow with two immiscible fluids

bubble generates a velocity field within the fluid which in turn generates a stress field.

Compute the velocity v_r, the pressure distribution in the fluid, the governing equation for the bubble dynamics and investigate the treatment of the interface.

Chapter 4
Vorticity and Vortex Kinematics

In Sect. 1.8, the incompressible Navier–Stokes equations were derived for a viscous Newtonian fluid in terms of primitive variables: velocity and pressure. The phenomena observed in fluid flows have been interpreted by an equilibrium between the inertial forces, the pressure gradient, the volume forces such as gravity, and the viscous forces. In this chapter, we take a different point of view based on the concept of vorticity.

The presence of vorticity in a flow is an indication of the importance of the viscous effects, given that they are generated by viscous stresses. However rotational flows are computed by solving Euler equation, which show the presence of vortices. For example, the flow over a delta wing may be obtained by solving Euler equation. Vorticity can also be generated by a baroclinic mechanism for compressible flow as in Rayleigh–Taylor instability.

Therefore, under certain assumptions, vorticity possesses the following properties:

(i) in the absence of viscosity, it is transported by the flow as an elementary material vector;
(ii) in the presence of viscosity, it diffuses into the surrounding fluid while being continually produced at the solid walls that delimit the flow.

Thus the vorticity produced on a solid wall introduces the notion of a boundary layer for which we are led to modify certain conclusions coming from the theory of irrotational perfect fluids. In turbulence, flow dynamics is mostly the result of the stretching or shortening of vortex filaments and their deformation.

M. O. Deville, *An Introduction to the Mechanics of Incompressible Fluids*,
https://doi.org/10.1007/978-3-031-04683-4_4

4.1 Kinematic Considerations

The velocity gradient tensor $\boldsymbol{L}$ can be decomposed into the sum of a symmetric strain rate tensor $\boldsymbol{d}$ and an antisymmetric rotation rate tensor $\dot{\boldsymbol{\omega}}$ according to Eq. (1.36). The tensor $\boldsymbol{d}$ is given by (1.33) and $\dot{\boldsymbol{\omega}}$ by (1.35). Recall that the dual vector $\dot{\boldsymbol{\Omega}}$, corresponding to the rotation rate tensor, is the rotation rate vector introduced by (1.37).

In fluid mechanics, we classically introduce the vorticity vector $\boldsymbol{\omega}$, defined as the curl of the velocity (1.40). To acquire familiarity with the concept of vorticity, we study the flow near a stagnation point at the origin. The velocity components are such that we have, with a constant C,

$$v_1 = Cx_1,\ v_2 = -Cx_2,\ v_3 = 0\,. \tag{4.1}$$

We easily calculate that for this flow $\boldsymbol{\omega} = \boldsymbol{0}$. A flow with zero vorticity is called ***irrotational***.

Now consider the plane Poiseuille flow in a channel of height h. If the coordinate system has its origin on the lower wall, the velocity profile, (3.19) with definition (3.24), is given by the relation

$$v_1 = 4v_{max}\frac{x_2}{h}(1 - \frac{x_2}{h})\,, \tag{4.2}$$

with v_{max} being the maximum velocity on the centerline of the channel at $x_2 = h/2$. The only component of the vorticity is ω_3. It is perpendicular to the plane of the flow and its value is

$$\omega_3 = \varepsilon_{321}\frac{\partial v_1}{\partial x_2} = -\frac{4v_{max}}{h}(1 - \frac{2x_2}{h})\,. \tag{4.3}$$

In this case, the absolute value of the vorticity attains a maximum at the two walls and goes to zero on the centerline of the channel.

From these examples we can conclude that the concept of vorticity has no relation to the curvature of the streamlines. In the first case, the streamlines are curved ($\psi = Cx_1x_2$), but the vorticity is zero; while in the second example, the streamlines are straight lines and there is finite vorticity.

The Stokes theorem or the curl theorem transforms the flux of the curl of a vector through a surface S into the line integral of that vector around the curvy boundary C of the surface. The theorem reads

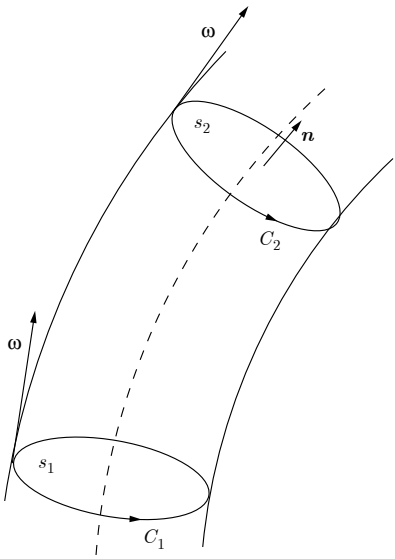

Fig. 4.1 Vortex tube

Theorem 4.1 (Stokes theorem)

$$\int_S \boldsymbol{\omega} \cdot \boldsymbol{n}\, dS = \oint_C \boldsymbol{v} \cdot \boldsymbol{\tau}\, dl\ . \tag{4.4}$$

From the definition of vorticity, (1.40), and the Stokes theorem (4.4), we obtain the identity

$$I(S) = \int_S \boldsymbol{\omega} \cdot \boldsymbol{n}\, dS = \int_S \mathbf{curl}\, \boldsymbol{v} \cdot \boldsymbol{n}\, dS = \oint \boldsymbol{v} \cdot \boldsymbol{\tau}\, dl = \Gamma\ , \tag{4.5}$$

where $I(S)$ is the intensity of the vortex tube. The curvilinear integral in (4.5) defines the velocity circulation, Γ, along the closed curve C, of the unit tangent vector $\boldsymbol{\tau}$. It is thus equal to the vorticity vector flux through an arbitrary surface bounded by the curve. In the following, this property will permit us to systematically link the concept of circulation to an interpretation in terms of vorticity.

Recall that a vortex line (Fig. 4.1) is a line tangent at all its points to the vorticity vector, and that a vortex tube is a family of vortex lines circumscribed by a closed curve. The intensity of a vortex tube, for a surface S defined by a closed line enclosing the vortex tube, is the flux $I(S)$ of vorticity through the surface.

Theorem 4.2 (Helmholtz) (Vorticity properties) *Helmholtz main theorems about vorticity are as follows:*

- *the vorticity flux through a closed surface is always zero;*
- *the intensity of a vortex tube does not depend on the transverse section considered;*

- *a vortex tube can only end connected to itself or extend to infinity unless it is cut by a wall.*

The proof of these theorems can be found in Panton's book [71].

4.2 Dynamic Vorticity Equation

4.2.1 General Equation

The formulation of the equation that governs vorticity dynamics requires the establishment of certain preliminary relations.

The acceleration term $\boldsymbol{a}$ can be written as follows:

$$\boldsymbol{a} = \frac{\partial \boldsymbol{v}}{\partial t} + \boldsymbol{\omega} \times \boldsymbol{v} + \boldsymbol{grad}\left(\frac{\boldsymbol{v}\cdot\boldsymbol{v}}{2}\right) , \tag{4.6}$$

that can be proved by induction

$$\begin{aligned} a_i &= \frac{\partial v_i}{\partial t} + \varepsilon_{ijk}\omega_j v_k + \frac{\partial}{\partial x_i}\left(\frac{v_j v_j}{2}\right) , \\ &= \frac{\partial v_i}{\partial t} + \varepsilon_{ijk}\varepsilon_{jlm}\left(\frac{\partial v_m}{\partial x_l}\right) v_k + v_j \frac{\partial v_j}{\partial x_i} , \\ &= \frac{\partial v_i}{\partial t} + (\delta_{kl}\delta_{im} - \delta_{km}\delta_{il})\left(\frac{\partial v_m}{\partial x_l} v_k\right) + v_j \frac{\partial v_j}{\partial x_i} , \end{aligned}$$

or

$$a_i = \frac{\partial v_i}{\partial t} + v_k \frac{\partial v_i}{\partial x_k} .$$

This last expression is none other than the definition of acceleration (1.23). Thus, relation

$$\mathbf{curl}\,\boldsymbol{a} = \frac{D\boldsymbol{\omega}}{Dt} - \boldsymbol{\omega}\cdot\boldsymbol{grad}\,\boldsymbol{v} \tag{4.7}$$

is an identity. As can be seen, applying the curl operator to relation (4.6) leads to

$$\mathbf{curl}\,\boldsymbol{a} = \frac{\partial}{\partial t}\mathbf{curl}\,\boldsymbol{v} + \mathbf{curl}(\boldsymbol{\omega}\times\boldsymbol{v}) + \mathbf{curl}\,\boldsymbol{grad}\left(\frac{\boldsymbol{v}\cdot\boldsymbol{v}}{2}\right)$$

or

$$\mathbf{curl}\,\boldsymbol{a} = \frac{\partial \boldsymbol{\omega}}{\partial t} + \mathbf{curl}(\boldsymbol{\omega}\times\boldsymbol{v}) . \tag{4.8}$$

The term $\mathbf{curl}(\boldsymbol{\omega} \times \boldsymbol{v})$ can be developed as follows:

$$\mathbf{curl}(\boldsymbol{\omega} \times \boldsymbol{v}) = \boldsymbol{v} \cdot \boldsymbol{grad}\, \boldsymbol{\omega} - (\nabla \boldsymbol{v})\ \boldsymbol{\omega} + \boldsymbol{\omega}\, \mathrm{div}\, \boldsymbol{v} - \boldsymbol{v}\, \mathrm{div}\, \boldsymbol{\omega}\ . \tag{4.9}$$

The last term of (4.9) is zero as div $\mathbf{curl}\ \boldsymbol{v} = 0$. From (4.8) and (4.9), it follows that

$$\mathbf{curl}\, \boldsymbol{a} = \frac{D\boldsymbol{\omega}}{Dt} - (\nabla \boldsymbol{v})\ \boldsymbol{\omega} + \boldsymbol{\omega}\, \mathrm{div}\, \boldsymbol{v}\ .$$

From the mass conservation equation (1.50), we obtain the relation

$$\mathbf{curl}\, \boldsymbol{a} = \frac{D\boldsymbol{\omega}}{Dt} - (\nabla \boldsymbol{v})\ \boldsymbol{\omega}\ ,$$

which is equivalent to Eq. (4.7) that can be written in the form

$$\frac{D\boldsymbol{\omega}}{Dt} = (\boldsymbol{\omega} \cdot \boldsymbol{grad})\, \boldsymbol{v} + \mathbf{curl}\, \boldsymbol{a}\ . \tag{4.10}$$

From the conservation of momentum (1.58), we write

$$\frac{D\boldsymbol{\omega}}{Dt} = (\boldsymbol{\omega} \cdot \boldsymbol{grad})\, \boldsymbol{v} + \mathbf{curl}\, (\boldsymbol{b} + \frac{1}{\rho}\, \mathbf{div}\, \boldsymbol{\sigma})\ . \tag{4.11}$$

Using the constitutive equation (1.67) in (4.11), we have

$$\frac{D\boldsymbol{\omega}}{Dt} = (\boldsymbol{\omega} \cdot \boldsymbol{grad})\, \boldsymbol{v} + \mathbf{curl}\, \boldsymbol{b} - \frac{1}{\rho}\mathbf{curl}(\nabla p) + 2\nu\, \mathbf{curl}(\mathbf{div}\, \boldsymbol{d})\ . \tag{4.12}$$

If the body force is conservative, it can be derived from a potential χ, as is the case for gravity. Then we write

$$\boldsymbol{b} = -\nabla\, \chi\ . \tag{4.13}$$

Consequently, $\mathbf{curl}\, \boldsymbol{b} = \mathbf{0}$, and this term disappears from (4.12). We adopt this hypothesis for the rest of the discussion. Furthermore as for the scalar field p one has $\mathbf{curl}\ (\nabla\ p) = 0$, Eq. (4.12) is simplified as

$$\frac{D\boldsymbol{\omega}}{Dt} = (\boldsymbol{\omega} \cdot \boldsymbol{grad})\, \boldsymbol{v} + 2\nu\, \mathbf{curl}(\mathbf{div}\, \boldsymbol{d})\ . \tag{4.14}$$

The left-hand side of relation (4.14) contains the material derivative of the vorticity. On the right-hand side, we find two terms that describe the deformation (stretching and shrinking) and the curvature (bending-tilting) of the vortex lines and the viscous diffusion of the vorticity. We notice that in the incompressible case, the vorticity equation does not contain any pressure contribution unlike the compressible case where a baroclinicity term appears (cf. Botsis-Deville [16]).

4.2.2 *Physical Interpretation of Vorticity Dynamics for the Incompressible Perfect Fluid*

For an incompressible fluid ($\rho = constant$), that is inviscid ($\nu = 0$), Eq. (4.14) yields

$$\frac{D\boldsymbol{\omega}}{Dt} = (\boldsymbol{\nabla v})\ \boldsymbol{\omega} = (\boldsymbol{\omega}\cdot\boldsymbol{\nabla})\boldsymbol{v}\ . \tag{4.15}$$

The term

$$(\boldsymbol{\omega}\cdot\boldsymbol{\nabla})\boldsymbol{v}$$

does not correspond to any term in the Navier–Stokes equations written with the primitive variables, velocity and pressure. Let us examine what that term means from the physical point of view.

In Fig. 4.2, consider two neighboring points Pr and Q on a vortex line. The points P and Q also define a material line of length $dx = \| d\boldsymbol{x} \|$, and we can show the equality

$$\frac{D(dx_i)}{Dt} = dv_i = \frac{\partial v_i}{\partial x_j}dx_j \ \text{ or } \ \frac{D(d\boldsymbol{x})}{Dt} = d\boldsymbol{x}\cdot\boldsymbol{grad}\ \boldsymbol{v}\ . \tag{4.16}$$

This last equation simultaneously expresses the changes in length and direction of a material line element. Comparison of (4.15) and (4.16) shows that the vorticity vector $\boldsymbol{\omega}$ plays a role analogous to that of the vector $d\boldsymbol{x}$. Thus, $\boldsymbol{\omega}$ behaves *as if* it were a material line element instantaneously coinciding with a portion of the vortex line. Let $\delta\boldsymbol{v}$ be the relative velocity of the fluid at Q with respect to P. In relation (4.15), we can make the substitution

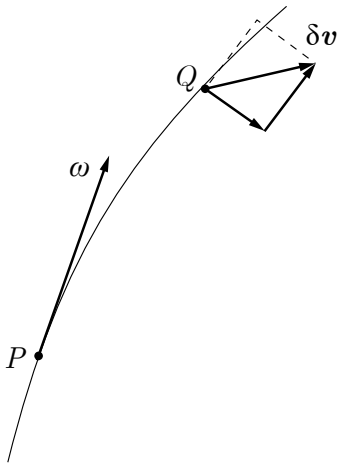

Fig. 4.2 Portion of a vortex line

$$(\nabla \boldsymbol{v})\ \boldsymbol{\omega} = \| \ \boldsymbol{\omega} \ \| \lim_{PQ \to 0} \frac{\delta \boldsymbol{v}}{PQ} \ .$$

One part of the change of $\boldsymbol{\omega}$ measured by (4.15) comes from the rigid body rotation of the material line element (from the component of $\delta \boldsymbol{v}$ normal to $\boldsymbol{\omega}$), and the other part is generated by the shrinking or stretching of the elementary line (from the component $\delta \boldsymbol{v}$ parallel to $\boldsymbol{\omega}$). Finally, Eq. (4.15) can be interpreted as follows: the vorticity is transported by the fluid particles, while being oriented and deformed *as if* it were an elementary material vector.

4.2.3 The Vorticity Number

Truesdell [110] proposed to measure the vorticity in a flow by means of a dimensionless invariant named the vorticity number. This number evaluates the relative strengths of the rotation and stretching and is defined by the relation

$$\mathcal{W} = \sqrt{\frac{\dot{\boldsymbol{\omega}} : \dot{\boldsymbol{\omega}}}{\boldsymbol{d} : \boldsymbol{d}}} \ , \tag{4.17}$$

where $\dot{\boldsymbol{\omega}}$ and $\boldsymbol{d}$ are the vorticity tensor (1.35) and rate of deformation tensor (1.33), respectively. The symbol : defines the scalar product of two tensors. For example, $\boldsymbol{d} : \boldsymbol{d} = d_{ij} d_{ij}$.

The two limit cases are the irrotational motion where $\dot{\boldsymbol{\omega}} = 0$ and $\mathcal{W} = 0$, and the rigid body motion where $\boldsymbol{d} = 0$ with $\dot{\boldsymbol{\omega}} \neq 0$ and thus $\mathcal{W} = \infty$. All flows with non zero vorticity will be measured through the vorticity number the range of which is in between 0 and infinity.

As an example, let us consider a generalized Poiseuille flow with the following velocity profile

$$v_1 = v_2 = 0, \quad v_3 = v_3(x_1, x_2) \ . \tag{4.18}$$

It is easily computed that $\mathcal{W} = 1$.

4.3 Vorticity Equation for a Viscous Newtonian Fluid

We assume now that the viscosity μ is invariable. With (1.68), we write

$$\mathbf{div}\, \boldsymbol{d} = \frac{1}{2} \left(\boldsymbol{grad} \ (\mathrm{div}\ \boldsymbol{v}) + \Delta \ \boldsymbol{v} \right) \tag{4.19}$$

or using the identity for an arbitrary vector $\boldsymbol{a}$

$$\Delta \boldsymbol{a} = \nabla \cdot \nabla \boldsymbol{a} = \nabla(\nabla \cdot \boldsymbol{a}) - \mathbf{curl}\ \mathbf{curl}\ \boldsymbol{a} \tag{4.20}$$

the relation (4.19) becomes

$$\mathbf{div}\, \boldsymbol{d} = \boldsymbol{grad}\ (\mathrm{div}\ \boldsymbol{v}) - \frac{1}{2}\, \mathbf{curl}\, \mathbf{curl}\, \boldsymbol{v}\ . \tag{4.21}$$

Taking the curl of (4.21) leads to

$$\mathbf{curl}(\mathbf{div}\, \boldsymbol{d}) = -\frac{1}{2}\mathbf{curl}(\,\mathbf{curl}\, \boldsymbol{\omega})\ . \tag{4.22}$$

The vorticity dynamics equation is obtained by combining (4.14) and (4.22):

$$\frac{D\boldsymbol{\omega}}{Dt} = (\boldsymbol{\omega} \cdot \boldsymbol{grad})\, \boldsymbol{v} - \nu\, \mathbf{curl}\, \mathbf{curl}\, \boldsymbol{\omega}\ . \tag{4.23}$$

Equation (4.23) may be rewritten with the help of (4.20) as

$$\frac{D\boldsymbol{\omega}}{Dt} = (\boldsymbol{\omega} \cdot \boldsymbol{grad})\, \boldsymbol{v} + \nu\, \Delta \boldsymbol{\omega}\ . \tag{4.24}$$

Special Case for Two-Dimensional Flow

For an incompressible two-dimensional flow, Eq. (4.23) becomes, with the notation $\omega_3 = \omega$,

$$\frac{D\omega}{Dt} = \nu\, \Delta\omega\ \ , \tag{4.25}$$

because in this special case the term $(\boldsymbol{\omega} \cdot \boldsymbol{grad}\, \boldsymbol{v})$ is zero since $\boldsymbol{\omega}$ is orthogonal to the flow plane and thus to $\boldsymbol{grad}\, \boldsymbol{v}$. We note that Eq. (4.25) is analogous to that for heat conduction, with the kinematic viscosity replacing the thermal diffusivity. We also notice that Eq. (4.25) is satisfied for $\omega = 0$, that is, for an irrotational flow. However, that solution is inadequate. To understand why, we reason by analogy with the heat equation, which also allows an identically zero solution. We know from the study of heat flow, that any non-uniform distribution of temperature at the wall or non-zero heat flux will generate a variable temperature field in the material. Thus the analogy leads us to conclude that, in the case of a viscous fluid, the vorticity that is generated at the walls will diffuse out by shear and then be carried away by the flow. The creation of vorticity at the wall is the result of the shear stress on the wall. To obtain the value of vorticity at the wall, we can resort to the classical method of Green's functions [101].

4.4 Circulation Equation

In the context of the hypotheses introduced in the previous section, we prove that for a material curve $C(t)$, along which the circulation of the velocity vector is $\Gamma(t)$, we can write the following:

$$\frac{d\Gamma}{dt} = -\oint_{C(t)} \nu(\mathbf{curl\ curl}\ \boldsymbol{v}) \cdot d\boldsymbol{x}\ . \tag{4.26}$$

This relation expresses the fact that the variation of the circulation along the material curve is due to the viscosity which dampens the motion.

To obtain (4.26), we must first prove that for a material curve $C(t)$, we have the following identity:

$$\frac{d\Gamma}{dt} = \oint_{C(t)} \boldsymbol{a} \cdot d\boldsymbol{x}\ . \tag{4.27}$$

For that purpose, we can write the equation

$$\frac{d\Gamma}{dt} = \frac{d}{dt}\oint_{C(t)} v_i dx_i = \frac{d}{dt}\oint_{C_0} V_i \frac{\partial x_i}{\partial X_j} dX_j\ ,$$

in which C_0 denotes the material curve $C(t)$ at the instant $t = t_0$ and X_i are the associated Lagrangian coordinates. Denoting by A_i and V_i the Lagrangian representations of acceleration (1.22) and velocity (1.9), we have:

$$\begin{aligned}\frac{d}{dt}\oint_{C_0} V_i \frac{\partial x_i}{\partial X_j} dX_j &= \oint_{C_0} \left(A_i \frac{\partial x_i}{\partial X_j} + V_i \frac{\partial V_i}{\partial X_j} \right) dX_j \\ &= \oint_{C(t)} a_i dx_i + \oint_{C_0} \frac{\partial}{\partial X_j} \left(\frac{V_i V_i}{2} \right) dX_j\ .\end{aligned}$$

The last term of the right-hand side of this equality is zero on a closed curve.

With relation (1.67), which we use in the motion equation (4.21), taking into account the vector identity (4.20) and Eq. (1.74), we can write

$$\boldsymbol{a} = -\boldsymbol{grad}\ \chi - \frac{1}{\rho}\boldsymbol{grad}\ p + 2\nu\ \boldsymbol{grad}\ (\mathrm{div}\ \boldsymbol{v}) - \nu\ \mathbf{curl\ curl}\ \boldsymbol{v}\ .$$

By the conservation of mass, it leads to

$$\boldsymbol{a} = -\boldsymbol{grad}\left(\frac{p}{\rho} + \chi \right) - \nu\ \mathbf{curl\ curl}\ \boldsymbol{v}\ . \tag{4.28}$$

Inserting (4.28) in (4.27), we obtain (4.26).

4.5 Vorticity Equation for a Perfect Fluid

For an incompressible, perfect ($\nu = 0$) fluid, the vorticity dynamics equation (4.24) becomes

$$\frac{D\boldsymbol{\omega}}{Dt} = \boldsymbol{\omega} \cdot \boldsymbol{grad}\, \boldsymbol{v} \ . \tag{4.29}$$

In the two-dimensional case, $\boldsymbol{\omega}$ is orthogonal to $\boldsymbol{grad}\, \boldsymbol{v}$ and this relation reduces to

$$\frac{D\omega}{Dt} = 0 \ . \tag{4.30}$$

From Eq. (4.29), we deduce that, for a perfect incompressible fluid, if the flow is irrotational at an instant, it remains so. In particular, an initially uniform flow will remain irrotational afterwards.

In the case of a perfect fluid, Eq. (4.26) yields Kelvin's theorem (cf. [71], Sect. 13.10)

Theorem 4.3 (Kelvin theorem) *The circulation of the velocity along a closed material line does not change, for an incompressible perfect fluid*

$$\frac{d\Gamma}{dt} = 0 \ . \tag{4.31}$$

4.6 Bernoulli's Equation

Bernoulli's equation is obtained from the Navier–Stokes equation (1.74) written for perfect fluids ($\mu = 0$). Assume that the volume forces can be derived from a potential (4.13), then

$$\frac{D\boldsymbol{v}}{Dt} = -\frac{1}{\rho}\boldsymbol{\nabla}\, p - \boldsymbol{\nabla}\chi \ . \tag{4.32}$$

Using the vector identity

$$\boldsymbol{v} \cdot \boldsymbol{\nabla}\boldsymbol{v} = \boldsymbol{\omega} \times \boldsymbol{v} + \boldsymbol{\nabla}\left(\frac{\boldsymbol{v} \cdot \boldsymbol{v}}{2}\right) \ , \tag{4.33}$$

in the material derivative of the velocity, we obtain

$$\frac{\partial \boldsymbol{v}}{\partial t} = -\boldsymbol{\omega} \times \boldsymbol{v} - \frac{1}{\rho}\boldsymbol{\nabla}\, p - \boldsymbol{\nabla}\left(\frac{v^2}{2} + \chi\right) \ . \tag{4.34}$$

We also assume that the flow is irrotational, $\boldsymbol{\omega} = \boldsymbol{0}$. This assumption is strong, because real fluids produce rotational flows, such as those produced, for example, by the viscous effects near a wall. Thus, Eq. (4.34) can now be written as

$$\frac{\partial \boldsymbol{v}}{\partial t} = -\frac{1}{\rho}\nabla\, p - \nabla\left(\frac{v^2}{2} + \chi\right) . \tag{4.35}$$

Since the flow is irrotational, the velocity field can be derived from a potential, Φ, such that

$$\boldsymbol{v} = \nabla\Phi . \tag{4.36}$$

Applying the divergence to (4.36) shows that the potential satisfies a Laplace equation

$$\Delta\Phi = 0 . \tag{4.37}$$

The Euler equation (4.35) yields

$$\nabla\left(\frac{\partial\Phi}{\partial t} + \frac{v^2}{2} + \chi\right) = -\frac{1}{\rho}\nabla\, p. \tag{4.38}$$

As the left-hand side of (4.38) corresponds to the gradient of a scalar function, the same must be the case for the right-hand side. Consequently, Eq. (4.38) becomes with the assumption $\rho = \text{cnst}$

$$\nabla\left(\frac{\partial\Phi}{\partial t} + \frac{v^2}{2} + \chi + \frac{p}{\rho}\right) = 0 . \tag{4.39}$$

We integrate this equation to obtain the general form of *Bernoulli's equation:*

$$\frac{\partial\Phi}{\partial t} + \frac{p}{\rho} + \frac{v^2}{2} + \chi = C(t) . \tag{4.40}$$

If the flow is stationary, then (4.40) yields the steady state form of Bernoulli's equation

$$\frac{p}{\rho} + \frac{v^2}{2} + \chi = C, \tag{4.41}$$

which, as is suggested by the second term, is an integral of the energy. Therefore, Bernoulli's equation is a first integral of the Euler equation for the case of a stationary, irrotational, perfect fluid.

4.7 Vorticity Production on a Solid Wall

The presence of a solid wall in a flow generates vorticity. An important fact to report is the direct link between the viscous wall shear stress and the produced vorticity. It is proposed in this section to establish certain properties of the effort exercised by a viscous fluid on a fixed wall. To this end, we can show that for a viscous

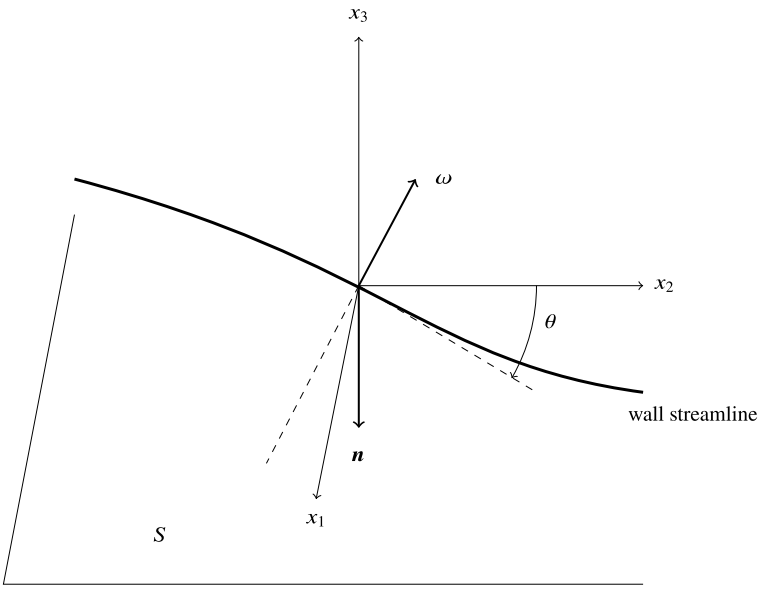

Fig. 4.3 Vorticity generated on a plane wall

incompressible fluid, considered in a point of the fixed wall, we have the following properties:

- the normal component of the contact force is the pressure;
- the tangential component of the contact force is equal to the product of the dynamic viscosity by the vorticity vector $\boldsymbol{\omega}$ rotated by 90° in the plane tangent to the wall, in the positive direction around the normal to this plane.

Let S be a plane wall, $\boldsymbol{n}$ the unit normal vector to S pointing to the outside of the fluid. The system of Cartesian rectangular axes is chosen such that the axes x_1, x_2 are located in S and the normal $\boldsymbol{n}$ is oriented in the negative direction of the axis x_3, cf. Fig. 4.3.

The continuity equation expressed at the origin of the axes reads

$$\frac{\partial v_1}{\partial x_1} + \frac{\partial v_2}{\partial x_2} + \frac{\partial v_3}{\partial x_3} = 0 \,. \tag{4.42}$$

As the components v_1, v_2 vanish on the wall, we obtain

$$\frac{\partial v_1}{\partial x_1} = \frac{\partial v_2}{\partial x_2} = 0 \,. \tag{4.43}$$

The relations (4.42) and (4.43) imply consequently

$$\frac{\partial v_3}{\partial x_3} = 0 \,. \tag{4.44}$$

Taking these relations into account, we develop the velocity components in Taylor series with respect to the normal direction to the wall. The dominating terms are

$$v_1 = 0 + \frac{\partial v_1}{\partial x_3} \mid_0 x_3 + \cdots \,, \tag{4.45}$$

$$v_2 = 0 + \frac{\partial v_2}{\partial x_3} \mid_0 x_3 + \cdots \tag{4.46}$$

$$v_3 = 0 + 0 + \frac{\partial^2 v_3}{\partial x_3^2} \mid_0 \frac{x_3^2}{2} + \cdots \,. \tag{4.47}$$

It is then possible to evaluate the slope of the wall streamline (w.s.), i.e. the streamline obtained when the distance to the wall goes to zero

$$\frac{dx_2}{dx_1} \mid_{w.s.} = \tan\theta = \lim_{x_3 \to 0} \frac{v_2}{v_1} = \frac{\frac{\partial v_2}{\partial x_3}|_0}{\frac{\partial v_1}{\partial x_3} \mid_0} \,. \tag{4.48}$$

In this relation θ is the angle at the origin of the axes between the wall streamline and the x_2 axis. This particular streamline is indeed in the wall as the angle that it makes with the planes (x_3, x_1) and (x_3, x_2), that is the limits of the respective ratios v_3/v_1 and v_3/v_2, vanish altogether.

Let us consider now the vorticity lines. On the wall at the origin of the axes, the vorticity components are

$$\begin{aligned} \omega_1 \mid_0 &= \frac{\partial v_3}{\partial x_2} - \frac{\partial v_2}{\partial x_3} = -\frac{\partial v_2}{\partial x_3}|_0 \,, \\ \omega_2 \mid_0 &= \frac{\partial v_1}{\partial x_3} - \frac{\partial v_3}{\partial x_1} = \frac{\partial v_1}{\partial x_3} \mid_0 \,, \\ \omega_3 \mid_0 &= \frac{\partial v_2}{\partial x_1} - \frac{\partial v_1}{\partial x_2} = 0 \,. \end{aligned} \tag{4.49}$$

The normal component of the wall vorticity is zero. It results that the vorticity vector is entirely located in the plane of the wall, where it is generated. We can also show that the wall vorticity lines (v.l.) are always orthogonal to the wall streamlines. Indeed, we have the relationship

$$\frac{dx_2}{dx_1} \mid_{v.l.} = \frac{\omega_2}{\omega_1} = \frac{\frac{\partial v_1}{\partial x_3} \mid_0}{-\frac{\partial v_2}{\partial x_3} \mid_0} = -\frac{1}{\frac{dx_2}{dx_1}|_{w.s.}} \tag{4.50}$$

When moving away from the wall, vorticity lines and streamlines do not necessarily remain orthogonal, especially in a three-dimensional flow.

Let us rotate the system of axes around the x_3 axis in such a way that the angle θ be zero. By (4.48), one has

$$\frac{\partial v_2}{\partial x_3} \mid_0 = 0 \,. \tag{4.51}$$

The viscous component of the contact force exerted on the wall by the fluid will be denoted $\boldsymbol{t}^v$. We evaluate its value by the relations (4.43), (4.44), (4.51) and the Cauchy theorem (1.53)

$$t_1^v = n_3 \sigma_{13} = -\mu \frac{\partial v_1}{\partial x_3} = -\mu \, \omega_2 \,. \tag{4.52}$$

The wall contact viscous force is thus tangential and directly proportional to the wall vorticity. It is possible to generalize (4.52) for an arbitrary system of axes for a wall that is not a plane, cf. Berker [14]. One obtains the relation

$$\boldsymbol{t} = p \, \boldsymbol{n} + \mu (\boldsymbol{n} \times \boldsymbol{\omega}) \,. \tag{4.53}$$

In the same way that the temperature of a wall gives no indication of the amount of energy leaving it, the wall vorticity does not give information on the vorticity intensity which goes in or out the flow. For the sake of comparison, the theory of heat flow establishes that the heat flux through a plane of normal $\boldsymbol{n}$ is given by the product $\boldsymbol{n} \cdot \boldsymbol{q}$ where $\boldsymbol{q}$ denotes the heat flux vector. By analogy, we define the diffusive vorticity flux for a viscous incompressible fluid by the equation

$$\begin{aligned} \boldsymbol{\zeta} &= -(\nabla \boldsymbol{\omega}) \, \boldsymbol{n} \\ \zeta_i &= -n_j \frac{\partial \omega_i}{\partial x_j} \,. \end{aligned} \tag{4.54}$$

The wall value of ζ_i is computed from Eq. (4.6) and the momentum equation (1.74) with no body force term

$$\frac{\partial \boldsymbol{v}}{\partial t} + \nabla \left(\frac{\boldsymbol{v} \cdot \boldsymbol{v}}{2} + \frac{p}{\rho} \right) = -\boldsymbol{\omega} \times \boldsymbol{v} - \nu \, \mathbf{curl} \, \boldsymbol{\omega} \,. \tag{4.55}$$

On a fixed wall the velocity $\boldsymbol{v}$ is zero and (4.55) yields

$$\nabla p = -\mu \, \mathbf{curl} \, \boldsymbol{\omega} \,. \tag{4.56}$$

By (4.49), (4.54) and (4.56), one obtains

$$\frac{\partial p}{\partial x_1} = \mu \frac{\partial \omega_2}{\partial x_3} = \mu \, \zeta_2, \tag{4.57}$$

$$\frac{\partial p}{\partial x_2} = -\mu \frac{\partial \omega_1}{\partial x_3} = -\mu \, \zeta_1. \tag{4.58}$$

We notice that it is necessary to have a pressure gradient along the wall to maintain vorticity production inside the fluid.

The third component of the diffusive vorticity flux is computed by the property $\nabla \cdot \boldsymbol{\omega} = 0$. One has

$$\zeta_3 = -n_3 \frac{\partial \omega_3}{\partial x_3} = -\left(\frac{\partial \omega_1}{\partial x_1} + \frac{\partial \omega_2}{\partial x_2}\right) . \tag{4.59}$$

The necessary pressure gradient for the wall vorticity generation is produced at the flow start-up as the term $\rho\, \partial \boldsymbol{v}/\partial t$ is the only one during the first instants that can be compensated by $-\nabla p$, because the viscous part of the Navier–Stokes operator comes into play on longer time scales, especially when the Reynolds number is large, cf. Morton [61].

4.8 Flow Behind a Grid

Kovasznay [45] examines the steady state two-dimensional exact solution of the Navier–Stokes equation for the laminar flow behind a periodic array of cylinders or rods. The velocity field is assumed to be such that $v_1 = U + u_1$, $v_2 = u_2$, where U is the mean velocity in the x_1 direction. The vorticity equation (4.25) yields

$$\frac{\partial \omega_3}{\partial t} + (U + u_1)\frac{\partial \omega_3}{\partial x_1} + u_2 \frac{\partial \omega_3}{\partial x_2} = \nu \Delta \omega_3 . \tag{4.60}$$

Denoting the grid spacing by δ, we define the Reynolds number as $Re = \delta U/\nu$. The dimensionless vorticity becomes $\omega = \omega_3\, \delta/U$. The other dimensionless variables are $x = x_1/\delta$, $y = x_2/\delta$, $\tau = tU/\delta$, $1 + u = v_1/U$, $v = v_2/U$. The governing equation (4.60) becomes

$$\frac{\partial \omega}{\partial \tau} + (1 + u)\frac{\partial \omega}{\partial x} + v\frac{\partial \omega}{\partial y} = \frac{1}{Re}\Delta \omega . \tag{4.61}$$

As steady state solutions are sought, the term $\partial \omega/\partial \tau$ vanishes. We are left with

$$\Delta \omega - Re\frac{\partial \omega}{\partial x} - Re\left(u\frac{\partial \omega}{\partial x} + v\frac{\partial \omega}{\partial y}\right) = 0 . \tag{4.62}$$

To build up the analytical solution, the trick consists in finding an expression that cancels the nonlinear term. The streamfunction is introduced to satisfy the continuity equation

$$u = \frac{\partial \psi}{\partial y}, \quad v = -\frac{\partial \psi}{\partial x} , \tag{4.63}$$

and therefore the vorticity is

$$\omega = -\Delta \psi . \tag{4.64}$$

Taking the y periodicity into account, the streamfunction is set up such that

$$\psi = f(x)\sin 2\pi y \,. \tag{4.65}$$

With (4.65), the nonlinear term of (4.62) gives

$$f' f'' - f f''' = 0 \,. \tag{4.66}$$

Assuming that none of the derivatives vanish, we write

$$\frac{f'''}{f''} = \frac{f'}{f} \,. \tag{4.67}$$

Integrating (4.67) we obtain

$$f'' = k^2 f \,, \tag{4.68}$$

where k is a real or complex arbitrary constant. A further integration yields

$$f = Ce^{kx} \,. \tag{4.69}$$

With the stream function

$$\psi = Ce^{kx}\sin 2\pi y \tag{4.70}$$

canceling the nonlinear term in (4.62), we have to seek a solution of the equation

$$\Delta\omega - Re\frac{\partial\omega}{\partial x} = 0 \,. \tag{4.71}$$

Setting

$$\omega = g(x)\sin 2\pi y \,, \tag{4.72}$$

we have

$$g'' - Re\, g' - 4\pi^2 g = 0 \,, \tag{4.73}$$

the solution of which is

$$g(x) = Ae^{\lambda_1 x} + Be^{\lambda_2 x} \,, \tag{4.74}$$

where

$$\lambda_{1,2} = \frac{Re}{2} \pm \sqrt{\frac{Re^2}{4} + 4\pi^2} \,. \tag{4.75}$$

Combining (4.72) and (4.74), the vorticity is

$$\omega = \left(Ae^{\lambda_1 x} + Be^{\lambda_2 x}\right)\sin 2\pi y \,, \tag{4.76}$$

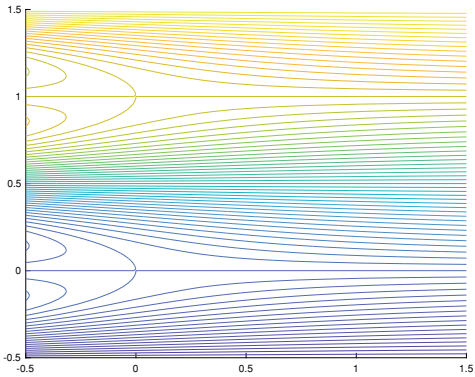

Fig. 4.4 Streamlines of the Kovasznay flow for $Re = 40$

while Eqs. (4.64) and (4.70) give

$$\omega = C(4\pi^2 - k^2)e^{kx} \sin 2\pi y \, . \tag{4.77}$$

Comparison of (4.76) and (4.77) shows that two solutions are possible

$$k = \lambda_1, \quad A = -Re\lambda_1 C, \quad B = 0, \tag{4.78}$$

$$k = \lambda_2, \quad A = 0, \quad B = -Re\lambda_2 C \, . \tag{4.79}$$

The constant C is obtained by fixing the stagnation point at $x = 0$ and therefore $C = -1/2\pi$. The corresponding streamfunction is

$$\psi = y - \frac{1}{2\pi} e^{\lambda_2 x} \sin 2\pi y \, . \tag{4.80}$$

With $Re = 40$ and the corresponding λ_2, the streamlines are shown in Fig. 4.4, with pairs of eddies generated behind the cylinders. The flow recovers uniformity downstream through the exponential term of the solution.

As the Kovasznay flow incorporates the nonlinear term, it is a good benchmark to test the numerical accuracy and space convergence of computational methods integrating the Navier–Stokes equation.

4.9 Taylor–Green Vortex

Taylor and Green [104] proposed an idealized model of a three-dimensional vortex field in order to test the dynamics of turbulence.

Orszag [66, 68] modified this model by shifting the origin of axis x_3 by a factor of $\frac{1}{2}\pi$ to obtain a two-dimensional initial velocity field that was simpler to handle by spectral Fourier methods in a cubic box of period 2π. The velocity is given as

$$\begin{aligned} v_1 &= \cos x_1 \sin x_2 \cos x_3 \\ v_2 &= -\sin x_1 \cos x_2 \cos x_3 \\ v_3 &= 0 \,. \end{aligned} \tag{4.81}$$

The corresponding vorticity components are

$$\begin{aligned} \omega_1 &= -\sin x_1 \cos x_2 \sin x_3 \\ \omega_2 &= -\cos x_1 \sin x_2 \sin x_3 \\ \omega_3 &= -2 \cos x_1 \cos x_2 \cos x_3 \,. \end{aligned} \tag{4.82}$$

The initial streamlines are planar curves given by $\cos x_1 \cos x_2 = const$ in planes $x_3 = const$. Nonetheless, the velocity that will develop at later times is fully three-dimensional. The initial vortex lines are the curves

$$\sin x_1 / \sin x_2 = \text{const}, \ \sin^2 x_1 \cos x_3 = \text{const}, \tag{4.83}$$

so they are twisted and induce a velocity field able to stretch them. The Taylor–Green vortex is perhaps the simplest example of self-induced vortex stretching by a three-dimensional velocity field.

Orszag did not give any detail to obtain (4.83). Therefore, to compute the vorticity lines, we will rely on a paper by Nore et al. [63], especially the appendix "Taylor–Green Clebsch potentials".

The Clebsch potentials allow to decompose the velocity field as follows

$$\boldsymbol{v} = \nabla\varphi + \lambda \nabla\mu \,, \tag{4.84}$$

i.e. in a potential part (first term of the r.h.s.) and a rotational part (second term of r.h.s.). The rotational part is chosen to be a complex-lamellar field, that is a flow where the velocity field is orthogonal to its own **curl**. Call it $\boldsymbol{v}^{(\omega)}$. The complex-lamellar field may be considered as a potential if it is divided by an integration factor λ such that

$$\boldsymbol{v}^{(\omega)} = \lambda \nabla\mu \,. \tag{4.85}$$

The potential $\varphi(\boldsymbol{x})$, $\lambda(\boldsymbol{x})$, $\mu(\mathbf{x})$ are named Clebsch variables. Note that the decomposition (4.84) is not unique.

Taking into account the identity $\nabla \times (\lambda \nabla\mu) = \lambda(\nabla \times \nabla\mu) + \nabla\lambda \times \nabla\mu$, the vorticity of the field (4.84) yields

$$\boldsymbol{\omega} = \mathbf{curl}\, \boldsymbol{v}^{(\omega)} = \nabla\lambda \times \nabla\mu \,. \tag{4.86}$$

Geometrically speaking, the relation (4.86) shows that the surfaces of constant λ and μ are material vorticity surfaces. As λ and μ both contain vortex lines, their intersection describes the vortex lines. The potentials λ and μ must be invariants under vorticity flow dynamics.

Looking for a general invariant $\mathcal{I}$, one must satisfy the transport equation

$$\boldsymbol{\omega} \cdot \nabla \mathcal{I} = 0 \quad \text{or} \quad \omega_j \frac{\partial \mathcal{I}}{\partial x_j} = 0 \,. \tag{4.87}$$

Carrying through the algebra and dividing by $\cos x_1 \cos x_2 \sin x_3$, one writes

$$\tan x_1 \frac{\partial \mathcal{I}}{\partial x_1} + \tan x_2 \frac{\partial \mathcal{I}}{\partial x_2} + 2 \frac{\frac{\partial \mathcal{I}}{\partial x_3}}{\tan x_3} = 0 \,. \tag{4.88}$$

This equation is solved by separation of variables. We divide (4.88) by $\mathcal{I} = u(x_1)v(x_2)w(x_3)$ to obtain the relation

$$\tan x_1 \frac{\partial [\ln u(x_1)]}{\partial x_1} + \tan x_2 \frac{\partial [\ln v(x_2)]}{\partial x_2} + 2 \frac{\partial [\ln w(x_3)]/\partial x_3}{\tan x_3} = 0 \,. \tag{4.89}$$

Each term in (4.89) must be equal to a constant c_1, c_2, c_3 such that

$$c_1 + c_2 + 2c_3 = 0 \,. \tag{4.90}$$

The first two terms of (4.89) are of the form

$$\tan x_1 \frac{\partial [\ln u(x_1)]}{\partial x_1} = c_1 \,, \tag{4.91}$$

with a general solution given by $u(x_1) = \text{const}\,(\sin x_1)^{c_1}$. The last term yields the equation

$$\frac{\partial [\ln w(x_3)]/\partial x_3}{\tan x_3} = c_3 \,, \tag{4.92}$$

with the solution given by $w(x_3) = \text{const}\,(\cos x_3)^{-c_3}$.

Two independent solutions of (4.90) are $c_1 = 1, c_2 = 0, c_3 = -1/2$ and $c_1 = 0, c_2 = 1, c_3 = -1/2$. The Clebsch potentials are

$$\lambda = \sin(x_1)\sqrt{\cos(x_3)} \tag{4.93}$$

$$\mu = \sin(x_2)\sqrt{\cos(x_3)} \,, \tag{4.94}$$

that give the vorticity lines (4.83).

Unlike the three-dimensional case that has no closed form solution, the two-dimensional Taylor–Green vortex is amenable to an analytical solution

$$\begin{aligned} v_1 &= e^{-2\nu t} \sin x_1 \cos x_2 \,, \\ v_2 &= -e^{-2\nu t} \cos x_1 \sin x_2 \,, \end{aligned} \tag{4.95}$$

$$p = -\frac{1}{4} e^{-4\nu t} \left(\cos(2x_1) + \cos(2x_2)\right) \,. \tag{4.96}$$

This solution is used in numerical fluid mechanics to check the accuracy and stability of Navier–Stokes solvers.

Exercises

4.1 Compute the vorticity in the circular Couette flow and verify the Stokes theorem (4.5).

4.2 By applying Bernoulli's theorem for perfect fluids (4.41), show that the velocity of a jet exiting an orifice in a wall at a distance h from the free surface of the fluid in a container is

$$v = \sqrt{2gh}\ . \tag{4.97}$$

4.3 Hill's Vortex

Hill's vortex [38] in an incompressible fluid represents the limit case where the vorticity is distributed in the volume inside a sphere of radius R. Outside the sphere the flow is considered irrotational. For example this situation concerns the constant velocity fall of a water drop in oil. The other limit case corresponds to filament vorticity distribution.

The problem in spherical coordinates has the $\boldsymbol{\omega}$ vorticity components

$$\omega_\varphi = \frac{\omega r \sin\theta}{R}, \quad \omega_r = \omega_\theta = 0, \quad \forall r \leq R \tag{4.98}$$

$$\boldsymbol{\omega} = \mathbf{0} \quad \forall r > R\ , \tag{4.99}$$

with C a constant.

We assume the problem is axisymmetric with $v_\varphi = 0$.

- Evaluate the velocity components $v_r = f(r)\cos\theta$ and $v_\theta = g(r)\sin\theta$ inside the vortex.
- Obtain with the velocity potential the velocity components outside the spherical vortex.
- Compute the streamfunction.

4.4 Simplified Vortex Study of the Draining of a Container

The physical situation concerns the draining of a container whose free surface is located at the altitude $z = 0$ in a cylindrical coordinate system, with the z axis oriented downwards. The fluid flow is axisymmetric, irrotational, incompressible with radial and axial velocity components given respectively by

$$v_r = -\frac{ar}{2}, \quad v_z = az\ , \tag{4.100}$$

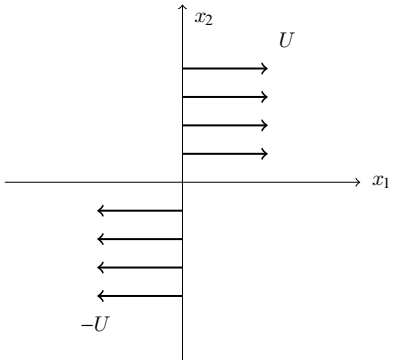

Fig. 4.5 Initial velocity distribution of the vortex sheet

with a a positive constant. We suppose that the flow is perturbed by the introduction of a low amplitude vortex (draining vortex) of vorticity $\boldsymbol{\omega} = \omega_z(r)\boldsymbol{e}_z$.

- Verify that the unperturbed flow is incompressible.
- Show that the unperturbed flow is irrotational.
- Show that ω_z verifies the steady state equation

$$\frac{a}{2}\omega_z r^2 + \nu r \frac{d\omega_z}{dr} = C \ , \tag{4.101}$$

  with C a constant.
- Show that the constant C in (4.101) vanishes by inspection of the ω_z behavior on short and long distances.
- Compute the solution for $\omega_z(r)$.
- Highlight the existence of a characteristic distance δ which will be expressed with the problem data.
- What is the physical meaning of δ?

4.5 Diffusion of a vortex sheet

At the initial time $t = 0$, a vortex sheet coinciding with the plane $x_2 = 0$ of the Cartesian coordinate system is given. This vortex sheet is a singularity that we will ignore. On each side of the sheet, the velocity distribution is uniform and such that (cf. Fig. 4.5)

$$\begin{aligned} v_1(x_2, 0) &= \ \ U \quad \forall x_2 > 0 \\ v_1(x_2, 0) &= -U \quad \forall x_2 < 0 \ . \end{aligned} \tag{4.102}$$

The fluid is incompressible. The body forces are neglected. The pressure is uniform. The flow is one-dimensional in the plane Ox_1x_2.

Compute the time evolution of the vorticity resulting from the effects of viscous diffusion. To this end, follow the next steps.

- Show that the dynamic vorticity equation reduces to

$$\frac{\partial \omega_3}{\partial t} = \nu \frac{\partial^2 \omega_3}{\partial x_2^2} \,. \tag{4.103}$$

- Introduce the dimensionless variables $\eta = \frac{x_2}{\sqrt{\nu t}}$, $\upsilon = \frac{U^2 t}{\nu}$. Assuming that the vorticity may be written as $\omega_3(x_2, t) = f(\eta)g(\upsilon)$, show that ω_3 depends only on η.
- Solve the f equation with the hypotheses that $f(0)$ and $f'(0)$ have finite non zero values.
- Describe qualitatively the time evolution of ω_3.

Chapter 5
Stokes Flow

In this chapter, let us consider first the Stokes equation, valid for very slow flows that we conventionally call creeping flows or Stokes flows. These flows are dominated by viscous forces which are much larger than inertial forces. Examples come from technologies in such diverse domains as convection currents in high temperature glass melting furnaces, lubricants in bearings, and the flow of oils and mud (although the latter may have pronounced non-Newtonian behavior). In nature (another source of interesting cases), we find convection in terrestrial magma, the flow of lava, the swimming of fish, the propulsion of microorganisms, and the squirming of spermatozoon.

We assume that the Reynolds number $Re \ll 1$ and therefore the Navier–Stokes equations reduce to the Stokes equation. As the latter is linear, a complete analytic treatment is possible.

Taking the divergence of the Stokes equation (2.54) and taking into account the solenoidal character of the velocity field, we get

$$\Delta p = 0 \,. \tag{5.1}$$

The pressure is thus a harmonic function for a Stokes flow.

Taking the curl of the Stokes equation (2.54), we obtain

$$\frac{\partial \boldsymbol{\omega}}{\partial t} = \nu \Delta \boldsymbol{\omega} \,, \tag{5.2}$$

where we have introduced the vorticity, $\boldsymbol{\omega} = \mathbf{curl}\, \boldsymbol{v}$ using Eq. (1.40). If the flow is stationary, the components of the vorticity are also harmonic functions.

M. O. Deville, *An Introduction to the Mechanics of Incompressible Fluids*,
https://doi.org/10.1007/978-3-031-04683-4_5

5.1 Plane Creeping Flows

Consider a plane flow for which we have

$$\boldsymbol{v} = (v_1(x_1, x_2, t),\ v_2(x_1, x_2, t),\ 0); \quad p = p(x_1, x_2, t)\ . \tag{5.3}$$

In such a two-dimensional problem, incompressibility (1.73) is automatically satisfied by the introduction of a ***stream function*** ψ so that

$$v_1 = \frac{\partial \psi}{\partial x_2}, \quad v_2 = -\frac{\partial \psi}{\partial x_1}\ . \tag{5.4}$$

As the vorticity reduces to a single component $\boldsymbol{\omega} = (0, 0, \omega)$, it follows that

$$\omega = \frac{\partial v_2}{\partial x_1} - \frac{\partial v_1}{\partial x_2} = -\Delta \psi\ , \tag{5.5}$$

and relation (5.2) becomes

$$\frac{\partial \Delta \psi}{\partial t} = \nu \Delta \Delta \psi\ . \tag{5.6}$$

For a stationary problem, we will have

$$\Delta \Delta \psi = 0\ , \tag{5.7}$$

showing that in this case the stream function is a biharmonic function.

In polar coordinates (r, θ), the conservation of mass becomes

$$\frac{1}{r}\frac{\partial}{\partial r}(r v_r) + \frac{1}{r}\frac{\partial v_\theta}{\partial \theta} = 0\ . \tag{5.8}$$

A stream function ψ also exists such that

$$v_r = \frac{1}{r}\frac{\partial \psi}{\partial \theta}, \quad v_\theta = -\frac{\partial \psi}{\partial r}\ . \tag{5.9}$$

5.1.1 Flow in a Corner

Let us consider the flow in a corner as presented in Fig. 5.1. The lower wall is fixed while the wall inclined at an angle θ_0 is in uniform translational motion at the constant velocity U in the direction x_1. Near the origin, the velocity gradients are large; nonetheless, we expect the viscous forces to dominate in the neighborhood of the origin. To formulate the problem in steady state, we choose a coordinate system with the origin at the intersection of the two walls, in motion with the inclined wall. In this case, the boundary conditions are written as

$$\frac{1}{r}\frac{\partial \psi}{\partial \theta} = -U, \qquad \frac{\partial \psi}{\partial r} = 0 \quad \text{at} \quad \theta = 0 \tag{5.10}$$

$$\frac{1}{r}\frac{\partial \psi}{\partial \theta} = 0, \qquad \frac{\partial \psi}{\partial r} = 0 \quad \text{at} \quad \theta = \theta_0 \, . \tag{5.11}$$

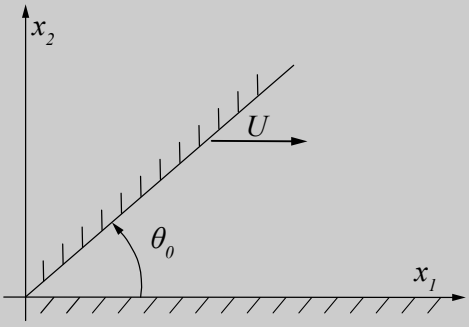

Fig. 5.1 Flow in a corner of angle θ_0. The coordinate system moves at the upper wall velocity U

The form of the boundary conditions suggests that we can write ψ in the following form:

$$\psi = r\, f(\theta) \, . \tag{5.12}$$

Substituting (5.12) in the biharmonic equation

$$\nabla^4 \psi = \left(\frac{1}{r}\frac{\partial}{\partial r} + \frac{\partial^2}{\partial r^2} + \frac{1}{r^2}\frac{\partial^2}{\partial \theta^2}\right)\left(\frac{1}{r}\frac{\partial \psi}{\partial r} + \frac{\partial^2 \psi}{\partial r^2} + \frac{1}{r^2}\frac{\partial^2 \psi}{\partial \theta^2}\right) = 0 \, , \tag{5.13}$$

we find the relation

$$\frac{1}{r^3}\left(\frac{d^4 f}{d\theta^4} + 2\frac{d^2 f}{d\theta^2} + f\right) = 0 \, , \tag{5.14}$$

for which the solution is

$$f(\theta) = A\sin\theta + B\cos\theta + C\theta\sin\theta + D\theta\cos\theta\ . \tag{5.15}$$

(Recall that if H is a harmonic function, θH is a biharmonic function). The imposition of the boundary conditions (5.10) and (5.11) allows us to evaluate the constants which are

$$A, B, C, D = \left(-\theta_0^2, 0, \theta_0 - \sin\theta_0\cos\theta_0, \sin^2\theta_0\right)\frac{U}{\theta_0^2 - \sin^2\theta_0}\ . \tag{5.16}$$

For the special case of a right angle, we have

$$\psi = \frac{rU}{(\frac{\pi}{2})^2 - 1}\left(-(\frac{\pi}{2})^2\sin\theta + \frac{\pi}{2}\theta\sin\theta + \theta\cos\theta\right)\ , \tag{5.17}$$

from which we can easily obtain the velocity components

$$v_r = \frac{U}{(\frac{\pi}{2})^2 - 1}\left((1 - \frac{\pi^2}{4})\cos\theta + \frac{\pi}{2}(\sin\theta + \theta\cos\theta) - \theta\cos\theta\right) \tag{5.18}$$

$$v_\theta = -\frac{U}{(\frac{\pi}{2})^2 - 1}\left(-(\frac{\pi}{2})^2\sin\theta + \frac{\pi}{2}\theta\sin\theta + \theta\cos\theta\right)\ . \tag{5.19}$$

In retrospect we can examine the correctness of the creeping flow assumption. We see that the acceleration components (A.11) and (A.12) evaluated with the preceding solution are proportional to U^2/r with a factor that depends on θ, that is, of the order of unity. As for the viscous effects, they are of the order of $\mu U/r^2$. Thus the creeping flow assumption is met when $\rho rU/\mu \ll 1$. This is the case in the region close to the origin such that $r \ll \nu U$. Further away, the solution will no longer be correct as the inertial forces rapidly become of the same order of magnitude as the viscous forces.

It is interesting to compute the pressure from Eq. (A.22):

$$\frac{\partial p}{\partial\theta} = r\mu\left(\triangle v_\theta + \frac{2}{r^2}\frac{\partial v_r}{\partial\theta} - \frac{v_\theta}{r^2}\right) = r\mu\left(-\triangle\frac{\partial\psi}{\partial r} + \frac{2}{r^3}\frac{\partial^2\psi}{\partial\theta^2} + \frac{1}{r^2}\frac{\partial\psi}{\partial r}\right)\ , \tag{5.20}$$

which yields

$$p = \frac{2\mu}{r(\theta_0^2 - \sin^2\theta_0)}\left((\frac{1}{2}\sin 2\theta_0 - \theta_0)\sin\theta - \sin^2\theta_0\cos\theta\right)\ . \tag{5.21}$$

Observe that the pressure varying like r^{-1} becomes unbounded when we approach the corner. This dismal performance comes from the fact that at the corner the boundary conditions are not consistent with the real problem, which has always a tiny gap so that the forces remain finite.

5.2 Two-Dimensional Corner Moffatt Eddies

Plane Stokes flows occur in engineering or physical problems in the neighborhood of slots or cracks in a wall. This situation is modeled by analyzing the creeping flow close to the vertex of a sharp wedge with an aperture angle 2α formed by the walls $\theta = \pm\alpha$ as shown in Fig. 5.2.

The forcing mechanism generating the corner flow is "far" from the wedge vertex. For example, in the lid-driven square cavity problem, corner vortices are generated by the influence of the main primary vortex.

For the flow in a wedge, two geometrical configurations are possible: the flow is asymmetric with respect to the symmetry axis $\theta = 0$; the flow is symmetric in θ and the symmetry axis plays the role of a mirror.

Here we will concentrate on the asymmetric case shown in Fig. 5.2 with the assumption of 2D creeping flow described by the stream function. The governing equation is still (5.7) which in polar coordinates is given by

$$\Delta\Delta\psi = \left(\frac{\partial^2}{\partial r^2} + \frac{1}{r}\frac{\partial}{\partial r} + \frac{1}{r^2}\frac{\partial^2}{\partial\theta^2}\right)^2 \psi \,. \tag{5.22}$$

We look for separable solutions of (5.22) expressed by

$$\psi = r^\lambda f(\theta) \,, \tag{5.23}$$

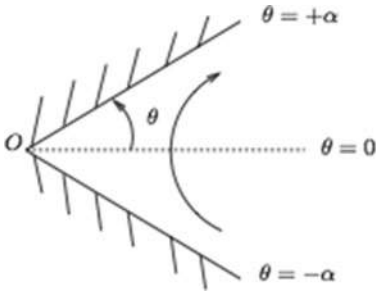

Fig. 5.2 Geometry of the corner flow

where λ is a real or complex number. Carrying through the algebra, the biharmonic equation yields

$$\Delta\Delta\psi = r^{\lambda-4}\left(\frac{d^2}{d\theta^2}+\lambda^2\right)\left(\frac{d^2}{d\theta^2}+(\lambda-2)^2\right) f = 0\,. \tag{5.24}$$

For $\lambda \neq 0, 1, 2$, the solution of (5.24) is given by

$$\psi = r^{\lambda}(Ae^{i\lambda\theta} + Be^{i(\lambda-2)\theta})\,. \tag{5.25}$$

Following Moffatt [60], the two-dimensional streamfunction is expanded in a series of basic solutions $\psi = r^{\lambda} f(\theta)$

$$\psi = \Re \sum_{n=1}^{\infty} A_n r^{\lambda_n} f_{\lambda_n}(\theta)\,, \tag{5.26}$$

where the A_n are complex numbers and the λ_n satisfy the condition

$$1 < \Re\lambda_1 < \Re\lambda_2 < \cdots \tag{5.27}$$

The first inequality imposes that the flow vanish at the origin, which is located at the corner. The remaining inequalities indicate that the first term in (5.26) dominates over the others and then

$$\psi \approx A_1 r^{\lambda_1} f_{\lambda_1}(\theta) = A r^{\lambda} f_{\lambda}(\theta)\,. \tag{5.28}$$

As for the asymmetric solution $v_r(r, -\theta) = -v_r(r, \theta)$ and $v_\theta(r, -\theta) = v_\theta(r, \theta)$, the function f_λ has to be even in θ. The term in between parentheses in solution (5.25) is rewritten as

$$A\sin\lambda\theta + B\cos\lambda\theta + C\cos(\lambda-2)\theta + D\sin(\lambda-2)\theta\,, \tag{5.29}$$

and is such that the constants A and D vanish:

$$f_\lambda = B\cos\lambda\theta + C\cos(\lambda-2)\theta\,. \tag{5.30}$$

The no slip boundary conditions on the two walls $f_\lambda(\pm\alpha) = f'_\lambda(\pm\alpha) = 0$ yield the system

$$B\cos\lambda\alpha + C\cos(\lambda-2)\alpha = 0\,, \tag{5.31}$$

$$B\lambda\sin\lambda\alpha + C(\lambda-2)\sin(\lambda-2)\alpha = 0\,. \tag{5.32}$$

For a nonzero solution the determinant of this system must vanish, i.e.

$$\sin 2(\lambda - 1)\alpha + (\lambda - 1)\sin 2\alpha = 0\,. \tag{5.33}$$

5.2.1 Real Solutions for λ ($\alpha > 73.15^{\nabla}$)

The nonlinear equation (5.33) gives real solutions for an angle $\alpha > 73.15°$. Figure 5.3 shows the real solutions obtained as the intersections of the sine function $\sin 2(\lambda - 1)\alpha$ in black and the straight line $-(\lambda - 1)\sin 2\alpha$ in green with respect to the variable $(\lambda - 1)\alpha$. The smallest value is the relevant one when we approach the corner $r \to 0$ as the solution goes like r^{λ}.

5.2.2 Complex Solutions for λ ($\alpha < 73.15^{\nabla}$)

Let us write $\lambda = p + 1 + iq$. The azimuthal velocity component is

$$v_\theta(r,\theta) = -\frac{\partial \psi}{\partial r} = \Re\left(-\lambda r^{\lambda-1} f(\theta)\right)\,. \tag{5.34}$$

On the symmetry axis of the corner, $\theta = 0$, and therefore

$$v_\theta(r,0) = \Re\left(-\lambda r^{\lambda-1} f(0)\right) = \Re\left(r^{\lambda-1} C\right)\,, \tag{5.35}$$

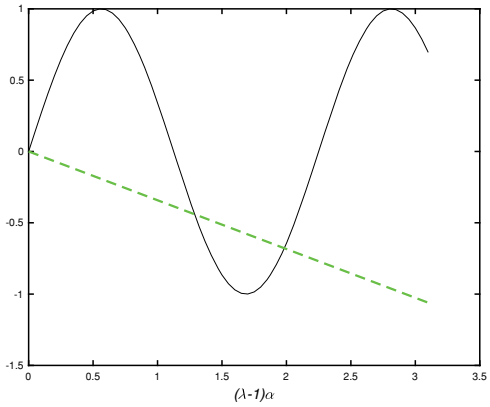

Fig. 5.3 Real solutions for $\alpha = 80°$

where $C = |C|e^{i\beta} \equiv -\lambda f(0)$. Equation (5.35) yields

$$v_\theta(r,0) = \Re\left(r^p|C|e^{iq\ln r}e^{i\beta}\right) = r^p|C|\cos(q\ln r + \beta)\ . \tag{5.36}$$

When $r \to 0$, $\ln r \to -\infty$ and the velocity $v_\theta(r,0)$ changes sign infinitely often. This behavior means that a string of counter-rotating vortices is present in the corner. The center of the nth corner eddy denoted by r_n is the distance of this center to the origin. It is given by the relation $v_\theta(r,0) = 0$ leading to

$$q\ln r_n + \beta = -(2n+1)\frac{\pi}{2},\ n = 0,1,2,\ldots, \quad \text{or} \quad r_n = e^{-(2n+1)\frac{\pi}{2q}}e^{-\frac{\beta}{q}}\ . \tag{5.37}$$

A simple calculation yields

$$\frac{r_n}{r_{n+1}} = \frac{r_n - r_{n+1}}{r_{n+1} - r_{n+2}} = e^{\frac{\pi}{q}}\ , \tag{5.38}$$

which shows that the sizes of the vortices fall off in geometrical progression with a common ratio $e^{\pi/q}$, depending on the aperture angle of the corner. If we now inspect the velocity maxima, we find $v_{\theta,max} = r^p|C|$ at points $r_{n+\frac{1}{2}} = e^{-n\frac{\pi}{2q}}e^{-\frac{\beta}{q}}$. The maximum velocity will be called the intensity of the eddy. The corner vortices have their intensities falling off in geometrical progression with the common ratio

$$\left|\frac{v_n}{v_{n+1}}\right| = \left|\frac{r_{n+\frac{1}{2}}}{r_{n+\frac{3}{2}}}\right|^p = e^{\pi p/q}\ , \tag{5.39}$$

which also depends on α.

The numerical solution of Eq. (5.33) for the angle α is given in Table 5.1.

We observe that λ decreases when α increases. Furthermore, the imaginary part $\Im\lambda$ goes to zero when α reaches the value 73.15°, meaning that λ then becomes real.

Table 5.1 Main eigenvalue λ with respect to the corner half angle

α	λ
2°	$61.34043791 + i\ 32.2266675$
10°	$13.0794799 + i\ 6.3843883$
20°	$7.0578309 + i\ 3.0953659$
30°	$5.0593290 + i\ 1.9520499$
40°	$4.0674345 + i\ 1.3395862$
50°	$3.4792155 + i\ 0.9303733$
60°	$3.0941391 + i\ 0.6045850$
70°	$2.8268686 + i\ 0.2616953$
73.155°	$2.7634862 + i\ 0$

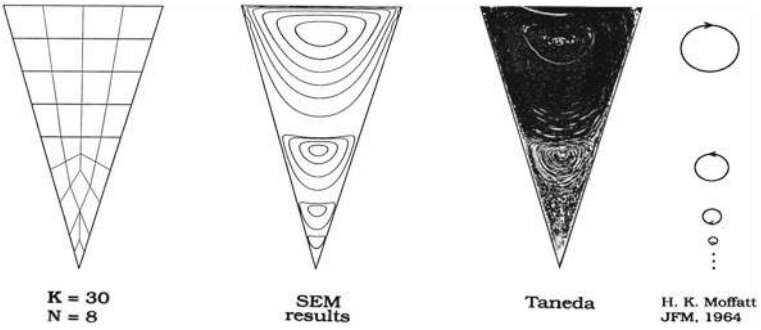

Fig. 5.4 Corner flow in a wedge of aperture $\alpha = 28.5°$. (Courtesy of E. Rønquist [81]. Taneda picture [102] (c) (1979) The Physics Society of Japan, is reprinted with permission)

Figure 5.4 shows a spectral element solution computed by Einar Rønquist [81] for the Stokes flow in a wedge. As the top lid moves at unit velocity, a series of Moffat corner eddies is generated. These eddies are stacked from top to bottom in an infinite cascade to the tip. The wedge shown has an aperture angle of 28.5°. The asymptotic ratio of successive eddy intensities is 405. With the discretization comprising 30 elements of polynomial degree 8 shown in the figure, one obtains four eddies. The ratio of the strength of two successive eddies is from top to bottom 386, 406, and 411. We observe also that the computed results are very close to the experimental data provided by Taneda [102] and Van Dyke [114].

5.3 Stokes Eigenmodes

Most state-of-the-art numerical methods dealing with the Navier–Stokes equation rely on an implicit treatment of the Stokes operator and an explicit scheme for the nonlinearity (rejecting it as a source term). Hence it is essential to understand the structure of the Stokes operator. Furthermore if we can write the eigenmodes in closed form, or if we can compute them accurately, then we are able to use those modes as the basis for the approximation of the Stokes equation, see for example Batcho-Karniadakis [12].

The Stokes eigenproblem is defined by setting $\frac{\partial \boldsymbol{v}}{\partial t} = \lambda \boldsymbol{v}$ in Eq. (2.54) and assuming that $\boldsymbol{b} = \boldsymbol{0}$. The eigenvalue λ provides the growth or decay rate of the velocity field. Now the eigensystem becomes

$$\lambda \boldsymbol{v} - \nu \Delta \boldsymbol{v} + \nabla p = \boldsymbol{0} \quad \text{in} \quad \Omega\,, \tag{5.40}$$

$$\operatorname{div} \boldsymbol{v} = 0 \quad \text{in} \quad \Omega\,, \tag{5.41}$$

$$\boldsymbol{v} = \boldsymbol{0} \quad \text{on} \quad \partial\Omega\,, \tag{5.42}$$

where p is normalized by ρ, Ω the problem domain and $\partial\Omega$ its boundary.

5.3.1 Periodic Stokes Eigenmodes

Let us consider the fully periodic solutions of the transient Stokes problem Eqs. (2.54) in the open square domain $\Omega =]-1, +1[^2$ with the Fourier approximation

$$\begin{aligned} \boldsymbol{v}(\boldsymbol{x}, t) &= \sum_{\|\boldsymbol{k}\|<\infty} \widehat{\boldsymbol{v}}(\boldsymbol{k}) e^{i(\boldsymbol{k}\cdot\boldsymbol{x}+\omega t)}, \quad p = \sum_{\|\boldsymbol{k}\|<\infty} \widehat{p}(\boldsymbol{k}) e^{i(\boldsymbol{k}\cdot\boldsymbol{x}+\omega t)} , \\ \boldsymbol{b}(\boldsymbol{x}, t) &= \sum_{\|\boldsymbol{k}\|<\infty} \widehat{\boldsymbol{b}}(\boldsymbol{k}) e^{i(\boldsymbol{k}\cdot\boldsymbol{x}+\omega t)} , \end{aligned} \tag{5.43}$$

where $\widehat{\boldsymbol{v}}$, $\widehat{p}$, $\widehat{\boldsymbol{b}}$ are the complex Fourier coefficients, $\boldsymbol{k}$ the wavevector and ω a complex frequency. The notation $\|\boldsymbol{k}\| < \infty$ is defined to mean $-\infty < k_i < +\infty$ for $i = 1, 2$.

Let us denote $\boldsymbol{e_k}$ the unit vector in the direction of $\boldsymbol{k}$. Then $\boldsymbol{k} = k\, \boldsymbol{e_k}$. The solution is easily obtained

$$\widehat{p} = -i \frac{\boldsymbol{e_k} \cdot \widehat{\boldsymbol{b}}}{k}, \quad (i\omega + \nu k^2)\widehat{\boldsymbol{v}} = \left(\widehat{\boldsymbol{b}} - \boldsymbol{e_k}(\boldsymbol{e_k} \cdot \widehat{\boldsymbol{b}}\right) . \tag{5.44}$$

The resulting periodic eigenmode corresponding to $\lambda = i\,\omega$ is

$$\widehat{p} = 0, \quad (\lambda + \nu k^2)\widehat{\boldsymbol{v}} = \boldsymbol{0}, \quad \boldsymbol{k} \cdot \widehat{\boldsymbol{v}} = 0 . \tag{5.45}$$

The periodic Stokes modes are constant pressure modes driven only by diffusion as $\lambda = -\nu k^2$. The incompressibility constraint div $\boldsymbol{v} = 0$ does not influence the space configuration, except that the wavevector $\boldsymbol{k}$ must be orthogonal to the velocity. Geometrically speaking the velocity is contained in a plane perpendicular to $\boldsymbol{k}$, while the pressure is aligned with the wavevector.

5.3.2 Channel Flow Stokes Eigenmodes

The problem is based on the plane channel flow between horizontal plates as treated in [69]. The flow is assumed periodic in the x_2 direction while it is confined by rigid walls in $x_1 = \pm 1$. We seek a solution of the two-dimensional Stokes equation in the form

$$\boldsymbol{v}(\boldsymbol{x}, t) = \left(u(x_1)e^{ikx_2+\lambda t}, v(x_1)e^{ikx_2+\lambda t}\right), \quad p = p(x_1)e^{ikx_2+\lambda t} , \tag{5.46}$$

where k is a chosen wavenumber and u, v are complex functions. The Stokes equations satisfied by u, v, p are

$$\begin{aligned}
\lambda u &= -\frac{dp}{dx_1} + \nu\left(\frac{d^2u}{dx_1^2} - k^2 u\right) , \\
\lambda v &= -ikp + \nu\left(\frac{d^2v}{dx_1^2} - k^2 v\right) , \\
\frac{du}{dx_1} &+ ikv = 0 ,
\end{aligned} \tag{5.47}$$

for $-1 \leq x_1 \leq +1$. The boundary conditions are

$$\boldsymbol{v}(\pm 1, x_2, t) = \mathbf{0} , \tag{5.48}$$

for no-slip walls. The elimination of v and p in Eqs. (5.47) yields

$$\lambda \left(D^2 - k^2\right) u = \nu \left(D^2 - k^2\right)^2 u , \tag{5.49}$$

with $u(\pm 1) = Du(\pm 1) = 0$, where $D = d/dx_1$. The solutions of Eq. (5.49) are either symmetric in x_1

$$u(x_1) = \cos\mu \cosh k x_1 - \cosh k \cos \mu x_1 , \tag{5.50}$$

or antisymmetric

$$u(x_1) = \sin\mu \sinh k x_1 - \sinh k \sin \mu x_1 . \tag{5.51}$$

The eigenvalues are

$$\lambda = -\nu(\mu^2 + k^2) , \tag{5.52}$$

satisfying the relations

$$k \tanh k = -\mu \tan \mu , \tag{5.53}$$

for (5.50) and

$$k \coth k = \mu \cot \mu , \tag{5.54}$$

for (5.51). For $k = 1$ and $k = 10$, the first symmetric eigenmode decays with $\lambda/\nu = -9.3137$ and $\lambda/\nu = -103.0394$, respectively, while, for $k = 1$ and $k = 10$, the antisymmetric eigenmode decays with $\lambda/\nu = -20.5706$ and $\lambda/\nu = -112.0836$. All the eigenvalues λ are real and negative, indicating strong damping by the viscous forces.

This problem is an excellent benchmark to test the accuracy of numerical methods treating the velocity-pressure formulation of the Navier–Stokes equations.

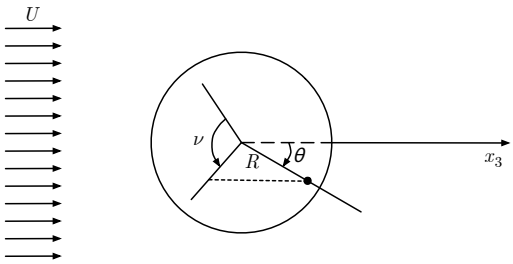

Fig. 5.5 Flow around a sphere

5.4 Parallel Flow Around a Sphere

A sphere of radius R is in a viscous steady state flow for which the velocity at infinity upstream is U. We assume a creeping flow such that we can have a solution of the Stokes equation (2.54). We place the Cartesian coordinate system such that the axis x_3 is oriented in the direction of the flow incident on the sphere (Fig. 5.5). The boundary conditions expressed in spherical coordinates (see Fig. B.1) are

$$\boldsymbol{v} = \boldsymbol{0} \quad \text{at} \quad r = R, \tag{5.55}$$

$$\boldsymbol{v} = U\boldsymbol{e}_3 \quad \text{at} \quad r = \infty\,. \tag{5.56}$$

The problem thus posed is symmetric about the axis Ox_3, and with respect to the longitude of the sphere. Consequently, $\partial(\bullet)/\partial\varphi \equiv 0$. Also then, $v_\varphi = 0$. Thus the mass conservation equation (B.20) reduces to

$$\frac{1}{r^2}\frac{\partial}{\partial r}(r^2\, v_r) + \frac{1}{r\sin\theta}\frac{\partial}{\partial\theta}(v_\theta \sin\theta) = 0\,. \tag{5.57}$$

We deduce that a stream function ψ exists such that

$$v_r = \frac{1}{r^2\sin\theta}\frac{\partial\psi}{\partial\theta}, \quad v_\theta = -\frac{1}{r\sin\theta}\frac{\partial\psi}{\partial r}\,. \tag{5.58}$$

Given the two-dimensional character of the flow, the vorticity will have a single component in the direction of the vector $\boldsymbol{e}_\varphi$ that we denote ω. We write (cf. (B.5))

$$\omega(r,\theta) = -\frac{1}{r}\left[\frac{1}{\sin\theta}\frac{\partial^2\psi}{\partial r^2} + \frac{1}{r^2}\frac{\partial}{\partial\theta}\left(\frac{1}{\sin\theta}\frac{\partial\psi}{\partial\theta}\right)\right]\,. \tag{5.59}$$

In the case of the Stokes equation, vorticity is a harmonic function. We have (recall that the Laplacian of a vector is not equal to the Laplacian of its components, cf. (B.7))

$$\Delta\omega - \frac{\omega}{r^2 \sin^2\theta} = \frac{1}{r^2}\left(\frac{\partial}{\partial r}\left(r^2 \frac{\partial \omega}{\partial r}\right) + \frac{1}{\sin\theta}\frac{\partial}{\partial \theta}\left(\sin\theta \frac{\partial \omega}{\partial \theta}\right) - \frac{\omega}{\sin^2\theta}\right)$$

$$= \frac{1}{r}\frac{\partial^2}{\partial r^2}(r\omega) + \frac{1}{r^2}\frac{\partial}{\partial \theta}\left(\frac{1}{\sin\theta}\frac{\partial}{\partial \theta}(\omega \sin\theta)\right) \tag{5.60}$$

$$= 0\,. \tag{5.61}$$

The combination of relations (5.59)–(5.61) gives the following biharmonic equation:

$$\left(\frac{\partial^2}{\partial r^2} + \frac{\sin\theta}{r^2}\frac{\partial}{\partial \theta}\left(\frac{1}{\sin\theta}\frac{\partial}{\partial \theta}\right)\right)^2 \psi = 0\,. \tag{5.62}$$

The boundary conditions (5.55) and (5.56), expressed in terms of the stream function, become

$$\begin{aligned} &\frac{\partial \psi}{\partial \theta} = \frac{\partial \psi}{\partial r} = 0, \quad \text{at} \quad r = R, \\ &v_r = U\cos\theta, \quad \frac{\partial \psi}{\partial \theta} = U r^2 \sin\theta\cos\theta, \quad \text{at} \quad r = \infty \\ &v_\theta = -U\sin\theta, \quad \frac{\partial \psi}{\partial r} = U r \sin^2\theta. \end{aligned} \tag{5.63}$$

The condition at infinity can be easily integrated. It follows that

$$\psi_\infty = \frac{1}{2} U r^2 \sin^2\theta\,. \tag{5.64}$$

The form of this expression for ψ suggests that the stream function can be written in the general form

$$\psi = \sin^2\theta\, f(r)\,. \tag{5.65}$$

Introducing (5.65) into (5.62), we find

$$\frac{d^4 f}{dr^4} - \frac{4}{r^2}\frac{d^2 f}{dr^2} + \frac{8}{r^3}\frac{df}{dr} - \frac{8}{r^4} f = 0\,. \tag{5.66}$$

Seeking a solution as a power series in r^n, we obtain the characteristic polynomial

$$(n-2)(n-1)\left(n^2 - 3n - 4\right) = 0\,,$$

whose roots are $n = -1, 1, 2,$ and 4. The function $f(r)$ is thus

$$f = \frac{C_{-1}}{r} + C_1 r + C_2 r^2 + C_4 r^4\,. \tag{5.67}$$

The imposition of the boundary condition at infinity, (5.64), requires $C_4 = 0$ and $C_2 = \frac{1}{2}U$, while at the sphere, with $v_r = v_\theta = 0$, we can determine $C_{-1} = (1/4)U\,R^3$, $C_1 = -(3/4)U\,R$. The stream function is then

$$\psi = \frac{U R^2}{2} \sin^2\theta \left(\frac{R}{2r} - \frac{3}{2}\frac{r}{R} + (\frac{r}{R})^2 \right) . \tag{5.68}$$

We can easily deduce the velocities from (5.58)

$$v_r = U \cos\theta \left[\frac{1}{2}(\frac{R}{r})^3 - \frac{3}{2}\frac{R}{r} + 1 \right] \tag{5.69}$$

$$v_\theta = U \sin\theta \left[\frac{1}{4}(\frac{R}{r})^3 + \frac{3}{4}\frac{R}{r} - 1 \right] . \tag{5.70}$$

The Cartesian velocity components are linked to the spherical components by the transformation

$$\begin{pmatrix} v_1 \\ v_2 \\ v_3 \end{pmatrix} = \begin{pmatrix} \sin\theta\cos\varphi & \cos\theta\cos\varphi & -\sin\varphi \\ \sin\theta\sin\varphi & \cos\theta\sin\varphi & \cos\varphi \\ \cos\theta & -\sin\theta & 0 \end{pmatrix} \begin{pmatrix} v_r \\ v_\theta \\ v_\varphi \end{pmatrix} . \tag{5.71}$$

Using (5.71), Eqs. (5.69) and (5.70) yield

$$\begin{aligned} v_1 &= -\frac{3}{4}\frac{U R x_1 x_3}{r^3}\left(1 - \frac{R^2}{r^2}\right) , \\ v_2 &= -\frac{3}{4}\frac{U R x_2 x_3}{r^3}\left(1 - \frac{R^2}{r^2}\right) , \\ v_3 &= U\left[1 - \frac{3}{4}\frac{R x_3^2}{r^3}\left(1 - \frac{R^2}{r^2}\right) - \frac{1}{4}\frac{R}{r}\left(3 + \frac{R^2}{r^2}\right)\right] , \end{aligned} \tag{5.72}$$

as we have

$$\begin{aligned} x_1 &= r\sin\theta\cos\varphi \\ x_2 &= r\sin\theta\sin\varphi \\ x_3 &= r\cos\theta . \end{aligned}$$

The vorticity field is written (cf. (5.59))

$$\omega = -\frac{3}{2} U R\,(\frac{\sin\theta}{r^2}) . \tag{5.73}$$

The calculation of the pressure field can easily be accomplished by taking into account the vector identity (4.20) which leads to the Stokes equation

$$\nabla p = -\mu \, \mathbf{curl}\, \boldsymbol{\omega} \, . \tag{5.74}$$

With (B.5), we generate the system of equations

$$\frac{\partial p}{\partial r} = -\frac{\mu}{r \sin\theta} \frac{\partial}{\partial \theta} (\omega \, \sin\theta) = 3\mu \, U \, R \frac{\cos\theta}{r^3} \, , \tag{5.75}$$

$$\frac{1}{r} \frac{\partial p}{\partial \theta} = \frac{\mu}{r} \frac{\partial (r\omega)}{\partial r} = \frac{3\mu}{2} U \, R \frac{\sin\theta}{r^3} \, . \tag{5.76}$$

Integration of (5.75) yields

$$p = -\frac{3\mu}{2} \, U \, R \frac{\cos\theta}{r^2} + q(\theta) \, .$$

Inserting this result in (5.76), we have

$$\frac{3\mu}{2} \, U \, R \frac{\sin\theta}{r^3} + \frac{q'(\theta)}{r} = \frac{3\mu}{2} U \, R \frac{\sin\theta}{r^3} \, .$$

The pressure field is then finally given by

$$p = -\frac{3\mu}{2} \, U \, R \frac{\cos\theta}{r^2} + p_0 \, , \tag{5.77}$$

with p_0 a constant reference pressure.

The uniform velocity flow around a sphere will generate pressure and shear forces. To calculate the pressure force in direction Ox_3, we integrate the elementary forces over the surface of the sphere

$$dF_{3,p} = -(\frac{3\mu}{2} \, U \, \frac{\cos\theta}{R} + p_0) \cos\theta \, (2\pi R^2 \sin\theta) \, d\theta \, . \tag{5.78}$$

The factor 2π comes from the symmetry of the problem which allows us to take into account the longitudinal part of the integral. Integrating from $\theta = 0$ to $\theta = \pi$, we obtain

$$F_{3,p} = -2\pi \mu \, U \, R \, . \tag{5.79}$$

Friction drag is obtained by integration over the sphere of the shear stress that acts on it, that is, $\sigma_{r\theta}$ (cf. (B.19)) which is $-3\mu U \sin\theta/(2R)$ for $r = R$. This leads to

$$F_{3,\sigma} = -\int_{\theta=0}^{\theta=\pi} (\sigma_{r\theta} \mid_{r=R} \sin\theta) \, (2\pi R^2 \sin\theta) \, d\theta = -4\pi \mu \, U \, R \, . \tag{5.80}$$

Total drag, $F_3 = F_{3,p} + F_{3,\sigma}$, known as ***Stokes drag***, is the sum of the pressure force and the friction force

$$F_3 = -6\pi \mu \, U \, R \, . \tag{5.81}$$

If we define the drag coefficient by

$$C_D = \frac{|F_3|}{\frac{1}{2}\rho U^2 \pi R^2}, \tag{5.82}$$

we obtain

$$C_D = \frac{24}{Re}, \tag{5.83}$$

where $Re = 2UR/\nu$. Note that the pressure drag represents one third of the total drag. Relation (5.83) is verified by experiments when $Re < 1$ which is valid in the neighborhood of the sphere. When we move away, the importance of the inertial terms grows and the Stokes solution diverges from the exact solution. Note that the solution that we have obtained is not applicable to the case of a set of spherical particles, as the presence of a spherical obstacle in the flow has impact relatively far away since the velocity profiles decrease as $1/r$.

The solution for uniform flow around a fixed sphere can be transposed to the case of translation at uniform velocity U of a sphere of radius R in a fluid at rest at infinity. In this case, the coordinate system is still attached to the sphere and thus in translation at uniform velocity. This modifies the sign of U to become $-U$ for the pressure and the vorticity. As for the velocity in the fluid, this is relative to the coordinate system, which leads to the following modifications: for the velocity and the stream function, U becomes $-U$ and the uniform velocity field must also be subtracted from the corresponding relations.

5.4.1 Oseen's Improvement

The Stokes solution was improved by Oseen [70] who proposed the solution of the Navier–Stokes equations (1.74) as a sum of uniform velocity field and a perturbation such that

$$\boldsymbol{v} = U\,\boldsymbol{e}_3 + \boldsymbol{v}'\,. \tag{5.84}$$

In the case of the flow around a fixed sphere, the velocity $\boldsymbol{v}'$ then takes into account the perturbation caused by the sphere in a flow uniform at infinity. With (5.84), the stationary inertial term takes the form

$$\rho \frac{D\boldsymbol{v}}{Dt} = \rho \left(v'_j \frac{\partial v'_i}{\partial x_j} + U \frac{\partial v'_i}{\partial x_3} \right)\,. \tag{5.85}$$

Oseen's assumption amounts to neglecting the first term with respect to the second term on the right-hand side of Eq. (5.85). We obtain a linearized Navier–Stokes equation

$$\rho\, U \frac{\partial \boldsymbol{v}'}{\partial x_3} = -\boldsymbol{\nabla}\, p + \mu\, \Delta \boldsymbol{v}' + \rho \boldsymbol{b}\,. \tag{5.86}$$

The drag coefficient obtained with Oseen's solution is

$$C_D = \frac{24}{Re}(1 + \frac{3}{16}Re) \, . \tag{5.87}$$

Experimental results show that (5.87) is approximately valid for $Re < 5$. Using matched asymptotic expansions [49], the corrected coefficient becomes

$$C_D = \frac{24}{Re}(1 + \frac{3}{16}Re - \frac{19}{1280}Re^2 + O(Re^3)) \, . \tag{5.88}$$

Another approximation for the drag coefficient is given as

$$C_D = \frac{24}{Re}[1 + \frac{3}{16}Re + \frac{9}{160}Re^2 \ln Re + O(Re^2)] \, . \tag{5.89}$$

For a quantitative outline of the analysis leading to (5.89), we refer the reader to Proudman and Pearson [75].

A more accurate relation for the drag is proposed by Ockendon and Ockendon [64]:

$$C_D = \frac{24}{Re}[1 + \frac{3}{16}Re + \frac{9}{160}Re^2 \ln Re + \frac{1}{160}(9\gamma + 15 \ln 2 - \frac{323}{40})Re^2 + \cdots] \, ,$$

where $\gamma = 0.5772156649$ is Euler's constant.

5.5 Parallel Flow Around a Cylinder

After the detailed study of the flow around a sphere, we would like to investigate the case of a uniform steady state parallel flow impinging a fixed circular cylinder. We will unfold the same steps as in the previous section in order to compare both theoretical developments and draw conclusions about the impact of the geometrical configurations on the analytical results.

A cylinder of radius R is placed in a uniform parallel flow for which the velocity at infinite upstream is U. We assume again a creeping flow described by the Stokes equation (2.54). We place the Cartesian coordinate system such that the axis x_3 is oriented in the direction of the flow incident on the cylinder (Fig. 5.6). The boundary conditions expressed in cylindrical or more precisely in polar coordinates are

$$\boldsymbol{v} = \boldsymbol{0} \quad \text{at} \quad r = R, \tag{5.90}$$

$$\boldsymbol{v} = U\boldsymbol{e}_3 \quad \text{at} \quad r = \infty \, . \tag{5.91}$$

The flow is two-dimensional and therefore $v_z = 0$. The velocity field is such that $\boldsymbol{v} = (v_r(r, \theta), v_\theta(r, \theta), 0)$. The mass conservation equation (A.2) reduces to

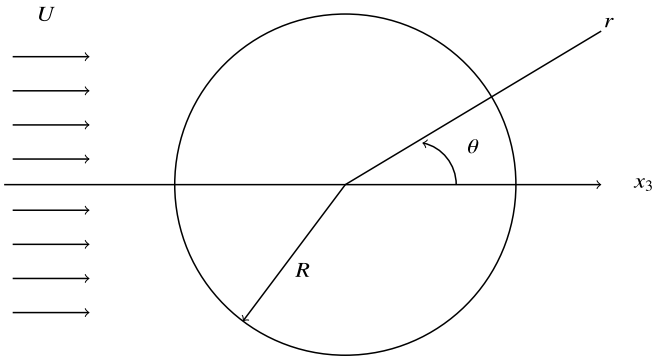

Fig. 5.6 Flow around a circular cylinder

$$\frac{1}{r}\frac{\partial}{\partial r}(r v_r) + \frac{1}{r}\frac{\partial v_\theta}{\partial \theta} = 0\,. \tag{5.92}$$

We deduce that a stream function ψ exists such that

$$v_r = \frac{1}{r}\frac{\partial \psi}{\partial \theta}, \quad v_\theta = -\frac{\partial \psi}{\partial r}\,. \tag{5.93}$$

Given the two-dimensional character of the flow, the vorticity will have a single component in the direction orthogonal to the plane that we denote ω. We can then write (see Eq. (A.6))

$$\omega(r,\theta) = -\frac{1}{r}\left(\frac{\partial}{\partial r}(r v_\theta) - \frac{\partial v_r}{\partial \theta}\right) \tag{5.94}$$

$$= -\left(\frac{1}{r}\frac{\partial \psi}{\partial r} + \frac{\partial^2 \psi}{\partial r^2} + \frac{1}{r^2}\frac{\partial^2 \psi}{\partial \theta^2}\right)\,. \tag{5.95}$$

As vorticity is a harmonic function, its Laplacian is given by

$$\Delta\omega = \frac{1}{r}\frac{\partial}{\partial r}\left(r\frac{\partial \omega}{\partial r}\right) + \frac{1}{r^2}\frac{\partial^2 \omega}{\partial \theta^2} = \frac{1}{r}\frac{\partial \omega}{\partial r} + \frac{\partial^2 \omega}{\partial r^2} + \frac{1}{r^2}\frac{\partial^2 \omega}{\partial \theta^2}\,. \tag{5.96}$$

The combination of relations (5.95)–(5.96) gives the following biharmonic equation:

$$\left(\frac{\partial^2}{\partial r^2} + \frac{1}{r}\frac{\partial}{\partial r} + \frac{1}{r^2}\frac{\partial^2}{\partial \theta^2}\right)^2 \psi = 0\,. \tag{5.97}$$

The boundary conditions (5.90) and (5.91), expressed in terms of the stream function, become

$$\frac{\partial \psi}{\partial \theta} = \frac{\partial \psi}{\partial r} = 0, \quad \text{at} \quad r = R, \tag{5.98}$$

$$v_r = U\cos\theta, \quad \frac{\partial \psi}{\partial \theta} = Ur\cos\theta, \quad \text{at} \quad r = \infty$$

$$v_\theta = -U\sin\theta, \quad \frac{\partial \psi}{\partial r} = U\sin\theta\ . \tag{5.99}$$

The condition at infinity suggests that the stream function can be written in the general form

$$\psi = f(r)\sin\theta\ . \tag{5.100}$$

Introducing (5.100) into (5.97), we find

$$\frac{d^4 f}{dr^4} + \frac{2}{r}\frac{d^3 f}{dr^3} - \frac{3}{r^2}\frac{d^2 f}{dr^2} + \frac{3}{r^3}\frac{df}{dr} - \frac{3}{r^4} f = 0\ . \tag{5.101}$$

Seeking a solution as a power series in r^n, we obtain the characteristic polynomial

$$(n-1)^2\left(n^2 - 2n - 3\right) = 0\ ,$$

whose roots are $n = -1, 1, 3$. Note that the root $n = 1$ is a double root. So far, the function $f(r)$ is

$$f = \frac{C_{-1}}{r} + C_1 r + C_3 r^3\ . \tag{5.102}$$

We need a fourth term to complete the expression of f. Michell [58] provided the full solution of the biharmonic equation in polar coordinates from which we extract the expression $r\log r$. Hence, eventually, we have

$$f = \frac{C_{-1}}{r} + C_1 r + C_3 r^3 + C_4 r\log r\ . \tag{5.103}$$

The r^3 term is rejected as it violates the regularity conditions at infinity. Using the boundary conditions on the cylinder (5.98), we obtain

$$\psi = C_1\sin\theta\left(\frac{1}{\overline{r}} - \overline{r} + 2\overline{r}\log\overline{r}\right)\ , \tag{5.104}$$

where $\overline{r} = r/R$. We note that it is impossible to satisfy the condition at infinity due to the presence of the logarithm.

Let us now satisfy the condition at infinity by setting $C_4 = 0$ and imposing $f(R) = 0$, one gets

$$f(\overline{r}) = C_1(\overline{r} - \frac{1}{\overline{r}})\ . \tag{5.105}$$

However it is impossible to satisfy $df/dr = 0$ at $r = R$.

This is Stokes paradox that shows there is no creeping flow around a circular cylinder unlike the flow around the sphere. To solve the paradox we need to resort to Oseen developments and matched asymptotic expansions for inner and outer expressions. We refer the reader to [46, 47].

5.6 Three-Dimensional Stokes Solution

In this section we present a three-dimensional solution for the steady Stokes equations

$$-\mu\Delta\boldsymbol{v} + \boldsymbol{\nabla} p = \boldsymbol{0} \quad \text{in} \quad \Omega\,, \tag{5.106}$$

$$\text{div}\ \boldsymbol{v} = 0 \quad \text{in} \quad \Omega\,. \tag{5.107}$$

This procedure is due to [106] and is based on harmonic solutions of the Laplace equation, assuming that separable solutions are relevant. The method works as follows. Suppose that $\boldsymbol{A}$ and B are vector and scalar fields satisfying Laplace's equations

$$A_{i,jj} = 0, \quad B_{,jj} = 0\,. \tag{5.108}$$

Then the velocity v_i and pressure p are given by the relationships

$$v_i = \frac{\partial}{\partial x_i}\left(r_j A_j + B\right) - 2A_i\,, \tag{5.109}$$

$$\frac{p}{\mu} = 2\,A_{j,j}\,, \tag{5.110}$$

where r_j are the components of the position vector. The proofs given in [106] are based on theoretical developments coming from elasticity theory, more precisely on the Papkovich–Neuber type of solution, cf. Chap. 7 in Botsis-Deville [16]. For the sake of simplicity, we will skip them. However let us examine how the methodology of solving both Laplace equations (5.108) and then combining the two harmonic solutions through (5.109)–(5.110) yields the Stokes solution. In Cartesian coordinates with $r_j = x_j$, Eqs. (5.109)–(5.110) give

$$v_i = \frac{\partial}{\partial x_i}(x_j A_j + B) - 2A_i = x_j A_{j,i} - A_i + B_{,i}\,, \tag{5.111}$$

$$\frac{p}{\mu} = 2A_{j,j}\,. \tag{5.112}$$

The incompressibility constraint is ensured

$$v_{i,i} = A_{i,i} + x_j A_{j,ii} - A_{i,i} + B_{,ii} = 0\,. \tag{5.113}$$

We next employ the equilibrium equation (5.106) and use (5.108) to eliminate some terms

$$\begin{aligned} v_{i,kk} &= \frac{\partial}{\partial x_k}\left(A_{k,i} + x_j A_{j,ik} - A_{i,k} + B_{i,k}\right) \\ &= A_{k,ik} + A_{k,ik} + x_j A_{j,ikk} - A_{i,kk} + B_{i,kk} = 2A_{k,ik} \\ &= \frac{1}{\mu}\frac{\partial p}{\partial x_i} \,. \end{aligned} \tag{5.114}$$

Let us apply the previous solution technique to the Stokes flow of a sphere of radius R moving at constant speed U in an infinite fluid, as reported in Sect. 5.4. We refer the problem to a Cartesian coordinate system with origin at the center of the sphere and with positive x_3-axis in the flow direction. The harmonic solutions are

$$A_1 = A_2 = 0, \quad A_3 = -U + \frac{3UR}{4r}, \qquad B = -\frac{Ux_3R^2}{4r^3} \,. \tag{5.115}$$

Using (5.115) in (5.111) we easily obtain the Eqs. (5.72).

Exercises

5.1 Hele-Shaw Flow

Let us consider the creeping flow between two fixed parallel plates, cf. Fig. 5.7, of a very viscous fluid in a layer of thickness $2h$. Inside the gap is placed an obstacle of cylindrical shape with its generators orthogonal to the plates, and of characteristic length L. The geometrical aspect ratio defined as

$$\varepsilon = \frac{h}{L} \,, \tag{5.116}$$

is such that $\varepsilon \ll 1$.

- With the incompressibility constraint (1.73) evaluate the order of magnitude of the velocity components.
- Evaluate the order of magnitude of the second order partial derivatives of v_1 and v_2.
- Show that the pressure is constant across the gap.
- Show that the velocity field may be written as

$$v_i(x_1, x_2, x_3) = v_i(x_1, x_2, 0)\, f(x_3) \,, \tag{5.117}$$

  with the origin of the axes located at mid-gap.
- Propose a solution for $f(x_3)$. Deduce the momentum equations for v_1, v_2.
- Show that

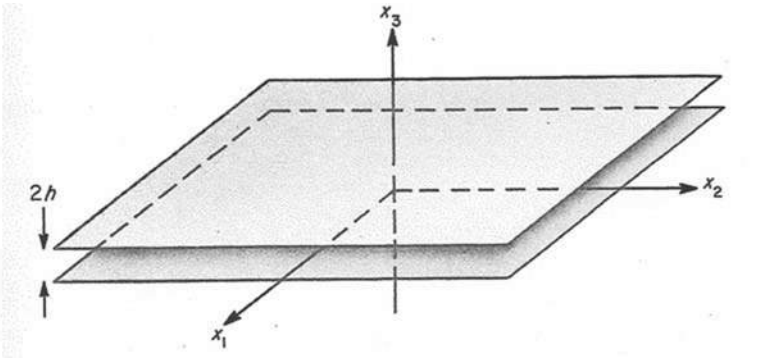

Fig. 5.7 Geometry for flow between parallel plates

$$v_i(x_1, x_2, 0) = -\frac{h^2}{2\mu}\frac{\partial p}{\partial x_i} \,. \tag{5.118}$$

- Compute the velocity potential.

5.2 Flow between parallel discs

In the parallel discs viscometer the fluid to be tested is contained in the cylindrical region of radius R between two discs. The lower plate is fixed and lies in the $z = 0$ plane, while the upper disc in the $z = h$ plane rotates at the angular velocity ω, cf. Fig. 5.8. This figure represents schematically such a viscosimeter. It is supposed that the angular velocity of the upper plate is small and that for small values of the applied torque, the velocities in a cylindrical coordinate system are such that

$$\boldsymbol{v} = (v_r, v_\theta, v_z) = (0, r\, f(z), 0) \tag{5.119}$$

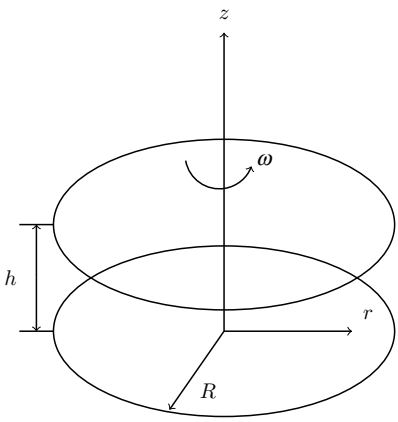

Fig. 5.8 Parallel discs and the associated coordinates

- Compute the velocity field
- As the angular velocity is small, it is assumed that $\partial p/\partial r = 0$. Deduce the hydrostatic pressure field.
- Evaluate the shear stress in the azimuthal direction. If the moment M to rotate the upper disc at velocity ω is known, generate the relation giving the viscosity μ as a function of M, h, ω, R.

Chapter 6
Plane Irrotational Flows of Perfect Fluid

In this chapter we consider the steady state two-dimensional irrotational flows of inviscid incompressible fluid. The monograph by L. M. Milne-Thomson [59] is a major contribution to the subject of this chapter.

In order to introduce the theory of complex variables, we will leave the index notation and use the standard coordinates, namely $x = x_1$, $y = x_2$. In that case the velocity components are $u = v_1$, $v = v_2$. We follow closely the book by Rhyming [83] that has been a cornerstone in the fluid mechanics courses of the Mechanical Engineering Department at the Swiss Institute of Technology Lausanne.

The assumption of irrotational flow induces the existence of a velocity potential such that

$$\boldsymbol{v} = \nabla\varphi \,. \tag{6.1}$$

The plane flow satisfies two relations

$$\nabla \cdot \boldsymbol{v} = \frac{\partial u}{\partial x} + \frac{\partial v}{\partial y} = 0 \tag{6.2}$$

$$\omega = \frac{\partial v}{\partial x} - \frac{\partial u}{\partial y} = 0 \,. \tag{6.3}$$

The incompressibility constraint is trivially satisfied by the stream function ψ

$$u = \frac{\partial \psi}{\partial y}, \quad v = -\frac{\partial \psi}{\partial x} \,. \tag{6.4}$$

On the other hand by the velocity potential, one has

$$u = \frac{\partial \varphi}{\partial x}, \quad v = \frac{\partial \varphi}{\partial y} \,. \tag{6.5}$$

M. O. Deville, *An Introduction to the Mechanics of Incompressible Fluids*,
https://doi.org/10.1007/978-3-031-04683-4_6

Let us show that the stream function and velocity potential are conjugate harmonic functions. Indeed, combining (6.1) and (6.2), one obtains $\Delta\varphi = 0$. Inserting (6.4) in (6.3), one gets $\Delta\psi = 0$. With (6.4) and (6.5), one writes

$$\frac{\partial\varphi}{\partial x} = \frac{\partial\psi}{\partial y}, \quad \frac{\partial\varphi}{\partial y} = -\frac{\partial\psi}{\partial x} . \tag{6.6}$$

These relations are the Cauchy-Riemann conditions. If the partial derivatives $\frac{\partial\varphi}{\partial x}, \frac{\partial\varphi}{\partial y}, \frac{\partial\psi}{\partial x}, \frac{\partial\psi}{\partial y}$ are continuous in a simply connected domain, relations (6.6) are necessary and sufficient conditions for the existence of a holomorphic (continuous, analytic and uniform) function $f(z)$ called the complex potential of the flow. It is defined as

$$f(z) = \varphi(x, y) + i\,\psi(x, y) \tag{6.7}$$

and depends on the complex variable $z = x + iy$, $i = \sqrt{-1}$. If the domain is multiply connected, the function given by (6.7) is analytic, although not necessarily uniform.

The complex analytic potential generates two sets of orthogonal curves: the equipotentials $\varphi = cst$ and the streamlines $\psi = cst$. From the definitions of the velocity potential and the stream function, it appears that the differentials $d\varphi$ and $d\psi$ are exact differentials

$$d\varphi = u\,dx + v\,dy , \tag{6.8}$$

$$d\psi = -v\,dx + u\,dy . \tag{6.9}$$

For an irrotational flow, the circulation of the velocity vector along a closed contour surrounding neither obstacle nor singularity is zero. We have using Stokes theorem

$$\Gamma = \int_C \boldsymbol{v}\cdot d\boldsymbol{\sigma} = \int_S \mathbf{curl}\,\boldsymbol{v}\cdot\boldsymbol{n}\,dS = 0 , \tag{6.10}$$

with $\boldsymbol{\sigma}$ the unit tangent vector to the curve C. In a simply connected domain, for any curvy segment located between points A and B, the circulation is independent on the followed path. One has

$$\Gamma = \int_A^B \boldsymbol{v}\cdot d\boldsymbol{\sigma} = \int_A^B (u\,dx + v\,dy) = \int_A^B d\varphi = \varphi_B - \varphi_A . \tag{6.11}$$

The flow rate Q across the segment AB is also independent on the path. One has

$$Q = \int_A^B \boldsymbol{v}\cdot\boldsymbol{n}\,d\tau = \int_A^B (un_x + vn_y)d\tau = \int_A^B (udy - vdx) = \int_A^B d\psi = \psi_B - \psi_A . \tag{6.12}$$

6.1 Complex Velocity

The use of complex variables enables the introduction of the velocity vector in the complex plane, namely $u + iv$. The conjugate velocity is called the *complex velocity*

$$w = u - iv \,, \tag{6.13}$$

which is evaluated by the derivative of the complex potential f by the relation

$$w = \frac{df}{dz} = u - iv \,. \tag{6.14}$$

As the function $f(z)$ is analytic, its derivative $f'(z)$ is independent on the way the limit is taken, i.e. on how the increment Δz goes to zero. As a reminder, by analogy with the derivative of a real function, one has

$$f'(z) = \frac{df}{dz} = \lim_{\Delta z \to 0} \frac{f(z + \Delta z) - f(z)}{\Delta z} \,. \tag{6.15}$$

It is easy to verify that using $\Delta z = \Delta x$ or $\Delta z = i\Delta y$, the same limit is obtained and one has

$$\frac{df}{dz} = \frac{\partial f}{\partial x} = \frac{\partial \varphi}{\partial x} + i\frac{\partial \psi}{\partial x} = u - iv \,, \tag{6.16}$$

$$\frac{df}{dz} = \frac{1}{i}\frac{\partial f}{\partial y} = -i\left(\frac{\partial \varphi}{\partial y} + i\frac{\partial \psi}{\partial y}\right) = u - iv \,. \tag{6.17}$$

The polar representation of complex numbers $z = re^{i\theta}$ gives the relation

$$dz = e^{i\theta}\, dr \,, \tag{6.18}$$

leading to the definition

$$f'(z) = \frac{1}{e^{i\theta}}\frac{\partial f}{\partial r} = w \,. \tag{6.19}$$

Examination of Fig. 6.1 shows that

$$v_r - iv_\theta = (u - iv)e^{i\theta} \,. \tag{6.20}$$

Combining Eqs. (6.19) and (6.20), one obtains

$$\frac{\partial f}{\partial r} = v_r - iv_\theta \,. \tag{6.21}$$

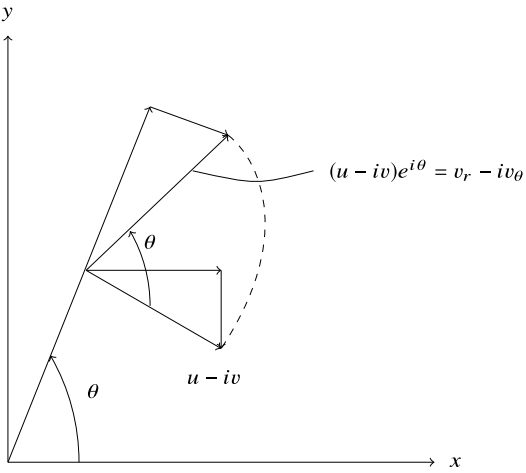

Fig. 6.1 Rotation of the complex velocity w by the angle θ

6.2 Complex Circulation Γ

Integration of the complex potential along an arbitrary path AB yields the following result

$$\int_A^B df(z) = \int_A^B (u - iv)\, dz = \int_A^B (udx + vdy) + i \int_A^B (udy - vdx)$$
$$= \Gamma + iQ = f_B - f_A \,. \tag{6.22}$$

The complex velocity w must be defined in a univocal manner at each point of the complex plane for obvious physical reasons. Thus it is a holomorphic function. If this velocity were a multiform (or multivalued) function, cuts must be used in order to make w uniform and therefore integrable. As far as the complex potential is concerned, the situation is different as it results from the integration of (6.19) and may be a multiform function.

Recall that every point, where $w(z)$ is holomorphic in a circle centered in z_0 and may be developed in Taylor series, is an ordinary or regular point. If this development is not possible, the point is singular. Singularities are poles, essential singular points and branch points. Without rigorous definitions, consider the next examples to illustrate these concepts. The function $1/z^2$ has a pole of order two at the origin. Function $1/(z^2 + 1)$ has two simple poles $z = \pm i$. Function $e^{\frac{1}{z-a}}$ has an essential singular point in $z = a$. Function $z^{\frac{1}{n}}$ presents a branch point at the origin.

Let us now examine two cases in detail.

1. If z_0 is the center of a circle of radius R where the flow is regular, cf. Fig. 6.2, it is possible to develop w as a Taylor series with complex coefficients such that

$$w = a_0 + a_1(z - z_0) + a_2(z - z_0)^2 + \ldots, \quad | z - z_0 | < R \,. \tag{6.23}$$

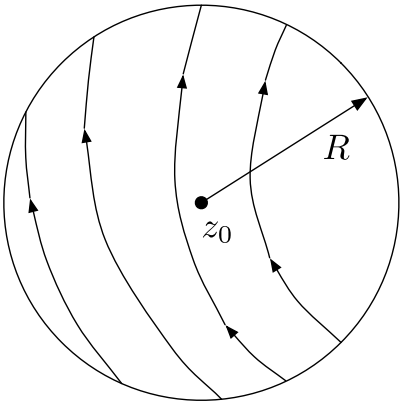

Fig. 6.2 Regular flow in a circle of radius R centered in z_0

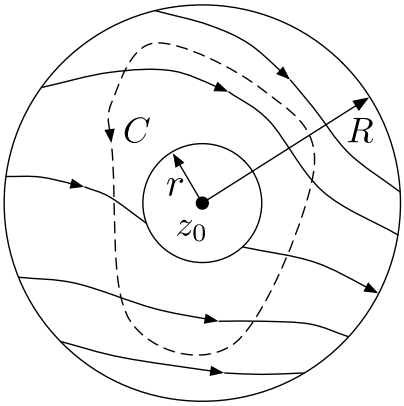

Fig. 6.3 Regular flow between two circles centered in z_0

2. If z_0 is the center of an annular domain comprised between two circles of respective radii r and R where the flow is regular, cf. Fig. 6.3, w is developed in Laurent series

$$w = \sum_{n=-\infty}^{n=\infty} a_n \, (z - z_0)^n, \quad r < \mid z - z_0 \mid < R \, . \tag{6.24}$$

The Laurent series includes two power series, one of ratio $z - z_0$ that converges for $\mid z - z_0 \mid < R$, the other one of ratio $1/(z - z_0)$ converging for $\frac{1}{|z-z_0|} < \frac{1}{r}$. Integrating the series (6.24), one obtains the complex potential

$$f(z) = \sum_{n=0}^{n=\infty} \frac{a_n}{n+1} (z - z_0)^{n+1} + a_{-1} \ln(z - z_0) + \sum_{n=-\infty}^{n=-2} \frac{a_n}{n+1} (z - z_0)^{n+1} + C \, . \tag{6.25}$$

In (6.25), the presence of the multiform complex function $\ln(z - z_0)$ influences the integration of the complex potential in relation (6.22). If the integration path is an arbitrary closed curve C that circles around z_0 only once, then the theorem of residues allows writing that the complex circulation $\mathbf{\Gamma}$ is

$$\mathbf{\Gamma}_C = \int_C df(z) = 2\pi i a_{-1} \ . \tag{6.26}$$

When the radius r is zero and the isolated singularity in z_0 is a pole, the calculus of residue utilises the relation

$$a_{-1} = \lim_{z \to z_0} (z - z_0) w \tag{6.27}$$

for a pole of order one and

$$a_{-1} = \lim_{z \to z_0} \frac{d^{n-1}}{dz^{n-1}} \frac{(z - z_0)^n w}{(n-1)!} \tag{6.28}$$

for a pole of order n. If R goes to infinity and the velocity at infinity is uniform, the complex potential (6.25) is such that $a_i = 0, i = 1, \ldots, \infty$ and the velocity at infinity is given by

$$w(\infty) = a_0 \ . \tag{6.29}$$

6.3 Elementary Complex Potential Flows

The irrotational flow is essentially a linear problem as the velocity potentials and the stream function satisfy each of them a Laplace equation. Thus in order to build up a somewhat complicated flow, we take full advantage of the superposition principle by combining simple complex potentials. This new potential will allow the calculation of the flow rate and the resulting circulation using the same superposition principle. For the pressure field, the Bernoulli equation will be our tool for analysis.

In the following figures, the equipotentials will be represented by dashed lines and the streamlines by solid lines with arrows pointing in the flow direction.

6.3.1 Parallel Homogeneous Flow

The complex potential

$$f(z) = Az, w = A = const \ , \tag{6.30}$$

is a homogeneous parallel flow. If A is real, the flow is parallel to direction x while if A is imaginary, it is in direction y. For complex A we have a superposition of both previous cases.

6.3.2 *Vortex and Source*

Let the potential be

$$f(z) = (A + iB)\ln z \tag{6.31}$$

with A and B real. In polar coordinates,

$$f(z) = (A + iB)(\ln r + i\theta) = (A\ln r - B\theta) + i(B\ln r + A\theta) \tag{6.32}$$

The complex velocity is

$$w = f'(z) = \frac{A + iB}{z}\,. \tag{6.33}$$

In polar coordinates, by (6.21),

$$\frac{\partial f}{\partial r} = v_r - i\,v_\theta = \frac{A + iB}{r}\,. \tag{6.34}$$

This velocity has a pole of order one and the residue is $(A + iB)$. The integration of the velocity involves a closed contour encircling once the origin. By (6.22), one has

$$\Gamma_0 + iQ_0 = 2\pi i(A + iB) \tag{6.35}$$

and thus

$$\Gamma_0 = -2\pi B, \quad Q_0 = 2\pi A\,. \tag{6.36}$$

Let us inspect the various cases corresponding to this potential.

6.3.2.1 Sink or Source

$$A \neq 0, \quad B = 0\,,$$

$$\varphi = A\ln r, \quad v_r = \frac{A}{r}, \quad \Gamma = 0\,, \tag{6.37}$$

$$\psi = A\theta, \quad v_\theta = 0, \quad Q = 2\pi A\,. \tag{6.38}$$

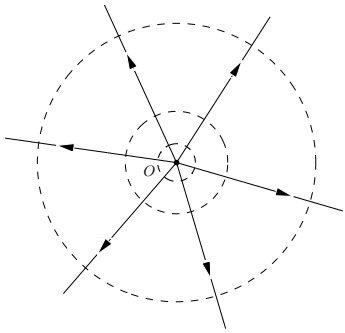

Fig. 6.4 Source flow, $f = A \ln z$

In Fig. 6.4, one observes that the equipotentials are circles centered at the origin and the streamlines are half-straight lines from the same point. The velocity is radial and inversely proportional to the distance to the origin. The flow is a source for $A > 0$ or a sink ($A < 0$) with a flow rate $2\pi A$.

6.3.2.2 Vortex

$$A = 0, \quad B \neq 0 \,,$$

$$\varphi = -B\theta, \quad v_r = 0, \quad \Gamma = -2\pi B \,, \tag{6.39}$$

$$\psi = B \ln r, \quad v_\theta = -\frac{B}{r}, \quad Q = 0 \,. \tag{6.40}$$

Here (cf. Fig. 6.5), we may just swap the streamlines and the equipotentials of the previous case. The equipotentials are radial lines while the streamlines are circles centered at the origin. A fluid particle rotates around the origin with a velocity inversely proportional to the distance to the origin. If $B > 0$, the rotation is clockwise (on an analog watch). Note that the motion is irrotational except at the origin where

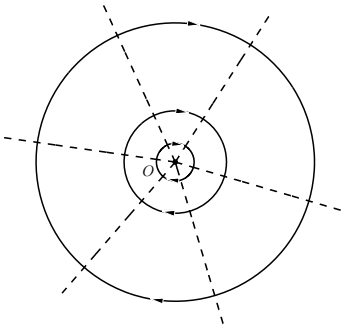

Fig. 6.5 Vortex flow, $f = iB \ln z$

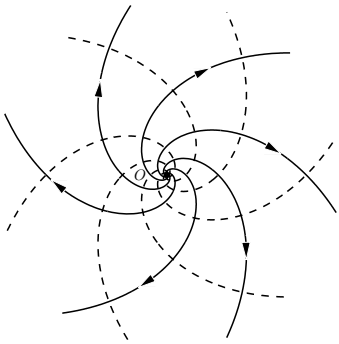

Fig. 6.6 Logarithmic spiral flow, $f = (A + iB)\ln z$

a vortex is concentrated in the singularity. This is the reason why Γ_0 is different from zero.

6.3.2.3 Spiral Flow

$$A \neq 0, \quad B \neq 0\,. \tag{6.41}$$

The velocity potential and the stream function read

$$\varphi = A\ln r - B\theta, \quad \psi = A\theta + B\ln r\,. \tag{6.42}$$

One deduces

$$v_r = A/r, \quad \Gamma = -2\pi B, \quad v_\theta = -B/r, \quad Q = 2\pi A\,. \tag{6.43}$$

The fluid particles rotate around the origin while moving away if there is a source at the origin. The equipotentials and the streamlines are orthogonal nets of logarithmic spirals as can be seen in Fig. 6.6.

6.3.3 Complex Potential in Power of z

Let the complex potential be

$$f(z) = Az^n = Ar^n\, e^{in\theta} = Ar^n(\cos n\theta + i\sin n\theta) \tag{6.44}$$

with $A \in \mathrm{R}$ and $A > 0$. The velocity potential is

$$\varphi = Ar^n \cos n\theta \tag{6.45}$$

and the stream function

$$\psi = Ar^n \sin n\theta \ . \tag{6.46}$$

The complex velocity reads

$$w = f'(z) = nAz^{n-1} \ , \tag{6.47}$$

and presents a singularity at the origin for n non-positive integer or negative n. In polar coordinates, by (6.21),

$$\frac{\partial f}{\partial r} = v_r - i\, v_\theta = nAr^{n-1}(\cos n\theta + i \sin n\theta) \ . \tag{6.48}$$

In order to obtain a uniform velocity everywhere in the complex plane, n must be an integer. The streamlines $\psi = 0$ are radial lines going through the origin given by

$$\theta = \frac{k\pi}{n}, k = 0, 1, \ldots \ . \tag{6.49}$$

For non-integer values of n, cuts in the complex plane are needed to make the velocity uniform. The stream lines $\psi = 0$ are again radial lines through the origin.

Let us examine successively the following cases: integer $n \geq 0$, non integer $n \geq 0$, integer $n < 0$.

6.3.3.1 Positive Integer *n*

1. $\mathbf{n = 0}$. The fluid is at rest, i.e. hydrostatic regime. One has

$$w = 0 \ . \tag{6.50}$$

2. $\mathbf{n = 1}$. This is the case of homogeneous and parallel flow described in Sect. 6.3.1.
3. $\mathbf{n = 2}$. The complex potential gives

$$f(z) = A(x^2 - y^2) + 2iAxy \ , \tag{6.51}$$

the velocity components of which are

$$u = 2Ax, \quad v = -2Ay \ . \tag{6.52}$$

The equipotentials are equilateral hyperbolas whose asymptotes are bisectors of the coordinate axes. The streamlines are also equilateral hyperbolas that are orthogonal to the previous ones and whose asymptotes are the coordinate axes, cf. Fig. 6.7. The origin of the axes is called the stagnation point.

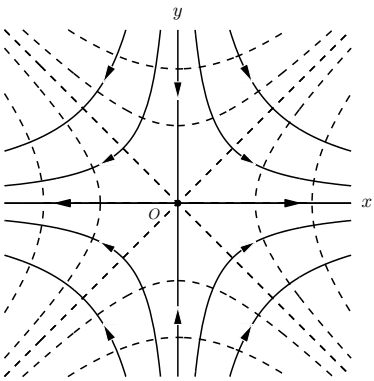

Fig. 6.7 Flow corresponding to $f = Az^2$

6.3.3.2 Non Integer $n \nabla 1/2$

The use of fractional values for n is possible inasmuch one carries out cuts in the complex plane to get a uniform velocity in the domain at hand. These cuts are made most of the time along streamlines that are assimilated to obstacles. The best choice to obtain a very wide domain consists in utilizing cut lines going through the origin.

1. $\mathbf{n} = \frac{1}{2}$. The potential

$$f(z) = Ar^{1/2}(\cos\frac{\theta}{2} + i\sin\frac{\theta}{2}) \tag{6.53}$$

produces the streamlines

$$\psi = Ar^{1/2}\sin\frac{\theta}{2}\,. \tag{6.54}$$

For values $\theta = 0$ or $\theta = 2\pi$, $\psi = 0$. One has the flow around a thin plate (cf. Fig. 6.8) that coincides with the semi-axis $x > 0$. One notices that the radial velocity component depends on $r^{-1/2}$ indicating that it goes to infinity at the origin.

2. $\mathbf{n} > \frac{1}{2}$ .The streamlines $\psi = 0$ are obtained for $\theta = \frac{k\pi}{n}$, $k = 0, 1, \ldots,$.
Figure 6.9 shows that the flow is generated in the concave part of a dihedron $n > 1$ or around the convex part of a dihedron $n < 1$. The velocity at the tip of the convex dihedron ($n < 1$) goes to infinity, cf. Fig. 6.10 (left) while for a concave dihedron cf. Fig. 6.10 (right), the velocity at the origin goes to zero. Bernoulli's law that connects pressure and the square of the velocity shows that for a convex dihedron, we will have an infinite negative pressure at the origin and for the concave dihedron, pressure will be maximum at the vertex (Fig. 6.10).

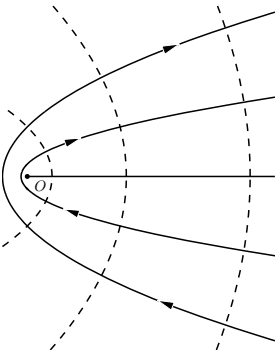

Fig. 6.8 Flow corresponding to $f = Az^{1/2}$

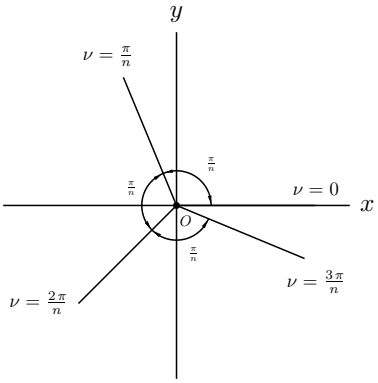

Fig. 6.9 Flow corresponding to $f = Az^n, n > 1/2$

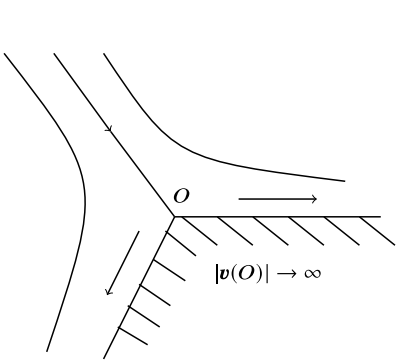

Convex dihedron

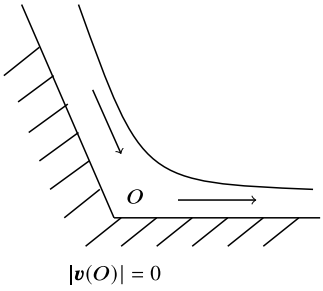

Concave dihedron

Fig. 6.10 Convex dihedron

6.3.3.3 Dipole

Consider the case $n = -1$. The complex potential

$$f(z) = \frac{A}{z} = \frac{A}{r}(\cos\theta - i\sin\theta) \tag{6.55}$$

yields real and imaginary parts

$$\varphi = \frac{Ax}{x^2+y^2} = \frac{A}{r}\cos\theta, \quad \psi = \frac{-Ay}{x^2+y^2} = -\frac{A}{r}\sin\theta\ . \tag{6.56}$$

The equipotential lines are circles centered on Ox and tangent to Oy at the origin, while the streamlines are circles centered on Oy and tangent to Ox in O, cf. Fig. 6.11. The f function and its derivative present a pole at the origin. The velocity

$$w = -\frac{A}{z^2} \tag{6.57}$$

has a pole of order two at the origin. The relations (6.57) and (6.22) show that the residue a_{-1} at the origin is zero. Thus the flow rate and the circulation associated to a closed contour around the origin also vanish. In fact everything happens as if we had at the origin a source and a sink of the same flow rate. This case corresponds to a doublet or dipole.

The shape of the streamlines (Fig. 6.11) show that they become tighter at the origin. The velocity increases when one approaches to the origin and goes to infinity at that precise point. It is possible to demonstrate that the potential of a dipole is the limit of the potential of a couple source-sink located from either side of the origin on the x axis, when the distance between the singularities goes to zero, while their opposite flow rates go to infinity (cf. Fig. 6.12)

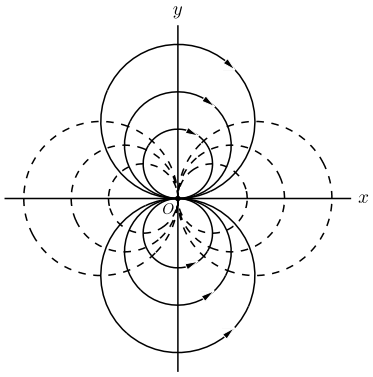

Fig. 6.11 Flow corresponding to $f = Az^{-1}$

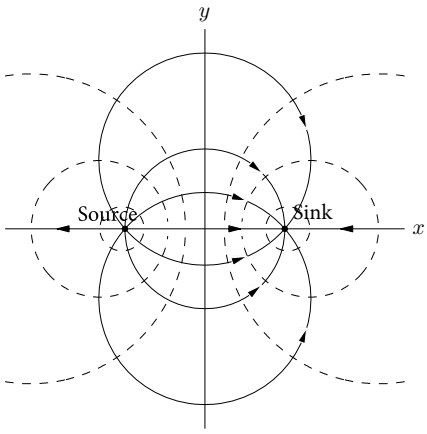

Fig. 6.12 Flow corresponding to a doublet

6.4 Flow Around a Circular Cylinder

For the sake of simplicity, the cylinder has a circular cross section of radius a centered at the origin.

6.4.1 Flow Without Circulation Around a Cylinder

Let us apply the superposition principle by combining a dipole with a homogeneous parallel flow. The complex potential reads

$$f(z) = U\left(z + \frac{a^2}{z}\right) . \tag{6.58}$$

This potential corresponds to the definition (6.25). Decomposing real and imaginary parts, the velocity potential is given by

$$\varphi = Ux\left(1 + \frac{a^2}{x^2 + y^2}\right) \tag{6.59}$$

and the streamline

$$\psi = Uy\left(1 - \frac{a^2}{x^2 + y^2}\right) . \tag{6.60}$$

The streamline $\psi = 0$ is composed of the circle of radius a centered at the origin $x^2 + y^2 = a^2$ and of the abscissa axis $y = 0$. The velocity is easily evaluated as

$$w = f'(z) = U\left(1 - \frac{a^2}{z^2}\right) = U[1 - \frac{a^2(x^2 - y^2 - 2ixy)}{(x^2 + y^2)^2}] . \tag{6.61}$$

Inspection of (6.61) shows that the velocity is zero at the two points of intersection of the abscissa axis with the circle in $x = \pm a$, $y = 0$; these are the stagnation points S_1 and S_2 of the flow. We note also that the velocity reaches its maximum norm equal to $2U$ at the intersection points of the circle with the ordinates axis in $x = 0$, $y = \pm a$.

To obtain the velocity on the cylinder, it is easier to work in polar coordinates. One has

$$f(z) = U\left(re^{i\theta} + \frac{a^2}{re^{i\theta}}\right) . \tag{6.62}$$

The equation of the circle is $z = ae^{i\theta}$. The components v_r and v_θ are obtained by (6.21)

$$v_r - iv_\theta = U\left(e^{i\theta} - \frac{a^2}{r^2 e^{i\theta}}\right) . \tag{6.63}$$

On the cylinder, the velocity is such that

$$v_r = 0, \quad v_\theta = -2U \sin\theta \tag{6.64}$$

showing that it is tangent to the cylinder with a sine variation.

For the steady state flow with the effects of gravity neglected, Bernoulli's relation (4.41) gives

$$C = \frac{p}{\rho} + \frac{\boldsymbol{v} \cdot \boldsymbol{v}}{2} , \tag{6.65}$$

We have

$$\frac{p_\infty}{\rho} + \frac{U^2}{2} = \frac{p}{\rho} + 2U^2 \sin^2\theta . \tag{6.66}$$

Defining the pressure coefficient C_p by

$$C_p = \frac{p - p_\infty}{\rho \frac{U^2}{2}} , \tag{6.67}$$

one obtains

$$C_p = 1 - 4\sin^2\theta . \tag{6.68}$$

The pressure field is symmetric with respect to the axial plane orthogonal to the flow direction and therefore if we integrate the pressure on the cylinder to obtain the lift force F_y, it will be zero. The streamlines are exhibited in Fig. 6.13.

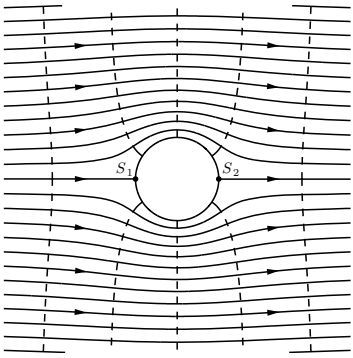

Fig. 6.13 Flow without circulation around a cylinder

6.4.2 Flow with Circulation Around a Cylinder

To produce circulation, it is necessary to introduce a logarithmic term in the potential

$$f(z) = U\left(z + \frac{a^2}{z}\right) - i\frac{\Gamma}{2\pi}\ln\frac{z}{a}\,. \tag{6.69}$$

This logarithmic term is modified in such a way that the streamline $\psi = 0$ contains the circle of radius a centered at the origin. The velocity is computed as

$$w = f'(z) = U\left(1 - \frac{a^2}{z^2}\right) - \frac{i\Gamma}{2\pi z}\,. \tag{6.70}$$

The velocity potential and the streamlines are easily obtained

$$\varphi = Ur\cos\theta\left(1 + \frac{a^2}{r^2}\right) + \Gamma\frac{\theta}{2\pi} \tag{6.71}$$

$$\psi = Ur\sin\theta\left(1 - \frac{a^2}{r^2}\right) - \frac{\Gamma}{2\pi}\ln\frac{r}{a}\,. \tag{6.72}$$

The velocity components are

$$v_r = \frac{1}{r}\frac{\partial\psi}{\partial\theta} = U\cos\theta\left(1 - \frac{a^2}{r^2}\right) \tag{6.73}$$

$$v_\theta = -\frac{\partial\psi}{\partial r} = -U\sin\theta\left(1 + \frac{a^2}{r^2}\right) + \frac{\Gamma}{2\pi r}\,. \tag{6.74}$$

The radial component vanishes on the circle. The calculation of the flow stagnation points is carried out via (6.70)

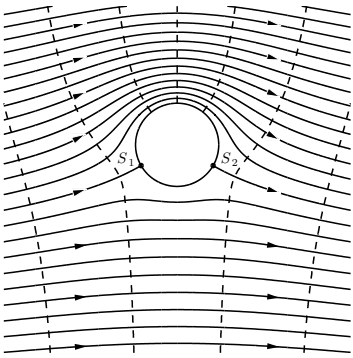

Fig. 6.14 Flow around a circular cylinder with $\Gamma = 4\pi U a \sin\theta$

$$z^2 - \frac{i\Gamma}{2\pi U} z - a^2 = 0 \,. \tag{6.75}$$

The solution reads

$$z = \frac{i\Gamma}{4\pi U} \pm \sqrt{a^2 - (\frac{\Gamma}{4\pi U})^2} \,. \tag{6.76}$$

Consider the case of a positive discriminant

$$a^2 - (\frac{\Gamma}{4\pi U})^2 > 0 \,. \tag{6.77}$$

Let us set $\sin\theta = \Gamma/(4\pi U a)$. The solution (6.76) becomes

$$z = a(\pm\cos\theta + i\sin\theta) \,. \tag{6.78}$$

If $|\ \Gamma\ | < 4\pi U a$, Eq. (6.78) shows that two stagnation points are located symmetrically with respect to the vertical axis and the streamlines are shown in Fig. 6.14. For $\Gamma = 4\pi U a$ with $\Gamma < 0$, $\sin\theta = -1$ and $\theta = 3\pi/2$, $z = -ia$ and the stagnation point is unique and situated at the bottom point of the cylinder. Figure 6.15 displays the streamlines of this particular case.

If $|\ \Gamma\ | > 4\pi U a$, then one finds

$$z = i\left(\frac{\Gamma}{4\pi U} \pm \sqrt{(\frac{\Gamma}{4\pi U})^2 - a^2}\right) \,. \tag{6.79}$$

The two stagnation points are conjugated with respect to the circle of radius a. One of these points is inside the circle and does not participate to the flow, cf. Fig. 6.16.

The streamline $\psi = 0$ separates the flow in two distinct regions. The fluid close to the cylinder stays locked up because of the vortex strength. The velocities in that region are high and consequently, pressure decreases. The pressure on the cylinder surface is obtained by the Bernoulli equation (4.41)

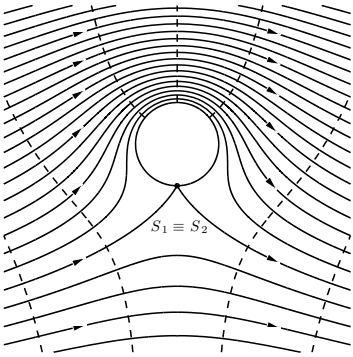

Fig. 6.15 Flow around a circular cylinder with $\Gamma = 4\pi U a$

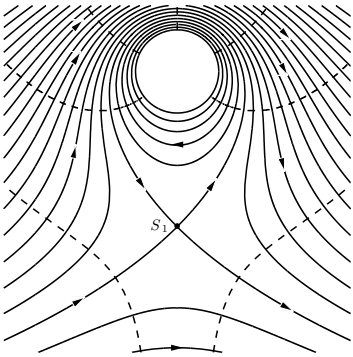

Fig. 6.16 Flow around a circular cylinder with $|\ \Gamma\ | > 4\pi U a$

$$\frac{p}{\rho} = \frac{p_\infty}{\rho} + \frac{1}{2}U^2 - \frac{1}{2}\left(4U^2 \sin^2\theta + \frac{\Gamma^2}{4\pi^2 a^2} - \frac{2\Gamma U}{\pi a}\sin\theta\right) . \tag{6.80}$$

The last term in the parenthesis generates the lift as we will verify in the sequel.

6.5 Blasius Theorem: Forces and Moment

Let C be a closed contour corresponding to the wall of a rigid obstacle in the steady irrotational flow of an inviscid fluid, cf. Fig. 6.17.

The wall coincides with a streamline. To evaluate the force exerted by the fluid on the wall, one integrates the density of the contact forces on the curve C. Using Cauchy theorem (1.53) and the constitutive relation for the perfect fluid (1.70), one obtains

$$\boldsymbol{F} = \int_C \boldsymbol{t}(\boldsymbol{n})ds = \int_C -p\boldsymbol{n}\, ds\ . \tag{6.81}$$

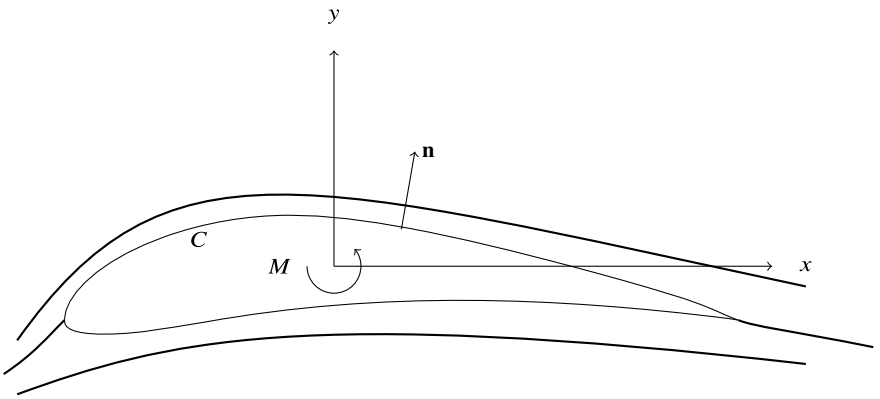

Fig. 6.17 Flow around an airfoil

In complex variables, the wall unit normal is given by

$$\boldsymbol{n} = n_x + i n_y = \frac{dy}{ds} - i\frac{dx}{ds} = -i\frac{dz}{ds} , \tag{6.82}$$

where s is a curvilinear coordinate along C.

Combining (6.81) and (6.82) we find

$$\boldsymbol{F} = i \int_C p \, dz . \tag{6.83}$$

The pressure field on the profile C is governed by Bernoulli equation

$$\frac{p}{\rho} + \frac{(\boldsymbol{v} \cdot \boldsymbol{v})_C}{2} = \frac{p_0}{\rho} , \tag{6.84}$$

with the last term evaluated at the upstream airfoil stagnation point. The term $(\boldsymbol{v} \cdot \boldsymbol{v})_C$ is given by

$$(\boldsymbol{v} \cdot \boldsymbol{v})_C = (u^2 + v^2)_C = [(u - iv)(u + iv)]_C = (w\overline{w})_C = (\frac{df}{dz}\frac{d\overline{f}}{d\overline{z}})_C , \tag{6.85}$$

with the overline indicating complex conjugation. Therefore the Bernoulli equation is rewritten as

$$\frac{p}{\rho} + \frac{1}{2}\frac{df}{dz}\frac{d\overline{f}}{d\overline{z}} = \frac{p_0}{\rho} . \tag{6.86}$$

Consequently, the force vector $\boldsymbol{F}$ (6.83) becomes

$$\begin{aligned}\boldsymbol{F} = F_x + iF_y &= i\int_C (p_0 - \frac{\rho}{2}\frac{df}{dz}\frac{d\overline{f}}{d\overline{z}})dz \\ &= ip_0\int_C dz - \frac{i\rho}{2}\int_C \frac{d\overline{f}}{d\overline{z}}df\ .\end{aligned} \tag{6.87}$$

On the streamline C, $\psi = cst$, thus the differential $df = d\varphi + id\psi$ is real as $d\psi = 0$ and thus $df = d\overline{f}$. Moreover $d\overline{f}/d\overline{z} = df/dz$. By Cauchy theorem, the first term of the right hand side of (6.87) is zero. One obtains

$$\overline{\boldsymbol{F}} = \frac{i\rho}{2}\int_C (\frac{df}{dz})^2 dz = \frac{i\rho}{2}\int_C w^2 dz\ . \tag{6.88}$$

The moment exerted by the fluid on the obstacle with respect to the origin of the axes is given by

$$\begin{aligned}M &= \int_C -p\,\boldsymbol{n}\times\boldsymbol{x}\,ds = -\int_C p(n_x y - n_y x)ds = \int_C -p(x\frac{dx}{ds} + y\frac{dy}{ds})ds \\ &= -\int_C p\Re(zd\overline{z}) = \Re[\int_C -p_0(zd\overline{z}) + \frac{\rho}{2}\int_C z\frac{df}{dz}d\overline{f}]\ ,\end{aligned} \tag{6.89}$$

where $\Re$ indicates the real part of the expression. Along a streamline, one has

$$M = \frac{\rho}{2}\Re\int_C z\overline{w}^2 dz = \frac{\rho}{2}\Re\int_C zw^2 dz\ , \tag{6.90}$$

as $(\overline{w}d\overline{z})_C = (w\,dz)_C$.

Let us apply these force and moment relations to the case of the cylinder in a flow with circulation. By (6.70) and the theorem of residues, one gets

$$\overline{\boldsymbol{F}} = i\rho\Gamma U, \quad F_x = 0, \quad F_y = -\rho\Gamma U\ . \tag{6.91}$$

We find a zero drag and a lift proportional to the circulation. As we assumed $\Gamma < 0$ and $U > 0$, the force F_y is positive and oriented in direction Oy.

Let us now examine the moment. From (6.70) and (6.90), we have

$$\begin{aligned}M &= \frac{\rho}{2}\Re\int_C \left(U(1-\frac{a^2}{z^2}) - i\frac{\Gamma}{2\pi\,z}\right)^2 zdz \\ &= \frac{\rho}{2}\Re\left(2\pi\,i\,a^2\left[-2U^2 + \frac{\Gamma^2}{4\pi^2 a^2}\right]\right) = 0\ .\end{aligned} \tag{6.92}$$

Thus the couple exerted on the cylinder vanishes as the resulting M is purely imaginary.

6.6 The Method of Conformal Transformation

Let z and ζ be two complex planes, the first one with variable $z = x + iy$ and the second one with variable $\zeta = \xi + i\eta$. We consider a one-to-one correspondance, i.e. a bijective transformation between these two planes, given by

$$\zeta = \zeta(z) \,, \tag{6.93}$$

such that each point z in the z plane has an image in the ζ plane. Therefore a curve in z plane is equivalent to another curve in ζ plane in such a way that the second curve is an image or mapping of the first one.

6.6.1 A Few Properties of the Conformal Transformation

The mapping is conformal because it preserves or conserves the angles but allows stretching or shortening of lengths. In Fig. 6.18, two elementary vectors dz_1 and dz_2 of the z plane are mapped onto the corresponding counterpart vectors $d\zeta_1$ and $d\zeta_2$. We write

$$d\zeta_1 = \frac{d\zeta}{dz} dz_1, \quad d\zeta_2 = \frac{d\zeta}{dz} dz_2 \,. \tag{6.94}$$

As ζ is an analytic function, the value of $d\zeta/dz$ depends on the location of point z and is independent of the orientation. Therefore by (6.94) with the relations $z = re^{i\theta}$, $\zeta = se^{i\vartheta}$, one obtains

$$\arg d\zeta_1 - \arg d\zeta_2 = \vartheta_1 - \vartheta_2 = \arg dz_1 - \arg dz_2 = \theta_1 - \theta_2 \,. \tag{6.95}$$

The angle between the two vectors is conserved by the transformation. Moreover, it is easily shown that

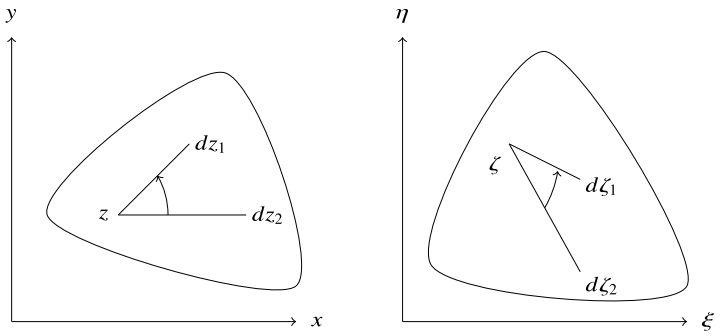

Fig. 6.18 z (left) and ζ (right) planes

$$\left|\frac{dz_2}{dz_1}\right| = \left|\frac{d\zeta_2}{d\zeta_1}\right| . \tag{6.96}$$

The ratio of the length of two infinitesimal vectors in a plane is equal to the ratio of the length of the corresponding vectors in the other plane.

6.6.2 Application to Potential Flows

In the z plane, the complex potential $f(z)$ transformed via (6.93) yields the complex potential G in the ζ plane. Indeed we have

$$f(z) = f(z(\zeta)) \equiv G(\zeta) . \tag{6.97}$$

The argument $z(\zeta)$ is the inverse function of the transformation (6.93). The analytical function $G(\zeta)$ defines a flow in the ζ plane. The streamlines and the equipotentials in the original plane z are transformed and present different shapes in the ζ plane. By analogy with the definition (6.7) one has

$$G(\zeta) = \Phi(\xi, \eta) + i\Psi(\xi, \eta) . \tag{6.98}$$

Equating f and G by (6.97), one obtains

$$\Re f(z) = \Re G(\zeta), \quad \Im f(z) = \Im G(\zeta) , \tag{6.99}$$

along homologous curves. The symbol $\Im$ denotes the imaginary part.

The complex velocity in the ζ plane is computed as

$$w_\zeta = G'(\zeta) = \frac{df}{dz}\frac{dz}{d\zeta} = \frac{w(z)}{\zeta'(z)} . \tag{6.100}$$

Let us note that both velocities w_ζ and w vanish at homologous points inasmuch $\zeta'(z) \neq 0$, i.e. when the mapping remains conformal.

The transformation is no longer conformal at the singular points $\zeta'(z) = 0$. A first case occurs when the z point is a stagnation point ($w = 0$) and the derivative ζ' is finite, then the velocity w_ζ remains finite. The second case corresponds to $\zeta'(z) = 0$ with the second derivative $\zeta''(z) \neq 0$. The homologous point ζ is a cusp (cf. Fig. 6.19) because by (6.93), we write

$$d\zeta = 0 + \frac{1}{2}\frac{d^2\zeta}{dz^2}dz^2 , \tag{6.101}$$

where the infinitesimal quantity $d\zeta$ is the dominating term in the development in series of the difference $\zeta(z + dz) - \zeta(z)$. This leads to the result that two infinitesimal

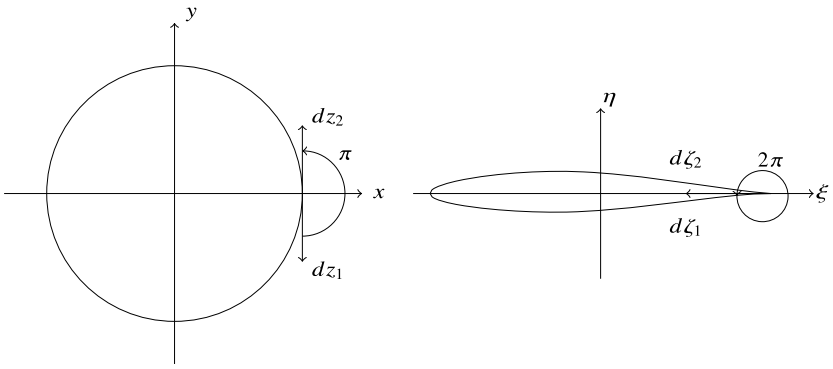

Fig. 6.19 Cusp in the ζ plane. The airfoil on the right is a NACA 64-1112 profile

segments dz_1 and dz_2 tangents to the circle in the z plane are transformed into two segments $d\zeta_1$ and $d\zeta_2$ such that

$$\frac{d\zeta_2}{d\zeta_1} = \left(\frac{dz_2}{dz_1}\right)^2 . \tag{6.102}$$

Therefore one has

$$\arg d\zeta_1 - \arg d\zeta_2 = 2(\arg dz_1 - \arg dz_2) . \tag{6.103}$$

As $\arg dz_1 - \arg dz_2 = \pi$, we obtain $\arg d\zeta_1 - \arg d\zeta_2 = 2\pi$ that corresponds indeed to a cusp.

The complex circulation remains unchanged in the transformation

$$(\Gamma + i\,Q)_\zeta = \int_{C_\zeta} G'(\zeta)d\zeta = \int_{C_z} \frac{w}{\zeta'(z)}\frac{d\zeta}{dz}dz = (\Gamma + i\,Q)_z . \tag{6.104}$$

6.7 Schwarz-Christoffel Transformation

The polygonal boundary of a domain located in the complex plane z with interior angles $\alpha, \beta, \gamma, \ldots$ can be transformed in the real axis ξ of the complex plane ζ by a conformal transformation. The transformed domain is the half plane $\eta > 0$ in Fig. 6.20. The transformation is given by a differential equation that is integrated for any polygonal shape. The equation defining the transformation $z = f(\zeta)$ is given by the relationship

$$\frac{dz}{d\zeta} = K(\zeta - a)^{\frac{\alpha}{\pi}-1}(\zeta - b)^{\frac{\beta}{\pi}-1}(\zeta - \gamma)^{\frac{\gamma}{\pi}-1}\ldots , \tag{6.105}$$

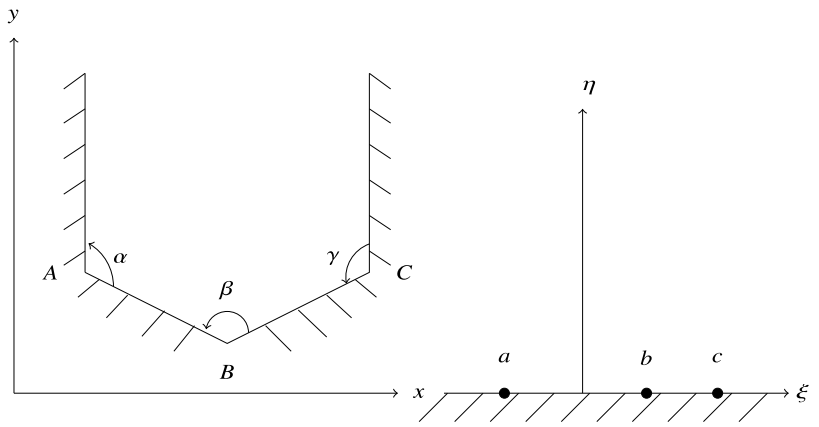

Fig. 6.20 Schwarz-Christoffel transformation of polygonal contour

where K is a constant and $a, b, c, \ldots$ are the real values of the complex variables corresponding to the polygon vertices in the z plane. If the polygon is closed and possesses n vertices, from Euclid's geometry, the quantities $\alpha, \beta, \gamma, \ldots$ are such that $\alpha + \beta + \gamma + \cdots = (n-2)\pi$. The function f can be expressed by an indefinite integral

$$z = z_0 + K \int (\zeta - a)^{\frac{\alpha}{\pi}-1} (\zeta - b)^{\frac{\beta}{\pi}-1} (\zeta - \gamma)^{\frac{\gamma}{\pi}-1} \ldots d\zeta \, . \tag{6.106}$$

The K and z_0 constants allow the determination of the position and the size of the domain.

It is sometimes convenient to place at infinity the point in the ζ plane corresponding to one of the vertices, e.g. $\zeta = a$. The factor $(\zeta - a)^{\frac{\alpha}{\pi}-1}$ is incorporated in the K constant generating a new constant $K' = (-a)^{\frac{\alpha}{\pi}-1}$ such that we can write

$$\frac{dz}{d\zeta} = K' \zeta - b)^{\frac{\beta}{\pi}-1} (\zeta - \gamma)^{\frac{\gamma}{\pi}-1} \ldots \, . \tag{6.107}$$

It is possible to show that two real values corresponding to the vertices may be chosen arbitrarily. This will be implemented in the following examples.

6.7.1 Mapping of a Semi-infinite Strip

Let us consider in Fig. 6.21 a semi-infinite strip A, B, C, D of height h. This strip may be assimilated to a rectangle with two vertices at infinity. The point A will be mapped on the point $\zeta = -\infty$, while B, C will be at $\zeta = b, \zeta = c$, respectively. We

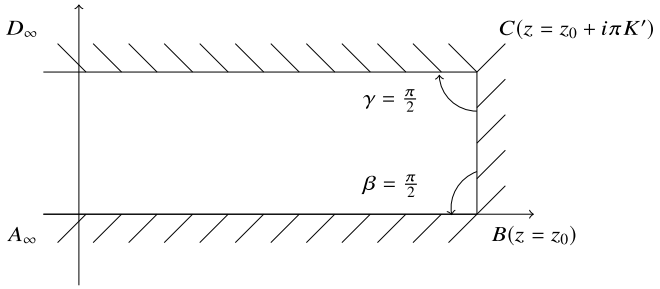

Fig. 6.21 Schwarz-Christoffel transformation of a semi-infinite strip

can conclude easily that D will be at $\zeta = \infty$. The interior angles that are relevant for the transformation are those at B and C, and then $\beta = \gamma = \pi/2$.

Eq. (6.107) is

$$\frac{dz}{d\zeta} = K'(\zeta - b)^{-\frac{1}{2}}(\zeta - c)^{-\frac{1}{2}} = \frac{K'}{\sqrt{(\zeta - b)(\zeta - c)}}$$
$$= \frac{K'}{\sqrt{(\zeta - \frac{b+c}{2})^2 - (\frac{b-c}{2})^2}} . \tag{6.108}$$

Let us set

$$\delta = \frac{\zeta - \frac{b+c}{2}}{\left|\frac{b-c}{2}\right|} . \tag{6.109}$$

Therefore the Schwarz-Christoffel relation (6.108) becomes

$$\frac{dz}{d\delta} = \frac{K'}{\sqrt{\delta^2 - 1}} . \tag{6.110}$$

The integration leads to (cf. [1])

$$z = z_0 + K' \ln(\delta + \sqrt{\delta^2 - 1}) = z_0 + K' \cosh^{-1} \delta . \tag{6.111}$$

Consequently

$$\delta = \cosh\left(\frac{z - z_0}{K'}\right) . \tag{6.112}$$

Using 6.109) and (6.112), we write

$$\zeta = \frac{b + c}{2} + \left|\frac{b - c}{2}\right| \cosh\left(\frac{z - z_0}{K'}\right) . \tag{6.113}$$

If $b \geq c$ and $z = z_0$, (6.113) yields $\zeta = b$. With $z = z_0 + i\pi\ K'$, we obtain $\zeta = c$.

6.7.2 *Mapping of a Plane Channel*

The problem of plane channel may be considered as a polygon with two vertices located at infinity with zero angles as shown in Fig. 6.22.

The Schwarz-Christoffel formula (6.106) allows writing

$$\frac{dz}{d\zeta} = K(\zeta - a)^{0-1}(\zeta - b)^{0-1} . \tag{6.114}$$

Let us choose a at infinity and b any value. Equation (6.114) becomes

$$\frac{dz}{d\zeta} = K'(\zeta - b)^{0-1} , \tag{6.115}$$

which gives

$$\zeta = b + e^{(z-z_1)/K'} , \tag{6.116}$$

where z_1 is a complex constant corresponding to any point of the channel. Note that $\zeta = b$ for $z \to -\infty$ and $\zeta = b + 1$ when $z = z_1$.

A point $z_1 + d$ with real d is transformed in a real $\zeta = b + e^{d/K'}$. The real half-line ζ with $\zeta > b$ corresponds to the channel boundary going through z_1. This was expected as the goal of the Schwarz-Christoffel transformation consists in building up the correspondance of the domain boundary with the real axis of the ζ plane. We also desire that the other plane channel wall corresponds to another portion of the real axis $\xi = 0$. Let H denote the channel height and d be a positive real value. We write

$$z = z_1 + iH + d \quad \Rightarrow \quad \zeta = b + e^{iH/K'} e^{d/K'} . \tag{6.117}$$

Therefore ζ will be real if $e^{iH/K'}$ is also real, i.e. if $\sin(H/K') = 0$. We deduce that we must have the condition $H/K' = n\pi$ with n, an integer. If we require that the second channel wall corresponds to the real half-line ζ with $\zeta < b$, one must choose an odd n and $K' = H/\pi$.

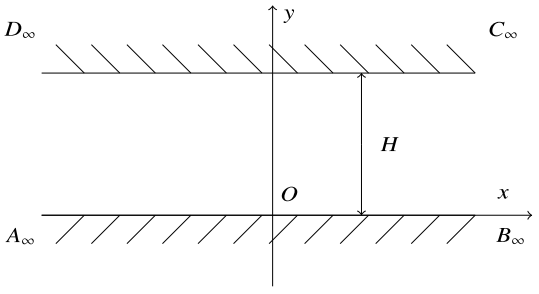

Fig. 6.22 Schwarz-Christoffel transformation of a plane channel

A parallel line to the channel walls is defined as

$$z = z_1 + i\alpha H + d \quad \text{with} \quad 0 \leq \alpha \leq 1 \,, \tag{6.118}$$

where α is a constant and d a variable parameter. The corresponding transformation reads

$$\zeta = b + e^{\pi d/H} e^{i\pi\alpha} \,. \tag{6.119}$$

This corresponds to a half-line that begins at point $\zeta = b$ and making an angle α with the positive real axis. Moreover, as $0 \leq \alpha \leq 1$, this half-line is located in the upper half-plane $\eta > 0$.

A straight line orthogonal to the channel walls is defined by the relationship (6.118), except that now α is varying and d is constant. Its transformation (6.119) is a semicircle centered in $\zeta = b$ with the radius $e^{\pi d/H}$.

6.7.3 *Schwarz-Christoffel Transformation of a Converging Channel*

In order to tackle the flow in a converging channel as shown in Fig. 6.23, the problem is solved with the help of the Schwarz-Christoffel transformation. We notice the following considerations:

- The first polygon angle is located at the vertices [2] and [3] coinciding at infinity. Therefore $\alpha_2 = \alpha_3 = 0$. The corresponding point in the ζ plane may be placed at the origin without loss of generality $\xi_2 = \xi_3 = 0$.
- For point [4], we have $\alpha_4 = 3\pi/4$ and $\xi_4 = a^4$.
- For point [5], we have $\alpha_5 = 5\pi/4$ and $\xi_5 = 1$.
- Point [1] (resp. [6]) is sent to $\xi = -\infty$ (resp. $\xi = \infty$) with zero angles in [1] and [6] (Fig. 6.23).

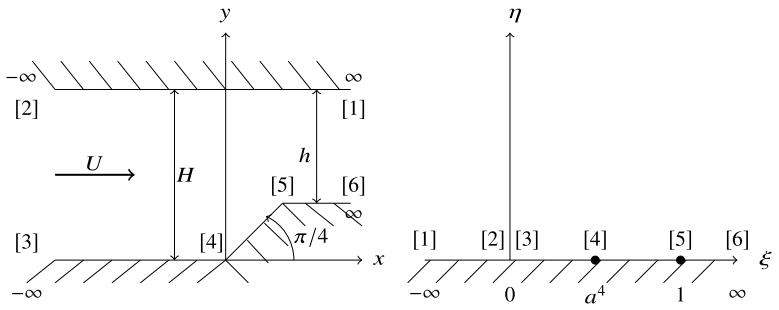

Fig. 6.23 Flow through a converging channel by the Schwarz-Christoffel method

With the help of (6.107), we write

$$\frac{dz}{d\zeta} = K'(\zeta - 0)^{0-1}(\zeta - a^4)^{3/4-1}(\zeta - 1)^{5/4-1} = \frac{K'}{\zeta}\left(\frac{\zeta - 1}{\zeta - a^4}\right)^{1/4} . \tag{6.120}$$

In the z plane, the entry flow is uniform with the velocity U. The volume flow rate Q is UH. In the ζ plane, we look for a complex potential with this flow rate generated between points [2] and [3] that coincide in $\xi = 0$. This is achieved by a source located at the origin with the complex potential

$$f(\zeta) = \frac{Q}{2\pi}\ln\zeta = \frac{UH}{\pi}\ln\zeta . \tag{6.121}$$

The last equality is due to the fact that $Q = 2UH$ as the source flows also in the half-plane $\eta < 0$. The complex velocity in the ζ plane is given by

$$w_\zeta = \frac{df}{d\zeta} = \frac{UH}{\pi\zeta} . \tag{6.122}$$

At the corresponding points in the z plane, the velocity is

$$w_z(z) = \frac{df}{d\zeta}\frac{d\zeta}{dz} = \frac{UH}{\pi K'}\left(\frac{\zeta - a^4}{\zeta - 1}\right)^{1/4} . \tag{6.123}$$

Let us determine the K' value in order that the velocity at [6] in the z plane be equal to the velocity at point [6] in the ζ plane. Due to the flow rate conservation, one has

$$w_z([6]) = \frac{UH}{h} \quad \Rightarrow \quad \frac{UH}{\pi K'}\left(\frac{\xi_6 - a^4}{\xi_6 - 1}\right)^{1/4} = \frac{UH}{h} . \tag{6.124}$$

But $\xi_6 = \infty$. Taking the limit of (6.124), one gets

$$\frac{UH}{\pi K'} = \frac{UH}{h} \quad \rightarrow \quad K' = \frac{h}{\pi} . \tag{6.125}$$

We must now compute the abscissa of point [4] in the ζ plane such that $\zeta_4 = \xi_4$. The z velocity in [4] is U. Using (6.123), we have

$$U = \frac{UH}{h}\left(\frac{0 - a^4}{0 - 1}\right)^{1/4} \quad \Rightarrow \quad a = \frac{h}{H} \quad \Rightarrow \quad \xi_4 = a^4 = \left(\frac{h}{H}\right)^4 . \tag{6.126}$$

With (6.120) and (6.125), we write

$$dz = \frac{h}{\pi\zeta}\left(\frac{\zeta - 1}{\zeta - a^4}\right)^{1/4} d\zeta \tag{6.127}$$

In order to ease the integration of (6.127), we introduce the change of variable

$$t^4 = \frac{\zeta - a^4}{\zeta - 1} \,. \tag{6.128}$$

Inverting (6.128) we have

$$\zeta = \frac{t^4 - a^4}{t^4 - 1} \,. \tag{6.129}$$

We can compute $d\zeta/\zeta$ and with this intermediate result, Eq. (6.127) becomes using factorization

$$dz = \frac{2h}{\pi}\left(\frac{1/2a}{t-a} - \frac{1/2a}{t+a} - \frac{1}{2(t-1)} + \frac{1}{2(t+1)} + \frac{1}{t^2+a^2} - \frac{1}{t^2+1}\right) dt \,. \tag{6.130}$$

Integrating we get

$$z = z_0 + \frac{h}{\pi}\left(-\frac{1}{a}\ln(t+a) + \frac{1}{a}\ln(t-a) + \ln(t+1) - \ln(t-1) + \frac{2}{a}\arctan(\frac{t}{a}) - 2\arctan t\right) . \tag{6.131}$$

The integration constant z_0 is obtained by imposing that the point $\zeta_4 = a^4 \leftrightarrow t = 0$ correspond to the origin in the z plane. This leads to the following expression (as $\ln(-1) = (2k+1)i\pi$)

$$z_0 = i(H + h) \,. \tag{6.132}$$

6.8 Joukowski Transformation

The Joukowski transformation is defined by

$$\zeta = z + \frac{a^2}{z} \,, \tag{6.133}$$

with a a real number. For large values of z, one has $\zeta \simeq z$ and the homologous flows given by (6.133) are identical at infinity. Let us consider the transformation of the region outside a circle of radius R in the z plane given by

$$z = R\, e^{i\theta} \,. \tag{6.134}$$

With (6.133) and (6.134), one obtains

$$\zeta = \xi + i\eta = \left(R + \frac{a^2}{R}\right)\cos\theta + i\left(R - \frac{a^2}{R}\right)\sin\theta \,. \tag{6.135}$$

Eliminating θ one gets

$$\frac{\xi^2}{r^2} + \frac{\eta^2}{s^2} = 1 \,, \tag{6.136}$$

$$r = R + \frac{a^2}{R}, \quad s = R - \frac{a^2}{R} \,. \tag{6.137}$$

The counterpart of the circle of radius R is an ellipse of semi-axes r and s. The two foci[1] of the ellipse are located on the ξ axis in $\xi = \pm 2a$. If the circle of ζ plane is such that $R = a$, it is transformed in the segment $-2a \le \xi \le 2a$ of the ξ axis. From Eq. (6.135) we have

$$\xi = a\, e^{i\theta} + a\, e^{-i\theta} = 2a\cos\theta \,. \tag{6.138}$$

For $\theta = 0, \pi/2, \pi, 3\pi/2, 2\pi$, one has $\xi = 2a, 0, -2a, 0, 2a$. Therefore when a point goes around the circle $R = a$ in the z plane, the homologous point in the ζ plane sweeps first the upper part of the segment and afterwards the bottom part. This means that in the ζ plane we have a flat plate of span $4a$.

The singular points of the transformation are the zeroes of the relation

$$\frac{d\zeta}{dz} = 1 - \frac{a^2}{z^2} \,. \tag{6.139}$$

These are the points $z = \pm a$ and thus $\zeta = \pm 2a$. The transformed circle generates cusps at those points.

6.8.1 Flow over a Flat Plate

Let us consider the flow over a circular cylinder with circulation that is inclined by an angle α with respect to the x axis. This is taken into account by the transformation $z = z_0 e^{i\alpha}$ where z_0 corresponds to the case of a horizontal incoming flow. With reference to relation (6.69) corresponding to z_0, the complex potential reads

$$f(z) = U\left(ze^{-i\alpha} + \frac{a^2}{z}e^{i\alpha}\right) - i\frac{\Gamma}{2\pi}\ln\left(\frac{z}{a}e^{-i\alpha}\right) \,. \tag{6.140}$$

Taking the derivative of (6.140) with respect to z and taking (6.139) into account, one produces the velocity relation on the plane $\zeta = a\, e^{i\theta}$

[1] The distance of the focus c to the ellipse center is such that $c = \sqrt{a^2 - b^2}$, where a and b are the semi-axes and the ellipse equation is $(x/a)^2 + (y/b)^2 = 1$.

$$w_\zeta = \frac{U}{1 - e^{-2i\theta}} \left(e^{i\alpha} - e^{i(\alpha - 2\theta)} - i \frac{\Gamma}{2\pi a U} e^{-i\theta} \right) . \tag{6.141}$$

With the identity

$$\frac{1}{1 - e^{-2i\theta}} = \frac{1 - e^{2i\theta}}{4 \sin^2 \theta} \tag{6.142}$$

we obtain

$$w_\zeta|_{plate} = \frac{U}{2 \sin^2 \theta} \left(\cos\alpha - \cos(\alpha - 2\theta) - \frac{\Gamma}{2\pi a U} \sin\theta \right) . \tag{6.143}$$

One notes that for the particular values $\alpha = \Gamma = 0$, one gets $w_\zeta|_{plate} = U$, corresponding to the uniform and parallel flow not perturbed by the presence of the plate.

For $\Gamma = 0$, $w_\zeta = 0$ when

$$\cos\alpha = \cos(\alpha - 2\theta) \quad \text{or} \quad \theta_1 = \alpha, \quad \theta_2 = \alpha + \pi . \tag{6.144}$$

Figure 6.24 shows the streamlines for $\alpha = 25°$, $\Gamma = 0$. We notice the stagnation points S_1 and S_2 on the pressure and suction sides. The velocities at $x = \pm 2a$ are infinite. Using the identity

$$\cos\alpha - \cos(\alpha - 2\theta) = 2 \sin^2\theta \cos\alpha - 2 \sin\alpha \sin\theta \cos\theta$$

the velocity is

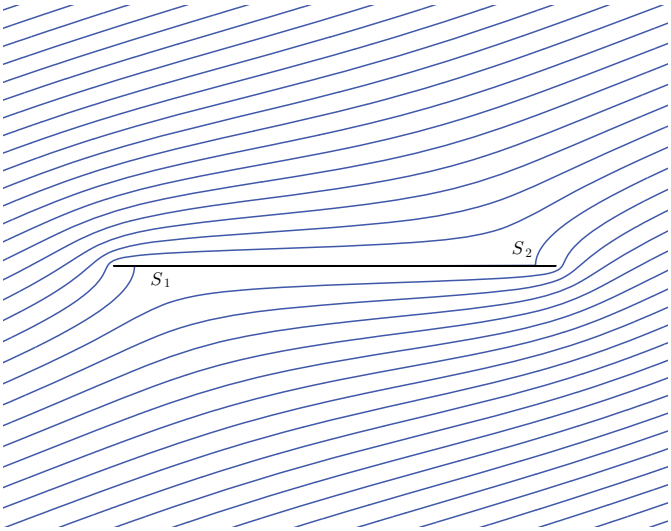

Fig. 6.24 Flow without circulation, inclined by an angle $\alpha = 25°$ around a flat plate

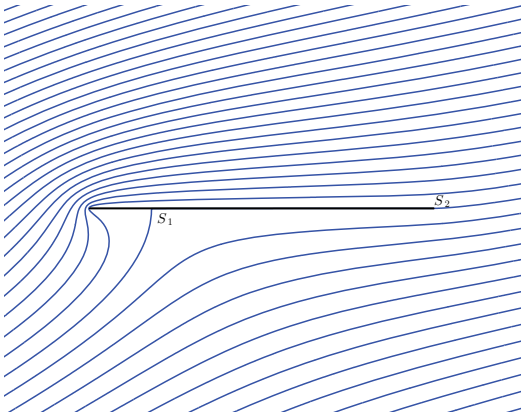

Fig. 6.25 Flow inclined by an angle $\alpha = 25°$ around a flat plate with $|\Gamma| = 4\pi aU \sin\alpha$

$$w_\zeta|_{plate} = U\cos\alpha - \frac{U}{2\sin\theta}\left(\frac{\Gamma}{2\pi aU} + 2\sin\alpha\cos\theta\right) . \tag{6.145}$$

In order to avoid an infinite velocity at the trailing edge that corresponds to $\xi = 2a$ and $\theta = 0$, we choose a Γ value that generates a finite velocity at that point. One has

$$|\Gamma| = 4\pi aU\sin\alpha . \tag{6.146}$$

Figure 6.25 presents the streamlines for this particular value of Γ, corresponding to a finite velocity at the trailing edge S_2.

6.8.2 *Joukowski Profiles*

With the help of Joukowski transformation, it is possible to generate a series of various profiles; among them, the ellipse and the flat plate constitute particular cases. This series called Joukowski profiles is obtained by locating the center of the circle of the transformation in a position different from the origin of the axes.

In Fig. 6.26, the circle is shifted in the negative direction of x axis. This procedure generates a thick symmetric profile such that the leading edge presents an elliptic shape and the trailing edge corresponds to the cusp of the flat plate case.

If the center of the circle is now located on the η axis, as it is shown in Fig. 6.27, one obtains an arc of a thin circle. This type of off-set generates a cambered profile.

Finally, Fig. 6.28 corresponds to the more general situation where the center of the circle is located inside the interior of the complex plane. We wish that the trailing edge be no longer a cusp, but a dihedral with a small aperture angle. This dihedral will be tied up with the intersection of the cylinder with the ξ axis. The center of the circle is off-set at point $z = z_{off}$. The transformation is given by the relationship

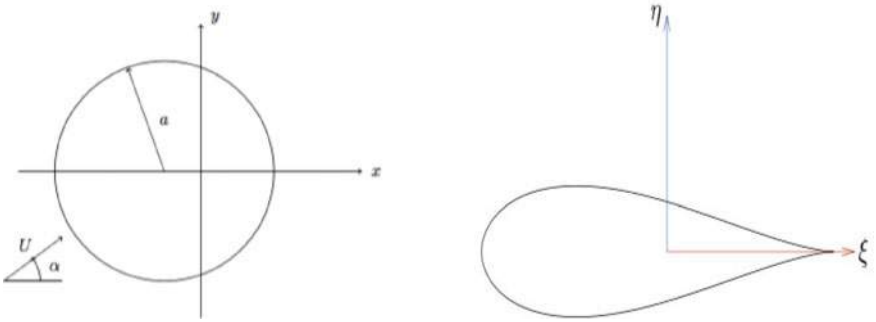

Fig. 6.26 Symmetric Joukowski profile

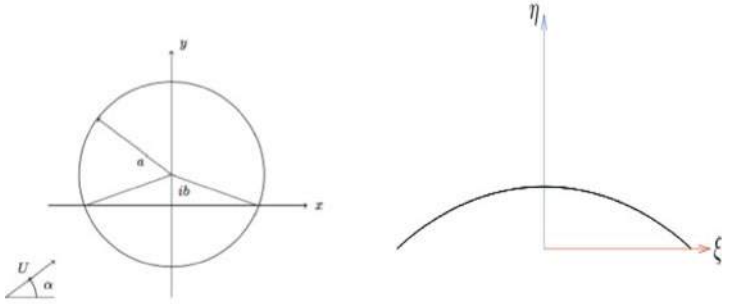

Fig. 6.27 Cambered Joukowski profile

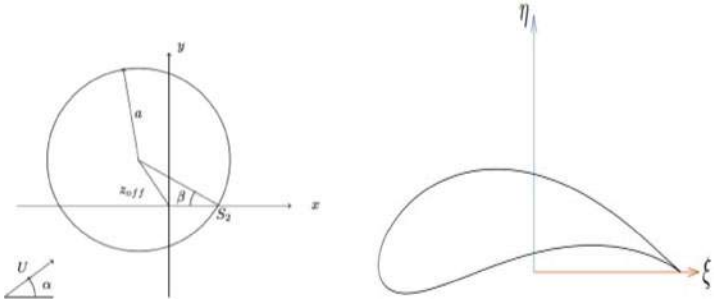

Fig. 6.28 General Joukowski profile

$$z = z_0 e^{i\alpha} + z_{off} \ . \tag{6.147}$$

The complex potential of the flow is then

$$f(z) = U\left(z - z_{off}\right) e^{-i\alpha} + \frac{Ua^2}{z - z_{off}} e^{i\alpha} - i\frac{\Gamma}{2\pi} \ln\left(\frac{z - z_{off}}{a} e^{-i\alpha}\right) \ . \tag{6.148}$$

The S_2 point corresponds to the intersection of the circle with ξ axis. Referring to Fig. 6.28, where the line connecting S_2 to the center of the circle makes the angle β, one gets by (6.147)

$$z_{S_2} = ae^{i\beta} + z_{off} \, . \tag{6.149}$$

Imposing a zero velocity at the trailing edge point S_2, we obtain

$$w(S_2) = U\left(e^{-i\alpha} - e^{+i(\alpha+2\beta)}\right) - \frac{i\Gamma}{2\pi a}e^{i\beta} = 0 \, . \tag{6.150}$$

We are then able to compute the circulation Γ

$$|\Gamma| = 4\pi aU \sin(\alpha + \beta) \, . \tag{6.151}$$

The lift on the profile is therefore

$$F_y = 4\pi\rho U^2 \sin(\alpha + \beta) \, . \tag{6.152}$$

Imposing this value for the circulation constitutes the Kutta condition which yields a finite velocity at the trailing edge on the pressure and suction sides of the profile. In the steady state plane case, there is no downstream vortex sheet. On the contrary, in the unsteady flow or downstream a three-dimensional profile, such a vortex sheet is present. From the physical point of view, this will generate a wake and some instabilities.

Consequently, the pressure coefficient is given by the relation

$$C_p = 1 - \frac{u^2 + v^2}{U^2} = 1 - \frac{w\overline{w}}{U^2} \, . \tag{6.153}$$

Figure 6.29 shows the flow with an incidence angle of five degrees. The circle of the transformation is in $z_{off} = 0.1 + i\,0.14$ with radius $a = 1.16$. One notices that the pressure side (intrados) is subjected to high pressure and the suction side (extrados)

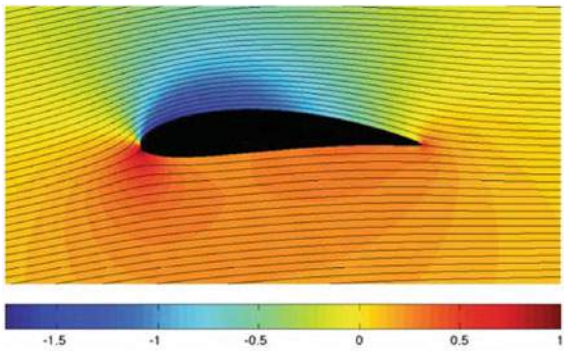

Fig. 6.29 Streamlines and isocontours of the pressure coefficient on a Joukowski airfoil for an incidence angle $\alpha = 5°$

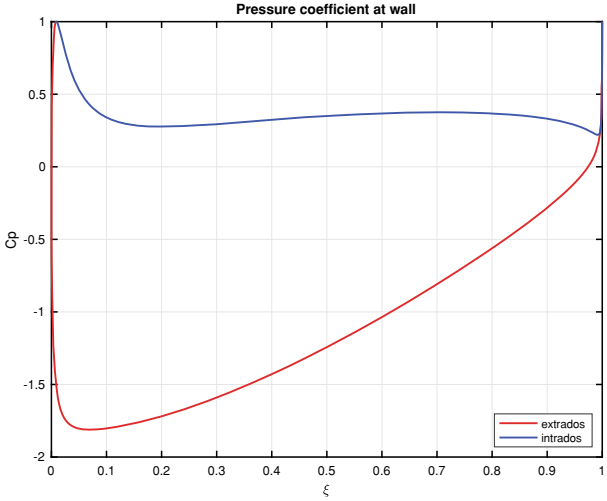

Fig. 6.30 Pressure coefficient on a Joukowski airfoil for an incidence angle $\alpha = 5°$

is low pressured. This phenomenon induces the lift of the airfoil. The next Fig. 6.30 shows the pressure variation between pressure and suction sides allowing computing the center of pressure which is the average location of the pressure variation. Through the center of pressure acts the aerodynamic force that is lift for an inviscid fluid and lift and drag in the viscous case.

Exercises

6.1 Let the complex potential of the flow be given by the expression

$$f(z) = m \ln\left(z - \frac{1}{z}\right), \quad m > 0\,. \tag{6.154}$$

- Find the locations of the sources and sinks.
- Compute the velocity potential φ and the streamfunction ψ and show that with these expressions it is possible to examine the flow in a positive half-disk $r < 1$.
- Evaluate the flow rate crossing the line between the points $z_1 = \frac{1}{2} + \frac{i}{2}$ and $z_2 = \frac{1}{2}$.

6.2 The complex potential of the flow reads

$$f(z) = (1+i)\ln(z^2-1) + (2-3i)\ln(z^2+4) + \frac{1}{z}\,. \tag{6.155}$$

- Find the positions of the singular points.
- Compute the flow rate across the circle $C : x^2 + y^2 = 9$ and the circulation around C.

6.3 The complex potential of the flow is given as

$$z = \cosh f \ . \tag{6.156}$$

- Compute the streamlines ψ and the equipotentials φ.
- Evaluate the velocity along the segment $[-1, 1]$ of the real axis.

Reminder

$$\cosh \alpha = \frac{e^{\alpha} + e^{-\alpha}}{2}$$
$$\sinh \alpha = \frac{e^{\alpha} - e^{-\alpha}}{2}$$
$$\cosh^2 \alpha - \sinh^2 \alpha = 1 \ .$$

6.4 Flow in front of a circular obstacle

Let us consider in the upper part ($\eta \geqslant 0$) of the ζ complex plane, the flow generated by a source with flow rate Q, at a distance $a < 1$ from a plane wall, and a sink with the same flow rate at a unit distance. The complex potential in the ζ plane is given by

$$g(\zeta) = \frac{Q}{2\pi} \ln \frac{\zeta^2 - a^2}{\zeta^2 - 1} \ . \tag{6.157}$$

- Justify the relation for the complex potential $g(\zeta)$ using the concept of hydrodynamic images analogous to that of electrical images in electrostatics.
- Express the complex velocity w_{ζ} in the ζ complex plane.

Consider now the conformal transformation between the complex ζ plane and the physical z plane :

$$z = g(\zeta) = \frac{1 + \zeta}{1 - \zeta} \ , \tag{6.158}$$

where $z = x + iy$ represents the point in the physical plane. This transformation is applied to the upper half plane $\eta \geq 0$.

- Evaluate the image in the z plane of the line $\xi = 0$ by the conformal transformation g.

Fig. 6.31 Flow over a step

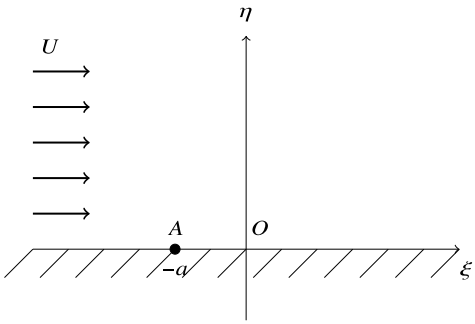

- Obtain the images in the z plane of the sources and sinks in the ζ plane. For the sake of simplicity, set $b = (1 + a)/(1 - a)$.
- Calculate the image in the z plane of the half-plane $\eta \geq 0$.
- Express the complex velocity $w(z)$ in the physical plane as a function of w_ζ. Deduce the analytical expression of $w(z)$.
- Show that the complex potential in the physical plane reads

$$f(z) = \frac{Q}{2\pi}\left[\ln\left(1 - \frac{b}{z}\right) + \ln\left(z - \frac{1}{b}\right)\right] . \tag{6.159}$$

6.5 Flow over a forward facing step

Let us consider the conformal mapping $\zeta = f(z)$ of the upper half plane $\eta \geq 0$ towards the physical plane z defined by

$$\frac{dz}{d\zeta} = \left(\frac{\zeta}{\zeta + a}\right)^{1/2} , \tag{6.160}$$

where a is a positive real number. We denote by A the corresponding point of the complex plane such that $\zeta = \xi = -a$ as is exhibited in Fig. 6.31. Moreover, it is assumed that the origin O of the ζ plane corresponds to the origin of the physical plane.

- Evaluate the image of the half line $\xi > 0$ and $\eta = 0$ by the conformal mapping. To this end, use arguments based on angles.
- As in the previous item, evaluate the image of the segment AO and of the half line $\xi < -a$. Deduce the flow domain in the physical plane.
- The flow in the ζ plane is uniform and represented by the complex potential $g(\zeta) = U\zeta$. Express the complex velocity $w(z)$ in the physical plane as a function of ξ for the domain boundary $\eta = 0$. Show that the image of point A in the z plane is a stagnation point. Compute in the transformed plane the velocity at the origin (Fig. 6.31).

Chapter 7
Boundary Layer

In Chap. 6, we considered the model of incompressible inviscid fluid in plane irrotational flow. Through the application of the theory of complex potential around an airfoil profile, we discovered that the model can deduce the lift while the drag associated with the perfect fluid vanishes. This is in perfect contradiction to experimental observations that show that drag affects all flows of real fluids. As these fluids are viscous, in principle they stick to the walls and the tangential velocity component is zero if the wall is fixed. This last condition is never met by the inviscid fluid. Furthermore, the irrotationality condition is far from representing the reality as we observed in Chap. 4 that vorticity production occurs at the walls. In order to remedy the deficiencies of perfect fluid theory, one resorts to the theory of boundary layer that brings a necessary correction for the flows at high Reynolds numbers. The boundary layer theory is due to Ludwig Prandtl who was a distinguished aerodynamicist. Initially developed within the framework of fluid mechanics, the boundary layer theory knew a great success and today belongs to the corpus of applied mathematics methods. A complete presentation is given in the excellent book by Bender and Orszag [13]. On the fluid side, the reference monographs are the ones by Hermann Schlichting [85] and Louis Rosenhead [82].

The boundary layer is the flow zone close to the wall, either of an obstacle sitting in a uniform upstream flow, either of a container that confines an inner flow. Inside the boundary layer which is a very thin zone, one assumes that the viscous effects are of the same order of magnitude as the inertial effects (the *local* Reynolds number in the boundary layer is of the order of unity), whatever the value of the *global* Reynolds number characterizing the full flow is. The boundary layer is the location of intense vorticity generation that will diffuse and advect in the exterior region in the long run. Therefore we reach a very modern approach of the complete problem by decomposing it in two sub-domains: on the one hand the boundary layer where viscous effects will be handled by a simplified Navier-Stokes model, and on the other hand, the outer region where the theory of complex potential for the irrotational flow

M. O. Deville, *An Introduction to the Mechanics of Incompressible Fluids*,
https://doi.org/10.1007/978-3-031-04683-4_7

of perfect fluid will be used. Note that this outer region is characterized by velocities that are of the same order of magnitude as those of the incoming flow.

The boundary layer along an obstacle is consequently thin as the fluid flows over long distances downstream the leading edge during the time interval in which the vorticity diffuses slowly over a short orthogonal distance starting from the wall. The vorticity creation within the boundary layer allows for the physical realization of the fluid circulation around the profile. The circulation generates a wake in the region close to the trailing edge. The wake size will depend on the obstacle shape and the angle of attack of the upstream flow at the leading edge.

7.1 The Equations of the Laminar Boundary Layer

To set up these equations, we will carry out a dimensional analysis of the problem at hand. For the sake of facility, let us consider the uniform upstream flow of a viscous incompressible fluid with constant velocity U on a plane horizontal wall of characteristic length L. A laminar boundary layer develops from the leading edge of the plane wall. We use a Cartesian (x_1, x_2) coordinate system. Inside the boundary layer, in the x_2 direction orthogonal to the wall, the velocity goes from a zero value at the wall to a value of the order of U at the edge of the boundary layer. We conclude that the thickness of the boundary layer is always small with respect to the distances measured in the parallel direction to the wall along which it is developed.

7.1.1 Dimensional Analysis

Therefore we assume that the variation of every unknown in the x_2 direction across the boundary layer will be more important than the variation in x_1 direction. This allows us to write the following approximations on the next derivatives

$$| \frac{\partial v_1}{\partial x_1} | << | \frac{\partial v_1}{\partial x_2} |, \quad | \frac{\partial^2 v_1}{\partial x_1^2} | << | \frac{\partial^2 v_1}{\partial x_2^2} | \ . \tag{7.1}$$

Let us inspect the momentum equation in the x_1 direction taking the previous inequalities into account and neglecting the body forces. One writes

$$\rho \frac{Dv_1}{Dt} = -\frac{\partial p}{\partial x_1} + \mu \frac{\partial^2 v_1}{\partial x_2^2} \ . \tag{7.2}$$

If one neglects viscosity in (7.2), one recovers the Euler equation. This relation will be adequate in the region outside the boundary layer where the fluid viscosity does

not supposedly affect the flow physics. As the local Reynolds number in the boundary layer is of the order of unity, one obtains

$$| \rho \frac{Dv_1}{Dt} | = O\left(| \mu \frac{\partial^2 v_1}{\partial x_2^2} | \right), \quad x_2 \to 0 . \tag{7.3}$$

The order of magnitude of the left hand side may be evaluated through the term $\rho v_1 \partial v_1 / \partial x_1$ for a steady state flow. We will observe that the term $\rho v_2 \partial v_1 / \partial x_2$ is of the same order of magnitude. One replaces (7.3) by

$$| \rho v_1 \frac{\partial v_1}{\partial x_1} | = O\left(| \mu \frac{\partial^2 v_1}{\partial x_2^2} | \right), \quad x_2 \to 0 \tag{7.4}$$

Taking U as the reference velocity, L as reference length and δ_0 the average thickness of the boundary layer as reference length in the x_2 direction, we estimate the order of magnitude of the terms appearing in (7.4), namely

$$\rho \frac{U^2}{L} = O(\mu \frac{U}{\delta_0^2}), \quad x_2 \to 0 , \tag{7.5}$$

or

$$\left(\frac{\delta_0}{L} \right)^2 = O\left(\frac{\mu}{\rho L U} \right) = O(Re^{-1}), \quad x_2 \to 0 . \tag{7.6}$$

This last dimensionless number is the *global* Reynolds number. As per the definition of the Bachmann symbol O, the product $(\frac{\delta_0}{L})^2 \, Re$ is bounded by a constant. If $Re \to \infty$, the ratio $\frac{\delta_0}{L}$ becomes very small, while remaining finite. One concludes the following estimate

$$\frac{\delta_0}{L} \sim Re^{-\frac{1}{2}}, \quad \text{for} \quad Re \to \infty . \tag{7.7}$$

For example, on a wing profile with a chord of the order of one meter and a Reynolds number $Re \sim 10^6$, the boundary layer thickness will be of the order of a few millimeters $(2 - 3)$.

By the incompressibility constraint (1.50), it is possible to obtain the order of magnitude of the vertical velocity component in the boundary layer. One has

$$v_2 \sim \frac{\delta_0}{L} U \sim U \, Re^{-\frac{1}{2}} . \tag{7.8}$$

For high Reynolds numbers, the vertical velocity will be several orders of magnitude less than the flow characteristic velocity.

7.1.2 Prandtl's Equations

As we mentioned in the preceding paragraphs, the boundary layer possesses essentially two normative space scales: the length L in the main flow direction and the thickness of the boundary layer we will now denote by δ. For this reason, we perform a multi-scale approach to write down the dimensionless form of the Navier-Stokes equations, using these normative scales in the plane case. Let us define the dimensionless variables

$$x_1' = \frac{x_1}{L}, \quad x_2' = \frac{x_2}{\delta} = \frac{x_2}{L} Re^{\frac{1}{2}}, \quad t' = \frac{tU}{L}, \tag{7.9}$$

$$v_1' = \frac{v_1}{U}, \quad v_2' = \frac{v_2}{U} Re^{\frac{1}{2}}, \quad p' = \frac{p - p_\infty}{\rho U^2}, \tag{7.10}$$

where p_∞ is the pressure at infinity upstream. With these variables, the Navier-Stokes equations become

$$\frac{\partial v_1'}{\partial t'} + v_1' \frac{\partial v_1'}{\partial x_1'} + v_2' \frac{\partial v_1'}{\partial y'} = -\frac{\partial p'}{\partial x_1'} + \frac{1}{Re} \frac{\partial^2 v_1'}{\partial x_1'^2} + \frac{\partial^2 v_1'}{\partial x_2'^2}, \tag{7.11}$$

$$\frac{1}{Re} \left(\frac{\partial v_2'}{\partial t'} + v_1' \frac{\partial v_2'}{\partial x_1'} + v_2' \frac{\partial v_2'}{\partial x_2'} \right) = -\frac{\partial p'}{\partial x_2'} + \frac{1}{Re^2} \frac{\partial^2 v_2'}{\partial x_1'^2} + \frac{1}{Re} \frac{\partial^2 v_2'}{\partial x_2'^2}, \tag{7.12}$$

$$\frac{\partial v_1'}{\partial x_1'} + \frac{\partial v_2'}{\partial x_2'} = 0. \tag{7.13}$$

Assuming that the velocities v_1', v_2' and pressure p' together with their derivatives with respect to space and time variables remain bounded, when $Re \to \infty$, one produces the reduced form of the equations of the laminar boundary layer

$$\frac{\partial v_1'}{\partial t'} + v_1' \frac{\partial v_1'}{\partial x_1'} + v_2' \frac{\partial v_1'}{\partial x_2'} = -\frac{\partial p'}{\partial x_1'} + \frac{\partial^2 v_1'}{\partial x_2'^2}, \tag{7.14}$$

$$0 = -\frac{\partial p'}{\partial x_2'}, \tag{7.15}$$

$$\frac{\partial v_1'}{\partial x_1'} + \frac{\partial v_2'}{\partial x_2'} = 0. \tag{7.16}$$

Equation (7.15) expresses that pressure remains constant over the boundary layer thickness. Therefore the boundary layer pressure will be equal to the pressure prevailing at its border, i.e. the one in the outer flow. The pressure gradient of the exterior region is thus the development engine of the boundary layer.

Coming back to dimensional variables, the boundary layer or Prandtl's equations are

$$\frac{\partial v_1}{\partial t} + v_1 \frac{\partial v_1}{\partial x_1} + v_2 \frac{\partial v_1}{\partial x_2} = -\frac{1}{\rho} \frac{\partial p_e(x_1, 0, t)}{\partial x_1} + \nu \frac{\partial^2 v_1}{\partial x_2^2} , \tag{7.17}$$

$$\frac{\partial v_1}{\partial x_1} + \frac{\partial v_2}{\partial x_2} = 0 , \tag{7.18}$$

with the following boundary conditions

$$v_1 = v_2 = 0, \quad \text{for} \quad x_2 = 0 \tag{7.19}$$

$$v_1 \to U_e(x, 0, t) \quad \text{for} \quad x_2 \to \infty . \tag{7.20}$$

The subscript e for p and U characterizes these variables in the exterior (inviscid) sud-domain. In the Eqs. (7.17) and (7.20), the variables p_e and U_e are evaluated by the Euler equation

$$\rho U_e \frac{dU_e}{dx_1} = -\frac{dp_e}{dx_1} . \tag{7.21}$$

Note that in (7.20), one imposes that at the location where the boundary layer meets the zone of perfect fluid, it is considered that the distance to the wall goes to infinity, namely $x_2 \to \infty$. For the perfect fluid region, everything occurs as if the boundary layer did not exist or at least is so thin that we use $U_e(x, 0, t)$ on the solid wall, while for the boundary layer, everything is treated as if it would ignore the presence of the outer zone, whence $x_2 \to \infty$. In Sect. 6.5.2 of [83], Ryhming writes "According to (7.20) one requires that when the inner solution approaches the outer solution, the value of the inner solution for $x_2 \to \infty$ be equal to the value of the outer solution for $x_2 \to 0$." A similar line of reasoning introduces in (7.17) the exterior pressure p_e evaluated at the wall $x_2 = 0$.

The link between the inner and outer solutions may be explained by a simple example proposed by von Mises and Friedrichs [116]. The problem is given by a second-order linear ordinary differential equation for a function $f(x_2)$ defined on the interval [0, 1] with two boundary conditions

$$\varepsilon f'' + f' = a , \tag{7.22}$$

$$f(0) = 0, \qquad f(1) = 1 , \tag{7.23}$$

where a is a positive constant and ε a positive coefficient such that $\varepsilon \ll 1$. This equation mimics the full Navier-Stokes equations. The small parameter ε that multiplies the second-order derivative corresponds to ν and is proportional to Re^{-1}. Therefore when the viscosity ν goes to zero, the mathematical nature of the problem changes. Instead of having a second-order problem with two boundary conditions, we are facing a first-order problem with the same conditions. This is typical of a singular perturbation problem.

In (7.22) the linearity of the problem allows for an exact solution of the problem comprising a particular solution and the general solution of the homogeneous ordinary differential equation. We obtain

$$f(x_2) = ax_2 + (1-a)\frac{1-e^{-\frac{x_2}{\varepsilon}}}{1-e^{-\frac{1}{\varepsilon}}} \,. \tag{7.24}$$

If we set the limit $\varepsilon \to 0$ for any fixed value of x_2, we get

$$\lim_{\varepsilon \to 0} f(x_2) = ax_2 + 1 - a = f_e(x_2) \,. \tag{7.25}$$

This exterior solution f_e satisfies the outer condition $f(1) = 1$ but not the inner condition as $f_e(0) \neq 0$. Let us inspect now the limit of $f(x_2)$ when $\varepsilon \to 0$ for a fixed value of x_2/ε. We obtain

$$\begin{aligned} \lim_{\substack{fixed\ \frac{x_2}{\varepsilon} \\ \varepsilon \to 0}} f(x_2) &= a\frac{x_2}{\varepsilon}\varepsilon + (1-a)(1-e^{-x_2/\varepsilon}) \\ &= (1-a)(1-e^{-x_2/\varepsilon}) = f_i(x_2) \,. \end{aligned} \tag{7.26}$$

The inner solution f_i satisfies the inner condition $f_i(0) = 0$ but fails to satisfy the exterior condition, $f_i(1) \neq 1$. However we note that the exterior limit $x_2/\varepsilon \to \infty$ of the inner solution is equal to the inner limit $x_2 \to 0$ of the exterior solution

$$f_i(\infty) = f_e(0) = 1 - a \,. \tag{7.27}$$

Therefore the solution of a singular perturbation problem is built by addition of the inner and outer solutions and by subtraction of their common quantity, which in our case is $1 - a$. The approximate complete solution for $\varepsilon \ll 1$ reads

$$f_a = f_i + f_e - (1-a) = ax_2 + (1-a)(1-e^{-x_2/\varepsilon}) \,. \tag{7.28}$$

In Fig. 7.1 we observe that the approximate (red) f_a solution is not very far from the (green) analytical solution f.

The condition (7.20) with the use of $p_e(x_1, 0, t)$ at $x_2 = 0$ in Eq. (7.17) must be justified. As the thickness δ_0 given by (7.7) is small, we can imagine an intermediary length ζ small with respect to the dimension L and large with respect to δ_0 as is shown in Fig. 7.2.

Let us choose

$$\frac{\delta_0}{\zeta} \sim Re^{-1/4} \,. \tag{7.29}$$

This induces

$$\frac{\zeta}{L} \sim Re^{-1/4} \,. \tag{7.30}$$

The exterior solution will not vary much when x_2 will go from ζ to 0. Indeed, the exterior solution changes significantly over distances of the order of magnitude of L, much larger than ζ. Therefore we can approximate the following quantities

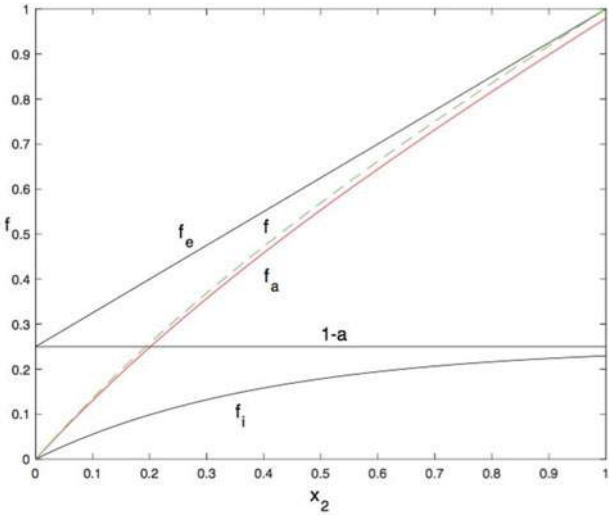

Fig. 7.1 Solutions of problem (7.22)

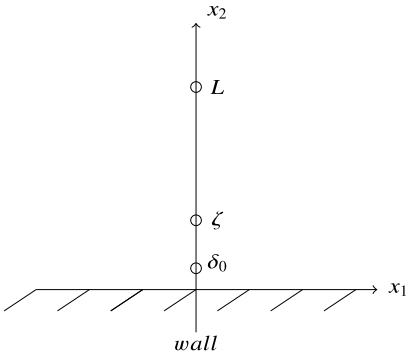

Fig. 7.2 Scales in the boundary layer theory

$$v_{1e(}x_1, \zeta, t) \simeq U_e(x_1, 0, t) \tag{7.31}$$

$$p_e(x_1, \zeta, t) \simeq p_e(x_1, 0, t)\ . \tag{7.32}$$

On the other hand, the interior solution is totally linked to the exterior solution at distances ζ from the wall which are larger than the thickness δ_0 of the boundary layer. Consequently, we write the following approximations

$$v_1(x_1, \zeta, t) \simeq U_e(x_1, \zeta, t) \tag{7.33}$$

$$p(x_1, \zeta, t) \simeq p_e(x_1, \zeta, t)\ . \tag{7.34}$$

Taking these various approximations into account, we conclude

$$v_1(x_1, \zeta, t) \simeq U_e(x_1, 0, t) \, . \tag{7.35}$$

If $Re \to \infty$, we can write the relation

$$\lim_{x_2 \to \infty} v_1(x_1, x_2, t) = U_e(x_1, 0, t) \, . \tag{7.36}$$

For the pressure, via a similar reasoning, we write

$$p(x_1, \zeta, t) \simeq p_e(x_1, 0, t) \, . \tag{7.37}$$

As the pressure is constant over the boundary layer thickness, we replace in the Prandtl equations the pressure $p(x_1, x_2, t)$ by $p(x_1, \zeta, t)$, leading to

$$p(x_1, x_2, t) \simeq p_e(x_1, 0, t), \quad x_2 \leq \zeta. \tag{7.38}$$

The pressure $p_e(x_1, 0, t)$ and the velocity $U_e(x_1, 0, t)$ will be computed by (7.21).

7.2 Boundary Layer on a Flat Plate

In this section we analyze the development of the boundary layer on a semi-infinite flat plate located in steady-state uniform flow parallel to direction x_1 of a Cartesian coordinates system. We will solve Prandtl's equations and introduce several relevant considerations about boundary layer thicknesses and friction coefficient.

7.2.1 Solution of Prandtl's Equations

We will assume that the boundary layer thickness is sufficiently thin not to affect the velocity distribution in the exterior zone modeled by the perfect fluid. Then the exterior flow is such that $U_e = U$, $v_{2e} = 0$. The pressure distribution is obtained by the Euler equation (7.21) giving with $U_e = U$

$$\frac{dp_e}{dx} = 0 \, . \tag{7.39}$$

With (7.39), the Prandtl's equations simplify

$$v_1 \frac{\partial v_1}{\partial x_1} + v_2 \frac{\partial v_1}{\partial x_2} = \nu \frac{\partial^2 v_1}{\partial x_2^2} \tag{7.40}$$

$$\frac{\partial v_1}{\partial x_1} + \frac{\partial v_2}{\partial x_2} = 0 \,. \tag{7.41}$$

We position the origin of the axes at the leading edge of the plate. The boundary conditions are

$$v_1 = v_2 = 0, \quad \text{for} \quad x_2 = 0, \quad x_1 \geq 0, \tag{7.42}$$

$$v_1 = U, \quad \text{for} \quad x_2 \to \infty, \quad x_1 \geq 0 \,. \tag{7.43}$$

To impose a zero boundary layer thickness at the leading edge, we prescribe

$$v_1 = U, \quad \text{for} \quad x_1 = 0, \quad x_2 \neq 0 \,. \tag{7.44}$$

The boundary layer thickness will grow with the distance x_1 and therefore

$$\delta_0 = \delta_0(x_1) \,. \tag{7.45}$$

As the semi-infinite plate has no normative scale that can be derived from the geometry, the abscissa x_1 will fulfill this purpose. The Eq. (7.7) becomes

$$\frac{\delta_0(x_1)}{x_1} = \left(\frac{U x_1}{\nu}\right)^{-1/2} = Re_{x_1}^{-\frac{1}{2}} \tag{7.46}$$

with the definition of a local Reynolds number Re_{x_1} based on the distance to the leading edge. We conclude

$$\delta_0(x_1) = \left(\frac{\nu\, x_1}{U}\right)^{1/2} \,. \tag{7.47}$$

Let us write the system (7.40)–(7.41) in dimensionless form (cf. Chap. 2). We search a solution of these equations such that

$$\frac{v_1}{U} = F\left(\frac{U x_1}{\nu}, \frac{U x_2}{\nu}\right) \,. \tag{7.48}$$

Relation (7.48) can be simplified by writing it in self-similar form. Indeed, if x_1, x_2, v_1, v_2 are replaced respectively by $\alpha^2 x_1, \alpha x_2, \alpha^2 v_1, \alpha v_2$, the Eqs. (7.40)–(7.41) are not modified. This suggests to write relation (7.48) as

$$\frac{v_1}{U} = g(s) \tag{7.49}$$

with the variable

$$s = \frac{Ux_2/\nu}{(Ux_1/\nu)^{1/2}} = x_2\sqrt{\frac{U}{\nu x_1}} = \frac{x_2}{\delta_0(x_1)} \,. \tag{7.50}$$

This type of solution is self-similar as the function that will describe the velocity profile at various stations x_1 will be the same with respect to the variable x_2, normalized by the local boundary layer thickness $\delta_0(x_1)$, this thickness taking the variation of the solution in direction x_1 into account.

The incompressibility constraint (7.41) is trivially satisfied by the introduction of the stream function $\psi(x_1, x_2)$. One has

$$\psi = \int_0^{x_2} v_1 \, dx_2' = U\delta_0 \int_0^{\infty} g(s') \, ds' = U\delta_0 f(s) = (U\nu x_1)^{1/2} f(s) \,, \tag{7.51}$$

with $f'(s) = df/ds = g(s)$. The component v_2 is obtained easily

$$v_2 = -\frac{\partial \psi}{\partial x_1} = \frac{1}{2}\sqrt{\frac{\nu U}{x_1}}[sf'(s) - f(s)] \,. \tag{7.52}$$

With the help of relations (7.49) and (7.52), Eq. (7.40) produces the third-order non linear ordinary differential equation, named Blasius equation

$$f'''(s) + \frac{1}{2} f''(s) f(s) = 0 \tag{7.53}$$

with the boundary conditions

$$f(s\,) = f'(s) = 0, \quad \text{for} \quad s = 0, \tag{7.54}$$

$$f'(s\,) = 1, \quad \text{for} \quad s \to \infty \,. \tag{7.55}$$

This equation is numerically integrated by a fourth-order Runge-Kutta method for example. As we have only two initial conditions in $s = 0$, we must calculate a third condition, namely $f''(0)$, in an iterative fashion. This is nicely performed by a shooting method [39].

One notes that v_1 goes quickly towards the value U of the perfect fluid flow as numerical results yield

$$\frac{v_1}{U} = 0.99 \quad \text{for} \quad s = 4.99 \,, \tag{7.56}$$

$$\frac{v_1}{U} = 0.999 \quad \text{for} \quad s = 5.99 \,. \tag{7.57}$$

We observe in Fig. 7.3 the excellent concordance of the theory and the experimental results represented by small circles. The boundary layer theory constitutes one of the major achievements of the twentieth century fluid mechanics.

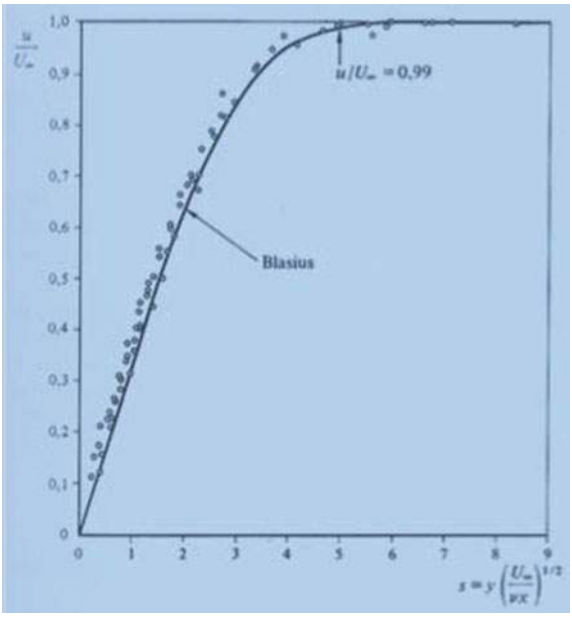

Fig. 7.3 Blasius profile and experimental data [83] where $u = v_1, x = x_1, y = x_2$

7.2.2 Boundary Layer Thicknesses

There exists several ways to define with accuracy the boundary layer thickness. We know that the component v_1 tends asymptotically towards the value U when one approaches this thickness. A first definition giving the sensitive thickness δ_∞ is the value of the ordinate x_2 where v_1 is equal to 99% of U_e. For the flat plate, one obtains

$$\delta_\infty = \delta_{0.99} \simeq 5\sqrt{\frac{\nu x_1}{U}} \,. \tag{7.58}$$

We notice that this thickness depends on the chosen accuracy indicated by the index of δ_∞. Note also that the thickness grows along the obstacle according to $\sqrt{x_1}$.

The concept of displacement thickness δ^* is based on the effective displacement of the exterior flow generated by the reduction of the mass flow rate inside the boundary layer close to the wall, because of the viscous effects as can be seen in Fig. 7.4. It is defined by the relation

$$\delta^* = \int_0^\infty \left(1 - \frac{v_1}{U}\right) dx_2 \,. \tag{7.59}$$

This notion corresponds to the idea of a thickened obstacle, the displacement thickness being defined in such a way to maintain the flow rate conservation between transverse sections made in the flow. We write the relation

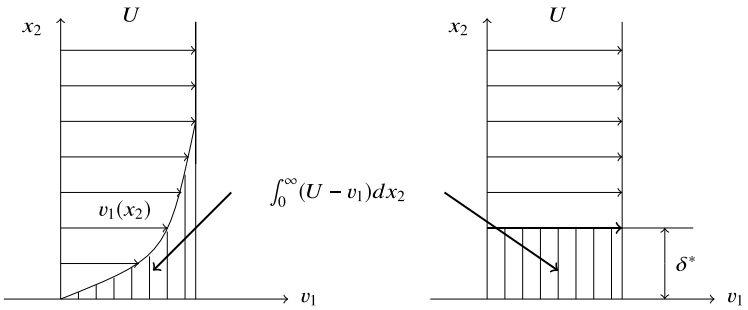

Fig. 7.4 Displacement thickness δ^* in relation with the velocity v_1 at position x_1

$$U\delta^* = \int_0^\zeta (U - v_1)\, dx_2 \tag{7.60}$$

or

$$\int_0^\zeta v_1 dx_2 = U(\zeta - \delta^*) \tag{7.61}$$

expressing the flow rate conservation over the height ζ introduced by (7.29). This length is large with respect to the boundary layer thickness so that it can stretch to infinity. In this case, (7.61) becomes (7.59). For the flat plate, the computation gives

$$\delta^* = 1.721\sqrt{\frac{\nu x_1}{U}}\,. \tag{7.62}$$

Last but not least, the momentum thickness θ defined by the relation

$$\theta = \int_0^\infty \frac{v_1}{U}\left(1 - \frac{v_1}{U}\right) dx_2 \tag{7.63}$$

is linked to the loss of momentum in the boundary layer with respect to the one in the exterior flow. We calculate it as follows

$$\rho \int_0^\infty v_1(U - v_1)\, dx_2 = \rho U^2 \theta\,. \tag{7.64}$$

For the flat plate, one has

$$\theta = 0.664\sqrt{\frac{\nu x_1}{U}}\,. \tag{7.65}$$

These various thicknesses are in the ratio

$$\frac{\delta^*}{\delta_\infty} = \frac{1}{3}, \quad \frac{\theta}{\delta_\infty} = \frac{1}{8}\,. \tag{7.66}$$

7.2.3 Friction and Drag Coefficients

The knowledge of the velocity profile in the vicinity of the flat plate allows the calculation of the wall shear stress and the drag on the plate in the flow. The wall shear stress is given by the relation

$$\tau_w = \mu \frac{\partial v_1}{\partial x_2} \mid_{x_2=0} \ . \tag{7.67}$$

With the stream function (7.51), we obtain

$$v_1 = \frac{\partial \psi}{\partial x_2} = U f'(s) \tag{7.68}$$

$$\frac{\partial v_1}{\partial x_2} = U f''(s) \frac{1}{\delta_0} \ . \tag{7.69}$$

Consequently,

$$\tau_w = \mu U f''(s) \mid_{s=0} \frac{1}{\delta_0} = 0.33 \mu U \sqrt{\frac{U}{\nu x_1}} \ . \tag{7.70}$$

The drag on a plate of length L and of unit width is worth

$$2F_{x_1} = 2 \int_0^L \tau_w \, dx_1 \ . \tag{7.71}$$

The factor of 2 takes into account the existence of the two faces of the plate. By (7.70), one gets

$$F_{x_1} = 0.33 \mu U \sqrt{\frac{U}{\nu}} \int_0^L x_1^{-1/2} dx_1 = 0.66 \sqrt{\mu \rho U^3 L} \ . \tag{7.72}$$

In practice, one expresses the wall shear stress and the drag by dimensionless quantities: the local friction coefficient and the drag coefficient

$$C_f = \frac{\tau_w}{\frac{1}{2}\rho U^2}, \quad C_{x_1} = \frac{F_{x_1}}{\frac{1}{2}\rho U^2 L} \tag{7.73}$$

this last expression corresponding to a plate with unit width.

For the flat plate, one has

$$C_f = 0.66 \frac{\nu}{U} \sqrt{\frac{U}{\nu_1 x}} = \frac{0.66}{Re_{x_1}^{1/2}} \ , \tag{7.74}$$

with the Reynolds number defined by (7.46). The drag coefficient is

$$C_{x_1} = \frac{1.33}{Re_{x_1}^{1/2}} \,. \tag{7.75}$$

7.3 von Kármán Integral Equation

Prandtl's equations become difficult to integrate in closed form as soon as we do not deal with thin profiles. Of course we may always resort to numerical integration; however in this monograph we like to use the analytical tools as much as possible. Therefore we will use another approach based on the integral equation of the momentum relation for the boundary layer. This method is valid for an obstacle shape placed in a moving fluid inasmuch the considered ordinates are small with respect to the local radius of curvature of the obstacle profile.

We integrate Eq. (7.17) in x_2 direction between $x_2 = 0$ and $\zeta(x_1) > \delta_0$. This procedure will generate an ordinary differential equation for θ, called the von Kármán integral equation. The detailed development goes as follows. The first term of (7.17) yields

$$\int_0^{\zeta(x_1)} v_1 \frac{\partial v_1}{\partial x_1} dx_2 = \frac{1}{2} \int_0^{\zeta(x_1)} \frac{\partial v_1^2}{\partial x_1} dx_2 \,. \tag{7.76}$$

An analytical formula that will be most helpful is Leibnitz relation

$$\frac{d}{dx_1} \int_0^{\zeta(x_1)} f(x_2, x_1) dx_2 = \int_0^{\zeta(x_1)} \frac{\partial f}{\partial x_1} dx_2 + f(x_2 = \zeta(x_1), x_1) \frac{d\zeta}{dx_1} \,. \tag{7.77}$$

Using (7.77), we obtain

$$\int_0^{\zeta(x_1)} \frac{\partial v_1^2}{\partial x_1} dx_2 = \frac{d}{dx_1} \int_0^{\zeta(x_1)} v_1^2 dx_2 - v_1^2(\zeta(x_1)) \frac{d\zeta}{dx_1} \,. \tag{7.78}$$

The second term of (7.17) reads

$$\int_0^{\zeta(x_1)} v_2 \frac{\partial v_1}{\partial x_2} dx_2 = v_1 v_2 \Big|_0^{\zeta(x_1)} - \int_0^{\zeta(x_1)} v_1 \frac{\partial v_2}{\partial x_2} dx_2 \,. \tag{7.79}$$

At the wall $x_2 = 0$, we have $v_1 = v_2 = 0$. We assume that at $x_2 = \zeta(x_1)$, $v_1(\zeta(x_1)) = U_e(x_1)$. Furthermore by the incompressibilty constraint, $v_2(\zeta(x_1))$ is expressed by the integral

$$v_2(\zeta(x_1)) = \int_0^{\zeta(x_1)} \frac{\partial v_2}{\partial x_2} dx_2 = -\int_0^{\zeta(x_1)} \frac{\partial v_1}{\partial x_1} dx_2 \,. \tag{7.80}$$

Consequently we write

$$\int_0^{\zeta(x_1)} v_2 \frac{\partial v_1}{\partial x_2} dx_2 = -U_e(x_1) \int_0^{\zeta(x_1)} \frac{\partial v_1}{\partial x_1} dx_2 + \frac{1}{2} \int_0^{\zeta(x_1)} \frac{\partial}{\partial x_1} \left(v_1^2\right) dx_2 \,. \tag{7.81}$$

Applying Leibnitz formula to both integrals on the right-hand side of (7.81), one gets

$$\int_0^{\zeta(x_1)} \left(v_1 \frac{\partial v_1}{\partial x_1} + v_2 \frac{\partial v_1}{\partial x_2} \right) dx_2 = \frac{d}{dx_1} \int_0^{\zeta(x_1)} v_1^2 dx_2 - U_e \frac{d}{dx_1} \int_0^{\zeta(x_1)} v_1 dx_2 \,. \tag{7.82}$$

Using Eq. (7.21) the pressure gradient becomes

$$\int_0^{\zeta(x_1)} -\frac{1}{\rho} \frac{dp_e}{dx_1} dx_2 = \int_0^{\zeta(x_1)} U_e \frac{dU_e}{dx_1} dx_2 \,. \tag{7.83}$$

The viscous term yields

$$\frac{1}{\rho} \int_0^{\zeta(x_1)} \frac{\partial}{\partial x_2} \left(\mu \frac{\partial v_1}{\partial x_2} \right) dx_2 = \frac{1}{\rho} \left[\mu \frac{\partial v_1}{\partial x_2} \right] \Big|_0^{\zeta(x_1)} = -\frac{\tau_w}{\rho} \,, \tag{7.84}$$

as in the exterior region, we have a perfect fluid (no shear stress involved). At this stage, Prandtl's equation is transformed into the relation

$$\frac{d}{dx_1} \int_0^{\zeta(x_1)} v_1^2 dx_2 - U_e \frac{d}{dx_1} \int_0^{\zeta(x_1)} v_1 dx_2 - \int_0^{\zeta(x_1)} U_e \frac{dU_e}{dx_1} dx_2 = -\frac{\tau_w}{\rho} \,. \tag{7.85}$$

Using Leibnitz formula again, let us compute the following term with $U_e = U_e(x_1)$

$$\frac{d}{dx_1}\int_0^{\zeta(x_1)} v_1 U_e dx_2 = \int_0^{\zeta(x_1)} \frac{\partial}{\partial x_1}(v_1 U_e) dx_2 + v_1 U_e(\zeta(x_1))\frac{d\zeta}{dx_1}$$
$$= \int_0^{\zeta(x_1)} U_e \frac{\partial v_1}{\partial x_1} dx_2 + \int_0^{\zeta(x_1)} v_1 \frac{dU_e}{dx_1} dx_2 + v_1 U_e(\zeta(x_1))\frac{d\zeta}{dx_1}$$
$$= U_e \int_0^{\zeta(x_1)} \frac{\partial v_1}{\partial x_1} dx_2 + \frac{dU_e}{dx_1}\int_0^{\zeta(x_1)} v_1 dx_2 + v_1 U_e(\zeta(x_1))\frac{d\zeta}{dx_1}$$
$$= U_e \frac{d}{dx_1}\int_0^{\zeta(x_1)} v_1 dx_2 - v_1 U_e(\zeta(x_1))\frac{d\zeta}{dx_1} + v_1 U_e(\zeta(x_1))\frac{d\zeta}{dx_1}$$
$$+ \frac{dU_e}{dx_1}\int_0^{\zeta(x_1)} v_1 dx_2 \,. \tag{7.86}$$

With (7.86) the second term of relation (7.85) is rewritten

$$U_e \frac{d}{dx_1}\int_0^{\zeta(x_1)} v_1 dx_2 = \frac{d}{dx_1}\int_0^{\zeta(x_1)} v_1 U_e dx_2 - \frac{dU_e}{dx_1}\int_0^{\zeta(x_1)} v_1 dx_2 \,. \tag{7.87}$$

The left hand side of (7.85) leads to the relationship

$$\frac{d}{dx_1}\int_0^{\zeta(x_1)} (v_1^2 - v_1 U_e) dx_2 + \frac{dU_e}{dx_1}\int_0^{\zeta(x_1)} (v_1 - U_e) dx_2$$
$$= -\frac{d}{dx_1}\left[U_e^2 \int_0^{\zeta(x_1)} \frac{v_1}{U_e}\left(1 - \frac{v_1}{U_e}\right) dx_2\right] - U_e \frac{dU_e}{dx_1}\int_0^{\zeta(x_1)} \left(1 - \frac{v_1}{U_e}\right) dx_2 \,. \tag{7.88}$$

As $\zeta(x_1)$ is still arbitrary, we impose now that $\zeta(x_1) \to \infty$. Therefore, with (7.88) and the definitions (7.59) and (7.63), the relation (7.85) reads

$$\frac{d}{dx_1}(U_e^2 \theta) + U_e \frac{dU_e}{dx_1}\delta^* = \frac{\tau_w}{\rho} \,. \tag{7.89}$$

Dividing through by U_e^2 and carrying the algebra, we find the classical form of von Kármán equation

$$\frac{d\theta}{dx_1} = \frac{\tau_w}{\rho U_e^2} - \frac{1}{U_e}\frac{dU_e}{dx_1}(2\theta + \delta^*)$$
$$= \frac{C_f}{2} - \frac{\theta}{U_e}(H+2)\frac{dU_e}{dx_1}\,, \tag{7.90}$$

where H is the shape factor defined by

$$H = \frac{\delta^*}{\theta}\,. \tag{7.91}$$

The increase of the momentum thickness θ depends on the wall shear stress. If the exterior flow is accelerated, i. e. $dU_e/dx_1 > 0$, the θ growth is penalized. On the contrary, if $dU_e/dx_1 < 0$, the thickness θ will grow. If the deceleration is strong enough, the boundary layer will separate from the wall involving that $\tau_w = 0$ and therefore the separation criterion is

$$\frac{\partial v_1}{\partial x_2}|_{x_2=0} = 0\,. \tag{7.92}$$

7.4 von Kármán-Pohlhausen Approximate Method

When the boundary layer theory was proposed by Prandtl, the computational resources of today did not exist. The integral equation of the previous section was very much in use. The von Kármán-Pohlhausen method is a solution procedure that consists in assuming the approximate shape of the velocity profile. Pohlhausen considered a fourth degree polynomial. For the sake of simplicity we will restrict ourselves to a third degree case and we then write the velocity as follows

$$\frac{v_1}{U_e(x_1,0)} = a(x_1) + b(x_1)s + c(x_1)s^2 + d(x_1)s^3, s = x_2/\delta_\infty, 0 \le s \le 1\,. \tag{7.93}$$

This profile is subjected to several boundary conditions. On the obstacle, the fluid sticks to the wall

$$v_1 = 0 \quad \text{for} \quad s = 0\,. \tag{7.94}$$

Furthermore along the wall, the velocity profile must satisfy Prandtl's equation (7.17). We write

$$\frac{1}{\rho}\frac{dp}{dx_1} = \nu\frac{\partial^2 v_1}{\partial x_2^2} \quad \text{for} \quad s = 0. \tag{7.95}$$

The velocity v_1 for $x_2 = \delta_\infty$ where the boundary layer meets the exterior flow, must be very close to $U_e(x_1, 0)$. Thus we have

$$v_1 = U_e(x_1, 0), \quad \left.\frac{\partial v_1}{\partial x_2}\right|_{x_2=\delta_\infty} = 0 \quad \text{for} \quad s = 1. \tag{7.96}$$

The variable $U_e(x_1, 0)$ will be computed from the theory of perfect fluids taking the shape of the obstacle into account. Then the conditions (7.94) and (7.95) with the integral equation (7.89) will provide the evaluation of the four coefficients introduced in (7.93) and the thickness for the matching condition. When the shape of the profile is more complex, one utilizes a polynomial of higher degree. We thus impose that derivatives of degree equal or higher than two are zero at $s = 1$ and expressions obtained by successive derivatives of Prandtl's equation with respect to the x_2 variable vanish at $s = 1$.

We illustrate the Pohlhausen method for the uniform flow over a flat plate. Conditions (7.94) and (7.95) show immediately that coefficients a and c are zero. Imposing conditions (7.96), the two other coefficients must satisfy the relationships

$$\begin{aligned} b + d &= 1\,, \\ b + 3d &= 0\,. \end{aligned} \tag{7.97}$$

The polynomial reads

$$\frac{v_1}{U_e} = \frac{s}{2}\left(3 - s^2\right)\,. \tag{7.98}$$

We are able now to calculate the approximate displacement thickness

$$\delta^* = \delta_\infty \int_0^1 (1 - \frac{v_1}{U_e})ds = \frac{3}{8}\delta_\infty \tag{7.99}$$

and the approximate momentum thickness

$$\theta = \delta_\infty \int_0^1 \frac{v_1}{U_e}\left(1 - \frac{v_1}{U_e}\right)ds = \frac{117}{840}\delta_\infty\,. \tag{7.100}$$

The wall shear stress is given by

$$\frac{\tau_w}{\rho} = \nu \left.\frac{\partial v_1}{\partial x_2}\right|_{x_2=\infty} = \nu \frac{3}{2}\frac{U_e}{\delta_\infty}\,. \tag{7.101}$$

To compute the matching thickness δ_∞ we use Prandtl's equation which is simplified as the variable $U_e(x_1, 0)$ is equal to the constant velocity U

$$\frac{\tau_w}{\rho} = U^2 \frac{d\theta}{dx_1}\,. \tag{7.102}$$

Combining (7.100)–(7.102), we obtain

$$\frac{3\nu U}{2\delta_\infty} = U^2 \frac{117}{840} \frac{d\delta_\infty}{dx_1} \,. \tag{7.103}$$

Integrating (7.103) we eventually get

$$\delta_\infty = \sqrt{\frac{840}{39}} \sqrt{\frac{\nu x_1}{U}} = 4.64 \sqrt{\frac{\nu x_1}{U}} \,. \tag{7.104}$$

This last equation shows that the approximate method is not that far from the exact solution (7.58).

Exercises

7.1 Evaluate by the von Kármán-Pohlhausen method the velocity profile for the plane plate case. The profile is approximated by the fourth degree polynomial

$$\frac{v_1}{U_e(x_1)} = a(x_1) + b(x_1)s + c(x_1)s^2 + d(x_1)s^3 + e(x_1)s^4, s = \frac{x_2}{\delta_\infty}, 0 \le s \le 1 \,. \tag{7.105}$$

where x_2 is the normal distance to the wall and δ_∞ the thickness of the boundary layer.

Deduce the boundary layer thicknesses, the displacement thickness δ^*, the momentum thickness θ and the wall shear stress τ_w.

7.2 The velocity profile of a laminar boundary layer over a flat plate can be approximated by the relation

$$v_1(x_2) = A \sin(Bx_2) + C \,. \tag{7.106}$$

- Enumerate the boundary conditions for the problem and obtain the values of the constants A, B, C.
- Compute the expression of the boundary layer thickness $\delta_0 = \delta_0(x_1)$.

The method goes through the following steps

1. Calculate θ the momentum thickness as

$$\theta = \int_0^{\delta_0} \frac{v_1}{U} \left(1 - \frac{v_1}{U}\right) dx_2 \,. \tag{7.107}$$

2. Show that the equation for θ is

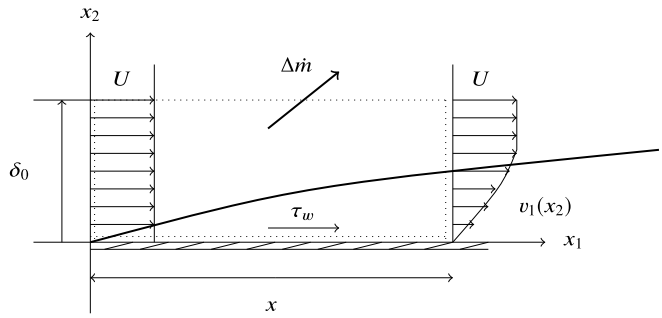

Fig. 7.5 Boundary layer over a flat plate

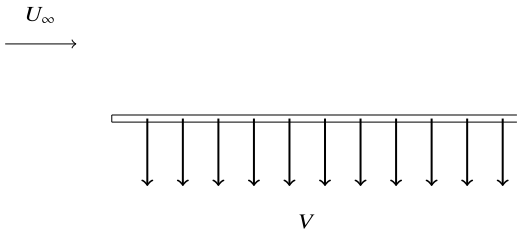

Fig. 7.6 Boundary layer over a porous wall

$$\frac{\partial \theta}{\partial x_1} = \frac{\tau_w}{\rho U^2} \,, \tag{7.108}$$

using the momentum conservation and continuity on the control volume (dotted lines) displayed in Fig. 7.5.

- Calculate the wall shear stress τ_w and deduce δ_0.

7.3 We consider the plane flow of an incompressible fluid over a porous plate. Through evenly distributed small holes, part of the laminar boundary layer is sucked. Let us denote by V the normal component of the velocity to the plate surface at $x_2 = 0$. Assuming V is constant, it is possible to demonstrate that for very small values of the aspiration velocity, i.e. $V/U_\infty \ll 1$, the boundary layer thickness becomes constant and the shape of the velocity profile invariable at long distance from the leading edge (Fig. 7.6).

At a long distance from the leading edge, it is requested to calculate

- from Prandtl's equations, the velocity profile $v_1(x_2)/U_\infty$.
- the value of the wall shear stress τ_w.
- the displacement and momentum thicknesses. Compute the shape factor (7.91). Compare this factor to the one of the laminar boundary layer over a non porous plate.

Chapter 8
Instability

8.1 Transition

The transition between laminar flow and turbulence is generated by instability mechanisms. Those mechanisms do not occur in the same operational mode in every geometrical configuration. The associated dynamics. i. e. the temporal behavior of the flow field may be sometimes smooth, sometimes brutal.

We will distinguish two types of transition. The first one, named spectral transition, characterizes the passage to turbulence by numerous bifurcations. The most exemplary flow of this situation is the circular Couette flow between two concentric cylinders. Suppose that the outer cylinder of radius R_2 is fixed, while the inner cylinder of radius R_1 rotates with an angular constant velocity ω. The Reynolds number can be defined by the relation

$$Re = \frac{\omega R_1 (R_2 - R_1)}{\nu} \, . \tag{8.1}$$

For small values of the Reynolds number, the flow is laminar and the Navier-Stokes equations allow to calculate the azimuthal velocity profile (3.41)

$$v_\theta = Ar + B/r \, , \tag{8.2}$$

with $A = -\omega R_1^2/(R_2^2 - R_1^2)$ and $B = \omega R_1^2 R_2^2/(R_2^2 - R_1^2)$. If the rotational speed ω is increased, for a critical Reynolds number, a new configuration containing Taylor vortices appears, cf. Fig. 1.1. On top of the fundamental flow (8.2) is superimposed a secondary flow in such a way that a fluid particle moves on a toroidal axisymmetric material surface. At higher Reynolds numbers, the torus is deformed in the azimuthal direction, cf. Fig. 1.2. For high enough Reynolds numbers, turbulence is developing.

The second type of transition is catastrophic transition where the passage from laminar state to turbulence occurs suddenly and instantaneously without a cascade of transitions. This is the case of developed Poiseuille flow in a cylindrical pipe. This

M. O. Deville, *An Introduction to the Mechanics of Incompressible Fluids*,
https://doi.org/10.1007/978-3-031-04683-4_8

instability was first observed by O. Reynolds [77] who gave his name to the eponym dimensionless number.

Fluid instability is a very rich and subtle subject. It influences all flows and the investigations for a full understanding of those complex phenomena involve both experiments, theoretical developments and today numerical simulations. Therefore the reader is facing the challenge of selecting his preferences and choices. The recent books by Tapan Sengupta [87, 88] constitute an updated review of those crucial subjects. As far as I am concerned I will concentrate on parallel flows and the circular Couette flow.

8.2 Orr-Sommerfeld Equation

The theory of hydrodynamic stability is a complicated subject from the mathematical point of view. We will tackle it in the framework of parallel flows of homogeneous fluids. This theory consists in analysing a base flow on which perturbations of small amplitude are superimposed. The non-linear term of the Navier-Stokes equations will generate an interaction with these perturbations. If they grow with respect to time, then the flow is unstable. If, on the contrary, the viscosity is sufficient to prevent those perturbations to grow, then the flow is stable.

Let us resume the dimensionless Navier-Stokes equations (2.47)–(2.48) where the body force is neglected and the accents are omitted to alleviate the notation. Let us consider the steady-state plane base flow satisfying the Navier-Stokes equations such that

$$\boldsymbol{v} = (V_1(x_1, x_2), V_2(x_1, x_2), 0) \tag{8.3}$$

and let us suppose that it is almost parallel to x_1 axis, namely

$$| V_2 | \ll | V_1 |, \quad | \partial V_1 / \partial x_1 | \ll | \partial V_1 / \partial x_2 | \ . \tag{8.4}$$

In order to enforce the flow stability criterion, three-dimensional velocity $\boldsymbol{v}'$ and pressure p' perturbations are superimposed on the fundamental flow. We have

$$\boldsymbol{v} = (V_1(x_1, x_2) + v_1'(\boldsymbol{x}, t), V_2(x_1, x_2) + v_2'(\boldsymbol{x}, t), v_3'(\boldsymbol{x}, t)), \tag{8.5}$$

$$p = P + p' \ . \tag{8.6}$$

Inserting (8.5)–(8.6) in (2.47)–(2.48) and neglecting the quadratic perturbations terms, one obtains taking (8.4) into account the linearized equations

$$\boldsymbol{\nabla} \cdot \boldsymbol{v}' = 0 \ , \tag{8.7}$$

$$\frac{\partial \boldsymbol{v}'}{\partial t} + V_1 \frac{\partial \boldsymbol{v}'}{\partial x_1} + v_2' \frac{\partial V_1}{\partial x_2} \boldsymbol{e}_1 = -\boldsymbol{\nabla} p' + \frac{1}{Re} \Delta \boldsymbol{v}' \ . \tag{8.8}$$

As stability theory is more developed for shear flows, we will restrict our attention to the fundamental parallel flow corresponding to $\boldsymbol{v} = (V_1(x_2), 0, 0)$. The stability problem is considerably simplified if Squire theorem [97] is evoked:

Theorem 8.1 (Squire theorem) *The behavior of three-dimensional perturbations can be deduced from the behavior of two-dimensional perturbations in a parallel flow of incompressible fluid.*

A proof is given in Rieutord [79]. Note that Squire's theorem pertains to disturbance growth in time, while in actual flow the disturbances actually grow spatio-temporally.

Therefore, for every three-dimensional unstable perturbation, there exists a corresponding two-dimensional perturbation that is still more unstable. This allows us to search the flow stability limit as a function of the Reynolds number, using a plane perturbation, while being assured that this procedure yields the inferior stability limit.

To verify the incompressibility constraint in a plane problem, it is natural to resort to the streamfunction. We get rid of the pressure variable by dealing with the dynamic vorticity equation. We have

$$v_1 = \frac{\partial \psi}{\partial x_2}, \quad v_2 = -\frac{\partial \psi}{\partial x_1}, \tag{8.9}$$

and consequently, by the vorticity definition (1.40)

$$\omega = -\Delta \psi \ . \tag{8.10}$$

Using (8.10) in (4.25), we obtain

$$\frac{\partial \Delta \psi}{\partial t} + \frac{\partial \psi}{\partial x_2}\frac{\partial \Delta \psi}{\partial x_1} - \frac{\partial \psi}{\partial x_1}\frac{\partial \Delta \psi}{\partial x_2} = \frac{1}{Re}\,\Delta \Delta \psi \ . \tag{8.11}$$

The boundary conditions to integrate (8.11) are no-slip conditions at the fixed lower and upper walls located in $x_2 = x_{2,lo}, x_{2,up}$ expressed in term of the streamfunction

$$\psi = const, \ \frac{\partial \psi}{\partial x_2} = 0, \quad \text{for } x_2 = x_{2,lo}, x_{2,up}. \tag{8.12}$$

Decomposing the streamfunction as $\psi = \Psi + \psi'$, where $\Psi = \int V_1(x_2)\, dx_2$ represents the fundamental flow and ψ' the perturbation, (8.11) is linearized

$$\frac{\partial \Delta \psi'}{\partial t} + V_1 \frac{\partial \Delta \psi'}{\partial x_1} - \frac{d^2 V_1}{dx_2^2}\frac{\partial \psi'}{\partial x_1} = \frac{1}{Re}\,\Delta \Delta \psi' \ . \tag{8.13}$$

The perturbation is approximated in normal modes

$$\psi' = \phi(x_2) e^{i\alpha(x_1 - ct)} \ . \tag{8.14}$$

Insertion of the normal mode (8.14) in (8.13) leads to the Orr-Sommerfeld equation [Orr [65]- Sommerfeld [93]]

$$(\frac{d^2}{dx_2^2} - \alpha^2)^2\phi = i\alpha\, Re\left[(V_1 - c)(\frac{d^2\phi}{dx_2^2} - \alpha^2\phi) - \phi\,\frac{d^2V_1}{dx_2^2}\right] . \tag{8.15}$$

This equation is the cornerstone of hydrodynamic stability. Numerical solutions have been given by Jordinson [41] and Orszag [66] more than half a century after its discovery. Equation (8.15) with the boundary conditions

$$\phi = \frac{d\phi}{dx_2} = 0 \quad \text{for } x_2 = x_{2,lo}, x_{2,up} \tag{8.16}$$

can be solved if the profile $V_1(x_2)$, the Reynolds number Re and the dimensionless wavenumber α are given. The equation will produce the eigenfunction $\phi(x_2)$, but also the complex wave velocity $c = c_R + i\, c_I$ as the associated eigenvalue. For fixed α and Re, the eigenvalue problem generates a discrete spectrum of eigenvalues $c_1, c_2, c_3, \ldots$. We consider that the eigenvalues are function of α and Re

$$\begin{aligned} c_R &= c_R(\alpha, Re) \\ c_I &= c_I(\alpha, Re) \, . \end{aligned} \tag{8.17}$$

The perturbation growth goes like $e^{\alpha c_I t}$. The flow is unstable for $c_I > 0$. A neutral stability mode is obtained for $c_I = 0$. Consequently, imposing $c_I = 0$ in (8.17) gives the neutral stability curve $c_I(\alpha, Re) = 0$. If, moreover, it is possible to show that c_I changes sign when we cross the neutral curve, then this curve is also that of marginal stability. The marginal stability curve separates the stable and unstable regions in the domain (α, Re).

Figure 8.1 shows the stability diagram in the plane (α, Re) for the plane Poiseuille flow (3.19). Instability occurs for parameter values inside the marginal stability curve. The critical Reynolds number Re_{crit} is obtained at the lowest value of the Reynolds number defining the stability curve and corresponds to the vertical tangent line in Fig. 8.1. The critical Reynolds number is 5772 for $\alpha = 1.02$.

The numerical solution of the Orr-Sommerfeld equation by S. A. Orszag used the Chebyshev Tau method [36, 66]. The Fortran program as coded in the 1970s is given in the Appendix D.

8.3 Stability of the Circular Couette Flow

Referring to the radial Navier-Stokes equation (3.39) for the circular Couette flow, we observe that the centrifugal force is balanced by the radial pressure gradient. Therefore the destabilizing physical force of the laminar Couette flow is this centrifugal force that is no longer in equilibrium with pressure and viscous forces.

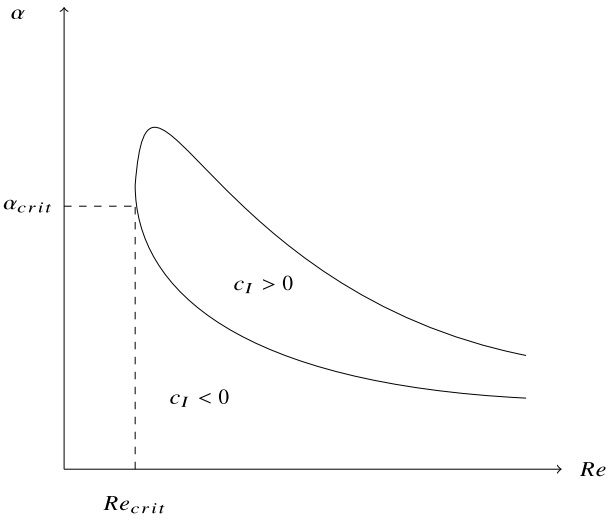

Fig. 8.1 Example of the marginal stability curve for the plane Poiseuille flow

8.3.1 Rayleigh's Criterion

The first analysis of this unstable phenomenon was carried out by Rayleigh [76] in the context of inviscid fluids. Suppose that the streamlines are circles and the disturbances are axisymmetric in a cylindrical coordinate system. As the pressure is independent of θ, the momentum equation in the azimuthal direction is

$$\frac{\partial v_\theta}{\partial t} + v_r \frac{\partial v_\theta}{\partial r} + \frac{v_\theta}{r}\frac{\partial v_\theta}{\partial \theta} + v_z \frac{\partial v_\theta}{\partial z} + \frac{v_r v_\theta}{r} = 0\,. \tag{8.18}$$

If we multiply (8.18) by r we obtain the relation

$$\frac{\partial (r v_\theta)}{\partial t} + v_r \frac{\partial (r v_\theta)}{\partial r} + \frac{v_\theta}{r}\frac{\partial (r v_\theta)}{\partial \theta} + v_z \frac{\partial (r v_\theta)}{\partial z} = \frac{D\Gamma}{Dt} = 0\,, \tag{8.19}$$

showing that the circulation $\Gamma = 2\pi r v_\theta$ should remain constant for a fluid element.

Let us consider two fluid annular elements of radii r_1 and r_2, respectively, with $r_1 < r_2$. The kinetic energy of these rings are $E_k = \frac{1}{2}\rho v_\theta^2 = \rho\Gamma^2/8\pi^2 r^2$. If we exchange these two elements, their mass and angular momentum will be conserved, while the kinetic energy will not. The total initial kinetic energy is

$$E_{k,init} = \frac{\rho}{8\pi^2}\left[\left(\frac{\Gamma_1}{r_1}\right)^2 + \left(\frac{\Gamma_2}{r_2}\right)^2\right]\,. \tag{8.20}$$

As this exchange is a perturbation with constant circulation, the final kinetic energy reads

$$E_{k,fin} = \frac{\rho}{8\pi^2}\left[\left(\frac{\Gamma_1}{r_2}\right)^2 + \left(\frac{\Gamma_2}{r_1}\right)^2\right] . \tag{8.21}$$

The difference between these two energies is

$$E_{k,fin} - E_{k,init} = \frac{\rho}{8\pi^2}(\Gamma_2^2 - \Gamma_1^2)(\frac{1}{r_1^2} - \frac{1}{r_2^2}) . \tag{8.22}$$

If $E_{k,fin}$ is larger than $E_{k,init}$, the perturbation needs receiving a definite quantity of energy. This cannot be provided by the flow at hand and therefore the physical situation is stable. On the contrary, if $E_{k,fin}$ is smaller than $E_{k,init}$, this means that the disturbance releases energy and it can be captured to feed the disturbance itself. Consequently, for a stable flow, we have Rayleigh's condition

$$\Gamma_2^2 > \Gamma_1^2 \quad \text{for} \quad r_2 > r_1 . \tag{8.23}$$

Rephrasing the condition with the velocity profile, we write

$$(r_2 v_{\theta 2})^2 > (r_1 v_{\theta 1})^2 . \tag{8.24}$$

With the solution of the circular Couette flow (3.41), we have

$$r v_\theta = A r^2 + B . \tag{8.25}$$

If the outer cylinder rotates in the positive direction $\omega_2 > 0$, the quantity (8.25) will increase with r provided the following condition obtained from the constant A in (3.41) holds

$$\omega_2 \geq \left(\frac{R_1}{R_2}\right)^2 \omega_1 . \tag{8.26}$$

If in (8.26) we use the equal sign, we obtained the Rayleigh line. Figure 8.2 exhibits the stability diagram for the perfect fluid in the (ω_1, ω_2) plane.

If the inner cylinder is fixed and the outer one rotates, the flow is stable. If the outer cylinder is fixed with the inner rotating, the flow is unstable according to the inviscid analysis. However, in the real world, viscosity is always present and damps all disturbances if the Reynolds number is not too high.

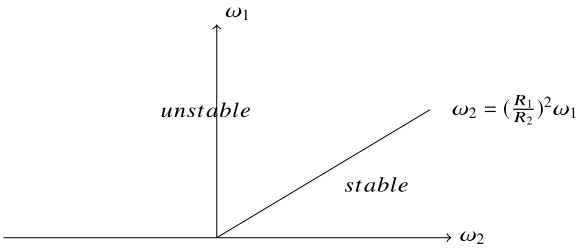

Fig. 8.2 For the inviscid fluid, the Rayleigh line $\omega_2 = (R_1/R_2)^2\omega_1$ separates the stable and unstable regions in the (ω_1, ω_2) plane

8.3.2 *Linear Stability of Viscous Circular Couette Flow*

Let us start from the Navier-Stokes equations written in cylindrical coordinates (A.21)–(A.23) with the incompressibility constraint (A.20). Assuming axial symmetry and neglecting the body force, with the simplification $\partial/\partial\theta = 0$, the equations read

$$\rho\left(\frac{\partial v_r}{\partial t} + v_r\frac{\partial v_r}{\partial r} + v_z\frac{\partial v_r}{\partial z} - \frac{v_\theta^2}{r}\right) = -\frac{\partial p}{\partial r} + \mu\left(\triangle v_r - \frac{v_r}{r^2}\right) \tag{8.27}$$

$$\rho\left(\frac{\partial v_\theta}{\partial t} + v_r\frac{\partial v_\theta}{\partial r} + v_z\frac{\partial v_\theta}{\partial z} + \frac{v_r v_\theta}{r}\right) = \mu\left(\triangle v_\theta - \frac{v_\theta}{r^2}\right) \tag{8.28}$$

$$\rho\left(\frac{\partial v_z}{\partial t} + v_r\frac{\partial v_z}{\partial r} + v_z\frac{\partial v_z}{\partial z}\right) = -\frac{\partial p}{\partial z} + \mu\triangle v_z \tag{8.29}$$

$$\frac{\partial v_r}{\partial r} + \frac{v_r}{r} + \frac{\partial v_z}{\partial z} = 0\,. \tag{8.30}$$

The stability analysis requires that the base flow be perturbed by three-dimensional axisymmetric velocity and pressure disturbances, denoted for ease of notation by (u, v, w) and p_p, respectively,

$$\boldsymbol{v} = (u, V + v, w) \quad \text{and} \quad p = P + p_p\,, \tag{8.31}$$

with V being the Couette flow solution (3.41). Inserting (8.31) in (8.27)–(8.30), we proceed to a linearization keeping only the first-order terms in the perturbations, while discarding higher order terms

$$\rho\left(\frac{\partial u}{\partial t} - \frac{(V+v)^2}{r}\right) = -\frac{\partial(P + p_p)}{\partial r} + \mu\left(\triangle u - \frac{u}{r^2}\right) \tag{8.32}$$

$$\rho\left(\frac{\partial v}{\partial t} + u\frac{dV}{dr} + \frac{u}{r}(V+v)\right) = \mu\left(\triangle v - \frac{v}{r^2}\right) \tag{8.33}$$

$$\rho\frac{\partial w}{\partial t} = -\frac{\partial(P + p_p)}{\partial z} + \mu\triangle w \tag{8.34}$$

$$\frac{\partial u}{\partial r} + \frac{u}{r} + \frac{\partial w}{\partial z} = 0\,. \tag{8.35}$$

With V satisfying the Navier-Stokes equations and carrying through a further step of the linearization process, we obtain

$$\rho\left(\frac{\partial u}{\partial t} - \frac{2Vv}{r}\right) = -\frac{\partial p_p}{\partial r} + \mu(\triangle u - \frac{u}{r^2}) \tag{8.36}$$

$$\rho\left(\frac{\partial v}{\partial t} + u(\frac{V}{r} + \frac{dV}{dr})\right) = \mu(\triangle v - \frac{v}{r^2}) \tag{8.37}$$

$$\rho\frac{\partial w}{\partial t} = -\frac{\partial p_p}{\partial z} + \mu\Delta w \tag{8.38}$$

$$\frac{\partial u}{\partial r} + \frac{u}{r} + \frac{\partial w}{\partial z} = 0\,. \tag{8.39}$$

This set of linear partial differential equations has coefficients depending only on the radial direction r. Therefore it is usual to search solutions in the form of normal axisymmetric modes such that

$$(u, v, w, p_p) = (\hat{u}(r), \hat{v}(r), \hat{w}(r), \hat{p_p}(r))e^{ikz+\sigma t}\,, \tag{8.40}$$

where k is the real wavenumber associated with the axial direction and σ the growth rate.

Let us set

$$D = \frac{d}{dr} \quad \text{and} \quad D_* = \frac{d}{dr} + \frac{1}{r}\,. \tag{8.41}$$

The stability equations become

$$\sigma\hat{u} - \frac{2V\hat{v}}{r} = -\frac{1}{\rho}D\hat{p_p} + \nu(DD_* - k^2)\hat{u} \tag{8.42}$$

$$\sigma\hat{v} + \hat{u}D_*V = \nu(DD_* - k^2)\hat{v} \tag{8.43}$$

$$\sigma\hat{w} = -ik\frac{\hat{p_p}}{\rho} + \nu(D_*D - k^2)\hat{w} \tag{8.44}$$

$$D_*\hat{u} + ik\hat{w} = 0\,. \tag{8.45}$$

From Eq. (8.45) we extract $\hat{w}$ in terms of $\hat{u}$. This expression is then inserted in Eq. (8.44) that yields the pressure

$$\frac{\hat{p_p}}{\rho} = \frac{1}{k^2}\left(\nu(D_*D - k^2) - \sigma\right)D_*\hat{u}\,. \tag{8.46}$$

Taking the derivative D of (8.46) and using it in (8.42) we are left with the relations

$$\nu\left(DD_* - k^2\right)^2 \hat{u} - 2k^2\frac{V}{r}\hat{v} = \sigma(DD_* - k^2)\hat{u} \tag{8.47}$$

$$\nu\left(DD_* - k^2\right)\hat{v} - (D_*V)\hat{u} = \sigma\hat{v} \tag{8.48}$$

$$\hat{u} = \hat{v} = D\hat{u} = 0 \qquad \text{for} \quad r = R_1, R_2\,. \tag{8.49}$$

The first analytical investigation of this eigenvalue problem was carried out by G. I. Taylor [103] with the narrow-gap approximation where the gap $d = R_2 - R_1$ is smaller than the mean radius $R_m = (R_1 + R_2)/2$. With this assumption, the operator D_* is approximated by D and the set of equations simplifies. The reader is referred to Chandrasekhar [18] and Drazin and Reid [27] for the detailed analysis. The stability problem is characterized by the dimensionless Taylor number Ta

$$Ta = 4\left(\frac{\omega_1 R_1^2 - \omega_2 R_2^2}{R_2^2 - R_1^2}\right)\frac{\omega_1 d^4}{\nu^2}\,. \tag{8.50}$$

Another definition of the Taylor number when the outer cylinder is fixed is

$$Ta = \left(\frac{\omega_1 R_1 d}{\nu}\right)^2 \frac{d}{R_m}\,. \tag{8.51}$$

The critical Taylor number is obtained for the fixed outer cylinder $\omega_2 = 0$, $Ta_{crit} = 1706$. Figure 8.3 exhibits the curve of marginal stability ($\sigma = 0$) for the apparatus used by Taylor [103] where the full dots are observed data while open circles are computational results. Above the marginal curve the flow is unstable. Note that the dotted line in the right quadrant is the Rayleigh stability line for inviscid perturbation. The axial wavenumber corresponding to the critical Taylor number, $k_{crit} = 3.12$, corresponds to a wavelength $\lambda_{crit} = 2\pi d/k_{crit} \approx 2d$. This means that the Taylor vortices have a height that is approximately equal to d so that each vortex has a shape close to a square.

To solve the set of Eqs. (8.45)–(8.49) high-order numerical discretizations are used like Chebyshev collocation or Tau methods or spectral elements [23]. The resulting discrete equations form a generalized eigenvalue problem that is solved using appropriate routines to be found in Lapack.

8.3.3 Non-linear Axisymmetric Taylor Vortices

The next step in analyzing the stability of Taylor vortices has been carried out by Davey [22] (see also Koschmieder [44]) who developed the velocity and pressure disturbances in Fourier series of k modes as non linearities excite high-order harmonics. Therefore we write

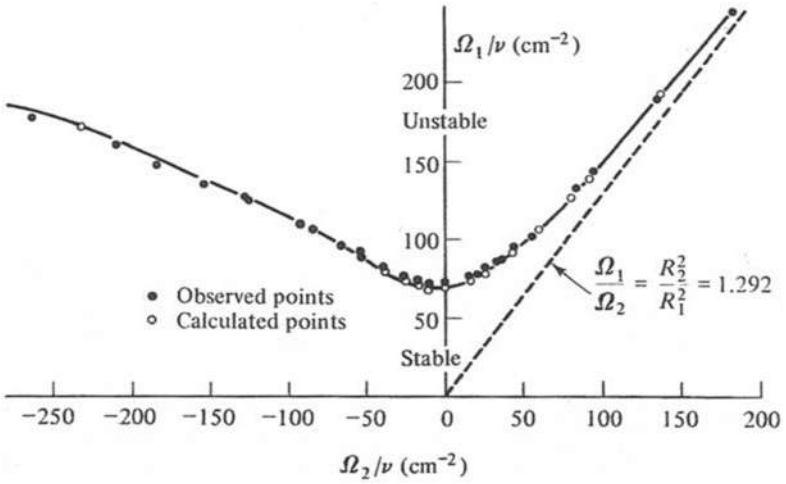

Fig. 8.3 Marginal stability curve for the Taylor-Couette flow with water. Experimental results and narrow-gap calculations. $R_1 = 3.55\,\text{cm}$ and $R_2 = 4.035\,\text{cm}$. Reproduced from [27]

$$u = \sum_{n=1}^{\infty} u_n(r,t)\cos nkz\ , \tag{8.52}$$

$$v = \overline{v}(r,t) + \sum_{n=1}^{\infty} v_n(r,t)\cos nkz\ , \tag{8.53}$$

$$w = \sum_{n=1}^{\infty} w_n(r,t)\sin nkz\ , \tag{8.54}$$

where $\overline{v}$ is the mean azimuthal velocity averaged in the z periodic direction. The elimination of the pressure p and the vertical velocity w leads to two differential equations.

Instead of solving the general initial value problem, Davey assumes that the spatial shape of the disturbance is unaltered and characterized in time by an unknown amplitude function $A(t)$. Because of the non-linear terms, the fundamental disturbance will grow according to the linear theory for $Ta > Ta_{crit}$, and will constrain the harmonics $\cos nkz$ and a mean motion term. As $\cos^2 kz = (1 + \cos 2kz)/2$, the first harmonic $\cos 2kz$ and the mean motion will be $O(A^2)$. Afterwards the fundamental mode interacting with the first harmonic $\cos kz \cos 2kz$ will generate a second harmonic $\cos 3kz$ and a correction to the fundamental $\cos kz$ of order $O(A^3)$. Consequently one writes

$$u_n(r,t) = A^n\left[u_n(r) + \sum_{n=1}^{\infty} A^{2m} u_{nm}(r)\right]\ , \quad n \geq 1 \tag{8.55}$$

$$v_n(r,t) = A^n \left[v_n(r) + \sum_{n=1}^{\infty} A^{2m} v_{nm}(r) \right] , \quad n \geq 1 \tag{8.56}$$

$$\overline{v} = \overline{v_{lam}} + \sum_{n=1}^{\infty} A^{2m} f_m(r) , \tag{8.57}$$

with $\overline{v_{lam}}$ the mean of the laminar state. With these expansions, the time dependent amplitudes are governed by the equation

$$\frac{dA}{dt} = f(A) = \sum_{m=0}^{\infty} a_m A^{2m+1} , \quad a_0 = \sigma . \tag{8.58}$$

We invoke the symmetry of the dynamical system following the line of reasoning in Rieutord [79]. If the system is invariant under the symmetry $A \to -A$ such that if A is a solution, $-A$ is also a solution, and we thus have $f(-A) = -f(A)$ because of the linearity of d/dt. We then conclude that all even derivatives in f are zero in (8.58). As the analysis is performed for small amplitudes, we discard all terms after the first two terms in f reducing (8.58) to the Landau equation (cf. Sect. 26 of Landau and Lifshitz [48] and Sect. 49.1 of Drazin and Reid [27])

$$\frac{dA}{dt} = \sigma A + a_1 A^3 . \tag{8.59}$$

Let us divide (8.59) by A^3 and solve for A^{-2}. Setting $x = A^{-2}$ we have

$$\frac{dx}{dt} + 2\sigma x = -2a_1 . \tag{8.60}$$

The integration of (8.60) gives

$$x = -\frac{a_1}{\sigma} + Ce^{-2\sigma t} . \tag{8.61}$$

Imposing the initial condition $A_0^{-2} = C - a_1/\sigma$ we find

$$\frac{1}{A^2} = \frac{a_1}{\sigma}(e^{-2\sigma t} - 1) + \frac{1}{A_0^2} e^{-2\sigma t} . \tag{8.62}$$

Eventually we obtain

$$A^2 = \frac{A_0^2 e^{2\sigma t}}{1 + \frac{a_1 A_0^2}{\sigma}(1 - e^{2\sigma t})} , \tag{8.63}$$

to be compared with Davey's solution

$$A^2 = \frac{A_0^2 e^{2\sigma t}}{1 - \frac{a_1 A_0^2}{\sigma} e^{2\sigma t}} \,. \tag{8.64}$$

Let us inspect Landau equation written a bit differently

$$\frac{dA}{dt} = (\sigma + a_1 A^2) A \,. \tag{8.65}$$

The equilibrium amplitude corresponding to an effective growth rate going to zero is such that

$$A_{eq}^2 = -\frac{\sigma}{a_1} \,. \tag{8.66}$$

Depending on $a_1 > 0$ or $a_1 < 0$ we have subcritical or supercritical disturbances that decay or amplify up to their equilibrium values, respectively. For the Taylor-Couette flow, experimental evidence shows that the instability is supercritical. Davey calculated the equilibrium amplitude for various cases, the wide and small gaps, and found that the equilibrium amplitude A_e^2 was proportional to $1 - Ta_{crit}/Ta$. This means that the amplitude increases as $\varepsilon^{1/2}$ with $\varepsilon = (Ta - Ta_{crit})/Ta_{crit}$.

To show the wealth of physical phenomena that can be generated in a Couette flow, Fig. 8.4 [2] offers the various regimes produced in a small-gap apparatus.

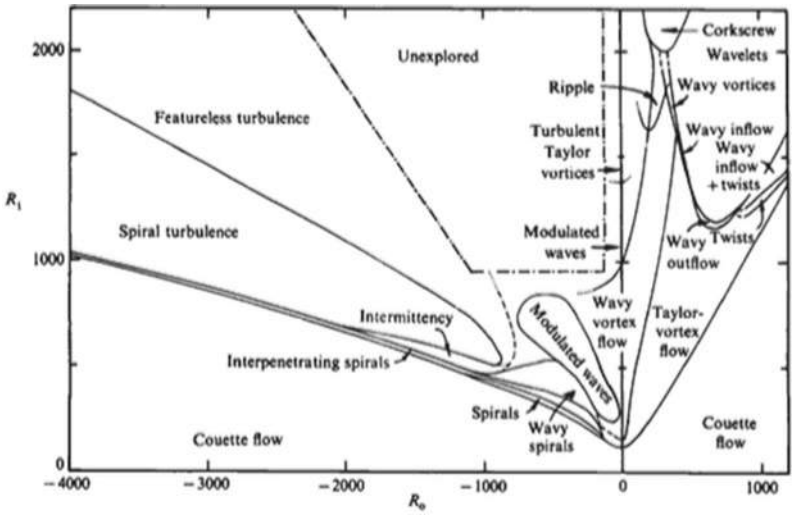

Fig. 8.4 Flow regimes in a Couette apparatus with long co-rotating cylinders. Reproduced from [2]

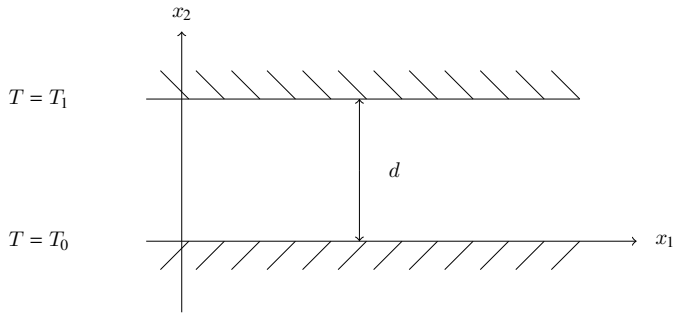

Fig. 8.5 Convection in a fluid layer between two parallel plates

Exercises

8.1 Obtain the linearized equations for the stability analysis of the spiral flow made of the combined circular Couette and Poiseuille flows under axisymmetric perturbations.

8.2 Rayleigh-Bénard instability A heat conducting fluid is at rest in between two parallel rigid plates, the lower one at temperature $T = T_0$, the upper one at $T = T_1$ such that $T_0 > T_1$, as shown in Fig. 8.5. The layer height is denoted by d. Using the Boussinesq approximation, the question is "When does the layer become unstable and show the presence of convection rolls?". The question makes sense since there are two stabilizing mechanics impeding the flow to start, namely the fluid viscosity and its thermal conductivity.

- Compute the base solution of the rest state: velocity, pressure p_{hyd} and temperature T_C.
- As this is a conduction/convection problem, the thermal diffusivity is used to define the reference velocity in the dimensionless equations (10.27)–(10.29). These relations are then linearized assuming that the perturbations are

$$\boldsymbol{v} = \mathbf{0} + \boldsymbol{v}' \,, \quad p = p_{hyd} + p' \,, \quad T = T_C + T' \,. \tag{8.67}$$

- Eliminate the pressure variable by taking the **curl** of the linearized momentum equation as $\mathbf{curl}\,\boldsymbol{\nabla} = 0$. The result is a governing relation for the vorticity.
- To recover the velocity perturbation as the main variable, the **curl** operator is applied to the vorticity equation. The velocity pops up as $\mathbf{curl}\,\omega = \mathbf{curl}\,\mathbf{curl}\boldsymbol{v} = -\triangle\triangle\boldsymbol{v}$.
- Write the governing equation for the x_2 perturbation velocity component.
- Obtain the fourth-order equation for the velocity perturbation by elimination of the temperature in the former governing relation and write the boundary conditions.
- Carry out the normal modes analysis of the perturbations system.

Chapter 9
Turbulence

As we already pinpointed several times in this monograph, turbulent flows occur in many situations in nature and technological applications. It is a subject that started during the nineteenth century and gained much momentum in the last century with the advent of powerful computers enabling solutions of statistical model equations or more recently tackling the full Navier–Stokes equations (without further modeling) through direct numerical simulation (DNS). Turbulence, its understanding and its modeling have been the main concern of many authors, researchers in the physical realm, or in engineering. Without being exhaustive, a few books may be referred to: Batchelor [11], Chassaing [19] (This book is only available in French. It is masterfully written with beautiful figures), Frisch [30], Lesieur [50], McComb [54], Manneville [55], Piquet [73], Pope [74], Tennekes and Lumley [105]. Turbulence modeling is the heart of Chap. 6 of the book by Deville and Gatski [24] where recent methodologies are presented and described in details.

In this chapter we will concentrate our attention to basic topics in turbulent phenomena and set up the standard models used in computational fluid dynamics.

9.1 General Considerations

Turbulence intervenes in most fluid flow phenomena in nature: meteorology, oceanography, hydrography,... or in industrial processes: pipe flows, mixing, melting. The study of turbulent physical phenomena is the main core of intense research, their understanding being not yet complete today.

It is difficult to propose an accurate definition of what is meant by turbulence. However, we can list the general characteristics of turbulent flows:

M. O. Deville, *An Introduction to the Mechanics of Incompressible Fluids*,
https://doi.org/10.1007/978-3-031-04683-4_9

1. **Unsteadiness**. Turbulent flows are irregular and present a random aspect. A full deterministic approach being impossible, we must resort to statistical methods.
2. **Diffusivity**. The diffusivity of turbulence is the cause of very quick mixings implying momentum and heat transfers.
3. **Dissipative character**. The viscous shear stresses perform a strain work that increases the internal fluid energy at the expense of its turbulent kinetic energy. Turbulence decreases rapidly, if we do not constantly provide energy to the fluid in order to oppose the friction losses, that are more important than in laminar state.
4. **Three-dimensional physics**. Turbulence is rotational and three-dimensional. It is characterized by high levels of vorticity fluctuations. This is the reason why vorticity dynamics plays such an important role.

Turbulence (more specifically developed turbulence) appears for relatively high values of the Reynolds number. It originates in the flow instability generated by the interaction, in the momentum equations, of the viscous and pressure terms and the non-linear terms in the acceleration. This interaction is present only when the inertial effects prevail, i.e. for high values of the Reynolds number. It is understood that turbulence is not an intrinsic characteristics of the fluid, but that it is related to the fluid flow properties.

9.2 General Equations of Incompressible Turbulence

We restrain ourselves in this chapter to the specific case of turbulent incompressible fluid flow. We will write the Navier–Stokes equations in conservative form while neglecting the body forces. Taking the continuity equation into account

$$\operatorname{div} \boldsymbol{v} = \boldsymbol{\nabla} \cdot \boldsymbol{v} = 0 \,, \tag{9.1}$$

the non-linear term reads as a divergence. We have

$$\frac{D\boldsymbol{v}}{Dt} = \frac{\partial \boldsymbol{v}}{\partial t} + (\boldsymbol{\nabla} \boldsymbol{v})\boldsymbol{v} = \frac{\partial \boldsymbol{v}}{\partial t} + \boldsymbol{\nabla} \cdot (\boldsymbol{v} \otimes \boldsymbol{v}) = -\frac{1}{\rho} \boldsymbol{\nabla}\, p + \nu\, \Delta \boldsymbol{v} \,, \tag{9.2}$$

where the symbol $\otimes$ denotes the tensor product of two vectors.

When we examine a velocity signal recorded as a function of time (cf. Fig. 9.1), we are struck by the random character of turbulence. As at each point in space, the velocity and pressure fields offer such temporal variations, we try to drastically reduce the amount of information necessary to interpret the physical phenomena and deduce prediction tools from them for design and engineering purposes. It is illusory to stick to the classical deterministic type modeling which would require following at each point the temporal evolution of velocity and pressure. This would produce a huge database that should be analyzed to extract useful information. Therefore

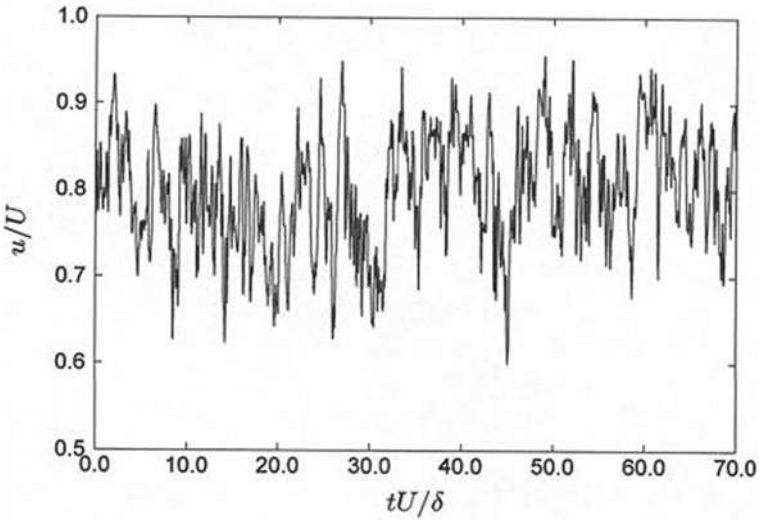

Fig. 9.1 Time variation of instantaneous velocity field at a fixed point within a turbulent boundary layer: $u = v_1$, U mean free-stream velocity and δ boundary layer thickness

the use of a statistical approach is unavoidable. To this end, the velocity vector $\boldsymbol{v}$ is decomposed in an averaged velocity $\overline{\boldsymbol{v}}$ and a fluctuation $\boldsymbol{v}'$ such that

$$\boldsymbol{v} = \overline{\boldsymbol{v}} + \boldsymbol{v}' \, . \tag{9.3}$$

An analogous relation is written for the pressure

$$p = \overline{p} + p' \, . \tag{9.4}$$

This is the Reynolds decomposition of velocity and pressure. The mean velocity $\overline{\boldsymbol{v}}$ is a time average defined by the equation

$$\overline{\boldsymbol{v}} = \lim_{T \to \infty} \frac{1}{T} \int_0^T \boldsymbol{v} \, dt \, . \tag{9.5}$$

This time average cannot be used for flows statistically evolving with time. Furthermore, from the experimental point of view, the measurement time T is such that we continue the averaging process until the moment when the fluctuations of $\overline{\boldsymbol{v}}$ are small enough. If the field is not statistically independent of time, we must take an ensemble average, i.e. the average obtained over a large set of similar experiences

$$< \boldsymbol{v} >= \lim_{N \to \infty} \frac{1}{N} \sum_{n=1}^{N} \boldsymbol{v}_n(\boldsymbol{x}, t) \, . \tag{9.6}$$

We suppose in the sequel that the averaging process is such that the derivatives with respect to space and time commute. The ensemble average satisfies always this property. If the ensemble average defined by (9.6) is an independent quantity of time, then the mean (9.5) is equal to the ensemble average. This is a result of the ergodic theorem, Tennekes and Lumley [105]. (From the statistical point of view, it is equivalent to toss one coin n times and toss n coins once). Note that the average process obtained by (9.6) is linear. However the mean of a product

$$< \boldsymbol{v}_1 \boldsymbol{v}_2 > \tag{9.7}$$

is generally not equal to the product of the means

$$< \boldsymbol{v}_1 >< \boldsymbol{v}_2 > \ .$$

By the definition of the mean, we have the relation

$$\overline{\boldsymbol{v}}' = 0 \ . \tag{9.8}$$

It also follows that given two random functions f and g, one obtains

$$\overline{\overline{f}\,\overline{g}} = \overline{f}\,\overline{g} \tag{9.9}$$

and

$$\overline{\overline{f}\,g'} = 0 \ . \tag{9.10}$$

With the decomposition (9.3), the average of Eq. (9.1) yields

$$\boldsymbol{\nabla} \cdot \overline{\boldsymbol{v}} = 0 \tag{9.11}$$

and therefore,

$$\boldsymbol{\nabla} \cdot \boldsymbol{v}' = 0 \ . \tag{9.12}$$

The fluctuating velocity field is incompressible as is the mean flow.

After inserting (9.3) and (9.4) in (9.2), we compute the mean. The average of the tensor product of the velocities yields

$$\begin{aligned} \overline{\boldsymbol{v} \otimes \boldsymbol{v}} &= \overline{(\overline{\boldsymbol{v}} + \boldsymbol{v}') \otimes (\overline{\boldsymbol{v}} + \boldsymbol{v}')} \\ &= \overline{\overline{\boldsymbol{v}} \otimes \overline{\boldsymbol{v}}} + \overline{\boldsymbol{v}' \otimes \overline{\boldsymbol{v}}} + \overline{\overline{\boldsymbol{v}} \otimes \boldsymbol{v}'} + \overline{\boldsymbol{v}' \otimes \boldsymbol{v}'} \\ &= \overline{\boldsymbol{v}} \otimes \overline{\boldsymbol{v}} + \overline{\boldsymbol{v}' \otimes \boldsymbol{v}'} \ . \end{aligned} \tag{9.13}$$

This procedure generates the Reynolds averaged Navier–Stokes equation (in short RANS)

$$\frac{\partial \overline{\boldsymbol{v}}}{\partial t} + \boldsymbol{\nabla} \cdot (\overline{\boldsymbol{v}} \otimes \overline{\boldsymbol{v}}) = -\frac{1}{\rho} \boldsymbol{\nabla} \overline{p} + \nu \Delta \overline{\boldsymbol{v}} - \boldsymbol{\nabla} \cdot (\overline{\boldsymbol{v}' \otimes \boldsymbol{v}'}) \ . \tag{9.14}$$

Using the average stress tensor defined by the expression

$$\overline{\boldsymbol{\sigma}} = -\overline{p}\,\boldsymbol{I} + 2\,\mu\,\overline{\boldsymbol{d}}\,, \tag{9.15}$$

with tensor $\overline{\boldsymbol{d}}$, the averaged strain rate

$$\overline{\boldsymbol{d}} = \frac{1}{2}(\nabla\overline{\boldsymbol{v}} + (\nabla\overline{\boldsymbol{v}})^T)\,, \tag{9.16}$$

Equation (9.14) reads

$$\frac{\partial\overline{\boldsymbol{v}}}{\partial t} + \nabla\cdot(\overline{\boldsymbol{v}}\otimes\overline{\boldsymbol{v}}) = \frac{1}{\rho}\nabla\cdot(\overline{\boldsymbol{\sigma}} - \rho\overline{\boldsymbol{v}'\otimes\boldsymbol{v}'})\,. \tag{9.17}$$

By similarity with the average Cauchy tensor $\overline{\boldsymbol{\sigma}}$, the second term under the operator $\nabla\cdot$ is assimilated to a stress, known as the symmetric Reynolds stress tensor $\boldsymbol{R}$

$$\boldsymbol{R} = -\rho\,\boldsymbol{\tau} = -\rho\overline{\boldsymbol{v}'\otimes\boldsymbol{v}'}\,, \tag{9.18}$$

while $\boldsymbol{\tau}$ has dimensions of squared velocities. This tensor will be named Reynolds tensor with no reference to stress. Note that $\boldsymbol{\tau}$ is similar to an energy tensor.

Equations (9.11) and (9.14) form a system of four equations with 10 unknowns, namely the three velocity components $\overline{v}_i$, the pressure $\overline{p}$ and the six components τ_{ij}. The Eqs. (9.17) and (9.18) exhibit the coupling between the average field and the fluctuation. We observe also that with more unknowns than equations, the closure problem is posed.

Subtracting the mean momentum equation (9.14) from the Navier–Stokes equation (9.2) gives the momentum equation of the fluctuating field that highlights the coupling with the mean field

$$\frac{\partial\boldsymbol{v}'}{\partial t} + \nabla\cdot(\boldsymbol{v}'\otimes\overline{\boldsymbol{v}}) = -\nabla\cdot(\overline{\boldsymbol{v}}\otimes\boldsymbol{v}') - \nabla\cdot(\boldsymbol{v}'\otimes\boldsymbol{v}' - \overline{\boldsymbol{v}'\otimes\boldsymbol{v}'}) - \frac{1}{\rho}\nabla p' + \nu\Delta\boldsymbol{v}'\,. \tag{9.19}$$

9.3 Kinetic Energy

Let us define the turbulent kinetic energy of the fluctuations, K, by the relation

$$K = \frac{1}{2}\overline{\boldsymbol{v}'\cdot\boldsymbol{v}'}\,. \tag{9.20}$$

This turbulent energy may be obtained as the half-trace of tensor $\boldsymbol{\tau}$

$$K = \frac{1}{2}\tau_{ii} \,. \tag{9.21}$$

The momentum equation of the turbulent kinetic energy is gotten by multiplying Eq. (9.19) by $\boldsymbol{v}'$ and taking the mean. We have

$$\frac{\partial K}{\partial t} + \overline{\boldsymbol{v}} \cdot \boldsymbol{\nabla} K = -\boldsymbol{\tau} : \boldsymbol{\nabla}\overline{\boldsymbol{v}} - \nu\overline{\boldsymbol{\nabla}\boldsymbol{v}' : \boldsymbol{\nabla}\boldsymbol{v}'} - \boldsymbol{\nabla} \cdot \boldsymbol{j} \,, \tag{9.22}$$

where the flux vector of turbulent kinetic energy $\boldsymbol{j}$ is defined by

$$\boldsymbol{j} = \frac{1}{\rho}\overline{p'\boldsymbol{v}'} + \frac{1}{2}\overline{(\boldsymbol{v}' \cdot \boldsymbol{v}')\boldsymbol{v}'} - \nu\boldsymbol{\nabla} K \,. \tag{9.23}$$

We notice in (9.23) the appearance of the triple velocity correlation. The first and second terms of the right hand side of (9.22) are the production rates of turbulent energy $\mathcal{P}$ and of dissipation of turbulent energy $\mathcal{D}$, respectively. We will denote them

$$\mathcal{P} = -\boldsymbol{\tau} : \boldsymbol{\nabla}\,\overline{\boldsymbol{v}} = -\boldsymbol{\tau} : \overline{\boldsymbol{d}}, \tag{9.24}$$

$$\mathcal{D} = \nu\overline{\boldsymbol{\nabla}\boldsymbol{v}' : \boldsymbol{\nabla}\boldsymbol{v}'} \,. \tag{9.25}$$

The production $\mathcal{P}$ is the result of the inner product of Reynolds tensor and the mean strain rate tensor. We observe that it is most often positive, although there might be situations where it is negative.

As the source of turbulent kinetic energy is the mean flow, we should retrieve this term with its sign changed in the equation governing the average kinetic energy, E_k, defined by the relation

$$E_k = \frac{1}{2}\overline{\boldsymbol{v}} \cdot \overline{\boldsymbol{v}} \,. \tag{9.26}$$

Let us multiply Eq. (9.14) by $\overline{\boldsymbol{v}}$. After some tedious but simple manipulations, one obtains:

$$\frac{\partial E_k}{\partial t} + \overline{\boldsymbol{v}} \cdot \boldsymbol{\nabla} E_k = -\frac{1}{\rho}\boldsymbol{\nabla} \cdot (\overline{p}\,\overline{\boldsymbol{v}}) - 2\nu\,\overline{\boldsymbol{d}} : \overline{\boldsymbol{d}} + 2\nu\,\boldsymbol{\nabla} \cdot (\overline{\boldsymbol{v}}\,\overline{\boldsymbol{d}}) - \mathcal{P} - \boldsymbol{\nabla} \cdot (\overline{\boldsymbol{v}}\,\boldsymbol{\tau}) \,. \tag{9.27}$$

In (9.27), appears the right product of tensor $\overline{\boldsymbol{d}}$ and the vector $\overline{\boldsymbol{v}}$. In indexed form, this product reads

$$(\overline{\boldsymbol{v}}\,\overline{\boldsymbol{d}})_j = \overline{v}_i\overline{d}_{ij} \,. \tag{9.28}$$

In the right hand side of (9.27), we find successively the following terms. The first one is associated with pressure and expresses the flow power. The two terms involving viscosity are one, the dissipation rate of turbulent kinetic energy by the molecular

viscous effects and the other, a reversible transfer of viscous power. The fourth term is a sink of mean turbulent kinetic energy $-\mathcal{P}$. Finally the last term is a divergence. If it is integrated on a sufficiently large volume, bounded by fluid in laminar flow, this term vanishes. Thus it takes into account a conservative transfer in the volume of mean kinetic energy.

9.4 Dynamic Equation of the Reynolds Tensor

This equation is developed by multiplying the momentum equation (9.19) of fluctuation v_i' by v_j' and the one of fluctuation v_j' by v_i'. Adding the resulting equations and averaging, one obtains

$$\frac{\partial \boldsymbol{\tau}}{\partial t} + \overline{\boldsymbol{v}} \cdot \boldsymbol{\nabla} \boldsymbol{\tau} = \boldsymbol{P} + \boldsymbol{\Pi} - \boldsymbol{D} - \boldsymbol{\nabla} \cdot \boldsymbol{J}^{(3)} \,. \tag{9.29}$$

Recall that the inner product of two tensors $\boldsymbol{A}$ and $\boldsymbol{B}$ is written in indexed notation as $(\boldsymbol{AB})_{ij} = A_{im} B_{mj}$; thus, $(\boldsymbol{AB}^T)_{ij} = A_{im} B_{jm}$. Consequently the production term

$$\boldsymbol{P} = -(\boldsymbol{\tau} \, (\boldsymbol{\nabla} \, \overline{\boldsymbol{v}})^T + (\boldsymbol{\nabla} \overline{\boldsymbol{v}}) \, \boldsymbol{\tau}^T) \tag{9.30}$$

is the source of the Reynolds stresses. We note that its trace yields

$$tr \, \boldsymbol{P} = 2\mathcal{P} \,. \tag{9.31}$$

The correlation term of pressure-strain rate

$$\boldsymbol{\Pi} = \frac{1}{\rho} \overline{p'(\boldsymbol{\nabla} \boldsymbol{v}' + (\boldsymbol{\nabla} \boldsymbol{v}')^T)} \tag{9.32}$$

possesses a zero trace. It redistributes the energy among the components of normal stresses as it contributes to an exchange between the components $\overline{v_1'^2}$, $\overline{v_2'^2}$, $\overline{v_3'^2}$ without modifying their sum. The dissipation-rate term

$$\boldsymbol{D} = 2\nu \, \overline{(\boldsymbol{\nabla} \boldsymbol{v}')(\boldsymbol{\nabla} \boldsymbol{v}')^T} \tag{9.33}$$

has a trace whose value is

$$tr \, \boldsymbol{D} = 2 \, \mathcal{D} \,. \tag{9.34}$$

Finally the tensor of order three, $\boldsymbol{J}^{(3)}$, is given by the equation

$$\boldsymbol{J}^{(3)} = \frac{1}{\rho} (\overline{p' \boldsymbol{v}'} \boldsymbol{I} + (\overline{p' \boldsymbol{v}'} \boldsymbol{I})^T) + \overline{\boldsymbol{v}' \otimes \boldsymbol{v}' \otimes \boldsymbol{v}'} - \nu \boldsymbol{\nabla} \boldsymbol{\tau} \,. \tag{9.35}$$

The first term is the exterior product of vector $\overline{p'\boldsymbol{v}'}$ and the identity tensor $\boldsymbol{I}$

$$(\overline{p'\boldsymbol{v}'}\boldsymbol{I})_{ijk} = \overline{p'v_i'}\,\delta_{jk}\ . \tag{9.36}$$

The second term is the transpose, the last index remaining unchanged, such that

$$(\overline{p'\boldsymbol{v}'}\boldsymbol{I})^T_{ijk} = \overline{p'v_j'}\delta_{ik}\ . \tag{9.37}$$

The third term $\overline{\boldsymbol{v}'\otimes\boldsymbol{v}'\otimes\boldsymbol{v}'}$ is the triple velocity correlation defined by the tensor product of three vectors, namely

$$(\overline{\boldsymbol{v}'\otimes\boldsymbol{v}'\otimes\boldsymbol{v}'})_{ijk} = \overline{v_i'v_j'v_k'}\ . \tag{9.38}$$

Finally the gradient of the second order tensor $\boldsymbol{\tau}$ is a third-order tensor with components

$$(\boldsymbol{\nabla\tau})_{ijk} = \frac{\partial}{\partial x_k}\tau_{ij}\ . \tag{9.39}$$

The tensor $\boldsymbol{J}^{(3)}$ is diffusive in essence and induces a spatial redistribution of energy (cf. the divergence theorem). We notice that in Eq. (9.29), the non-linear terms have generated triple velocity correlations $\overline{v_i'v_j'v_k'}$. It is possible to write the dynamic equations that govern the evolution of these triple correlations; they will call for quadruple correlations. The dynamics of quadruple correlations will entail quintuple correlations, and so forth. The mathematical complications will increase at each step. The hierarchy of the equations for the moments (averages of higher order products of velocity fluctuations) is not only infinite but also divergent, in the sense that additional unknowns produced at each stage appear in greater number than that of new equations. To overcome this difficulty, the problem is simplified in order to close the open equations hierarchy. This procedure is called the closure problem.

The simplest closure consists in truncating the set of equations with the assumption that the correlations are negligible beyond a certain order, in practice, the third or fourth order. We try then to express the high order correlations in terms of smaller order correlations.

A classification of turbulence models is based on the number of additional partial differential equations (with respect to the average Navier–Stokes equations) required to close the model.

The zero equation model consists in retaining only order two moments and therefore in linking the turbulent stress tensor to some characteristics of the mean flow via a turbulent viscosity. The one equation model, also called K model, is due to Prandtl. A partial differential equation is used to describe the dynamics of the turbulent kinetic energy. Eventually the two equation model is based on the dynamics of the turbulent kinetic energy and its dissipation rate. It is the well known $K-\varepsilon$ model.

9.5 Structures and Scales of Homogeneous Turbulence

Turbulence is homogeneous when the averaged quantities are invariant by spatial translation. Particularly, the mean velocity field in homogeneous turbulence is independent of the position $\boldsymbol{x}$. We then conclude that in homogeneous turbulence, all spatial points are statistically equivalent. If moreover, these statistical properties are independent of the orientation of the frame of reference, the field is called isotropic. The homogeneous and isotropic turbulence (HIT) allows using Fourier methods to build analytical turbulence models.

Experimentally and theoretically, it is observed that turbulence dynamics is strongly linked to vorticity dynamics. The vorticity filaments are stretched and twisted. This phenomenon is at the origin of the creation of large vorticity structures (large eddies). The large scales are very efficient to generate the Reynolds stresses that extract their energy from the mean flow. Through non-linear interactions, that are inviscid processes, the turbulent energy is transferred to smaller and smaller sized vortices. The viscosity only comes into play for sufficiently small vortices, of the order of Kolmogorov scale defined later, where this energy is dissipated.

Experiments lead to assuming the existence of an energy transfer from the large scales to the small ones without any dissipation. This is viewed as the energy cascade (or Richardson's cascade). Let us note that locally, "inverse" fluxes exist and give rise to the formation of larger scales from smaller ones. This is called retro-diffusion. Figure 9.2 shows the spectral energy $E(k)$ (introduced in the sequel) as a function of the Kolmogorov scale ℓ_K. Dissipation occurs for the small scale structures.

We will suppose that dissipation characterized by its dissipation rate ε ($\mathrm{m^2\,s^{-1}}$) operating at the level of small vortices arises from the large scales and that the turbulent energy is linked to them. Therefore if one chooses K and ε to qualify these large structures, by dimensional analysis, we obtain for their characteristic length

$$\ell = K^{3/2}/\varepsilon \tag{9.40}$$

with ε defined by the relation

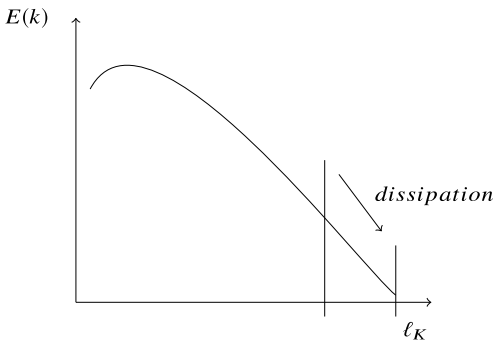

Fig. 9.2 Energy cascade

$$\varepsilon = 2\nu\,\overline{\boldsymbol{d}' : \boldsymbol{d}'} = \nu\,\overline{\frac{\partial v_i'}{\partial x_j}\left(\frac{\partial v_i'}{\partial x_j} + \frac{\partial v_j'}{\partial x_i}\right)} = \frac{\nu}{2}\overline{\left(\frac{\partial v_i'}{\partial x_j} + \frac{\partial v_j'}{\partial x_i}\right)^2}\,. \tag{9.41}$$

The characteristic time scale of these large vortices is given by

$$\tau = K/\varepsilon \tag{9.42}$$

with $K^{1/2}$ as the velocity scale. The turbulence Reynolds number rests upon the previous scales and reads

$$Re_T = \frac{K^{1/2}\ell}{\nu} = \frac{K^2}{\varepsilon\,\nu}\,. \tag{9.43}$$

Very often, the turbulence Reynolds number is smaller than the physical Reynolds number of the flow by a factor in between 20 and 100. The scale ℓ (9.40) of vortices energetic enough to influence the mean momentum is called mixing length. At the other end of the energy cascade, we find small vortices that are determined essentially by ε and ν. Dimensional analysis yields the Kolmogorov scale ℓ_K defined by the relationship

$$\ell_K = (\nu^3/\varepsilon)^{1/4} \tag{9.44}$$

corresponding to the scale where dissipative viscous phenomena start acting on the vortices that have a size of the order of that scale, and time τ_K

$$\tau_K = (\nu/\varepsilon)^{1/2} \tag{9.45}$$

characterizing the lifetime of a vortex of size $\sim \ell_K$. As we can admit that viscosity will fully play its role if the Reynolds number associated to small structures are of the order of unity, we can set that

$$\frac{v_K\,\ell_K}{\nu} \approx 1\,. \tag{9.46}$$

Thus we obtain

$$v_K = (\nu\varepsilon)^{1/4}\,. \tag{9.47}$$

Dividing (9.40) by (9.44), the ratio of large to small scales constitute an estimate of the spectrum:

$$\frac{\ell}{\ell_K} = {Re_T}^{3/4}\,. \tag{9.48}$$

With (9.48), when the Reynolds number increases, it is the chain of space structures that spreads (often over several decades). This large range limits the direct numerical simulations to low or moderate Reynolds numbers. On the contrary, the large eddy simulation where the structures of smaller size than the mesh step are modeled, depends precisely on these models. It is considered that small scale turbulence is

homogeneous and that small scales dynamics is isotropic, and consequently more universal than that of the large scales. Thus, it is necessary to understand what is meant by HIT.

9.6 Homogeneous Turbulence

Homogeneous turbulence is described within the framework of the statistical properties of random homogeneous fields. To this end, we need to introduce the concept of correlations and spectra. In this section we follow closely the presentation of the subject by W. C. Reynolds [78].

9.6.1 Correlations and Spectra

Let f and g denote two random fields. Then the two-point correlation of f and g is defined by the relation

$$Q_{fg}(\boldsymbol{x}, \boldsymbol{x}', t) = \langle \overline{f(\boldsymbol{x}, t) g(\boldsymbol{x}', t)} \rangle \tag{9.49}$$

with upper line for the volume average

$$\overline{f}(t) = \lim_{L \to \infty} \frac{1}{L^3} \int_0^L f(\boldsymbol{x}, t)\, d^3\boldsymbol{x} \tag{9.50}$$

and the brackets for the ensemble mean. For homogeneous fields, the ergodic assumption implies the equivalence of these two types of averaging.

For homogeneous fields, Q_{fg} depends only on the distance between the two points $\boldsymbol{r} = \boldsymbol{x}' - \boldsymbol{x}$ and on t

$$Q_{fg}(\boldsymbol{r}, t) = \langle \overline{f(\boldsymbol{x}, t) g(\boldsymbol{x} + \boldsymbol{r}, t)} \rangle \, . \tag{9.51}$$

In homogeneous turbulence, we use Fourier series to represent the fields, with the hypothesis that turbulence occurs in a cube with a periodicity of length L. Most of the time, for the sake of simplicity and ease of analysis, one chooses $L = 2\pi$. This procedure allows to forget about the influence of the boundary conditions on the flow and to rely on the space periodicity of the fields.

The representation of $f(\boldsymbol{x})$ reads

$$f(\boldsymbol{x}) = \sum_{\boldsymbol{k}} \hat{f}(\boldsymbol{k})\, e^{-i\boldsymbol{k}\cdot\boldsymbol{x}} \, , \quad -\infty < k < +\infty \, , \tag{9.52}$$

where $\hat{f}(\boldsymbol{k})$ is the associated spectrum to f. The three-dimensional wave-vector $\boldsymbol{k}$ is such that $\boldsymbol{k} = (k_1, k_2, k_3)$. Imposing that $f(\boldsymbol{x})$ be a real function implies

$$\hat{f}(\boldsymbol{k}) = \hat{f}^*(-\boldsymbol{k}) \tag{9.53}$$

with the symbol $*$ denoting the conjugate complex. The relation (9.53) is the Hermitian property.

To express the two point correlation between f and g, we write

$$\langle f(\boldsymbol{x}) g(\boldsymbol{x}') \rangle = \sum_{\boldsymbol{k}} \sum_{\boldsymbol{k}'} \langle \hat{f}(\boldsymbol{k}) \hat{g}(\boldsymbol{k}') \rangle e^{-i(\boldsymbol{k}\cdot\boldsymbol{x} + \boldsymbol{k}'\cdot\boldsymbol{x}')} . \tag{9.54}$$

Setting $\boldsymbol{k}'' = -\boldsymbol{k}'$ and $\boldsymbol{r} = \boldsymbol{x}' - \boldsymbol{x}$, we get

$$\langle f(\boldsymbol{x}) g(\boldsymbol{x} + \boldsymbol{r}) \rangle = \sum_{\boldsymbol{k}} \sum_{\boldsymbol{k}''} \langle \hat{f}(\boldsymbol{k}) \hat{g}^*(\boldsymbol{k}'') \rangle e^{-i\boldsymbol{x}\cdot(\boldsymbol{k} - \boldsymbol{k}'') + i\boldsymbol{k}''\cdot\boldsymbol{r}} . \tag{9.55}$$

By orthogonality of the Fourier modes, we have the relation

$$\int e^{i(\boldsymbol{k} - \boldsymbol{k}')\cdot\boldsymbol{x}} d^3\boldsymbol{x} = \begin{cases} 0 & \text{if } \boldsymbol{k} \neq \boldsymbol{k}', \\ L^3 \text{ or } (2\pi)^3 & \text{if } \boldsymbol{k} = \boldsymbol{k}' , \end{cases} \tag{9.56}$$

and the Eq. (9.55) becomes with $\boldsymbol{k}'' = \boldsymbol{k}$

$$Q_{fg}(\boldsymbol{r}) = \sum_{\boldsymbol{k}} \langle \hat{f}(\boldsymbol{k}) \hat{g}^*(\boldsymbol{k}) \rangle e^{i\boldsymbol{k}\cdot\boldsymbol{r}} . \tag{9.57}$$

In the Fourier representation (9.57), we use again L as the size of the cubic box with $k_i = 2\pi n_i / L$, $n_i = 0, \pm 1, \pm 2, \ldots$. If we let $L \to \infty$, the sums become integrals and one writes

$$Q_{fg}(\boldsymbol{r}) = \int \langle \hat{f}(\boldsymbol{k}) \hat{g}^*(\boldsymbol{k}) \rangle e^{i\boldsymbol{k}\cdot\boldsymbol{r}} d^3\boldsymbol{k} , \tag{9.58}$$

where $d^3\boldsymbol{k}$ denotes the elemental volume in Fourier space. Defining by $E_{fg}(\boldsymbol{k})$ the cospectrum of f and g as $\langle \hat{f}(\boldsymbol{k}) \hat{g}^*(\boldsymbol{k}) \rangle$, we obtain

$$E_{fg}(\boldsymbol{k}) = \frac{1}{(2\pi)^3} \int Q_{fg}(\boldsymbol{r}) e^{-i\boldsymbol{k}\cdot\boldsymbol{r}} d^3\boldsymbol{r} . \tag{9.59}$$

One notices that Q_{fg} and E_{fg} are Fourier transforms of each other.

9.6.2 Velocity Correlations and Associated Spectra

Setting $f = v_i'$ and $g = v_j'$, we define the two-point velocity correlation tensor

$$Q_{ij}(\boldsymbol{r}) = \overline{v_i'(\boldsymbol{x})v_j'(\boldsymbol{x}+\boldsymbol{r})} \,. \tag{9.60}$$

When $f = g = v_i'$, this is the self-correlation function. For $\boldsymbol{r} = \boldsymbol{0}$, we have

$$Q_{ii}(\boldsymbol{0}) = \overline{v_i'(\boldsymbol{x})v_i'(\boldsymbol{x})} = 2K \,. \tag{9.61}$$

The velocity spectrum tensor $\boldsymbol{E}$ is thus the Fourier transform of Q_{ij}

$$E_{ij}(\boldsymbol{k}) = \frac{1}{(2\pi)^3}\int Q_{ij}(\boldsymbol{r})e^{-i\boldsymbol{k}\cdot\boldsymbol{r}}d^3\boldsymbol{r} \,. \tag{9.62}$$

Moreover,

$$Q_{ij}(\boldsymbol{r}) = \int E_{ij}(\boldsymbol{k})e^{i\boldsymbol{k}\cdot\boldsymbol{r}}d^3\boldsymbol{k} \,. \tag{9.63}$$

The Reynolds tensor τ_{ij} is obtained by

$$\tau_{ij} = Q_{ij}(\boldsymbol{0}) \,. \tag{9.64}$$

With (9.63), we have

$$\tau_{ij} = \int E_{ij}(\boldsymbol{k})d^3\boldsymbol{k} \,. \tag{9.65}$$

It is easily shown that $\boldsymbol{Q}$ possesses a symmetry such that

$$\boldsymbol{Q}(-\boldsymbol{r}) = \boldsymbol{Q}^T(\boldsymbol{r}) \,. \tag{9.66}$$

Consequently, the tensor $\boldsymbol{E}$ has the property

$$\boldsymbol{E}(-\boldsymbol{k}) = \boldsymbol{E}^T(\boldsymbol{k}) \,. \tag{9.67}$$

Let us introduce the general tensor

$$D_{ijpq} = \overline{\frac{\partial v_i'}{\partial x_p}\frac{\partial v_j'}{\partial x_q}} \,. \tag{9.68}$$

From the definition (9.60), one obtains

$$\frac{\partial Q_{ij}(\boldsymbol{r})}{\partial r_q} = \overline{v_i'(\boldsymbol{x})\frac{\partial v_j'(\boldsymbol{x}+\boldsymbol{r})}{\partial r_q}} \,. \tag{9.69}$$

Replacing $\boldsymbol{x}$ by $\boldsymbol{x}' - \boldsymbol{r}$ in (9.69) and taking the derivative with respect to r_p, we have

$$\frac{\partial^2 Q_{ij}(\boldsymbol{r})}{\partial r_p \partial r_q} = -\overline{\frac{\partial v_i'(\boldsymbol{x}' - \boldsymbol{r})}{\partial r_p} \frac{\partial v_j'(\boldsymbol{x}')}{\partial r_q}} \,. \tag{9.70}$$

Letting $\boldsymbol{r}$ go to zero, the tensor D_{ijpq} yields

$$D_{ijpq} = -\frac{\partial^2 Q_{ij}(\boldsymbol{r})}{\partial r_p \partial r_q} \,|_{\boldsymbol{r}=\boldsymbol{0}} \,. \tag{9.71}$$

Applying Eqs. (9.73) to (9.63), we find

$$D_{ijpq} = \int k_p k_q E_{ij}(\boldsymbol{k}) d^3\boldsymbol{k} \,. \tag{9.72}$$

The dissipation rate ε (9.41) may be linked to the previous tensor by the relation

$$\varepsilon = \nu D_{iijj} \,. \tag{9.73}$$

With the Eqs. (9.72) and (9.73), we compute

$$\varepsilon = \nu \int k^2 E_{ii}(\boldsymbol{k}) d^3\boldsymbol{k} \,. \tag{9.74}$$

With Eq. (9.61) the turbulent kinetic energy is expressed as

$$K = \frac{1}{2} tr\ \boldsymbol{Q}(\boldsymbol{0}) = \frac{1}{2} \int E_{ii}(\boldsymbol{k}) d^3\boldsymbol{k} \,. \tag{9.75}$$

The k^2 factor in (9.74) shows that the main contribution to the dissipation comes from wave numbers higher than those characterizing the kinetic energy. This is a partial confirmation of the validity of Kolmogorov hypothesis for the energy cascade in homogeneous turbulence.

9.6.3 Correlations and Spectra in Isotropic Turbulence

In isotropic turbulence, the tensor $\boldsymbol{E}$ is an isotropic tensor function of only $k = \sqrt{\boldsymbol{k} \cdot \boldsymbol{k}}$. Its more general form is

$$\boldsymbol{E}(\boldsymbol{k}) = C_1 \boldsymbol{I} + C_2 \boldsymbol{k} \otimes \boldsymbol{k} \,. \tag{9.76}$$

The incompressibility condition (1.50) applied to the Fourier expansion of the velocity field

$$\boldsymbol{v}(\boldsymbol{x}) = \sum_{\boldsymbol{k}} \hat{\boldsymbol{v}}(\boldsymbol{k})\, e^{-i\boldsymbol{k}\cdot\boldsymbol{x}} \tag{9.77}$$

imposes $k_j \hat{v}_j(\boldsymbol{k}) = 0$ such that the Fourier coefficients of the velocity must be orthogonal to $\boldsymbol{k}$. Therefore, we have

$$k_i\, E_{ij} = k_j\, E_{ij} = 0, \tag{9.78}$$

and thus, one obtains

$$C_1 k_j + C_2 k^2 k_j = 0 \tag{9.79}$$

and consequently

$$C_2 = -C_1/k^2\,. \tag{9.80}$$

Redefining C_1 as

$$C_1 = \frac{E(k)}{4\pi k^2}, \tag{9.81}$$

(and that is justified by the isotropy in the spectral space with $dE = 4\pi k^2\, E(k)\, dk$ which gives the energy density between the spherical layers k and $k + dk$), we get

$$\boldsymbol{E}(\boldsymbol{k}) = \frac{E(k)}{4\pi k^2}\left(\boldsymbol{I} - \frac{\boldsymbol{k}\otimes\boldsymbol{k}}{k^2}\right)\,. \tag{9.82}$$

We call $E(k)$ the spectral energy function.

The turbulence energy via (9.75) and (9.82) becomes

$$K = \int \frac{1}{4\pi k^2} E(k) d^3\boldsymbol{k}\,. \tag{9.83}$$

This integral is computed in spherical coordinates as shown in Fig. 9.3.

We have

$$K = \frac{1}{4\pi}\int_{k=0}^{\infty}\int_{\theta=0}^{\pi}\int_{\phi=0}^{2\pi} \frac{E(k)}{k^2} k^2 \sin\theta\, d\theta\, d\varphi\, dk\,. \tag{9.84}$$

Integrating with respect to θ and φ, and because of the isotropy, we obtain

$$K = \int_0^{\infty} E(k)\, dk\,. \tag{9.85}$$

Let us note that $E(k)$ has dimension $m^3 s^{-2}$. In isotropic turbulence, the energy spectrum is completely determined as soon as $E(k)$ is specified.

As the $\boldsymbol{E}$ tensor is the Fourier transform of $\boldsymbol{Q}$ (Eq. (9.62)) in isotropic turbulence, the velocity correlation tensor is completely defined by two correlation functions (Fig. 9.4). The longitudinal correlation function

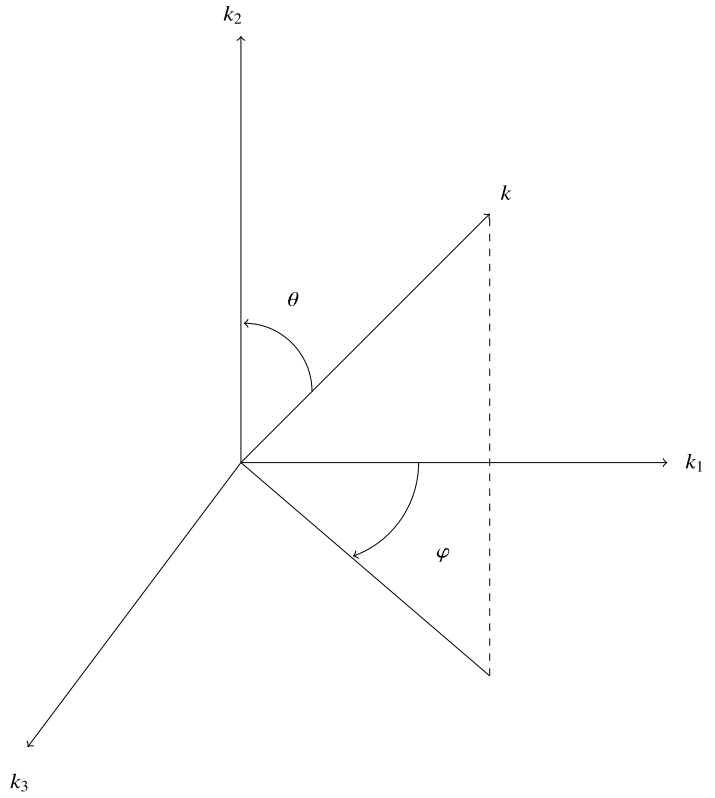

Fig. 9.3 Spherical coordinates for Fourier space integration

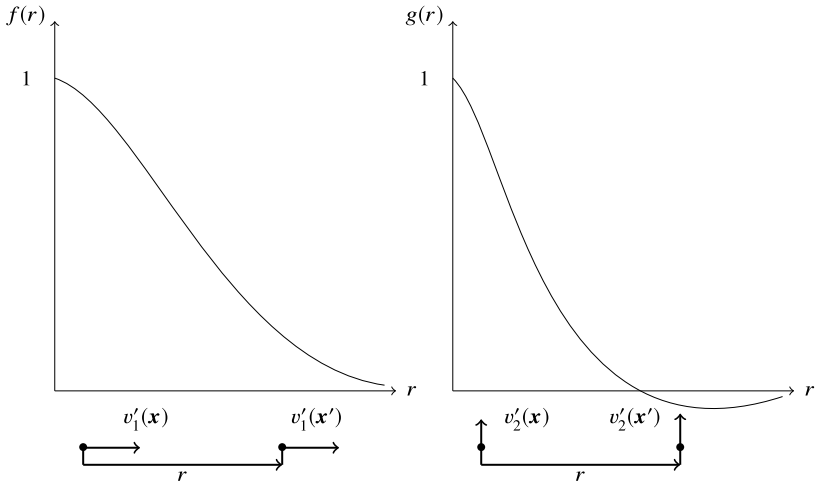

Fig. 9.4 Longitudinal and transverse correlations

$$f(r) = \frac{3}{2K} Q_{11}(r_1, 0, 0) \tag{9.86}$$

describes the coherence of fluctuations aligned in the direction of the vector separating the two points. The transverse correlation function

$$g(r) = \frac{3}{2K} Q_{22}(r_1, 0, 0) \tag{9.87}$$

is the image of the coherence of fluctuations of velocities orthogonal to the separation line. The most general expression of tensor $\boldsymbol{Q}$ is

$$\boldsymbol{Q}(\boldsymbol{r}) = C_1 \boldsymbol{I} + C_2 \, \boldsymbol{r} \otimes \boldsymbol{r} \tag{9.88}$$

with the definition

$$r = \sqrt{r_i r_i} \, . \tag{9.89}$$

The constants C_1 and C_2 are easily evaluated

$$\begin{aligned} Q_{22}(r_1, 0, 0) &= \frac{2K}{3} g(r) = C_1, \\ Q_{11}(r_1, 0, 0) &= \frac{2K}{3} f(r) = C_1 + C_2 r^2. \end{aligned}$$

Solving this system, we find

$$\boldsymbol{Q}(r) = \frac{2K}{3} \left[\frac{f(r) - g(r)}{r^2} \boldsymbol{r} \otimes \boldsymbol{r} + g(r) \boldsymbol{I} \right] . \tag{9.90}$$

In this last expression, we note that the functions f and g are scalar functions of the (scalar) distance of separation.

In theory, homogeneous isotropic turbulence evolves with time and we should measure the spectral tensor by taking measurements in many points. In reality, this is very difficult. Therefore the experimenters use Taylor's hypothesis which assumes that the turbulence time history mirrors the space history as turbulence is only advected around the measurement device. We conclude that the measurement of $v_1'(\boldsymbol{x}, t)$ yields $Q_{11}(r_1, 0, 0, t)$. In other words, we replace time correlations by space correlations.

Inserting (9.82) in (9.63), we obtain

$$Q_{11}(r_1, 0, 0) = \int \frac{E(k)}{4\pi k^2} \left(1 - \frac{k_1^2}{k^2} \right) e^{i k_1 r_1} d^3 \boldsymbol{k} \, . \tag{9.91}$$

Referring to Fig. 9.5 for the Fourier wavenumber integration, we observe that k_1 wavenumbers contribute substantially. As k_1 goes from $-\infty$ to $+\infty$, these terms

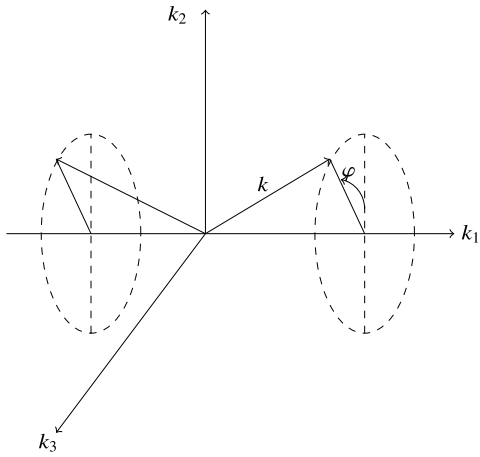

Fig. 9.5 k coordinates for Fourier spectral integration

have the imaginary parts of $e^{ik_1r_1}$ with opposite signs and therefore cancel each other leaving only cosines in the integral. This integral reads now

$$Q_{11}(r_1,0,0) = \int_{k_1=0}^{\infty}\int_{k=k_1}^{\infty}\int_{\varphi=0}^{2\pi}\frac{E(k)}{4\pi k^2}\left(1-\frac{k_1^2}{k^2}\right)2\cos(k_1r_1)kd\varphi dkdk_1\ . \quad (9.92)$$

The φ integration gives 2π and we are left with

$$Q_{11}(r_1,0,0) = \int_{k=k_1}^{\infty} E_1(k_1)\cos(k_1r_1)dk_1 \quad (9.93)$$

with the definition of the one-dimensional spectral function E_1

$$E_1(k_1) = \int_{k=k_1}^{\infty}\frac{E(k)}{k}\left(1-\frac{k_1^2}{k^2}\right)dk\ . \quad (9.94)$$

With relation (9.93), we notice that the Fourier cosine transform of measurements $Q_{11}(r_1,0,0)$ is an efficient tool to obtain $E_1(k_1)$. By taking twice the derivative of Eq. (9.94) with respect to k_1, one has

$$E(k_1) = \frac{k_1^2}{2}\frac{\partial^2 E_1(k_1)}{\partial k_1^2} - \frac{k_1}{2}\frac{\partial E_1(k_1)}{\partial k_1}\ . \quad (9.95)$$

This equation allows to establish $E(k)$. Its general shape is shown in Fig. 9.2. By (9.85), the surface beneath the curve gives the turbulent kinetic energy that receives its maximum contribution from wave-numbers located near the maximum.

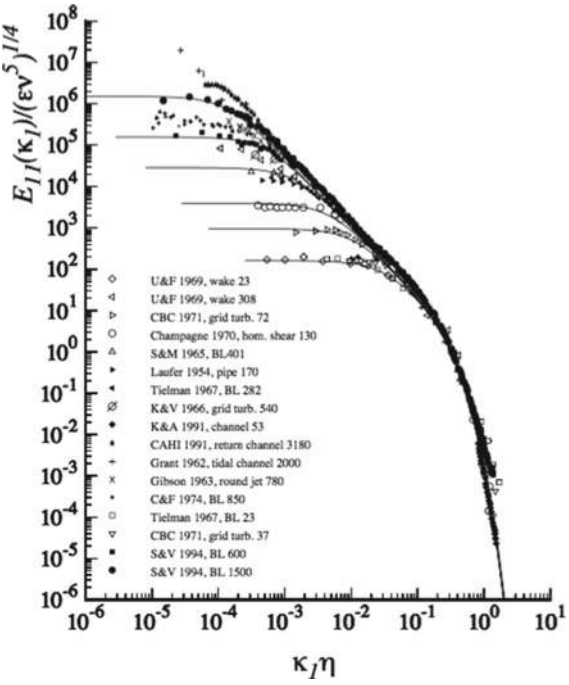

Fig. 9.6 Spectrum of the longitudinal fluctuation $\frac{E(k)}{\nu^{5/4}\varepsilon^{1/4}}$ with respect to the Kolmogorov variable $\frac{k\nu^{3/4}}{\varepsilon^{1/4}}$

It is supposed that the small scale motions in every turbulent flow become isotropic for high Reynolds numbers and that the Kolmogorov scales characterize the region of large wave-numbers (or of small spatial scales) of any turbulent flow. If we suppose the existence of a universal spectrum at small scale, by means of dimensional analysis, we have

$$\frac{E(k)}{v_K^2 \ell_K} = \frac{E(k)}{\nu^{5/4}\varepsilon^{1/4}} = F(\ell_K k) = F(\frac{k\nu^{3/4}}{\varepsilon^{1/4}}) \,. \tag{9.96}$$

Figure 9.6 shows that the experimental data for a vast diversity of flows fall effectively on a common curve when Kolmogorov variables are used.

Kolmogorov [42, 43] suggests that there exists a wave-number range for which the dominant physical mechanism consists in transmitting the energy of the large structures towards the small scales (cascade) and that the structure of this region depends only on the speed of the energy transfer. This interval is called the inertial zone or else inertial range. Since this cascade ends with the small-scale dissipation, the transfer rate is equal to the dissipation rate ε. We assume, therefore, that $E(k)$ depends only on k and ε. Applying dimensional analysis, we get

$$E(k) = C\,\varepsilon^{2/3}\,k^{-5/3} \,. \tag{9.97}$$

This is Kolmogorov spectrum. Note that this result proved in homogeneous isotropic turbulence remains valuable in many non homogeneous and non isotropic turbulent configurations.

The correlation functions f and g give a certain idea of the turbulent motion. The integral scales are useful for the large scale motion. One can define for example:

$$L_{11}(t) = \frac{\int_0^t Q_{11}(r_1, 0, 0, t)dr_1}{Q_{11}(0, 0, 0, t)} \tag{9.98}$$

giving a measure of the size of the vortices in direction x_1. Another scale that is often used is Taylor's microscale λ_T. A possible definition is

$$\varepsilon = \nu \frac{K}{\lambda_T^2} . \tag{9.99}$$

If we compare Taylor's microscale to Kolmogorov scale, we have

$$\frac{\lambda_T}{\ell_K} = Re_T^{1/4} . \tag{9.100}$$

If we compare λ_T to the size of energetic structures (9.40), we obtain

$$\frac{\ell}{\lambda_T} = Re_T^{1/2} . \tag{9.101}$$

Thus, the microscale is comprised between the smallest and the largest scales.

9.7 Fourier Spectral Solution

The assumption of spatial homogeneity naturally leads to a Fourier representation of the primitive variables of the Navier–Stokes equations. In this case, the absence of solid walls eases the elaboration of solutions and the differential operators are replaced by wavenumber multiplications in spectral space. Nevertheless, these Fourier tools yield direct access to spectra that are convenient and reliable theoretical instruments to interpret the physical phenomena. As might be expected, the field has been extensively explored and exploited by several authors arguably starting with the monograph by Batchelor [11]. Over the intervening decades there have been several reviews and these are nicely highlighted by Lesieur [50] and McComb [54].

The velocity field is approximated by the following Fourier series given in a 2π periodic box

$$\boldsymbol{v}(\boldsymbol{x}, t) = \sum_{\boldsymbol{k}} \boldsymbol{u}(\boldsymbol{k}, t) \exp(i\boldsymbol{k} \cdot \boldsymbol{x}) , \tag{9.102}$$

where the wavevector $\boldsymbol{k} = (k_1, k_2, k_3)$ goes from $-\infty$ to ∞. The k_i are integers.

For the sake of facility, we rewrite the Navier–Stokes equations with the non-linear term in conservative form taking the incompressibility into account

$$\frac{\partial \boldsymbol{v}}{\partial t} + \nabla \cdot (\boldsymbol{v} \otimes \boldsymbol{v}) = -\frac{1}{\rho}\nabla p + \nu \triangle \boldsymbol{v} \, . \tag{9.103}$$

With (9.102), the Fourier representation of the tensor product appearing in the non-linear term is obtained as follows

$$\begin{aligned} (\boldsymbol{v} \otimes \boldsymbol{v})_{ij} = v_i v_j &= \sum_{\boldsymbol{k}'} u_i(\boldsymbol{k}', t) e^{i\boldsymbol{k}'\cdot\boldsymbol{x}} \sum_{\boldsymbol{k}''} u_j(\boldsymbol{k}'', t) e^{i\boldsymbol{k}''\cdot\boldsymbol{x}} \\ &= \sum_{\boldsymbol{k}'+\boldsymbol{k}''=\boldsymbol{k}} u_i(\boldsymbol{k}', t) u_j(\boldsymbol{k}'', t) e^{i(\boldsymbol{k}'+\boldsymbol{k}'')\cdot\boldsymbol{x}} \, . \end{aligned} \tag{9.104}$$

The pressure field is also given by a Fourier series such that

$$\frac{1}{\rho} p = \sum_{\boldsymbol{k}} \hat{p}(\boldsymbol{k}, t) \exp(i\boldsymbol{k} \cdot \boldsymbol{x}) \, . \tag{9.105}$$

The insertion of the Fourier approximations of the various terms in (9.103), followed by the multiplication of the resulting relation by $e^{-i\boldsymbol{k}\cdot\boldsymbol{x}}$ and then integration on the periodic cube leads to the equation

$$\frac{du_i}{dt} + \nu k^2 u_i = -ik_i \hat{p} - C_i \, , \tag{9.106}$$

where C_i is the non-linear convective term which in Fourier space is given by

$$C_i = ik_m \sum_{\boldsymbol{k}'+\boldsymbol{k}''=\boldsymbol{k}} u_i(\boldsymbol{k}', t) u_m(\boldsymbol{k}'', t) \, . \tag{9.107}$$

Taking the divergence of (9.106) with the incompressibility constraint, we get the pressure Poisson equation

$$k^2 \hat{p} = ik_i C_i \, . \tag{9.108}$$

The pressure $\hat{p}$ is then

$$\hat{p} = i \frac{k_l}{k^2} C_l \, . \tag{9.109}$$

The dynamical Navier–Stokes equation (9.106) becomes

$$\left(\frac{d}{dt}+\nu k^2\right)u_i = \frac{k_i k_l}{k^2}C_l - C_i$$
$$= -(\delta_{il} - \frac{k_i k_l}{k^2})C_l$$
$$= -P_{il}C_l \ , \tag{9.110}$$

with $P_{il} = \delta_{il} - k_i k_l / k^2$, the projection tensor of the velocity field on a plane that is orthogonal to the $\boldsymbol{k}$ vector.

It is very often preferred to write (9.110) in symmetric form, i.e. in terms of the compound projection operator P_{ilm}

$$P_{ilm} = k_l P_{im} + k_m P_{il} \ , \tag{9.111}$$

such that

$$\left(\frac{d}{dt}+\nu k^2\right)u_i = -\frac{i}{2}P_{ilm}\sum_{\boldsymbol{k}'+\boldsymbol{k}''=\boldsymbol{k}} u_l(\boldsymbol{k}',t)u_m(\boldsymbol{k}'',t) \ , \tag{9.112}$$
$$k_i u_i = 0 \ . \tag{9.113}$$

Equations (9.112) and (9.113) are amenable to numerical Fourier spectral approximation if we apply a cut-off wavenumber k_c in the $\boldsymbol{k}$ space in such a way that $\|\boldsymbol{k}\| < k_c$. In the convolution term, $\|\boldsymbol{k}'\| < k_c$ and $\|\boldsymbol{k}''\| < k_c$, cf. S. A. Orszag [67].

Even though the numerical integration is carried out in spectral space, the non-linearity is computed in physical space by so-called pseudo-spectral or more appropriately collocation method. The passage between Fourier and physical space and vice-versa is performed by discrete Fourier transforms (DFT). All derivatives are accurately computed in spectral space. For the non-linear terms the various contributions are transformed in physical space by DFT on the collocation grid, where the product $\boldsymbol{v}\cdot\nabla\boldsymbol{v}$ is evaluated at these nodes and transformed back to Fourier space by inverse DFTs. Dealiasing procedures are needed to avoid spectral pollution in the high wave numbers.

9.8 Linear Turbulence Models

The real life applications are very seldom taking place in periodic geometries. Engineering practice implies complicated internal or external shapes and the presence of walls renders matters quite complex. Therefore a number of approaches of turbulent flows require the use of turbulent models following the lead of Lumley [52] and more recently Gatski [33]. We review some of them in the next subsections.

9.8.1 Zero Equation Model

This closure scheme is often called algebraic to clearly demonstrate the fact that there is no transport equation to describe the Reynolds stresses, but only algebraic expressions relating them to the velocity field $\overline{\boldsymbol{v}}(\boldsymbol{x})$. By analogy with the viscous Newtonian fluid model, we write the constitutive turbulent equation for the Reynolds stress as

$$\boldsymbol{R} = 2\mu_T \, \overline{\boldsymbol{d}} \, , \tag{9.114}$$

using the turbulent (dynamic) viscosity μ_T. This turbulent viscosity was introduced by Boussinesq [17]. It should be emphasized that we reason by analogy with the mechanics of continuous media where we deduce equations for the viscous Newtonian fluid. Here, however, we do not characterize a material behavior but the state of a flow. In order to ensure a correct writing of the Reynolds tensor, we write the Eq. (9.114) in the form:

$$\boldsymbol{\tau} - \frac{2K}{3}\boldsymbol{I} = -2\nu_T \overline{\boldsymbol{d}} \, . \tag{9.115}$$

The addition of the diagonal term allows to obtain in the left hand side a tensor with a zero trace as is $\overline{\boldsymbol{d}}$ and $\tau_{ii} = 2K$. The turbulent viscosity is fixed by K, ε and ℓ, the mixing length. By dimensional analysis, we have

$$\nu_T \simeq K^{1/2}\ell \quad \text{or} \quad \nu_T \simeq K^2/\varepsilon = \tau K \, , \tag{9.116}$$

where τ is the turbulent velocity time.

9.8.2 Turbulent Flow in a Plane Channel

Here we deal with the case of a particular flow that will enable us to write with full details the closure problem described by Eqs. (9.115)–(9.116). We consider a statistically steady state flow between two parallel planes of infinite horizontal extension that constitute a channel of height $2h$. The mean flow is a pure shear flow, homogeneous in direction x_1, such that

$$\overline{\boldsymbol{v}} = (\overline{v_1}(x_2), 0, 0) \, . \tag{9.117}$$

The Eqs. (9.14) of the mean motion become

$$0 = -\frac{\partial \overline{p}}{\partial x_1} + \mu \frac{\partial^2 \overline{v_1}}{\partial x_2^2} + \frac{\partial}{\partial x_2}(-\rho \overline{v_1' v_2'}), \tag{9.118}$$

$$0 = -\frac{\partial \overline{p}}{\partial x_2} + \frac{\partial}{\partial x_2}(-\rho \overline{v_2'^2}), \tag{9.119}$$

$$\frac{\partial \overline{v_1}}{\partial x_1} = 0 \, . \tag{9.120}$$

Integrating (9.119) yields

$$\overline{p} + \rho \overline{v_2'^2} = p_0(x_1) \, . \tag{9.121}$$

We may rewrite (9.118) as

$$\frac{\partial}{\partial x_2}(\mu \frac{\partial \overline{v_1}}{\partial x_2} - \rho \overline{v_1' v_2'}) = \frac{dp_0}{dx_1} = -A \, . \tag{9.122}$$

As the left hand side can only be a function of x_2 because of the hypotheses of steady state homogeneous turbulence and as the right hand side is only function of x_1, each side must be equal to a constant. One gets

$$\mu \frac{\partial \overline{v_1}}{\partial x_2} - \rho \overline{v_1' v_2'} = -Ax_2 + B \, . \tag{9.123}$$

In the left hand side, we have the total stress resulting from the viscous and Reynolds stresses. If the origin of the axes is located at mid-height of the channel, by symmetry, B must vanish in $x_2 = 0$.

Let us move the origin of the coordinate system on the lower wall. We assume that the mixing length increases linearly with the distance to the wall, i.e.

$$\ell = \kappa x_2 \, . \tag{9.124}$$

The vortices close to a wall have a characteristic dimension proportional to the wall distance. Let us note that turbulence is zero on this wall by the no-slip condition.

Using the model of turbulent viscosity (9.115) and assuming a steady state homogeneous turbulence, one obtains with (9.22)

$$\mathcal{P} = \mathcal{D}, \tag{9.125}$$

and

$$\mathcal{P} = 2\nu_T \overline{d}_{ij} \overline{d}_{ij} = \varepsilon \, . \tag{9.126}$$

By (9.40), (9.116) and (9.126), we eliminate $K^{1/2}$ and ε. We have

$$\begin{aligned} \nu_T &\approx K^{1/2} \ell = \varepsilon^{1/3} \ell^{4/3} \\ &= (2\nu_T \overline{d}_{ij} \overline{d}_{ij})^{1/3} \ell^{4/3} \end{aligned} \tag{9.127}$$

and therefore

$$\nu_T \approx \ell^2 (2\overline{d}_{ij}\overline{d}_{ij})^{1/2} . \tag{9.128}$$

For the flow between two parallel walls, we have $\overline{d}_{12} = \overline{d}_{21}$ and then,

$$\nu_T = \ell^2 \frac{\partial \overline{v_1}}{\partial x_2} . \tag{9.129}$$

9.8.3 The Logarithmic Velocity Profile

Combining (9.115), (9.123) and (9.129), we obtain

$$\left(\mu + \rho \ell^2 \frac{\partial \overline{v_1}}{\partial x_2}\right) \frac{\partial \overline{v_1}}{\partial x_2} = -Ax_2 + B , \tag{9.130}$$

where B is the wall shear stress that we denote τ_w. In the neighborhood of the wall assumed to be smooth, the turbulent exchanges are negligible with respect to the molecular viscosity effects. We are in the viscous sub-layer. The Eq. (9.130) reduces to:

$$\mu \frac{\partial \overline{v_1}}{\partial x_2} = \tau_w = \rho v_*^2, \quad | \, Ax_2 \, | \ll B , \tag{9.131}$$

with v_*, the friction velocity. The velocity profile is linear

$$\frac{\overline{v_1}}{v_*} = \frac{v_* x_2}{\nu} = Re_* . \tag{9.132}$$

In (9.132), Re_* is the wall Reynolds number.

Beyond the viscous sub-layer, we neglect the molecular diffusion with respect to the turbulent diffusion. The relation (9.130) with (9.124) becomes:

$$\rho \kappa^2 x_2^2 \left(\frac{d\overline{v_1}}{dx_2}\right)^2 = -Ax_2 + B . \tag{9.133}$$

The integration of this non-linear differential equation is not simple. We notice experimentally that the result obtained for $x_2/h < 0.2$ is very close to that obtained when Ax_2 is neglected compared to B. Consequently, in this zone, the shear stress remains constant. We have the relation:

$$\frac{d\overline{v_1}}{dx_2} = \frac{v_*}{\kappa x_2} . \tag{9.134}$$

Integrating Eq. (9.134) yields

$$\overline{v_1} = \frac{v_*}{\kappa} \log x_2 + C \ . \tag{9.135}$$

To know the velocity variation close to the wall, we need to determine the value of the integration constant C. To this end, we will admit that the velocity $\overline{v_1}$ vanishes, at a distance from the wall corresponding to the thickness δ_s of the viscous sub-layer. We set the condition:

$$\overline{v_1} = 0 \quad \text{in} \quad x_2 = \delta_s = \beta \frac{\nu}{v_*} \ , \tag{9.136}$$

β being a numerical constant. This way to express the thickness δ_s is classically adopted in order to get the wall distance x_2 dimensionless using the wall Reynolds number Re_*:

$$\frac{v_* x_2}{\nu} = Re_* \ . \tag{9.137}$$

Condition (9.136) applied to (9.135) yields

$$C = -\frac{v_*}{\kappa} \log \frac{\beta \nu}{v_*} \ . \tag{9.138}$$

The relation (9.135), with C given by (9.138), is written as:

$$\frac{\overline{v_1}}{v_*} = \frac{1}{\kappa} (\log \frac{x_2 v_*}{\nu} - \log \beta) = \frac{1}{\kappa} (\log Re_* - \log \beta) \ . \tag{9.139}$$

The experimental data show that κ, the von Kármán constant, has a value independent on the wall nature (rough or smooth) and is equal to 0.4. On the other hand, the β value, that is in the mean of the order of 0.1, is influenced by the wall roughness.

The logarithmic profile (9.139) is one of the most celebrated results of turbulence theory. Figure 9.7 is a semi-log plot. The straight line corresponding to Eq. (9.139) is obvious. When $x_2 v_*/\nu$ is <30, the molecular viscosity becomes important in this zone. The laminar stresses are dominant and the turbulent stresses are negligible, allowing to write the next equalities:

$$\tau_{12} = \mu \frac{\partial \overline{v_1}}{\partial x_2} = \tau_w = \rho v_*^2 \tag{9.140}$$

or

$$\frac{\overline{v_1}}{v_*} = \frac{v_* x_2}{\nu} = Re_* \ . \tag{9.141}$$

The curve corresponding to this profile is included in Fig. 9.7. The experimental data are in good agreement for $x_2 v_*/\nu < 8$. For $x_2/h > 0.2$, the logarithmic law no longer fits exactly the experimental results. In the region between $x_2/h = 0.2$ and

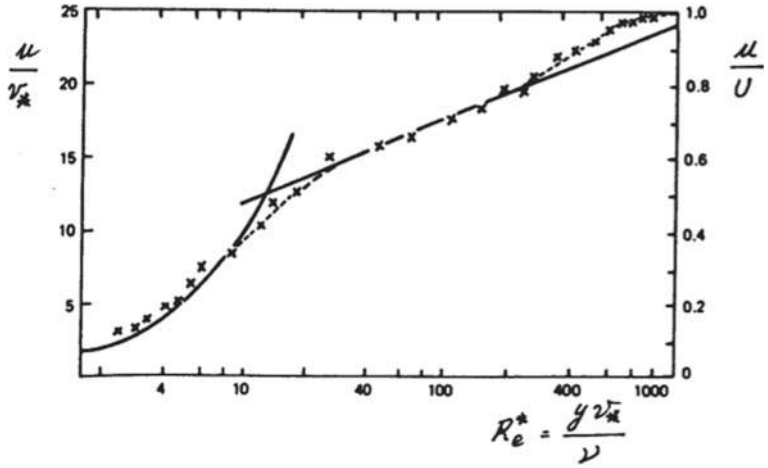

Fig. 9.7 Logarithmic velocity profile in a turbulent boundary layer with $u = v_1$, $y = x_2$. Crosses are experimental data

$x_2/h = 1$, one uses the wake function. The profile is then the logarithmic relation plus a function $w(x_2/\delta)$ with δ a characteristic thickness of the problem. One obtains

$$\frac{\overline{v_1}(x_2)}{v_*} = \frac{1}{\kappa}\log\frac{v_* x_2}{\nu} + C + \frac{1}{\kappa}\Pi w(\frac{x_2}{\delta}) \tag{9.142}$$

with

$$w = 2\sin^2(\frac{x_2}{\delta}\frac{\pi}{2}) \,. \tag{9.143}$$

The parameter Π is linked to the pressure gradient. In a boundary layer with constant pressure, $\Pi = 0.6$. For a pipe flow, $\Pi = 1/4$ with $\delta = R$.

9.9 The One-Equation Model: the $K - \ell$ Model

The algebraic closure of the zero equation model is often criticized for two reasons. The first one notices that there exists a number of flow experiments where $\overline{\boldsymbol{d}}$ and $\overline{\boldsymbol{v}' \otimes \boldsymbol{v}'}$ do not change sign at the same location. Therefore, the turbulent viscosity could be negative and this is physically not expected. However, experimentally the regions where the turbulent viscosity is negative, are spatially small in most industrial applications so that the local failure of this model has no major consequence.

The second reason consists in that the relationship between $\overline{\boldsymbol{d}}$ and $\overline{\boldsymbol{v}' \otimes \boldsymbol{v}'}$ is purely local, ignoring de facto the "history" of turbulence. In order to improve this situation, one adds a transport equation for a relevant velocity scale of the turbulent motion. The most significant scale from the physical point of view is $K^{1/2}$, cf. (9.20). With

the Eqs. (9.22) and (9.23) of the turbulent kinetic energy, we observe that we have generated new correlations in the diffusion and dissipation terms. In order to close the system of equations, the $K - \ell$ model introduces the following hypotheses. One replaces the first two terms of the turbulent kinetic energy flux (9.23) by a gradient and one develops a link between the dissipation rate ε and the kinetic energy by an algebraic relation. One gets

$$-\left(\frac{1}{\rho}\overline{p'\boldsymbol{v}'} + \overline{\frac{1}{2}(\boldsymbol{v}'\cdot\boldsymbol{v}')\boldsymbol{v}'}\right) = \frac{\nu_T}{\sigma_q}\nabla K \tag{9.144}$$

$$\varepsilon = \frac{C_D}{\ell}K^{3/2}\,, \tag{9.145}$$

with σ_q and C_D empirical constants. Usually, one sets $C_D = 0.164$. Similarly, one chooses μ_T as:

$$\mu_T = \rho K^{1/2}\ell\,, \tag{9.146}$$

where the mixing length ℓ is determined again by an algebraic relation. For completeness, it is worth noting that an alternative approach to determining the eddy viscosity is to solve a transport equation directly for the eddy viscosity ν_T (Spalart and Allmaras [94]). Such a one-equation model, though based primarily on empiricism and on dimensional analysis, is popular among industrial users, especially in aerodynamics and in turbomachinery, due to its ease of implementation and relatively inexpensive cost.

For three-dimensional flows, the concept of mixing length (9.124) can be generalized. With the gradient velocity tensor we have the Eq. (9.128) or if we use the vorticity

$$\nu_T = \ell^2(\overline{\boldsymbol{\omega}}\cdot\overline{\boldsymbol{\omega}})^{1/2}\,, \tag{9.147}$$

where $\overline{\boldsymbol{\omega}} = \mathbf{curl}\,\overline{\boldsymbol{v}}$ is the average vorticity. This is the Baldwin–Lomax mixing length model [7].

Consequently, the governing equation of the $K - \ell$ model reads:

$$\frac{\partial K}{\partial t} + \overline{\boldsymbol{v}}\cdot\nabla K = \nabla\cdot\left((\nu + \frac{\nu_T}{\sigma_K})\nabla K\right) + 2\nu_T\,\overline{\boldsymbol{d}} : \nabla\overline{\boldsymbol{v}} - C_D\frac{K^{3/2}}{\ell}\,. \tag{9.148}$$

Very often one sets σ_K equal to 1. This practice produces good results for various types of flows. To solve (9.148) the boundary condition imposes a vanishing K value on solid walls and a zero normal gradient on inflow and outflow sections.

9.10 The Two-Equation Models

In this section we will look at the widely used $K-\varepsilon$ and $K-\omega$ models. These approaches try to circumvent the deficiencies of the one-equation modeling by the addition of a second partial differential equation. Both models use (9.115) for the Reynolds stress tensor.

9.10.1 $K-\varepsilon$ Model

One takes the derivative of the dynamic equation for the velocity fluctuations (9.19) with respect to x_l. Then, one multiplies the resulting equation by $\partial v_i'/\partial x_l$. This last relation is averaged. We obtain

$$\begin{aligned}
&\frac{\partial}{\partial t}\frac{1}{2}\overline{\left(\frac{\partial v_i'}{\partial x_l}\right)^2}+\frac{\partial^2\overline{v_i}}{\partial x_l\partial x_j}\overline{v_j'\frac{\partial v_i'}{\partial x_l}}+\frac{\partial\overline{v_i}}{\partial x_j}\overline{\frac{\partial v_i'}{\partial x_l}\frac{\partial v_j'}{\partial x_l}}+\frac{\partial\overline{v_j}}{\partial x_l}\overline{\frac{\partial v_i'}{\partial x_l}\frac{\partial v_i'}{\partial x_j}}\\
&\quad+\overline{v_j}\frac{\partial}{\partial x_j}\frac{1}{2}\overline{(\frac{\partial v_i'}{\partial x_l})^2}+\overline{\frac{\partial v_i'}{\partial x_l}\frac{\partial v_j'}{\partial x_l}\frac{\partial v_i'}{\partial x_j}}+\overline{v_j'\frac{\partial}{\partial x_j}\frac{1}{2}(\frac{\partial v_i'}{\partial x_l})^2}\\
&\quad=-\frac{1}{\rho}\overline{\frac{\partial v_i'}{\partial x_l}\frac{\partial^2 p'}{\partial x_l\partial x_i}}+\nu\overline{\frac{\partial v_i'}{\partial x_l}(\frac{\partial^2}{\partial x_j^2}(\frac{\partial v_i'}{\partial x_l}))}\,.
\end{aligned}\tag{9.149}$$

Defining the dissipation rate ε

$$\varepsilon=\nu\overline{\frac{\partial v_i'}{\partial x_l}\frac{\partial v_i'}{\partial x_l}}\,,\tag{9.150}$$

we write Eq. (9.149) as follows

$$\begin{aligned}
\frac{\partial\varepsilon}{\partial t}+\overline{v_k}\frac{\partial\varepsilon}{\partial x_k}&=\frac{\partial}{\partial x_k}\left(\nu\frac{\partial\varepsilon}{\partial x_k}-\nu\overline{v_k'\frac{\partial v_i'}{\partial x_l}\frac{\partial v_i'}{\partial x_l}}-2\frac{\nu}{\rho}\overline{\frac{\partial p}{\partial x_i}\frac{\partial v_k'}{\partial x_i}}\right)\\
&\quad-2\nu\frac{\partial\overline{v_i}}{\partial x_k}\left(\overline{\frac{\partial v_i'}{\partial x_l}\frac{\partial v_k'}{\partial x_l}}+\overline{\frac{\partial v_l'}{\partial x_i}\frac{\partial v_l'}{\partial x_k}}\right)-2\nu\overline{v_k'\frac{\partial v_i'}{\partial x_l}}\frac{\partial}{\partial x_k}\left(\frac{\partial\overline{v_i}}{\partial x_l}\right)\\
&\quad-2\nu\overline{\frac{\partial v_i'}{\partial x_l}\frac{\partial v_k'}{\partial x_l}\frac{\partial v_l'}{\partial x_k}}-2\nu^2\overline{\left(\frac{\partial}{\partial x_k}\left(\frac{\partial v_i'}{\partial x_l}\right)\right)^2}\,.
\end{aligned}\tag{9.151}$$

On the left hand side of (9.151), we find the material derivative of the dissipation rate. Then in the first expression on the right hand side we have several diffusion terms: molecular, turbulent by velocity fluctuations, turbulent by pressure fluctuations. The two terms of the second line shows the production by the mean velocity gradients indicating the interaction between the turbulence and the mean flow. The penultimate

term in the third line shows the interaction between the gradients of the velocity fluctuations. Finally the last term is the dissipation of ε.

The Eq. (9.151) is often rewritten on the basis of empirical rather than theoretical considerations in the form

$$\frac{\partial \varepsilon}{\partial t} + \overline{\boldsymbol{v}} \cdot \boldsymbol{\nabla} \varepsilon = \boldsymbol{\nabla} \cdot \left((\nu + \frac{\nu_T}{\sigma_\varepsilon}) \boldsymbol{\nabla} \varepsilon \right) + 2 C_{\varepsilon_1} \frac{\varepsilon}{K} \nu_T \, \overline{\boldsymbol{d}} : \overline{\boldsymbol{d}} - C_{\varepsilon_2} \frac{\varepsilon^2}{K} , \tag{9.152}$$

where the eddy viscosity is defined as

$$\nu_T = C_\mu \frac{K^2}{\varepsilon} . \tag{9.153}$$

Observe the strong similarity of Eqs. (9.148) and (9.152).

There has been many attempts to obtain the numerical values for the constants appearing in the $K - \varepsilon$ model by a careful analysis of the experimental data. However a convincing theoretical approach is based on the renormalization group theory (RNG) proposed by Yakhot and Orszag [123]. The RNG theory is well beyond of the scope of this monograph and we refer the reader to the available literature. The constants are given by Yakhot et al. [124]

$$C_{\varepsilon_1} = 1.42 \quad C_{\varepsilon_2} = 1.68 \quad \sigma_\varepsilon = \sigma_K = 0.719 \quad C_\mu = 0.0845 . \tag{9.154}$$

The boundary conditions for K are identical to those proposed for the one-equation model. However for the two-equation approach, the appearance of ε induces complications to set up the boundary condition for that variable on the wall as its evaluation is rather tricky. The numericists and modelers resort to wall functions whereby the boundary conditions are not applied directly on the wall but at the beginning of the turbulent region close to the boundary. In the turbulent boundary layer, Eq. (9.126) yields

$$\nu_T \left(\frac{\partial \overline{v_1}}{\partial x_2} \right)^2 = \varepsilon . \tag{9.155}$$

We also know that in the turbulent boundary layer, the shear stress is constant

$$\mu_T \left(\frac{\partial \overline{v_1}}{\partial x_2} \right) = \tau_w . \tag{9.156}$$

Combining (9.155) and (9.156) with $\tau_w = \rho v_*^2$, we find

$$K = \frac{v_*^2}{\sqrt{C_\mu}} . \tag{9.157}$$

The dissipation rate is obtained from (9.156) and the velocity profile (9.139)

$$\varepsilon = \frac{|\, v_* \,|^3}{\kappa x_2} \,. \tag{9.158}$$

Sometimes, Neumann type conditions are needed

$$\frac{\partial K}{\partial n} = 0, \quad v_* = (K_w)^{1/2} C_\mu^{1/4} \,, \tag{9.159}$$

where K_w is the wall turbulence kinetic energy and $\partial/\partial n$ the normal derivative.

9.10.2 $K - \omega$ Model

In this model proposed by Wilcox [119, 120], K is still the turbulent kinetic energy while ω is the specific rate of dissipation of K, also referred to as the average frequency of the turbulence. The definition of ω is given as

$$\omega = \frac{\varepsilon}{K} \,. \tag{9.160}$$

The dimension of ω is indeed the inverse of time. The kinematic eddy viscosity is defined as

$$\nu_T = \frac{K}{\omega} \,. \tag{9.161}$$

The dynamic equation for ω may be obtained easily by formally dividing the variable in (9.148) by K and multiplying by ω yielding

$$\frac{\partial \omega}{\partial t} + \overline{\boldsymbol{v}} \cdot \nabla \omega = \nabla \cdot \left((\nu + \frac{\nu_T}{\sigma_\omega}) \nabla \omega \right) + 2\alpha \nu_T \frac{\omega}{K} \overline{\boldsymbol{d}} : \nabla \overline{\boldsymbol{v}} - \beta \omega^2 \,. \tag{9.162}$$

The constants have the following values $\alpha = 5/9$, $\beta = 3/40$, $\sigma_\omega = 1/2$.

Two important topics have played a central role in the formulation of recent models of the Reynolds stresses: realizability and objectivity. Realizability imposes that the tensor diagonal components be individually positive

$$R_{\alpha\alpha} \geq 0, \quad \alpha = 1, 2, 3, \tag{9.163}$$

the greek index α indicating that there is no summation on the repeated indices in this case. Objectivity is a more delicate topic and is beyond the framework of this monograph [21, 95].

9.11 Non-linear Turbulence Models

So far we have examined linear turbulence models. However the physical reality of turbulence, as it is generated by the non-linear terms of the Navier–Stokes equations, is definitely non-linear. Therefore in this section we will tackle the construction of non-linear models to be able to cope better with the experimental data and the knowledge of turbulent phenomena. The two-equation models present the following defects: firstly, the inability to take into account the curvature effects of the streamlines and the deformations due to rotation; secondly, the neglect of non-local effects and history on the anisotropy of the Reynolds stresses.

9.11.1 Anisotropy Tensor

The anisotropy tensor of the Reynolds tensor is defined by the relationship

$$b_{ij} = \frac{\tau_{ij} - \frac{2K}{3}\delta_{ij}}{2K} , \tag{9.164}$$

and describes the deviations with respect to the isotropic situation. This tensor offers interesting properties. We notice that its trace which is the first invariant I_1

$$b_{ii} = \mathrm{I}_1(\boldsymbol{b}) = 0 \tag{9.165}$$

is zero by Eq. (9.21). Most of the time, the use of the anisotropy tensor is related to its eigenvectors because then, the tensor is diagonal. As a consequence of (9.165) the sum of its eigenvalues vanish in such a way that only two such quantities are independent. Therefore the anisotropy is characterized by two independent invariants

$$\mathrm{I}_2(\boldsymbol{b}) = -b_{ij}b_{ji}/2 = -\frac{1}{2}\,\mathrm{tr}\,\boldsymbol{b}^2, \quad \mathrm{I}_3(\boldsymbol{b}) = b_{ij}b_{jk}b_{ki}/3 = \det \boldsymbol{b} . \tag{9.166}$$

If the turbulence is two-dimensional, because one velocity component in the direction of one of the principal axes always vanishes, we obtain

$$b_{\alpha\alpha} = -1/3 \quad \text{if} \quad \tau_{\alpha\alpha} = 0 . \tag{9.167}$$

There is no summation on Greek indices. If now all the energy is concentrated in a single component, we have

$$b_{\alpha\alpha} = 2/3 \quad \text{if} \quad \tau_{\alpha\alpha} = 2K . \tag{9.168}$$

This last case is named one-dimensional turbulence. We conclude that the eigenvalues of $\boldsymbol{b}$ are contained in the interval $[-1/3, 2/3]$.

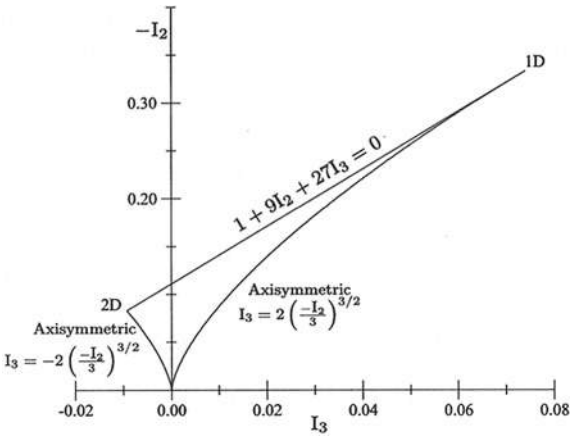

Fig. 9.8 Anisotropy invariant map. $1D$-axisymmetric boundary at $(I_3, -I_2) = (2/27, 1/3)$; $2D$-axisymmetric boundary at $(I_3, -I_2) = (-1/108, 1/12)$

Lumley [53] examined the limiting values associated with b_{ij} in incompressible flows. For isotropic turbulence, the anisotropies vanish and the corresponding point is the origin in the anisotropy invariant map defined with the axes $(I_3, -I_2)$. From the origin, two other limiting boundaries are associated with axisymmetric turbulence where two of the diagonal elements are equal and the third is the negative sum of the other two (incompressibility). For example the anisotropy tensor in the principal coordinates is given by

$$b_{ij} = \text{diag}(a, a, -2a) \; . \tag{9.169}$$

We compute

$$\text{I}_2 = -3a^2, \quad \text{I}_3 = -2a^3 \; . \tag{9.170}$$

For $a > 0$, we have $\text{I}_3 = +(-2\text{I}_2/3)^{3/2}$, corresponding to an axisymmetric expansion. When $a < 0$, $\text{I}_3 = -(-2\text{I}_2/3)^{3/2}$ that corresponds to an axisymmetric contraction.

As Fig. 9.8 shows, a straight line connects the one-component axisymmetric limit with the two-component axisymmetric limit. This turbulence case corresponds to a Reynolds tensor with only two non zero components

$$\tau_{ij} = \text{diag}(0, p, q) \; , \tag{9.171}$$

with p, q both positive and $p + q = 2K$. Now let us set $q = K(1 - a/3)$, with $0 \leq a \leq 3$. We have successively

$$\tau_{ij} = \text{diag}(0, K(1 + a/3), K(1 - a/3))) \tag{9.172}$$

and the anisotropy tensor reads

$$b_{ij} = \text{diag}(0, (1 + a)/6, (1 - a)/6) \; . \tag{9.173}$$

The invariants are

$$\mathrm{I}_2(\boldsymbol{b}) = -\frac{1}{12}\left(1+\frac{a^2}{3}\right) , \quad \mathrm{I}_3(\boldsymbol{b}) = \frac{a^2-1}{108} \tag{9.174}$$

For $a = 0$, $\mathrm{I}_3(\boldsymbol{b}) = -1/108$ and with $a = 3$, $\mathrm{I}_3(\boldsymbol{b}) = 2/27$.

Theorem 9.1 (Cayley–Hamilton theorem) *The Cayley–Hamilton theorem specifies that every tensor* $\boldsymbol{b}$ *satisfies its own characteristic equation*

$$\boldsymbol{b}^3 - I_1\boldsymbol{b}^2 + I_2\boldsymbol{b} - I_3\boldsymbol{I} = 0 . \tag{9.175}$$

In our case, (9.175) reduces to

$$b_{ij}^3 + \mathrm{I}_2 b_{ij} - \mathrm{I}_3\delta_{ij} = 0 . \tag{9.176}$$

Using (9.176) with (9.174), the straight line of Fig. 9.8 is given by the relation

$$1 + 9\mathrm{I}_2 + 27\mathrm{I}_3 = 0 . \tag{9.177}$$

Referring to Eq. (9.115) for the Reynolds stress, the anisotropy tensor yields

$$\boldsymbol{b} = \frac{-2\nu_T\overline{\boldsymbol{d}}}{2K} . \tag{9.178}$$

This relation shows that the principal axes of the stress and the averaged strain rate are aligned. However this is not true for a particularly important engineering application, namely shear flows.

9.11.2 Dynamic Equation for the Anisotropy Tensor

In this section, we will resort to the index notation for ease of mathematical developments. The dynamic equation for the Reynolds stress (9.29) reads

$$\frac{D\tau_{ij}}{Dt} = -\tau_{ik}\frac{\partial\overline{v}_j}{\partial x_k} - \tau_{jk}\frac{\partial\overline{v}_i}{\partial x_k} + \Pi_{ij} - \varepsilon_{ij} + \mathcal{D}_{ij} , \tag{9.179}$$

where the various terms are

$$\Pi_{ij} = \overline{p'\left(\frac{\partial v_i'}{\partial x_j} + \frac{\partial v_j'}{\partial x_i}\right)} \tag{9.180}$$

$$\varepsilon_{ij} = 2\nu\overline{\frac{\partial v_i'}{\partial x_k}\frac{\partial v_j'}{\partial x_k}} \tag{9.181}$$

$$\begin{aligned}\mathcal{D}_{ij} &= -\frac{\partial C_{ijk}}{\partial x_k} \\ &= -\frac{\partial}{\partial x_k}\left(\overline{v_i'v_j'v_k'} + \overline{p'v_i'}\delta_{jk} + \overline{p'v_j'}\delta_{ik} - \nu\frac{\partial \tau_{ij}}{\partial x_k}\right) .\end{aligned} \tag{9.182}$$

By incompressibility $\Pi_{ii} = 0$. Evaluating the trace of (9.179) leads to the dynamic equation of the turbulent energy

$$\frac{DK}{Dt} = \mathcal{P} - \varepsilon + \mathcal{D} , \tag{9.183}$$

where

$$\mathcal{P} = -\tau_{ik}\frac{\partial \overline{v}_i}{\partial x_k}, \quad \varepsilon = \frac{\varepsilon_{ii}}{2}, \quad \mathcal{D} = \frac{\mathcal{D}_{ii}}{2} . \tag{9.184}$$

Taking (9.179) and (9.183) into account, we obtain

$$\frac{Db_{ij}}{Dt} = \frac{1}{2K}\left(\frac{D\tau_{ij}}{Dt} - \frac{\tau_{ij}}{K}\frac{DK}{Dt}\right) . \tag{9.185}$$

Defining the anisotropy tensor for the dissipation-rate correlation

$$d_{ij} = \frac{\varepsilon_{ij} - \frac{2K}{2K}\delta_{ij}}{2K} \tag{9.186}$$

the combination of (9.179) and (9.183) gives using the definition

$$\overline{d}_{ij} + \overline{\dot{\omega}}_{ij} = \frac{\partial \overline{v}_i}{\partial x_j} , \tag{9.187}$$

the relationship

$$\begin{aligned}\frac{Db_{ij}}{Dt} &= -b_{ij}\left(\frac{\mathcal{P}}{K} - \varepsilon\right) - \frac{2}{3}\overline{d}_{ij} - \left(b_{ik}\overline{d}_{kj} + \overline{d}_{ik}b_{kj} - \frac{2}{3}b_{mn}\overline{d}_{mn}\delta_{ij}\right) \\ &+ \left(b_{ik}\overline{\dot{\omega}}_{kj} - \overline{\dot{\omega}}_{ik}b_{kj}\right) + \frac{\Pi_{ij}}{2K} + \frac{1}{2K}\left(\mathcal{D}_{ij} - \frac{\tau_{ij}}{K}\mathcal{D}\right) - \frac{1}{\tau}d_{ij} ,\end{aligned} \tag{9.188}$$

with $\tau = K/\varepsilon$.

To treat the pressure-strain rate correlation, we take the divergence of (9.19) that produces the pressure Poisson's equation

$$\frac{1}{\rho}\frac{\partial^2 p'}{\partial x_i^2} = -2\frac{\partial v_i'}{\partial x_j}\frac{\partial \overline{v_j}}{\partial x_i} - \left(\frac{\partial v_i'}{\partial x_j}\frac{\partial v_j'}{\partial x_i} - \overline{\frac{\partial v_i'}{\partial x_j}\frac{\partial v_j'}{\partial x_i}}\right) . \tag{9.189}$$

It is customary (cf. [24]) to decompose the turbulent pressure field p' into slow $p'^{(s)}$ and rapid $p'^{(r)}$ contributions

$$\frac{1}{\rho}\frac{\partial^2 p'^{(s)}}{\partial x_i^2} = -\left(\frac{\partial v_i'}{\partial x_j}\frac{\partial v_j'}{\partial x_i} - \overline{\frac{\partial v_i'}{\partial x_j}\frac{\partial v_j'}{\partial x_i}}\right) \tag{9.190}$$

$$\frac{1}{\rho}\frac{\partial^2 p'^{(r)}}{\partial x_i^2} = -2\frac{\partial v_i'}{\partial x_j}\frac{\partial \overline{v_j}}{\partial x_i} . \tag{9.191}$$

Equation (9.190) expresses the "slow" relaxation of the turbulence toward isotropy while (9.191) is concerned with the "rapid" response of turbulence to imposed mean velocity gradients.

The modeling of the pressure-strain rate correlation is based on the hypothesis of local homogeneity. Therefore, for the case of a one-point closure, the model is based on functionals of the Reynolds stress and the turbulent dissipation rate. We write

$$\Pi_{ij} = \varepsilon \mathcal{A}_{ij}(\boldsymbol{b}) + K\mathcal{M}_{ij}(\boldsymbol{b}) . \tag{9.192}$$

Gatski and Jongen [32] propose a nonlinear form in the anisotropy tensor b_{ij} that reads

$$\begin{aligned}\Pi_{ij} = &-\left(C_1^0 + C_1^1\frac{\mathcal{P}}{\varepsilon}\right)\varepsilon b_{ij} + C_2 K\overline{d}_{ij} \\ &+ C_3 K\left(b_{ik}\overline{d}_{jk} + b_{jk}\overline{d}_{ik} - \frac{2}{3}b_{mn}\overline{d}_{mn}\delta_{ij}\right) \\ &- C_4 K\left(b_{ik}\overline{\dot{\omega}}_{kj} - \overline{\dot{\omega}}_{ik}b_{kj}\right) \\ &+ C_5\varepsilon\left(b_{ik}b_{kj} - \frac{1}{3}b_{mn}b_{nm}\delta_{ij}\right) .\end{aligned} \tag{9.193}$$

Substituting (9.193) in (9.188) and rewriting yields

$$\begin{aligned}\frac{Db_{ij}}{Dt} &- \frac{1}{2K}\left(\mathcal{D}_{ij} - \frac{\tau_{ij}}{K}\mathcal{D}\right) \\ &= -\left(\frac{b_{ij}}{a_4} + a_3\left(b_{ik}\overline{d}_{kj} + \overline{d}_{ik}b_{kj} - \frac{2}{3}b_{mn}\overline{d}_{mn}\delta_{ij}\right)\right. \\ &- a_2\left(b_{ik}\overline{\omega}_{kj} - \overline{\omega}_{ik}b_{kj}\right) + a_1\overline{d}_{ij} \\ &\left. - \frac{1}{\tau}a_5\left(b_{ik}b_{kj} - \frac{1}{3}b_{mn}b_{nm}\delta_{ij}\right) + \frac{1}{\tau}d_{ij}\right) ,\end{aligned} \tag{9.194}$$

with the pressure-strain rate closure coefficients

$$a_1 = \frac{1}{2}\left(\frac{4}{3} - C_2\right) \ , \quad a_2 = \frac{1}{2}\left(2 - C_4\right) \ ,$$
$$a_3 = \frac{1}{2}\left(2 - C_3\right) \ , \tag{9.195}$$
$$a_4 = \tau\left(\frac{C_1^0}{2} - 1 + \left(\frac{C_1^1}{2} + 1\right)\frac{\mathcal{P}}{\varepsilon}\right)^{-1} \ ,$$
$$a_5 = \frac{1}{2}C_5 \ . \tag{9.196}$$

The closure coefficients are obtained from experimental data or numerical results on benchmark problems. Following Speziale et al. [96], we have $C_1^0 = 3.4$, $C_1^1 = 1.8$, $C_2 = 0.36$, $C_3 = 1.25$, $C_4 = 0.4$, $C_5 = 4.2$.

9.12 Reynolds Stress Tensor Representation Using Integrity Bases

From the previous section, we know that

$$\boldsymbol{b} = \boldsymbol{b}\left(\overline{\boldsymbol{d}}, \overline{\dot{\boldsymbol{\omega}}}, \tau\right) \ , \tag{9.197}$$

where τ is the integral turbulence time. The tensor $\boldsymbol{b}$ must satisfy the isotropy property, namely

$$\boldsymbol{Q}\boldsymbol{b}\left(\overline{\boldsymbol{d}}, \overline{\dot{\boldsymbol{\omega}}}, \tau\right)\boldsymbol{Q}^T = \boldsymbol{b}\left(\boldsymbol{Q}\overline{\boldsymbol{d}}\,\boldsymbol{Q}^T, \boldsymbol{Q}\overline{\dot{\boldsymbol{\omega}}}\,\boldsymbol{Q}^T, \tau\right) \ , \tag{9.198}$$

for all orthogonal transformation matrices $\boldsymbol{Q}$ such that $\boldsymbol{Q}\boldsymbol{Q}^T = \boldsymbol{Q}^T\boldsymbol{Q} = \boldsymbol{I}$ and $\det \boldsymbol{Q} = \pm 1$, where $\boldsymbol{Q}^T$ is the transpose of $\boldsymbol{Q}$ and det denotes the determinant. By (9.198), it is required that $\boldsymbol{b}$ be invariant to the full orthogonal group that includes all reflection and rotation matrices. By the Cayley–Hamilton theorem (9.175), given an arbitrary finite set of input tensors, it is possible to construct a finite basis of invariant tensors, called an integrity basis [24]. Any invariant tensor function of these given tensors, $\overline{\boldsymbol{d}}$, $\overline{\dot{\boldsymbol{\omega}}}$, will be a linear combination of the integrity basis tensors. These integrity bases have been tabulated in chapter two of Deville-Gatski monograph [24] where a clear presentation is aimed at achieving readability.

To summarize the theoretical development that is beyond the scope of this monograph, the integrity basis for a single symmetric tensor $\boldsymbol{T}$ is given by the associated matrix invariants

$$\text{tr}\ \boldsymbol{T}, \text{tr}\ \boldsymbol{T}^2, \text{tr}\ \boldsymbol{T}^3 \ . \tag{9.199}$$

For the case of a product of two tensors $\boldsymbol{T}, \boldsymbol{U}$ the matrix products to be considered are

$$\boldsymbol{T}\boldsymbol{U}, \boldsymbol{T}\boldsymbol{U}^2, \boldsymbol{U}\boldsymbol{T}^2, \mathbf{T}^2\boldsymbol{U}^2, \boldsymbol{T}\boldsymbol{U}\boldsymbol{T}^2\boldsymbol{U}^2 \tag{9.200}$$

and the invariants associated with the matrix products of $\boldsymbol{T}$ and $\boldsymbol{U}$ are

$$\text{tr}\ \boldsymbol{T}\boldsymbol{U}, \text{tr}\ \boldsymbol{T}\boldsymbol{U}^2, \text{tr}\ \boldsymbol{U}\boldsymbol{T}^2, \text{tr}\ \boldsymbol{T}^2\boldsymbol{U}^2, \text{tr}\ \boldsymbol{T}\boldsymbol{U}\boldsymbol{T}^2\boldsymbol{U}^2\ . \tag{9.201}$$

Of these five invariants the first four are irreducible. A polynomial invariant is called irreducible if it cannot be expressed as a polynomial in other invariants. The fifth invariant in (9.201) can be written in terms of the irreducible invariants. As a consequence, the resulting integrity basis for symmetric second-order tensors consist of

$$\text{tr}\ \boldsymbol{T}, \text{tr}\ \boldsymbol{T}^2, \text{tr}\ \boldsymbol{T}^3, \text{tr}\ \boldsymbol{T}\boldsymbol{U}, \text{tr}\ \boldsymbol{T}\boldsymbol{U}^2, \text{tr}\ \boldsymbol{U}\boldsymbol{T}^2, \text{tr}\ \boldsymbol{T}^2\boldsymbol{U}^2\ . \tag{9.202}$$

We want to develop a general representation for the anisotropy tensor for turbulent flows. Our minimal integrity basis for the tensors $\overline{\boldsymbol{d}}$ and $\overline{\dot{\boldsymbol{\omega}}}$ is given by

$$\begin{aligned}
&\eta_1 = \text{tr}\ \overline{\boldsymbol{d}}^2, \quad \eta_2 = \text{tr}\ \overline{\dot{\boldsymbol{\omega}}}^2, \quad \eta_3 = \overline{\boldsymbol{d}}^3, \\
&\eta_4 = \text{tr}\ \overline{\dot{\boldsymbol{\omega}}}^2\overline{\boldsymbol{d}}, \quad \eta_5 = \text{tr}\ \overline{\dot{\boldsymbol{\omega}}}^2\overline{\boldsymbol{d}}^2, \quad \eta_6 = \text{tr}\ \overline{\boldsymbol{d}}\,\overline{\dot{\boldsymbol{\omega}}}\,\overline{\boldsymbol{d}}^2\overline{\dot{\boldsymbol{\omega}}}^2\ .
\end{aligned} \tag{9.203}$$

Rivlin and Ericksen [80] showed that it is possible to write a linear relation between the dependent tensor $\boldsymbol{b}$ and a finite number N of other tensors $\boldsymbol{T}^{(1)}, \boldsymbol{T}^{(2)}, \ldots, \boldsymbol{T}^{(N)}$ formed from the elements of the independent tensors $\overline{\boldsymbol{d}}$ and $\overline{\dot{\boldsymbol{\omega}}}$

$$\alpha_0\boldsymbol{b} = \sum_{n=1}^{N} \alpha_n \boldsymbol{T}^{(n)}\ . \tag{9.204}$$

The linear system (9.204) is solved by projecting it onto the $\boldsymbol{T}^{(n)}$ basis in a way very similar to a Galerkin projection, the details of which are left for the curious and interested reader in the paper by Jongen and Gatski [40]. For a five term representation $N = 5$, the basis reduces to

$$\begin{aligned}
&\boldsymbol{T}^{(1)} = \overline{\boldsymbol{d}}, \quad \boldsymbol{T}^{(2)} = \overline{\boldsymbol{d}}\,\overline{\dot{\boldsymbol{\omega}}} - \overline{\dot{\boldsymbol{\omega}}}\,\overline{\boldsymbol{d}}, \quad \boldsymbol{T}^{(3)} = \overline{\boldsymbol{d}}^2 - \frac{1}{3}(\text{tr}\ \overline{\boldsymbol{d}}^2)\boldsymbol{I} \\
&\boldsymbol{T}^{(4)} = \overline{\dot{\boldsymbol{\omega}}}^2 - \frac{1}{3}(\text{tr}\ \overline{\dot{\boldsymbol{\omega}}}^2)\boldsymbol{I}, \quad \boldsymbol{T}^{(5)} = \overline{\dot{\boldsymbol{\omega}}}\,\overline{\boldsymbol{d}}^2 - \overline{\boldsymbol{d}}^2\overline{\dot{\boldsymbol{\omega}}}\ .
\end{aligned} \tag{9.205}$$

We leave at this stage the detailed writing of the final form of the equations. Further considerations may be found for turbulence modeling in Deville-Gatski [24] where are tackled the closure for the dissipation rate tensor, low-Reynolds turbulence modeling and the important engineering problem related to the constraints imposed by the presence of solid boundaries.

9.13 Large Eddy Simulation

RANS models even though as sophisticated as they might be have produced in some cases dismal performances and failed to resolve properly the turbulent physical phenomena. As the advent of more powerful computers made computational fluid dynamics (CFD) a more amenable way to tackle turbulence, the large eddy simulation (LES) became the appropriate tool.

LES comes from the observation that these large structures depend strongly on the flow type under scrutiny through the geometrical configuration, the boundary conditions, etc., while the small scales are more universal and therefore simpler to model. Moreover, as we will resort to numerical computation to integrate the equations (e.g. CFD), the large scales will be resolved by the simulation inasmuch the computational mesh be fine enough, while the small structures whose characteristic size is much lower than the mesh size, will be taken into account by a sub-grid model.

We will compute the motion of the large turbulent structures and their dynamics by the transient three-dimensional simulation in the flow domain. The statistical properties of the flow will be obtained by time averaging and/or by spatial means in the homogeneous (periodic) planes or by repeating several computations. This last possibility is never carried out because of its sky-rocketing cost.

This section is only an introduction to the subject and is missing a lot of details, interesting comments and presentation of the many LES models. The interested reader is referred to the monographs of P. Sagaut [84] and L. Berselli et al. [15] for a complete LES analysis.

9.13.1 Definitions

Let us consider the function $f(\boldsymbol{x}, t)$. The filtered field $\tilde{f}$ is defined by the convolution product

$$\tilde{f}(\boldsymbol{x}, t) = \int_{-\infty}^{\infty} G(\boldsymbol{x}, \boldsymbol{x}'; \Delta_{\boldsymbol{x}}) f(\boldsymbol{x}', t)\, d^3\boldsymbol{x}' \,. \tag{9.206}$$

The filtering function G allows to determine exactly which proportion (spatially speaking) of the flow will be incorporated in the large scales. The filtering parameter $\Delta_{\boldsymbol{x}}$ is used to fix this choice. In a compact form, this relation reads

$$\tilde{f} = G \star f \,, \tag{9.207}$$

where $G\star$ represents the filtering operator. The filter function is normalized such that

$$\int_{-\infty}^{\infty} G(\boldsymbol{x}, \boldsymbol{x}'; \Delta_{\boldsymbol{x}})\, d^3\boldsymbol{x}' = 1, \quad \forall \boldsymbol{x} \,. \tag{9.208}$$

The residual field f' is the complement of the filtered function

$$f(\boldsymbol{x},t) = \tilde{f}(\boldsymbol{x},t) + f'(\boldsymbol{x},t)\ . \tag{9.209}$$

The filtered field unlike what occurs in the Reynolds decomposition, **does not vanish**. Indeed, we can verify that

$$\tilde{\tilde{f}} \neq \tilde{f}, \quad \tilde{f}' \neq 0\ . \tag{9.210}$$

Filtering (9.209), one obtains the residual filtered field

$$\tilde{f}' = \tilde{f} - \tilde{\tilde{f}}\ . \tag{9.211}$$

In the particular case of homogeneous turbulence, the filter has the simpler form $G(\boldsymbol{x} - \boldsymbol{x}'; \Delta_{\boldsymbol{x}})$. Consequently, the equation

$$\tilde{f}(\boldsymbol{x},t) = \int G(\boldsymbol{x} - \boldsymbol{x}'; \Delta_{\boldsymbol{x}})\, f(\boldsymbol{x}',t)\, d^3\boldsymbol{x}' \tag{9.212}$$

is Fourier transformed into

$$\hat{\tilde{f}}(\boldsymbol{k},t) = \hat{G}(k; \Delta_{\boldsymbol{x}})\ \hat{f}(\boldsymbol{k},t)\ . \tag{9.213}$$

Here, we observe that G depends only on the norm k of the wavevector $\boldsymbol{k}$. For the Fourier case, various filters have been elaborated. The sharp cut-off filter corresponds to set all high frequency modes to zero beyond the cut-off frequency k_c in spectral space. This practice produces a clear separation between small and large scales

$$\hat{G} = \begin{cases} 1 \text{ if } \mid k_i - k_i' \mid \leq k_c, \\ 0 \text{ otherwise}\ . \end{cases} \tag{9.214}$$

However, the filtered signal obtained by inverse Fourier transform in the physical space presents a Gibbs phenomenon, which complicates the flow interpretation. A more even filter is defined with the Gaussian filter

$$G(\boldsymbol{x} - \boldsymbol{x}', \Delta_{\boldsymbol{x}}) = C \exp^{-6(x_i - x_i')^2/\Delta^2}\ , \tag{9.215}$$

where the constant C depends on the normalisation. The Fourier transform of the Gaussian filter is also Gaussian.

9.13.2 LES Equations

The velocity is decomposed as

$$\boldsymbol{v} = \tilde{\boldsymbol{v}} + \boldsymbol{v}'\ . \tag{9.216}$$

The filtered incompressibility equation yields

$$\nabla \cdot \tilde{\boldsymbol{v}} = 0\,, \tag{9.217}$$

so that by subtracting (9.217) from the continuity equation, one obtains

$$\nabla \cdot \boldsymbol{v}' = 0\,. \tag{9.218}$$

The resolved and residual velocity fields are incompressible. Filtering the Navier–Stokes equations, one gets

$$\frac{\partial \tilde{\boldsymbol{v}}}{\partial t} + \nabla \cdot (\tilde{\boldsymbol{v}}\,\tilde{\boldsymbol{v}}) \;=\; -\nabla \tilde{p} + \nu \triangle \tilde{\boldsymbol{v}} - \nabla \cdot \boldsymbol{\tau}, \tag{9.219}$$

$$\operatorname{div} \tilde{\boldsymbol{v}} = 0. \tag{9.220}$$

The sub-grid stress (SGS) tensor $\boldsymbol{\tau}$ takes into account the small scales effects on the dynamics of the resolved scales and is given by

$$\boldsymbol{\tau} = \widetilde{\boldsymbol{v}\boldsymbol{v}} - \tilde{\boldsymbol{v}}\,\tilde{\boldsymbol{v}}. \tag{9.221}$$

With the decomposition (9.216), the SGS tensor may be redefined as

$$\boldsymbol{\tau} = \boldsymbol{\mathcal{L}} + \boldsymbol{C} + \boldsymbol{\mathcal{R}}\,, \tag{9.222}$$

where

$$\begin{aligned} \boldsymbol{\mathcal{L}} &= \widetilde{\tilde{\boldsymbol{v}}\,\tilde{\boldsymbol{v}}} - \tilde{\tilde{\boldsymbol{v}}}\,\tilde{\tilde{\boldsymbol{v}}}\,, \\ \boldsymbol{C} &= (\tilde{\boldsymbol{v}}\,\widetilde{\boldsymbol{v}' + \boldsymbol{v}'\tilde{\boldsymbol{v}}}) - (\tilde{\tilde{\boldsymbol{v}}}\,\tilde{\boldsymbol{v}}' + \tilde{\boldsymbol{v}}'\,\tilde{\tilde{\boldsymbol{v}}})\,, \\ \boldsymbol{\mathcal{R}} &= \widetilde{\boldsymbol{v}'\boldsymbol{v}'} - \tilde{\boldsymbol{v}}'\,\tilde{\boldsymbol{v}}'\,, \end{aligned} \tag{9.223}$$

are the Leonard stress, $\boldsymbol{\mathcal{L}}$, and the SGS cross terms, $\boldsymbol{C}$, together with the Reynolds stress, $\boldsymbol{\mathcal{R}}$, respectively. The Leonard term can be computed by the resolved quantities. The cross tensor $\boldsymbol{C}$ represents the interactions between resolved and unresolved scales. The turbulent stress tensor $\boldsymbol{\mathcal{R}}$ represents the interaction between unresolved small scales.

9.13.3 The Smagorinsky Model

The Smagorinsky SGS model (SM) [92] utilises the concept of turbulent viscosity ν_T and is given by the relation

$$\boldsymbol{\tau} - \frac{1}{3} tr(\boldsymbol{\tau})\, \mathbf{I} = -2\nu_T \tilde{\boldsymbol{S}} = -2C_S \tilde{\Delta}^2 (\mathrm{II}_{\tilde{S}})^{1/2} \tilde{\boldsymbol{S}} = -2C_S \boldsymbol{b}, \tag{9.224}$$

where $\tilde{\boldsymbol{S}}$ is the filtered strain rate tensor

$$\tilde{\boldsymbol{S}} = \frac{1}{2}(\widetilde{\nabla \boldsymbol{v}} + \widetilde{(\nabla \boldsymbol{v})^T}), \tag{9.225}$$

and the tensor $\boldsymbol{b}$ is defined as

$$\boldsymbol{b} = \tilde{\Delta}^2 (\mathrm{II}_{\tilde{S}})^{1/2} \tilde{\boldsymbol{S}}\,. \tag{9.226}$$

The constant C_S is the Smagorinsky constant such that $C_S \approx 0.18$, $\tilde{\Delta}$ the filter size and $\mathrm{II}_{\tilde{S}}$ the second invariant of $\tilde{\boldsymbol{S}}$. The symbol tr denotes the trace of the tensor. The SM presents several flaws. The most severe one consists in the C_S constant value during the computation and this defect produces too much dissipation. Furthermore, the SM does not allow backscatter that transfers kinetic energy from small to large scales in the opposite direction of Richardson cascade. Finally, in the a priori tests where the correlation between the modeled tensor and the exact SGS tensor (9.221) is evaluated, one obtains poor quality results.

9.13.4 The Dynamic Model

The dynamic model (DM) proposed by Germano et al. [35] circumvents the difficulty of the constant C_S by letting it depend on space and time. We thus have a dynamic parameter $C_d = C_d(\boldsymbol{x}, t)$. Let us introduce the length-scale of a test-filter $\hat{\Delta}$ that is larger than the mesh length-scale $\tilde{\Delta}$ (e.g. $\hat{\Delta} = 2\tilde{\Delta}$). Using the information provided by both filters and assuming that in the inertial part of the turbulent energy spectrum, the statistical self-similarity applies, we can better determine the characteristics of the SGS tensor. The scale-similarity hypothesis assumes that the behavior of the smallest resolved scales is similar to the subgrid unresolved scales being modeled. With the test filter, the previous LES equations (9.219) lead to a relation implying the sub-tests scales stresses

$$\boldsymbol{T} = \widehat{\tilde{\boldsymbol{v}}\tilde{\boldsymbol{v}}} - \hat{\tilde{\boldsymbol{v}}}\,\hat{\tilde{\boldsymbol{v}}}\,. \tag{9.227}$$

One introduces Germano's identity to obtain the relation between $\boldsymbol{T}$ and the SGS filtered tensor $\hat{\boldsymbol{\tau}}$ such that

$$\mathcal{G} = \boldsymbol{T} - \hat{\boldsymbol{\tau}} = \widehat{\tilde{\mathbf{v}}\,\tilde{v}} - \hat{\tilde{\mathbf{v}}}\,\hat{\tilde{v}}. \tag{9.228}$$

Applying the turbulent viscosity model to $\boldsymbol{T}$ and using the self-similarity hypothesis for the C_d constant, one obtains

$$\boldsymbol{T} - \frac{1}{3} tr(\boldsymbol{T})\,\mathbf{I} = -2C_d \hat{\Delta}^2 (\mathrm{II}_{\hat{\mathbf{S}}})^{1/2} \hat{\mathbf{S}} := -2C_d \boldsymbol{a}. \tag{9.229}$$

Inserting (9.224) and (9.229) in the deviatoric part of $\mathcal{G}$, one has

$$\mathcal{G} - \frac{1}{3} tr(\mathcal{G})\mathbf{I} = 2(\widehat{C_d \boldsymbol{b}} - C_d \boldsymbol{a}). \tag{9.230}$$

Supposing that C_d does not vary too much in space, we set $\hat{C}_d \approx C_d$ and then we deduce from a least square minimisation of the error linked to (9.230) (cf. [51] for details) that

$$C_d = -\frac{1}{2} \frac{\mathcal{M} : \mathcal{G}}{\mathcal{M} : \mathcal{M}}, \tag{9.231}$$

where

$$\mathcal{M} = \boldsymbol{a} - \hat{\boldsymbol{b}} \tag{9.232}$$

and the notation : designates the inner tensorial product (double contraction).

In the case where the flow has no homogeneous direction, the previous hypothesis about the slow spatial variation of C_d and its elimination of the filtering operation are no longer valid. To avoid this difficulty, we follow the procedure proposed by Piomelli and Liu [72]. Taking the scalar product of Eq. (9.230) with $\boldsymbol{a}$, one obtains the relation

$$C_d = -\frac{1}{2} \frac{(\mathcal{L} - \frac{1}{3} tr(\mathcal{L})\mathbf{I} - 2\widehat{C^* \boldsymbol{b}}) : \boldsymbol{a}}{\boldsymbol{a} : \boldsymbol{a}}, \tag{9.233}$$

where the known quantity $C^* = C_d^{n-1}$, i.e. the C_d value at the former time level in the CFD time integration scheme.

9.13.5 The Dynamic Mixed Model

The dynamic mixed model [126] introduced to simulate cavity flows is a blending of the mixed model of Bardina et al. [8] and of the previous dynamic model. Note that the mixed model is not a model based on the turbulent viscosity. On the contrary it belongs to the class of structural models [84] and rests upon the similarity principle of scales. It hardly produces dissipation and for that reason we must use it with the dynamic model. We decompose the velocity field in a resolved field and a sub-grid field as done in Eq. (9.216) and we redefine the stress as Germano [34] proposed in Eqs. (9.221)–(9.223). The Leonard term computed by the resolved quantities corresponds essentially to the mixed models. The other two terms are the non resolved residual stresses and they are treated via the Smagorinsky model. The dynamic procedure is applied to the C constant in order to obtain a dynamic coefficient. Let us introduce

a test filter denoted now by a hat $\hat{}$. By application of the test filter to (9.219), one generates the sub-tests scales stress

$$\boldsymbol{T} = \widehat{\tilde{\boldsymbol{v}}\tilde{\boldsymbol{v}}} - \hat{\tilde{\boldsymbol{v}}}\,\hat{\tilde{\boldsymbol{v}}} = \boldsymbol{L}^t + \boldsymbol{C}^t + \boldsymbol{R}^t, \tag{9.234}$$

with

$$\begin{aligned}
\boldsymbol{L}^t &= \widehat{\tilde{\tilde{\boldsymbol{v}}}\,\tilde{\boldsymbol{v}}} - \hat{\tilde{\tilde{\boldsymbol{v}}}}\,\hat{\tilde{\tilde{\boldsymbol{v}}}} \\
\boldsymbol{C}^t &= \widehat{(\tilde{\boldsymbol{v}}\,\boldsymbol{v}' + \boldsymbol{v}'\tilde{\boldsymbol{v}})} - (\hat{\tilde{\tilde{\boldsymbol{v}}}}\,\hat{\boldsymbol{v}'} + \hat{\boldsymbol{v}'}\,\hat{\tilde{\tilde{\boldsymbol{v}}}}), \\
\boldsymbol{R}^t &= \widehat{\boldsymbol{v}'\boldsymbol{v}'} - \hat{\boldsymbol{v}'}\,\hat{\boldsymbol{v}'}\,.
\end{aligned} \tag{9.235}$$

The deviatoric turbulent stress tensors associated with the sub-grid and sub-tests filters are expressed as follows

$$\begin{aligned}
\boldsymbol{\tau} - \frac{1}{3}tr(\boldsymbol{\tau})\,\mathbf{I} &= -2C_d\tilde{\Delta}^2(\mathrm{II}_{\tilde{\mathbf{S}}})^{1/2}\tilde{\boldsymbol{S}} + \boldsymbol{\mathcal{L}} - \frac{1}{3}tr(\boldsymbol{\mathcal{L}})\,\mathbf{I} \\
&= -2C_d\boldsymbol{b} + \boldsymbol{\mathcal{L}} - \frac{1}{3}tr(\boldsymbol{\mathcal{L}})\,\mathbf{I},
\end{aligned} \tag{9.236}$$

$$\begin{aligned}
\boldsymbol{T} - \frac{1}{3}tr(\boldsymbol{T})\,\mathbf{I} &= -2C_d\hat{\tilde{\Delta}}^2(\mathrm{II}_{\hat{\tilde{\mathbf{S}}}})^{1/2}\hat{\tilde{\mathbf{S}}} + \boldsymbol{L}^t - \frac{1}{3}tr(\boldsymbol{L}^t)\,\mathbf{I} \\
&= -2C_d\boldsymbol{a} + \boldsymbol{L}^t - \frac{1}{3}tr(\boldsymbol{L}^t)\,\mathbf{I}.
\end{aligned} \tag{9.237}$$

Substituting Eqs. (9.236) and (9.237) in Germano's identity (9.228) and introducing tensor $\mathcal{H}$

$$\mathcal{H} = \widehat{\tilde{\tilde{\boldsymbol{v}}}\,\tilde{\boldsymbol{v}}} - \hat{\tilde{\tilde{\boldsymbol{v}}}}\,\hat{\tilde{\boldsymbol{v}}} \tag{9.238}$$

one evaluates the C constant following the same steps as for the dynamic model

$$C = -\frac{1}{2}\frac{((\mathcal{G} - \mathcal{H}) - 2\widehat{C^*\boldsymbol{b}}) : \boldsymbol{a}}{\boldsymbol{a} : \boldsymbol{a}}. \tag{9.239}$$

9.13.6 The Approximate Deconvolution Method

The approximate deconvolution method (ADM) [98, 99] extracts the information of the resolved scales in order to deduce from them the behavior of the sub-grid scales. The founding hypothesis leading to ADM consists in the existence of G^{-1} that can be computed by a finite series in $\tilde{\boldsymbol{v}}$. As $G = I - (I - G)$, the inverse of G may be written as a non convergent series

$$G^{-1} = \sum_{n=0}^{\infty} (I - G)^n \, . \tag{9.240}$$

Van Cittert [113] proposed to approximate G^{-1} by a finite series such as

$$G_a^{-1} := Q_M = \sum_{n=0}^{M} (I_d - G)^n \, , \tag{9.241}$$

where I_d is the identity operator.

The ADM approach constructs an approximation of the velocity field $\boldsymbol{v}^*$ that must be used in the non-linear term

$$\boldsymbol{v}^* = Q_M \star (G \star \boldsymbol{v}). \tag{9.242}$$

The deconvolutions to order three and five yield

$$\boldsymbol{v}^* = Q_3 \star \tilde{\boldsymbol{v}} = 4(\tilde{\boldsymbol{v}}^{(1)} + \tilde{\boldsymbol{v}}^{(3)}) - 6\tilde{\boldsymbol{v}}^{(2)} - \tilde{\boldsymbol{v}}^{(4)}, \tag{9.243}$$

$$\boldsymbol{v}^* = Q_5 \star \tilde{\boldsymbol{v}} = 6(\tilde{\boldsymbol{v}}^{(1)} + \tilde{\boldsymbol{v}}^{(5)}) - 15(\tilde{\boldsymbol{v}}^{(2)} + \tilde{\boldsymbol{v}}^{(4)}) + 20\tilde{\boldsymbol{v}}^{(3)} - \tilde{\boldsymbol{v}}^{(6)}, \tag{9.244}$$

with the notation $\tilde{\boldsymbol{v}}^{(k)}$ indicating that the velocity field is filtered k times.

We then solve the set of equations

$$\frac{\partial \tilde{\boldsymbol{v}}}{\partial t} + \widetilde{(\nabla \cdot \boldsymbol{v}^* \boldsymbol{v}^*)} = -\nabla \tilde{p} + \nu \Delta \tilde{\boldsymbol{v}}, \tag{9.245}$$

$$\operatorname{div} \tilde{\boldsymbol{v}} = 0. \tag{9.246}$$

9.14 Concluding Remarks

At the end of this chapter the reader may feel overwhelmed, lonely and trapped in a chaotic ocean of equations, models and choices that are not obvious. Fortunately enough, some researchers felt the same and wrote review articles like the paper by Argyropoulos and Markatos [4] to delineate the pros and cons of each approach versus the target to be reached within a given time frame.

It is of course a complete different situation to solve an engineering problem using a RANS model because it should be done within minutes rather than getting a nice simulation by an LES approach that requires weeks or months of computing time on a large parallel machine. Therefore the choice of the turbulence model depends on many parameters: the time allotted to solving the problem, the computer available, the accuracy demanded (a few percents like in most engineering design or more

precision). Is computing a trend instead a full solution sufficient if one changes only one data, do we need a physically meaning solution?, etc.

Whatever complicated the situation is, there remains still hope for improvement and better comprehension of turbulence. I will finish by quoting Sébastien Galtier [31] in his introduction (my own translation) "A detailed analytical understanding of turbulence remains limited because of the difficulty intrinsic to non-linear physics. Therefore one often reads that turbulence is one of the last major non solved problems of the classical physics. This long conveyed affirmation that can be found in the book of Feynman [29] does no longer correspond to the modern view. Indeed, even though turbulence remains a very active research subject, we have today availability to many theoretical, experimental and observational results which allow us to know in detail the physics of turbulence".

Exercises

9.1 Prove relation (9.53)

9.2 Show that the two-point velocity correlation tensor (9.60) is symmetric.

9.3 Demonstrate Eqs. (9.243) and (9.244).

Chapter 10
Solutions of Exercises

10.1 Chapter One

1.1 Let us inspect the contribution of the contact force $\boldsymbol{t}$. With the help of (1.67) one has

$$\int_S \boldsymbol{t}\, dS = -\int_S p\boldsymbol{n}\, dS + \boldsymbol{F}\ , \tag{10.1}$$

where $\boldsymbol{F}$ is the shearing force exerted by the plate on the fluid. Indeed the shear contributions vanish on the vertical lines AB, CD and on BC of Fig. 10.1. On the closed surface S, the pressure is uniform and then, $-\int_S p\boldsymbol{n}\, dS = 0$. The integral equation (1.125) becomes

$$\boldsymbol{F} = \rho \int_S (\boldsymbol{v}\cdot\boldsymbol{n})\boldsymbol{v}\, dS\ . \tag{10.2}$$

We need to compute $F = \boldsymbol{F}\cdot\boldsymbol{e}_1$. Therefore from (10.2) one obtains

$$F = \rho \int_S (\boldsymbol{v}\cdot\boldsymbol{n}) v_1\, dS\ . \tag{10.3}$$

With the control volume of thickness Z in x_3 direction exhibited in Fig. 10.1, it is easy to proceed further

$$\rho \int_S (\boldsymbol{v}\cdot\boldsymbol{n})\, v_1\, dS = \rho \sum_{i=1}^{i=6} \int_{S_i} (\boldsymbol{v}\cdot\boldsymbol{n})_i\, v_1\, dS_i\ . \tag{10.4}$$

In section S_2 the velocity profile is

$$\begin{aligned} v_1(x_2) &= Ux_2/h, \text{for } 0 \le x_2 \le h, \\ v_1 &= U, \text{for } h \le x_2 \le H\ . \end{aligned} \tag{10.5}$$

M. O. Deville, *An Introduction to the Mechanics of Incompressible Fluids*,
https://doi.org/10.1007/978-3-031-04683-4_10

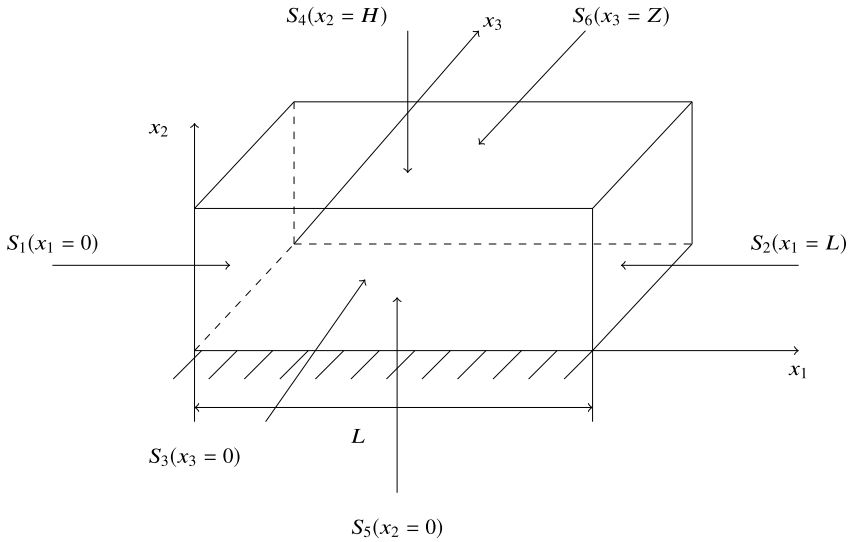

Fig. 10.1 Control volume for the flat plate problem

We have successively

$$\rho \int_{S_1} (\boldsymbol{v} \cdot \boldsymbol{n})_1 v_1 \, dS_1 = -\rho U^2 H Z \quad \boldsymbol{n} = (-1, 0, 0) \quad \boldsymbol{v} = (U, 0, 0)$$

$$\rho \int_{S_2} (\boldsymbol{v} \cdot \boldsymbol{n})_2 v_1 \, dS_2 = \rho U^2 \left((H - h) Z + \frac{hZ}{3} \right) \quad \boldsymbol{n} = (1, 0, 0) \quad \boldsymbol{v} = (v_1(x_2), 0, 0)$$

$$\rho \int_{S_3} (\boldsymbol{v} \cdot \boldsymbol{n})_3 v_1 \, dS_3 = 0 \quad \text{as } (\boldsymbol{v} \cdot \boldsymbol{n})_3 = 0$$

$$\rho \int_{S_4} (\boldsymbol{v} \cdot \boldsymbol{n})_4 v_1 \, dS_4 = \rho \int_0^L U v_2 Z \, dx_1 \quad \boldsymbol{n} = (0, 1, 0) \quad \boldsymbol{v} = (0, v_2, 0) \, .$$

It is forbidden to impose v_2 to be zero on S_4. The fluid flows in the vertical direction through S_4 as the flow rate in the exit S_2 is less than in the entry section S_1. The two last integrals yield $\rho \int_{S_5} (\boldsymbol{v} \cdot \boldsymbol{n})_5 v_1 \, dS_5 = \rho \int_{S_6} (\boldsymbol{v} \cdot \boldsymbol{n})_6 v_1 \, dS_6 = 0$ as the velocity has no component in x_3 direction.

One deduces that

$$F = \rho \int_0^L U v_2 Z \, dx_1 - \frac{2}{3} \rho U^2 h Z \, . \tag{10.6}$$

To evaluate the integral in (10.6) the control volume method is applied to the mass conservation law (1.120)

$$\rho \int_S \boldsymbol{v} \cdot \boldsymbol{n}\, dS = \rho \sum_{i=1}^{i=6} (\boldsymbol{v} \cdot \boldsymbol{n})_i dS_i \ . \tag{10.7}$$

We obtain

$$\begin{aligned}
&\rho \int_{S_5} (\boldsymbol{v} \cdot \boldsymbol{n})_5\, dS_5 = \rho \int_{S_6} (\boldsymbol{v} \cdot \boldsymbol{n})_6\, dS_6 = \rho \int_{S_3} (\boldsymbol{v} \cdot \boldsymbol{n})_3\, dS_3 = 0 \\
&\rho \int_{S_1} (\boldsymbol{v} \cdot \boldsymbol{n})_1\, dS_1 = -\rho U H Z \\
&\rho \int_{S_2} (\boldsymbol{v} \cdot \boldsymbol{n})_2\, dS_2 = \rho U \left((H-h)Z + \frac{hZ}{2} \right) \\
&\rho \int_{S_4} (\boldsymbol{v} \cdot \boldsymbol{n})_4\, dS_4 = \rho \int_0^L v_2 Z dx_1 \ .
\end{aligned}$$

Therefore one has

$$\rho \int_0^L v_2 Z dx_1 = \rho U \frac{hZ}{2} \tag{10.8}$$

Combining (10.6) and (10.8), the force F acting by the plate on the fluid is

$$F = -\frac{1}{6} \rho U^2 h Z \ . \tag{10.9}$$

1.2 Incompressibility requires $\nabla \cdot \boldsymbol{v} = 0$. Applying $\partial / \partial x_i$ to the velocity field, one has

$$\begin{aligned}
\frac{\partial v_i}{\partial x_i} &= \frac{Ar^3 \delta_{ii} - 3Ar^2 x_i \frac{\partial r}{\partial x_i}}{r^6} \\
&= \frac{Ar^3 \delta_{ii} - 3Ar^2 x_i \frac{x_i}{r}}{r^6} \\
&= 0
\end{aligned}$$

since $x_i x_i = r^2$.

It is also possible to solve the problem by computing

$$\begin{aligned}
\text{div}\, \boldsymbol{v} = \frac{\partial v_i}{\partial x_i} &= A \frac{\partial}{\partial x_i} \left(x_i (x_j x_j)^{-3/2} \right) \\
&= A \left(\delta_{ii} (x_j x_j)^{-3/2} - \frac{3}{2} x_i \cdot 2 (x_j x_j)^{-5/2} x_j \delta_{ji} \right) \\
&= A \left(\delta_{ii} (x_j x_j)^{-3/2} - \frac{3}{2} x_j \cdot 2 (x_j x_j)^{-5/2} x_j \right) = 0 \ ,
\end{aligned}$$

as $\delta_{ii} = 3$.

1.3 The incompressibility equation in cylindrical coordinates (A.2) is written as

$$\frac{1}{r}\frac{\partial(r v_r)}{\partial r} + \frac{1}{r}\frac{\partial v_\theta}{\partial \theta} + \frac{\partial v_z}{\partial z} = 0 .$$

It is easily deduced that the given velocity field is incompressible.

1.4 **Natural Convection between two parallel planes**

The $2D$ velocity field is such that $\boldsymbol{v} = (v_1(x_1, x_2), v_2(x_1, x_2), 0)$. However the flow is invariant with respect to translation in the x_2 direction. Therefore it depends only on the x_1 coordinate. With the incompressibility condition (1.115),

$$\frac{\partial v_1}{\partial x_1} = 0 . \tag{10.10}$$

As $v_1 = 0$ at the walls, $v_1 = 0$ and $\boldsymbol{v} = (0, v_2, 0)$. The temperature gradient is oriented in the horizontal direction, so that the temperature field is such that $T = T(x_1)$. The temperature Eq. (1.117) becomes

$$\frac{d^2 T}{dx_1^2} = 0 . \tag{10.11}$$

Integrating with the boundary conditions $T = T_2$ at $x_1 = -h$ and $T = T_1$ at $x_1 = h$ yields

$$T = -\frac{T_2 - T_1}{2h} x_1 + \frac{T_1 + T_2}{2} := A x_1 + \frac{T_1 + T_2}{2} . \tag{10.12}$$

The momentum equation (1.116) gives

$$-\frac{\partial p}{\partial x_2} + \mu \frac{d^2 v_2}{dx_1^2} - \rho_0 \, g \, (1 - a(T - T_0)) = 0 . \tag{10.13}$$

The reference temperature is chosen as the mean temperature $T_0 = (T_1 + T_2)/2$. The flow is not driven by an exterior pressure gradient; then the pressure is purely hydrostatic and results from the integration of

$$-\frac{\partial p}{\partial x_2} - \rho_0 \, g = 0 , \tag{10.14}$$

valid at equilibrium. Consequently the velocity field is driven by the buoyancy forces and one solves

$$\mu \frac{d^2 v_2}{dx_1^2} + \rho_0 \, g \alpha A x_1 = 0 . \tag{10.15}$$

With the boundary conditions $v_2 = 0$ at $x_1 \pm h$,

$$v_2 = -\frac{g\alpha A}{6\nu} x_1 (x_1^2 - h^2) = \frac{g\alpha}{12\nu h} (T_1 - T_2) x_1 (x_1^2 - h^2) \,. \tag{10.16}$$

It is a simple check to verify that this velocity profile corresponds to a vanishing flow rate across each horizontal cross section.

1.5

- The continuity equation applied to the control volume in dashed lines (Fig. 1.14) yields

$$\int_0^{R_0} v_z(r)\, 2\pi r dr = V \pi R_1^2 \,. \tag{10.17}$$

Using (1.126) in (10.17) one has

$$2 v_{max} \int_0^{R_0} \left(1 - \frac{r^2}{R_0^2}\right) r\, dr = V R_1^2 \,. \tag{10.18}$$

Carrying through the integration we obtain

$$\frac{V}{v_{max}} = \frac{1}{2} \frac{R_0^2}{R_1^2} \,. \tag{10.19}$$

- The momentum equation in integral form is applied to the control volume

$$\int_S \rho(\boldsymbol{v} \cdot \boldsymbol{n}) \boldsymbol{v} dS = 0 \,. \tag{10.20}$$

Indeed the contact force $\boldsymbol{t} = \boldsymbol{0}$ as there is no diffusion and the pressure is constant and equal to the atmospheric pressure. Consequently one writes successively

$$\begin{aligned}
\int_0^{R_0} (v_z(r) dS) v_z(r) &= \pi V^2 R_1^2 \,, \\
v_{max}^2 \int_0^{R_0} \left(1 - \frac{r^2}{R_0^2}\right)^2 2\pi r dr &= \pi V^2 R_1^2 \,, \\
2 v_{max}^2 \frac{R_0^6}{6} &= V^2 R_1^2 \,, \\
\left(\frac{V}{v_{max}}\right)^2 &= \frac{1}{3} \frac{R_0^2}{R_1^2} \,.
\end{aligned} \tag{10.21}$$

With (10.19) and (10.21) the contraction coefficient is

$$\beta = \frac{R_1^2}{R_0^2} = \frac{3}{4} \,. \tag{10.22}$$

10.2 Chapter Two

2.1 In thermal convection problems there is no reference velocity to be chosen like in aerodynamics where the upstream uniform velocity is a given data of the flow. As it is proposed in the problem statement there are three possible choices for the reference velocity. Note that the dimensional matrix of Table 2.1 is almost identical to the one corresponding to the Boussinesq variables. It is sufficient to add the column corresponding to α with $[\alpha|0\,0\,0\,-1]$.

If ρ, μ, L, T are chosen as primary variables, then the minor is not zero. The first and third dimensionless groups become $\Pi_1 = \nu t/L^2$, $\Pi_3 = \boldsymbol{v}L/\nu$. This shows that the reference velocity is indeed ν/L based on the viscous diffusivity. The alternate choice ρ, k, L, c_p with non zero minor generates $\Pi_1 = \Lambda t/L^2$, $\Pi_3 = \boldsymbol{v}L/\Lambda$.

We resort to the Boussinesq equations given by (1.118) and (1.119).

- Let us now consider the dimensionless Boussinesq equations with the viscous diffusivity as reference velocity. The dimensionless variables are

$$x_i = Lx_i' \ , \ t = \frac{L^2}{\nu}t' \ , \ v_i = \frac{\nu}{L}v_i' \ , \ P' = \frac{\tilde{p}L^2}{\rho\nu^2} \ , T - T_0 = (T_1 - T_0)T' \ .$$

  Dropping the primes for ease of notation we obtain

$$\operatorname{div} \boldsymbol{v} = 0, \tag{10.23}$$

$$\frac{D\boldsymbol{v}}{Dt} = -\boldsymbol{\nabla} P \ + \ \triangle \boldsymbol{v} + Gr\, T\boldsymbol{g}, \tag{10.24}$$

$$\frac{DT}{Dt} = \frac{1}{Pr} \triangle T. \tag{10.25}$$

- Referring to the thermal diffusivity for the reference velocity, the dimensionless variables become

$$x_i = Lx_i' \ , \ t = \frac{L^2}{\kappa}t' \ , \ v_i = \frac{\kappa}{L}v_i' \ , \ P' = \frac{\tilde{p}L^2}{\rho\kappa^2} \ , T - T_0 = (T_1 - T_0)T' \ . \tag{10.26}$$

  The dimensionless Boussinesq equations are now

$$\operatorname{div} \boldsymbol{v} = 0, \tag{10.27}$$

$$\frac{D\boldsymbol{v}}{Dt} = -\boldsymbol{\nabla} P \ + \ Pr \triangle \boldsymbol{v} + RaPr\, T\boldsymbol{g}, \tag{10.28}$$

$$\frac{DT}{Dt} = \triangle T. \tag{10.29}$$

- With the reference velocity $U = (g\alpha(T - T_0)L)^{1/2}$ the dimensionless Boussinesq equations are

$$\operatorname{div} \boldsymbol{v} = 0, \tag{10.30}$$

$$\frac{D\boldsymbol{v}}{Dt} = -\boldsymbol{\nabla} P + \frac{Pr}{Pe} \triangle \boldsymbol{v} - Gr\, T \boldsymbol{g}, \tag{10.31}$$

$$\frac{DT}{Dt} = \frac{1}{Pe} \triangle T. \tag{10.32}$$

2.2 Let us define the dimensionless coordinate variable and velocity as follows

$$\eta = \frac{x_1}{h}\,, \quad v_2^* = \frac{v_2 h}{\nu}\,. \tag{10.33}$$

In dimensionless form, the velocity profile (10.16) reads

$$v_2^* = \frac{1}{12} Gr\, \eta \left(\eta^2 - 1\right)\,, \tag{10.34}$$

where Gr is the Grashof number

$$Gr = \frac{g\alpha(T_2 - T_1)h^3}{\nu^2}\,. \tag{10.35}$$

10.3 Chapter Three

3.1 The solutions obtained in (3.7) and (3.19) for the plane Couette and Poiseuille flows, respectively, result from linear differential equations. As the non-linear terms of the Navier–Stokes equations do not intervene in this problem, one invokes the principle of linear superposition and the solution of the combined plane Couette–Poiseuille flow is written as

$$v_1 = -\frac{h^2}{2\mu}\frac{dP}{dx_1}\frac{x_2}{h}(1 - \frac{x_2}{h}) + \frac{U x_2}{h}\,.$$

The shear stress is

$$\sigma_{12} = \mu\frac{dv_1}{dx_2} = -\frac{h}{2}\frac{dP}{dx_1}(1 - \frac{2x_2}{h}) + \frac{\mu U}{h}\,.$$

Finally, the flow rate is

$$Q = \int_0^h v_1\, dx_2 = -\frac{h^3}{12\mu}\frac{dP}{dx_1} + \frac{Uh}{2}\,.$$

3.2 We will refer to the spherical coordinates (r, θ, φ) as in Fig. B.1. The rotation axis of the sphere with the angular velocity $\boldsymbol{\sigma} = \Omega \boldsymbol{e}_{x_3}$ is axis x_3. As a consequence

of the problem's symmetries, the velocity field has only one single component such that

$$\boldsymbol{v} = v_\varphi(r,\theta)\boldsymbol{e}_\varphi \,. \tag{10.36}$$

We solve the Stokes equations with the boundary conditions

$$\boldsymbol{v} = 0 \quad \text{in} \quad r = \infty \tag{10.37}$$

$$v_\varphi = \Omega R \sin\theta \quad \text{in} \quad r = R \,. \tag{10.38}$$

The form of the boundary conditions (10.38) suggests to search the solution under the form

$$v_\varphi = \Omega R f(r) \sin\theta \,, \quad p = p_\infty \,. \tag{10.39}$$

One verifies that the mass conservation equation (B.20) is trivially verified by (10.39). The pressure gradient does not intervene in (B.23) because of axial symmetry ($\partial/\partial\varphi = 0$). One has

$$\Delta v_\varphi - \frac{v_\varphi}{r^2\sin^2\theta} = \Omega R \sin\theta \left(f'' + \frac{2f'}{r} - \frac{2f}{r^2} \right) = 0 \,. \tag{10.40}$$

The f solution written as $f(r) = \sum_{n=-\infty}^{+\infty} C_n r^n$ gives

$$f(r) = C_1 r + \frac{C_2}{r^2} \,. \tag{10.41}$$

The boundary conditions (10.37) and (10.38) impose $C_1 = 0$ and $C_2 = R^2$, respectively. The velocity field around the rotating sphere is

$$v_\varphi = \Omega \frac{R^3}{r^2} \sin\theta \, \boldsymbol{e}_\varphi \,.$$

3.3 **Spherical Couette flow**

The boundary conditions are

$$v_\varphi = \Omega_1 R_1 \sin\theta \quad \text{in} \quad r = R_1 \tag{10.42}$$

$$v_\varphi = \Omega_2 R_2 \sin\theta \quad \text{in} \quad r = R_2 \,. \tag{10.43}$$

The considerations of the previous exercise remain valid for the velocity profile search under the form (10.39)

$$v_\varphi = f(r) \sin\theta \,, \quad p = p_\infty \,. \tag{10.44}$$

We will note that we do not use anymore the factor ΩR, as now we have two radii and two angular velocities to take care of. The equation to solve is thus

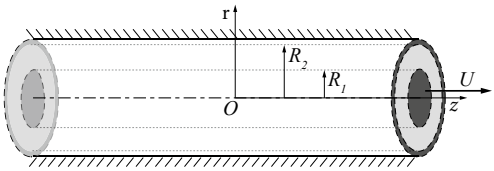

Fig. 10.2 Flow between two concentric cylinders, one fixed and the other moving with velocity U in the z direction

$$\Delta v_\varphi - \frac{v_\varphi}{r^2 \sin^2\theta} = \sin\theta \left(f'' + \frac{2f'}{r} - \frac{2f}{r^2} \right) = 0 \,, \tag{10.45}$$

whose solution is

$$f(r) = C_1 r + \frac{C_2}{r^2} \,. \tag{10.46}$$

The imposition of the boundary conditions (10.42) and (10.43) yields

$$C_1 = \frac{\Omega_2 R_2^3 - \Omega_1 R_1^3}{R_2^3 - R_1^3}, \quad C_2 = \frac{\Omega_1 - \Omega_2}{R_2^3 - R_1^3} R_1^3 R_2^3 \,. \tag{10.47}$$

3.4 We work in cylindrical coordinates with the z axis in the direction of the axes of both cylinders (cf. Fig. 10.2). The only non zero velocity component is clearly v_z. Moreover $v_z = v_z(r)$.

The flow is kinematically forced by the displacement of the inner cylinder. No pressure gradient is involved in the fluid motion.

Equation (A.23) gives

$$\frac{1}{r}\frac{d}{dr}\left(r \frac{dv_z}{dr} \right) = 0 \,. \tag{10.48}$$

Integrating (10.48), one finds

$$v_z = C_1 \ln r + C_2 \,. \tag{10.49}$$

The boundary conditions are

$$v_z(r = R_1) = U \tag{10.50}$$

$$v_z(r = R_2) = 0 \,. \tag{10.51}$$

Imposing (10.50) and (10.51) to (10.49), one obtains the velocity field

$$v_z = \frac{U}{\ln \frac{R_1}{R_2}} \ln \frac{r}{R_2} \,. \tag{10.52}$$

With the help of (A.4), the only non zero component of the stress tensor is σ_{rz} equal to

$$\sigma_{rz} = \mu\left(\frac{\partial v_z}{\partial r} + \frac{\partial v_r}{\partial z}\right) = \mu\frac{U}{\ln\frac{R_1}{R_2}}\frac{1}{r} \,. \tag{10.53}$$

The friction force per unit length acting on the moving cylinder is given by the integral

$$\int_0^1 \sigma_{rz}|_{r=R1} 2\pi R_1 dz = 2\pi\mu\frac{U}{\ln\frac{R_1}{R_2}} \,. \tag{10.54}$$

3.5 Couette flow with a free surface

- It is simple to obtain $B = 0$ and $A = \omega_2$ in the Couette solution (3.41).
- The Navier–Stokes equations involving the pressure contributions are

$$\frac{\partial p}{\partial r} = \rho\frac{v_\theta^2}{r} \,, \tag{10.55}$$

$$\frac{\partial p}{\partial z} = -\rho g \,. \tag{10.56}$$

Therefore we conclude that $p = p(r, z)$ and $dp = \frac{\partial p}{\partial r}dr + \frac{\partial p}{\partial z}dz$. As at the free surface $p = p_a = cst$, one has $dp = 0$. Then we obtain

$$\begin{aligned}\frac{dz}{dr} &= -\frac{\frac{\partial p}{\partial r}}{\frac{\partial p}{\partial z}} = -\frac{\rho\frac{v_\theta^2}{r}}{-\rho g} \\ &= \frac{1}{g}\omega_2^2 r \,.\end{aligned} \tag{10.57}$$

Integrating (10.57) one gets

$$z = \frac{1}{2g}\omega_2^2 r^2 + C \,, \tag{10.58}$$

with C a constant. Imposing $z(R_1) = z_1$ we find

$$z = \frac{1}{2g}\omega_2^2(r^2 - R_1^2) + z_1 \,. \tag{10.59}$$

The free surface has a parabolic shape.

3.6 Plane Couette flow with two layers

The flow is two-dimensional and $v_3 = 0$. Furthermore we have $\partial/\partial x_1 = \partial/\partial x_3 = 0$. The two components v_1 and v_2 are only dependent on x_2. The incompressibility constraint imposes that $v_2 = 0$ and $v_1 = v_1(x_2)$. The hypothesis on the pressure gradient implies $\partial p/\partial x_1 = 0$. The Navier–Stokes equations yield

$$\begin{aligned} \mu \frac{\partial^2 v_1}{\partial x_2^2} &= 0 \\ -\frac{\partial p}{\partial x_2} - \rho g &= 0 \\ -\frac{\partial p}{\partial x_3} &= 0 \,. \end{aligned} \tag{10.60}$$

In the two layers labeled 1 and 2 by upper indices we have

$$\begin{aligned} \frac{\partial^2 v_1}{\partial x_2^2} &= 0 \\ \frac{dp}{dx_2} + \rho g &= 0 \,. \end{aligned} \tag{10.61}$$

Integrating we obtain

$$\begin{aligned} v_1^1 &= A_1 x_2 + B_1, \quad p^1 = -\rho_1 g x_2 + C^1 \\ v_1^2 &= A_2 x_2 + B_2, \quad p^2 = -\rho_2 g x_2 + C^2 \,. \end{aligned} \tag{10.62}$$

The boundary conditions are $v_1^1(h_1) = U$ and $v_1^2(-h_2) = 0$. We have

$$A_1 h_1 + B_1 = U \tag{10.63}$$

$$-A_2 h_2 + B_2 = 0 \,. \tag{10.64}$$

As the two fluids do not slip at the interface, one gets

$$B_1 = B_2 \,. \tag{10.65}$$

The interface is in equilibrium and the contact forces satisfy Eq. (1.76). With $\boldsymbol{n}_{\mathrm{I}} = \boldsymbol{e}_2$, the unit vector in direction x_2, we have

$$\boldsymbol{\sigma}^1 \boldsymbol{e}_2 = \boldsymbol{\sigma}^2 \boldsymbol{e}_2 \,. \tag{10.66}$$

In terms of stress components, relation (10.66) yields

$$\sigma_{12}^1 = \sigma_{12}^2, \quad \sigma_{22}^1 = \sigma_{22}^2, \quad \sigma_{32}^1 = \sigma_{32}^2 \,. \tag{10.67}$$

With the definition of the constitutive equation (1.67), the stress components in (10.67) are

$$\sigma_{12}^1 = 2\mu_1 d_{12}^1 = \mu_1 \frac{dv_1^1}{dx_2} = \mu_1 A_1 \tag{10.68}$$

$$\sigma_{12}^2 = 2\mu_2 d_{12}^2 = \mu_2 \frac{dv_1^2}{dx_2} = \mu_2 A_2 \tag{10.69}$$

$$\sigma_{22}^1 = -p^1 + 2\mu_1 d_{22}^1 = -p^1 \tag{10.70}$$

$$\sigma_{22}^2 = -p^2 \tag{10.71}$$

$$\sigma_{32}^1 = \sigma_{32}^2 = 0\,. \tag{10.72}$$

The first condition on the stress components (10.67) imposes

$$\mu_1 A_1 = \mu_2 A_2\,. \tag{10.73}$$

The second condition produces $-p^1 = -p^2$ at $x_2 = 0$ and then $C_1 = C_2 = p_0$ the pressure at the interface. Using (10.63)–(10.65) and (10.73) we obtain

$$A_1 = \frac{\mu_2 U}{\mu_2 h_1 + \mu_1 h_2} \tag{10.74}$$

$$A_2 = \frac{\mu_1 A_1}{\mu_2} = \frac{\mu_1 U}{\mu_2 h_1 + \mu_1 h_2} \tag{10.75}$$

$$B_2 = B_1 = \frac{\mu_1 h_2 U}{\mu_2 h_1 + \mu_1 h_2}\,. \tag{10.76}$$

The velocity components and pressures are

$$v_1^1 = \frac{(\mu_2 x_2 + \mu_1 h_2)U}{\mu_2 h_1 + \mu_1 h_2}, \quad p^1 = -\rho_1 g x_2 + p_0 \tag{10.77}$$

$$v_1^2 = \frac{(\mu_1 x_2 + \mu_1 h_2)U}{\mu_2 h_1 + \mu_1 h_2}, \quad p^2 = -\rho_2 g x_2 + p_0\,. \tag{10.78}$$

Note that if $h_2 = 0$, we recover the velocity profile of the standard plane Couette flow.

The vorticity is orthogonal to the plane of flow and $\omega_3 = -dv_1/dx_2$. We have

$$\omega_3^1 = -\frac{\mu_2 U}{\mu_2 h_1 + \mu_1 h_2} = cst \tag{10.79}$$

$$\omega_3^2 = -\frac{\mu_1 U}{\mu_2 h_1 + \mu_1 h_2}\,. \tag{10.80}$$

3.7 **Bubble dynamics**

The spherical symmetry of the physical situation makes it convenient to work with a spherical coordinate system with origin at the center of the bubble as is shown in Fig. 10.3. All derivatives with respect to θ and φ vanish. It is obvious that the only velocity component relevant to the problem is v_r and $v_r = v_r(r, t)$. The continuity

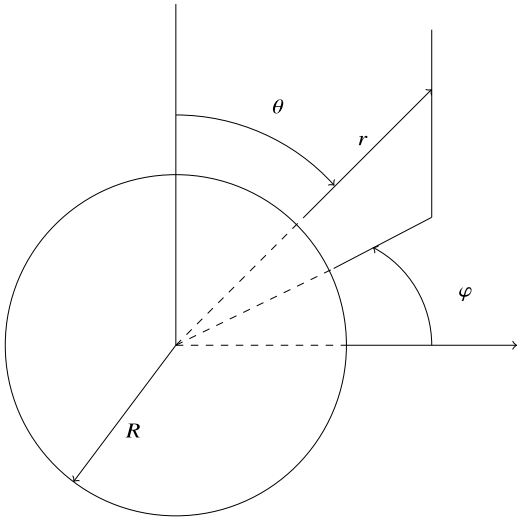

Fig. 10.3 Bubble geometry and associated spherical coordinates

equation and the Navier–Stokes equation for v_r give with the help of relations (B.20) and (B.21)

$$\frac{1}{r^2}\frac{\partial}{\partial r}(r^2\, v_r) = 0 \tag{10.81}$$

$$\rho\left(\frac{\partial v_r}{\partial t} + v_r\frac{\partial v_r}{\partial r}\right) = -\frac{\partial p}{\partial r} + \mu\left(\frac{1}{r^2}\frac{\partial}{\partial r}(r^2\frac{\partial v_r}{\partial r}) - \frac{2v_r}{r^2}\right) . \tag{10.82}$$

The integration of (10.81) gives $v_r = A/r^2$. With the boundary condition $v_r = \dot{R}$ at the bubble wall, $\dot{R}$ denoting the wall velocity, we obtain $A = R^2\dot{R}$. The dot denotes the time derivative. Then we have

$$v_r = \frac{\dot{R}R^2}{r^2} . \tag{10.83}$$

Inserting (10.83) in (10.82) we have

$$-\frac{\partial p}{\partial r} = \rho\left(2\frac{R\dot{R}^2}{r^2} + \frac{R^2\ddot{R}}{r^2} - 2\frac{R^4\dot{R}^2}{r^5}\right) . \tag{10.84}$$

Notice that the viscous term disappears by cancellation. We will integrate (10.84) from the bubble boundary $r = R$ to infinity $r \to \infty$. We obtain

$$-\frac{1}{\rho}\int_{p(R)}^{p(\infty)} dp = \int_R^\infty \left(\frac{1}{r^2}\left[2R\dot{R}^2 + R^2\ddot{R}\right] - 2\frac{R^4\dot{R}^2}{r^5}\right) dr . \tag{10.85}$$

Carrying the algebra further we get

$$\frac{p(R)-p_\infty}{\rho} = \left[-\frac{1}{r}\left[2R\dot{R}^2+R^2\ddot{R}\right]+\frac{R^4\dot{R}^2}{2r^4}\right]_R^\infty$$
$$= R\ddot{R}+\frac{3}{2}\dot{R}^2\,. \tag{10.86}$$

The stress components with the help of relations (B.19)–(B.23) are given by

$$\sigma_{rr} = -p-\frac{4\mu R^2\dot{R}}{r^3} \tag{10.87}$$
$$\sigma_{\theta\theta} = \sigma_{\varphi\varphi} = -p+\frac{2\mu R^2\dot{R}}{r^3} \tag{10.88}$$
$$\sigma_{\theta\varphi} = \sigma_{\varphi r} = \sigma_{r\theta} = 0\,. \tag{10.89}$$

Within the bubble

$$\sigma_{rr} = \sigma_{\theta\theta} = \sigma_{\varphi\varphi} = -p_g \tag{10.90}$$
$$\sigma_{\theta\varphi} = \sigma_{\varphi r} = \sigma_{r\theta} = 0\,. \tag{10.91}$$

The stress components $\sigma_{\varphi r}$ and $\sigma_{r\theta}$ must be continuous across the bubble surface. The comparison of (10.89) with (10.91) reveals that this requirement is automatically satisfied. The stress component σ_{rr} must experience a jump of magnitude $2\gamma/R$, where γ is the coefficient of interfacial tension (cf. Eq. (1.82)); the stress value inside the bubble is lower. Comparing Eq. (10.87) with (10.90), we find that the pressure just outside the bubble wall is given by

$$p(R+\varepsilon,t) = p_g(t)-\frac{(2\gamma+4\mu\dot{R})}{R}, \quad \varepsilon \ll 1\,. \tag{10.92}$$

Setting $r=(R+\varepsilon)$ in Eq. (10.86), we obtain an ordinary differential equation for the bubble radius as a function of time:

$$R\ddot{R}+\frac{3}{2}\dot{R}^2+\frac{4\mu\dot{R}}{\rho R}+\frac{2\gamma}{\rho R} = \frac{p_\infty(t)-p_b}{\rho}\,, \tag{10.93}$$

with p_g the pressure inside the bubble. Since (10.93) is a second-order equation, two initial conditions must be specified. Most simply, $R(0)$ and $\dot{R}(0)$ will be given. Equation (10.93) is the Rayleigh–Plesset equation.

The treatment given here has been restricted to spherical bubbles. In practice, the presence of a unidirectional gravitational field tends to destroy the spherical symmetry. It also causes the bubble to rise in the liquid, and our analysis does not account for streaming past the bubble.

However in certain physical problems the bubble is small enough so that interfacial tension causes it to remain essentially spherical. When streaming past the bubble is negligible, Eq. (10.93) can still be applied. Cavitation bubbles can be treated, but in the literature on cavitation in liquids, viscosity is usually neglected, so that the term $4\mu\dot{R}/\rho R$ is dropped from Eq. (10.93).

10.4 Chapter Four

4.1 The solution of the circular Couette flow is given by Eq. (3.41). Then $\boldsymbol{v} = (0, v_\theta(r), 0)$. The vorticity has the components

$$\boldsymbol{\omega} = (0, 0, \frac{1}{r}\frac{\partial}{\partial r}(r v_\theta)) \, . \tag{10.94}$$

Therefore $\omega_z = 2A$. The vorticity in the circular Couette flow is constant. It is interesting to note that if $B = 0$, i.e. $\omega_1 = \omega_2$, the fluid is in solid rotation and the vorticity value is twice the angular velocity.

Using Stokes theorem (4.4), the surface integral is easily computed as $\boldsymbol{\omega} \cdot \boldsymbol{n} = \omega_z$ and the surface $S = \pi(R_2^2 - R_1^2)$. Therefore $\int_S \boldsymbol{\omega} \cdot \boldsymbol{n} \, dS = 2\pi(R_2^2\omega_2 - R_1^2\omega_1)$. For the line integral, we define a contour made of a straight line orthogonal to the cylinders reaching the two boundary circumferences C_1 (inner) and C_2 (outer) at points L_1 and L_2. The contour is swept from the L_1 to L_2, goes counterclockwise around C_2 till L_2, crosses the annulus from L_2 to L_1 and then circumnavigates clockwise around C_1 until reaching L_1. It is obvious that both integrals on the line segment L_1L_2 do not contribute to the integral as the velocity is orthogonal to the integration path. For the integrals around C_1 and C_2 we have

$$\begin{aligned} \oint_{C_1} v_\theta(R_1) r d\theta &= \int_0^{2\pi} v_\theta(R_1) R_1 d\theta = -2\pi R_1 v_\theta(R1) = -2\pi R_1^2 \omega_1 \\ \oint_{C_2} v_\theta(R_2) r d\theta &= 2\pi R_2^2 \omega_2 \end{aligned} \tag{10.95}$$

We conclude that the Stokes theorem is satisfied.

4.2 We consider the streamline SA from the free surface S toward the orifice Or of the enclosure (cf. Fig. 10.4) and we apply to it the Bernoulli theorem (4.41) to obtain

$$p_S + \frac{\rho v_S^2}{2} + \rho\chi_S = p_A + \frac{\rho v_A^2}{2} + \rho\chi_A \, .$$

By (4.13), one obtains

$$-g = -\frac{\partial \chi}{\partial x_3} \, ,$$

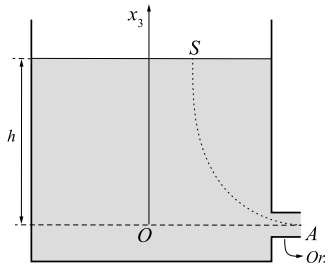

Fig. 10.4 Enclosure with free surface and orifice

and thus $\chi = gx_3 + C$. At the free surface the pressure is that of ambiant air; it is the same situation at the orifice. Therefore $p_S = p_A = p_{air}$. If we set the origin of the x_3 axis at the level of the orifice, the contribution of $\rho\chi$ is equal to C. For the sake of simplicity, we set $C = 0$, while at the free surface $x_3 = h$, $\rho\chi_S = \rho gh$. On the free surface, the velocity v_S is zero (this is especially true when the enclosure is large) and setting $v_A = v$ one has

$$\rho gh = \frac{\rho}{2} v^2 \,. \tag{10.96}$$

This gives the sought relation, which is known as Torricelli formula.

4.3 **Hill's Vortex**

We follow the solution described by Rieutord [79]. Another way of presenting and solving Hill's vortex leading to the same relationships is to be found in the book by Shivamoggi [91].

- Referring to the equations for the **curl** and div in spherical coordinates (Appendix B), the equations **curl** $= \mathbf{0}$ and div $\boldsymbol{v} = 0$ yield

$$\frac{1}{r}\frac{\partial}{\partial r}(r v_\theta) - \frac{1}{r}\frac{\partial v_r}{\partial \theta} = \frac{\omega r}{R}\sin\theta \tag{10.97}$$

$$\frac{1}{r^2}\frac{\partial}{\partial r}(r^2 v_r) + \frac{1}{r\sin\theta}\frac{\partial(\sin\theta\, v_\theta)}{\partial\theta} = 0 \,. \tag{10.98}$$

Using the suggested form of v_r and v_θ given in the statement, one gets from (10.98)

$$g(r) = -\frac{1}{2r}\frac{d}{dr}(r^2 f) \,. \tag{10.99}$$

Equation (10.97) with the help of Eq. (10.99) leads to relation

$$\frac{d^2}{dr^2}(r^2 f) - 2f = -\frac{2\omega r^2}{R} \,. \tag{10.100}$$

The particular solution f_p of (10.100) is sought as $f_p = Cr^2$ with C a constant. Inserting f_p in (10.100), one obtains $C = -\omega/5R$. The homogeneous solution

f_h gives $f = A/r^3 + B$. The boundary conditions allow the determination of the integration constants. First the velocity must be finite when $r \to 0$. This imposes $A = 0$. Secondly the radial component v_r vanishes for $r = R$. Eventually

$$v_r = \frac{\omega}{5R}(R^2 - r^2)\cos\theta \quad \text{and} \quad v_\theta = \frac{\omega}{5R}(2r^2 - R^2)\sin\theta\,. \tag{10.101}$$

Note that on the sphere the velocity is such that $v_\theta = \omega R \sin\theta/5$.

- Outside the sphere, the flow is irrotational and the velocity comes the velocity potential (4.36), solution of the Laplace equation

$$\Delta\Phi = 0\,. \tag{10.102}$$

We obtain

$$\Phi(r,\theta) = (Ar + \frac{B}{r^2})\cos\theta\,. \tag{10.103}$$

The boundary conditions are

$$v_r(r = R) = 0, \quad \text{and} \quad v_\theta(r = R) = \omega R \sin\theta/5\,. \tag{10.104}$$

Imposing (10.104) to (10.103) yields

$$v_r = \frac{2\omega R}{15}\left(-1 + (\frac{R}{r})^3\right)\cos\theta, \quad \text{and} \quad v_\theta = \frac{2\omega R}{15}\left(1 + \frac{1}{2}(\frac{R}{r})^3\right)\sin\theta\,. \tag{10.105}$$

- Introducing the streamfunction ψ such as

$$v_r = \frac{1}{r^2\sin\theta}\frac{\partial\psi}{\partial\theta} \quad \text{and} \quad v_\theta = -\frac{1}{r\sin\theta}\frac{\partial\psi}{\partial r}\,, \tag{10.106}$$

from the velocity components (10.105), the streamfunctions for the full flow are

$$\psi = \frac{\omega r^2}{10R}(R^2 - r^2)\sin^2\theta \quad \text{for} \quad r \le R \tag{10.107}$$

$$\psi = \frac{\omega R r^2}{15}\left(-1 + (\frac{R}{r})^3\right)\sin^2\theta \quad \text{for} \quad r > R \tag{10.108}$$

Figure 10.5 shows the streamlines associated to Hill's vortex in the meridian plane (r, z) of the cylindrical coordinates.

4.4 **Drain of a container**

- With Eqs. (4.100) and (A.20), it is obvious that div $\boldsymbol{v} = 0$.
- With Eqs. (4.100) and (A.6), we have $\mathbf{curl}\,\boldsymbol{\omega} = \mathbf{0}$.
- Using the unperturbed velocity component and the steady state vorticity Eq. (4.24) for ω_z, we obtain

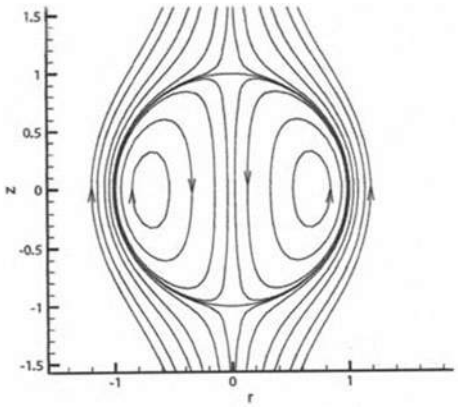

Fig. 10.5 Hill's vortex streamlines

$$\frac{D\omega_z}{Dt} = (\boldsymbol{v}\cdot\boldsymbol{\nabla})\omega_z = v_r\frac{\partial\omega_z}{\partial r} = \omega_z\frac{\partial v_z}{\partial z} + \frac{\nu}{r}\frac{\partial}{\partial r}\left(r\frac{\partial\omega_z}{\partial r}\right) . \tag{10.109}$$

This relationship yields

$$-\frac{ar}{2}\frac{d\omega_z}{dr} = a\omega_z + \frac{\nu}{r}\frac{d}{dr}\left(r\frac{d\omega_z}{dr}\right) . \tag{10.110}$$

Consequently

$$\frac{d}{dr}\left[\nu\, r\frac{d\omega_z}{dr} + \frac{a}{2}\omega_z r^2\right] = 0 . \tag{10.111}$$

Integration of (10.111) produces (4.101).

- The integration constant must be zero. If this were not the case, the vorticity ω_z would diverge logarithmically at small values of r as the viscous term would dominate the other terms. On the contrary, for large values of r, the viscous term is less influent and the vorticity decays as $1/r^2$. Therefore the total vorticity integrated over the flow volume is blowing up; nonetheless the vorticity must remain finite and constant as there exists no mechanism to create vorticity in this problem.
- With $C = 0$, the integration of (4.101) gives

$$\omega_z = \omega_z\big|_{r=0}\exp\left(-\frac{ar^2}{4\nu}\right) . \tag{10.112}$$

- The result (10.112) shows the presence of a characteristic length $\delta = \sqrt{\nu/a}$.
- Over the distance δ there is an equilibrium between the stretching effects of the elongational velocity field $\boldsymbol{v}$ and the sprawl by viscous diffusion. If the flow occurs through an orifice of diameter d with a reference velocity U, then we have

$$a \simeq \frac{U}{d} \ , \quad \frac{\delta}{d} \simeq \sqrt{\frac{\nu}{Ud}} = Re^{-\frac{1}{2}} \tag{10.113}$$

The higher the value of the Reynolds number, the more concentrated the vorticity in a small diameter core.

4.5 **Vortex sheet**

- From the problem statement, we have $v_2 = v_3 = 0$ and $v_1 = v_1(x_2, t)$. The non zero vorticity component is $\omega_3(x_2, t) = -\partial v_1/\partial x_2$. As the flow is two-dimensional and the vorticity is orthogonal to the plane flow, the term $(\boldsymbol{\omega} \cdot \boldsymbol{\nabla})\boldsymbol{v}$ vanishes. The vorticity governing equation (4.24) reduces to

$$\frac{\partial \omega_3}{\partial t} = \nu \frac{\partial^2 \omega_3}{\partial x_2^2} \ . \tag{10.114}$$

- This equation is of diffusion type as was (3.71). We introduce the dimensionless variables

$$\eta = \frac{x_2}{\sqrt{\nu t}} \quad \text{and} \quad \upsilon = \frac{U^2 t}{\nu} \ . \tag{10.115}$$

The vorticity is decomposed by separation of variables

$$\omega_3 = f(\eta) g(\upsilon) \ . \tag{10.116}$$

We have

$$\begin{aligned} \frac{\partial \omega_3}{\partial t} &= \frac{\partial \eta}{\partial t} f'(\eta) g(\upsilon) + f(\eta) \frac{\partial \upsilon}{\partial t} g'(\upsilon) \\ &= -\frac{\eta}{2t} f'(\eta) g(\upsilon) + \frac{U^2}{\nu} f(\eta) g'(\upsilon) \\ \frac{\partial \omega_3}{\partial x_2} &= \frac{1}{\sqrt{\nu t}} f'(\eta) g(\upsilon) \quad \Rightarrow \quad \frac{\partial^2 \omega_3}{\partial x_2^2} = \frac{1}{\nu t} f''(\eta) g(\upsilon) \ . \end{aligned} \tag{10.117}$$

Equation (10.114) reads now

$$-\frac{\eta}{2} f'(\eta) g(\upsilon) + \upsilon f(\eta) g'(\upsilon) = f''(\eta) g(\upsilon) \ . \tag{10.118}$$

Dividing through by (10.116) we get

$$\frac{\eta}{2} \frac{f'(\eta)}{f(\eta)} + \frac{f''(\eta)}{f(\eta)} = \upsilon \frac{g'(\upsilon)}{g(\upsilon)} = C \ . \tag{10.119}$$

If $g(0) \neq 0$ and $g'(0)$ is finite, then $C = 0$. This implies that $g'(\upsilon) = 0$ and thus $g(\upsilon)$ is constant.

- The f equation reads

$$f''(\eta) = -\frac{\eta}{2} f'(\eta) \, . \tag{10.120}$$

Integrating one obtains

$$f' = f'(0) e^{\frac{-\eta^2}{4}} \, . \tag{10.121}$$

Integrating again

$$f(\eta) = f(0) + f'(0) \int_0^\eta e^{\frac{-\zeta^2}{4}} d\zeta \, . \tag{10.122}$$

With the change of variable $\sigma = \frac{\zeta}{2}$, (10.122) becomes

$$f(\eta) = f(0) + 2 f'(0) \int_0^\eta e^{-\sigma^2} d\sigma \, . \tag{10.123}$$

Using the error function (3.79), we write

$$f(\eta) = f(0) + \sqrt{\pi} f'(0) \mathrm{erf}(\frac{\eta}{2}) \, . \tag{10.124}$$

- The thickness of the vortex sheet, i.e. the region where the vorticity does not vanish, increases like $\sqrt{\nu t}$.

10.5 Chapter Five

5.1 Hele-Shaw flow

- Inspection of (1.73) gives

$$\frac{\partial v_1}{\partial x_1} + \frac{\partial v_2}{\partial x_2} + \frac{\partial v_3}{\partial x_3} \simeq \frac{v_1}{L} + \frac{v_2}{L} + \frac{v_3}{h} \Rightarrow |v_3| \approx \varepsilon v_1 \simeq \varepsilon v_2 \ll |v_1| \simeq |v_2| \, . \tag{10.125}$$

- As the length scales in the directions parallel and orthogonal to the plates are quite different, we write

$$\left| \frac{\partial^2 v_1}{\partial x_1^2} \right| \approx \frac{v_1}{L^2} \ll \left| \frac{\partial^2 v_1}{\partial x_3^2} \right| \approx \frac{v_1}{\varepsilon^2 L^2}, \quad \left| \frac{\partial^2 v_2}{\partial x_1^2} \right| \approx \frac{v_2}{L^2} \ll \left| \frac{\partial^2 v_2}{\partial x_3^2} \right| \approx \frac{v_2}{\varepsilon^2 L^2} \, . \tag{10.126}$$

- The steady Stokes equations (1.73) and (2.54) reduce to the set

$$\frac{\partial v_i}{\partial x_i} = 0 \,, \tag{10.127}$$

$$\frac{\partial p}{\partial x_i} = \mu \nabla^2 v_i \,, \tag{10.128}$$

with $p = p(x_1, x_2)$ and $v_i = v_i(x_1, x_2)$, $i = 1, 2$. Since v_3 is of order ε, the $i = 3$ component of (2.54) indicates that the pressure is essentially constant across the gap and does not depend on x_3 as $\partial p/\partial x_3 = 0$, i.e., $p = p(x_1, x_2)$.

- This set of equations is meaningful in the symmetry plane parallel to the plates containing the origin of the coordinate axes. It is possible with the help of Eqs. (5.116) and (10.125)–(10.126) to write

$$v_i(x_1, x_2, x_3) = v_i(x_1, x_2, 0) f(x_3) \,, \tag{10.129}$$

as the variation of v_i with respect to x_1, x_2 is slower than that of f with respect to x_3.

- The Poiseuille flow solution (3.27) provides the relationship

$$f(x_3) = \left(1 - \frac{x_3^2}{h^2}\right) \,. \tag{10.130}$$

The momentum equations (10.128) become

$$\mu \frac{\partial^2 v_1}{\partial x_3^2} = \frac{\partial p}{\partial x_1} \,, \tag{10.131}$$

$$\mu \frac{\partial^2 v_2}{\partial x_3^2} = \frac{\partial p}{\partial x_2} \,. \tag{10.132}$$

- Taking Eqs. (10.129) and (10.130) into account, one obtains

$$v_i(x_1, x_2, 0) = -\frac{h^2}{2\mu} \frac{\partial p}{\partial x_i}, \quad \mathrm{i} = 1, 2 \,. \tag{10.133}$$

From (10.133) it is obvious that the velocity field is a gradient, is irrotational and hence, can be derived from a velocity potential. Introducing

$$v_i = \frac{\partial \varphi}{\partial x_i} \,, \tag{10.134}$$

Equation (10.133) yields

$$\varphi = -\frac{h^2 p}{2\mu} \,. \tag{10.135}$$

The streamline configuration will be the same in planes $x_3 = cst$. Furthermore they will be similar to those of a two-dimensional potential flow of an inviscid fluid around obstacles of the same shape. However near the obstacles the viscous fluid sticks to the walls, but this influence will be limited to a zone of thickness h. This discussion explains why the Hele-Shaw cell is used in many experiments to provide the observer with the geometrical pattern resulting from the presence of bodies inside an internal flow.

5.2 **Flow between parallel discs**

- With the velocity field given in Eq. (5.119), the continuity relation (A.20) gives

$$\frac{\partial v_\theta}{\partial \theta} = 0 \,, \tag{10.136}$$

showing that v_θ does not depend on θ.
The Navier–Stokes equations (A.21)–(A.23) reduce to

$$-\rho \frac{v_\theta^2}{r} = -\frac{\partial p}{\partial r} \tag{10.137}$$

$$0 = -\frac{1}{r}\frac{\partial p}{\partial \theta} + \mu \left[\frac{\partial}{\partial r}\left(\frac{1}{r}\frac{\partial}{\partial r}(r v_\theta) \right) + \frac{\partial^2 v_\theta}{\partial z^2} \right] \tag{10.138}$$

$$0 = -\frac{\partial p}{\partial z} + \rho b_z \,. \tag{10.139}$$

Because of the symmetry, the pressure term in (10.138) vanishes. Taking the particular form of (5.119) into account, Eq. (10.138) gives

$$f''(z) = 0 \,. \tag{10.140}$$

Integrating, we have $f(z) = C_1 z + C_2$. Imposing the boundary conditions

$$v_\theta(z = 0) = 0 \quad \text{and} \quad v_\theta(z = h) = \omega r \,, \tag{10.141}$$

we obtain $C_1 = \omega / h$ and $C_2 = 0$. Therefore the velocity field is

$$v_\theta = \frac{\omega}{h} r \, z \,. \tag{10.142}$$

- With (10.137), (10.139), (10.142) and $b_z = -g$, the pressure is

$$p(r, z) = -\rho g z + q(r) \,. \tag{10.143}$$

Setting $q(r) = 0$, Eq. (10.137) is satisfied provided $\omega \ll 1$ and $\partial p / \partial r = 0$.

- Throughout the fluid, the shear stress is

$$\sigma_{\theta z} = 2\mu d_{\theta z} = \mu \frac{\partial v_\theta}{\partial z} = \mu\omega \frac{r}{h} \,. \tag{10.144}$$

Consequently the moment M required to rotate the top disc, or to hold the bottom one still, is given by

$$M = \int_0^R (2\pi r)(r\sigma_{\theta z})dr = \frac{2\pi\mu\omega}{h} \int_0^R r^3 dr = \frac{\pi\mu\omega R^4}{2h} \,. \tag{10.145}$$

Since the quantities M, ω, a, h can presumably be measured, (10.145) can be used to determine the viscosity of the fluid, provided the underlying assumptions of creeping flow and idealized geometry are sufficiently well approximated.

10.6 Chapter Six

6.1

- The complex potential of the flow is

$$f(z) = m\,(\ln(z+1) + \ln(z-1) - \ln z) \tag{10.146}$$

corresponding to two sources located in $z = \pm 1$ and one sink in $z = 0$.

- The complex potential is expressed as

$$f(z) = m \ln\left(\frac{z^2-1}{z}\right) = m\left(\ln\left|\frac{z^2-1}{z}\right| + i\,\arg\left(\frac{z^2-1}{z}\right)\right) = \varphi + i\psi \,. \tag{10.147}$$

- With $z = re^{i\theta}$, we obtain

$$\varphi = m \ln\left(\frac{1}{r}\sqrt{r^4 - 2r^2\cos(2\theta) + 1}\right) \tag{10.148}$$

and

$$\psi = m \arctan\left(\frac{r^2+1}{r^2-1}\tan\theta\right) \,. \tag{10.149}$$

Therefore the streamlines are

$$\psi = cst, \quad \text{with} \quad \frac{r^2+1}{r^2-1}\tan\theta = \alpha \tag{10.150}$$

with α constant. Let us notice that the Eq. (10.150) is invariant by the transformation $r \to 1/r$. Replacing r^2 by $x^2 + y^2$ and $\tan\theta$ by y/x, Eq. (10.150) becomes

$$(x^2 + y^2 + 1)y = \alpha(x^2 + y^2 - 1)x \tag{10.151}$$

which is invariant by the following symmetry $(x, y) \to (-x, -y)$. Consequently we can inspect the flow in the positive half-disk $r < 1$.

- The flow rate across the line joining the points $z_1 = \frac{1}{2}(1 + i)$ and $z_2 = 1/2$ is given with (6.12)

$$\begin{aligned} Q &= \psi(z_2) - \psi(z_1) \\ &= m \arctan\left(\frac{r_2^2 + 1}{r_2^2 - 1} \tan\theta_2\right) - m \arctan\left(\frac{r_1^2 + 1}{r_1^2 - 1} \tan\theta_1\right) \\ &= m \arctan(3) \end{aligned} \tag{10.152}$$

as $r_2 = 1/2, \theta_2 = 0, r_1 = \sqrt{2}/2$ and $\theta_1 = \pi/4$.

6.2

- The singularities are located in

$$z_{1,1'} = \pm 1 \tag{10.153}$$
$$z_{2,2'} = \pm 2i \tag{10.154}$$
$$z_3 = 0\,. \tag{10.155}$$

- They are all inside the circle $C : x^2 + y^2 = 9$. The complex circulation $\mathbf{\Gamma}$ defined by (6.22) allows for the computation of the flow rate across C and the circulation around the circle

$$\begin{aligned} \mathbf{\Gamma} &= \int_C df, \quad z = 3e^{i\theta} \\ &= \int_0^{2\pi} df = f(3e^{i2\pi}) - f(3) \\ &= (1 + i)\left(\ln 8e^{i4\pi} - \ln 8\right) + (2 - 3i)\left(\ln 13e^{i4\pi} - \ln 13\right) \\ &+ \frac{e^{-i2\pi}}{3} - \frac{1}{3} \\ &= 4\pi i\,((1 + i) + (2 - 3i)) = 8\pi + 12\pi i\,. \end{aligned} \tag{10.156}$$

Then $Q = 12\pi$ and $\Gamma = 8\pi$.

6.3

- With the relation (6.156) we calculate

$$\begin{aligned} z = \cosh f &= \frac{e^f + e^{-f}}{2} = \frac{1}{2}\left(e^{\varphi + i\psi} + e^{-(\varphi + i\psi)}\right) \\ 2x + 2iy &= e^{\varphi}(\cos\psi + i\sin\psi) + e^{-\varphi}(\cos\psi - i\sin\psi)\,. \end{aligned} \tag{10.157}$$

Separating the real and imaginary contributions, we have

$$2x = e^{\varphi}\cos\psi + e^{-\varphi}\cos\psi = \cos\psi(e^{\varphi} + e^{-\varphi})$$
$$2y = e^{\varphi}\sin\psi + e^{-\varphi}\sin\psi = \sin\psi(e^{\varphi} - e^{-\varphi})\ ,$$

and

$$x = \cosh\varphi\cos\psi, \quad y = \sinh\varphi\sin\psi\ . \tag{10.158}$$

Therefore one has

$$\left(\frac{x}{\cosh\varphi}\right)^2 + \left(\frac{y}{\sinh\varphi}\right)^2 = 1 \tag{10.159}$$

$$\left(\frac{x}{\cos\psi}\right)^2 - \left(\frac{y}{\sin\psi}\right)^2 = 1\ . \tag{10.160}$$

Equations (10.159) and (10.160) show that the equipotentials are ellipses and streamlines hyperbolas that are drawn in Fig. 10.6. Note that for $y = 0$, there is no solution for $|x| > 1$.

- Let us evaluate the velocity for $y = 0$ and $-1 \le x \le 1$. Obviously by symmetry, $u = 0$. From (6.14) we have

$$\frac{dz}{df} = \frac{1}{w} = \frac{1}{u - iv} = \sinh f = \sqrt{\cosh^2 f - 1} = \sqrt{z^2 - 1}\ . \tag{10.161}$$

Therefore

$$u - iv = \frac{1}{\sqrt{z^2 - 1}} = \frac{1}{\sqrt{x^2 - 1}} = \frac{-i}{\sqrt{1 - x^2}}\ . \tag{10.162}$$

Consequently $v = -i/\sqrt{1 - x^2}$. Note the $|v| = \infty$ for $x = \pm 1$ and $|v| = 1$ for $x = 0$.

6.4 **Flow in front of a circular obstacle**

- The complex potential $g(\zeta)$ may be decomposed as a sum of noteworthy terms

$$g(\zeta) = \frac{Q}{2\pi}\left(\ln(\zeta - a) + \ln(\zeta + a) - \ln(\zeta - 1) - \ln(\zeta + 1)\right)\ . \tag{10.163}$$

The flow is thus created by two sources situated in $\zeta = \pm a$ and by two sinks in $\zeta = \pm 1$. The two images are the images of the singularities with respect to the wall, namely the η axis.

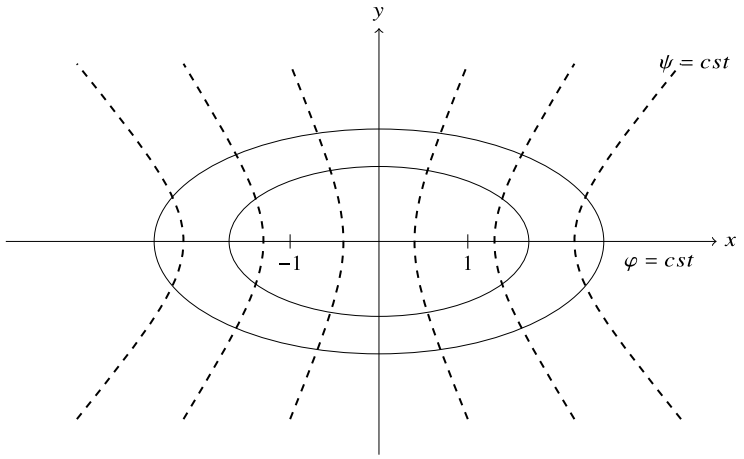

Fig. 10.6 Streamlines and equipotentials for $z = \cosh f$

- The complex velocity reads

$$w_\zeta = \frac{dg(\zeta)}{d\zeta} = \frac{Q}{2\pi}\left(\frac{1}{\zeta - a} + \frac{1}{\zeta + a} - \frac{1}{\zeta - 1} - \frac{1}{\zeta + 1}\right)$$
$$= \frac{Q}{2\pi}\left(\frac{2\zeta(a^2 - 1)}{(\zeta^2 - a^2)(\zeta^2 - 1)}\right) . \tag{10.164}$$

- With the conformal mapping (6.158), the wall $\xi = 0$ in the ζ plane is transformed in a circle of unit radius in the z plane as we have

$$x + iy = \frac{1 + i\eta}{1 - i\eta} \quad \Rightarrow \quad x^2 + y^2 = 1 . \tag{10.165}$$

- Introducing successively in $g(\zeta)$ the positions of the two sources and the two sinks, $\zeta = \pm a$ and $\zeta = \pm 1$ respectively, with the definition of b, we obtain that the source in $\zeta = a$ becomes a source in $x = b$, the image source in $\zeta = -a$ yields a source in $x = 1/b$, the sink in $\zeta = 1$ gives a sink at infinity, and eventually, the image sink in $\zeta = -1$ generates the sink in $z = 0$.
- Therefore the image of the half plane $\xi \geq 0$ in the z plane is the exterior of the unit circle centered at the origin as shown in Fig. 10.7.
- The complex velocity $w(z)$ in the z plane is

$$w = w_\zeta\left(\frac{z - 1}{z + 1}\right) \tag{10.166}$$

- The complex potential in the z plane is made of two sources and one sink

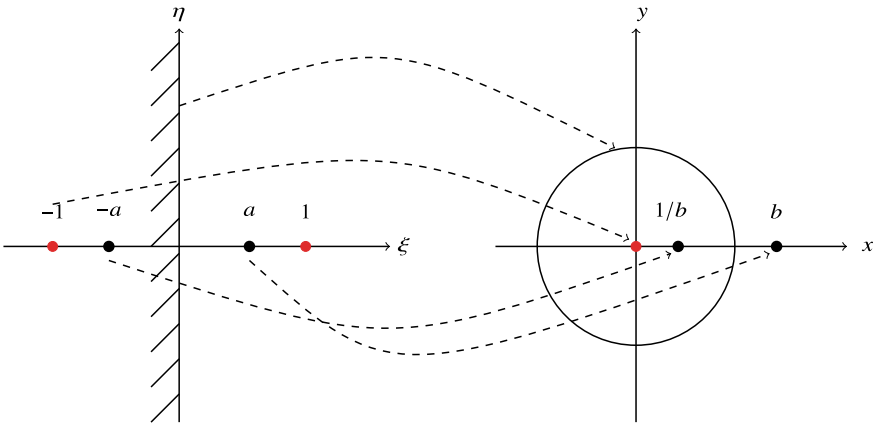

Fig. 10.7 Source in front of a circular obstacle with $a < 1$. Red dots are sinks and black dots sources

$$f(z) = \frac{Q}{2\pi}\left(\ln(z-b) + \ln(z-\frac{1}{b}) - \ln z\right) \tag{10.167}$$

which is exactly Eq. (6.159).

6.5 Flow over a forward facing step

- For the half line $\xi \geq 0$ and $\eta = 0$ we have $\arg dz - \arg d\zeta = (\arg\xi - \arg(\xi + a))/2 = 0$.
- For the AO segment, one has $\arg dz - \arg d\zeta = (\arg\xi - \arg(\xi + a))/2 = \pi/2$ and for $\xi < -a$, $\arg dz - \arg d\zeta = (\arg\xi - \arg(\xi + a))/2 = 0$. The geometry of the transformed domain is a forward facing step as shown in Fig. 10.8.
- The velocity in the physical plane is

$$w = g'(\zeta)\frac{d\zeta}{dz} = U\left(\frac{\zeta + a}{\zeta}\right)^{1/2}. \tag{10.168}$$

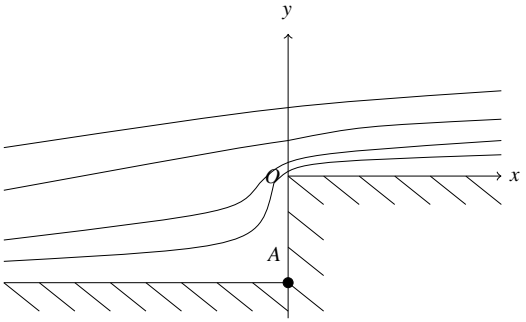

Fig. 10.8 Sketch of the flow over a forward facing step

In the limit $\eta \to 0$, we have

$$w = U \left(\frac{\xi + a}{\xi} \right)^{1/2} . \tag{10.169}$$

We notice that for $\xi = -a$, the velocity vanishes and this point is indeed a stagnation point; in $\xi = 0$, the velocity goes to infinity.

More details for this problem may be found in Sect. 10.6 of Milne-Thompson [59].

10.7 Chapter Seven

7.1 The boundary conditions are given by

$$x_2 = 0 \ : \ v_1 = v_2 = 0 \tag{10.170}$$

$$x_2 = \delta_\infty \ : \ v_1 = U_e(x_1), \ \frac{\partial v_1}{\partial x_2} = \frac{\partial^2 v_1}{\partial x_2^2} = 0 \, . \tag{10.171}$$

From the Navier–Stokes equations, we get

$$\nu \frac{\partial^2 v_1}{\partial x_2^2} = \frac{1}{\rho} \frac{\mathrm{d}p_e}{\mathrm{d}x_1} = -U_e \frac{\mathrm{d}U_e}{\mathrm{d}x_1}. \tag{10.172}$$

With the help of Eqs. (10.171) and (10.172), we calculate the coefficients a, b, c and d. With the substitution

$$\lambda = \frac{\delta_\infty^2}{\nu} \frac{dU_e}{dx_1}, \tag{10.173}$$

we find

$$a = \tfrac{\lambda}{6} + 2, \tag{10.174}$$

$$b = -\tfrac{\lambda}{2}, \tag{10.175}$$

$$c = \tfrac{\lambda}{2} - 2, \tag{10.176}$$

$$d = 1 - \tfrac{\lambda}{6}. \tag{10.177}$$

The velocity profile is then written

$$v_1/U_e = 2s - 2s^3 + s^4 + \frac{\lambda}{6} s(1-s)^3. \tag{10.178}$$

In the present case, the outer velocity is constant ($U_e = \mathrm{cst}$). Therefore $\lambda = 0$ and the velocity profile is simplified

$$\frac{u}{U_e} = 2s - 2s^3 + s^4. \tag{10.179}$$

The displacement thickness δ^* is

$$\delta^* = \int_0^\delta \mathrm{d}x_2 \left(1 - \frac{v_1}{U_e}\right) = \frac{3}{10}\delta_\infty. \tag{10.180}$$

For the momentum thickness θ, we have the definition

$$\theta = \int_0^\delta \mathrm{d}x_2 \left[\frac{v_1}{U_e}\left(1 - \frac{v_1}{U_e}\right)\right] = \frac{37}{315}\delta_\infty. \tag{10.181}$$

The wall shear stress τ_w is given by

$$\tau_w = -\int_0^{\delta_\infty} \mathrm{d}x_2 \frac{\partial}{\partial x_2}\left(\frac{\partial v_1}{\partial x_2}\right) = 2\mu\frac{U_e}{\delta_\infty}. \tag{10.182}$$

Finally, through the von Kármán equation (7.89), we have a relation between τ_w and θ

$$\frac{d\theta}{dx_1} = \frac{\tau_w}{\rho U_e^2}. \tag{10.183}$$

Substituting the above expressions for θ and τ_w, one finds

$$\frac{37}{315}\frac{d\delta}{dx_1} = \frac{2\nu}{\delta U_e} \Rightarrow \delta_\infty = 2\sqrt{\frac{315}{37}}\sqrt{\frac{\nu x_1}{U_e}} = 5.83\sqrt{\frac{\nu x_1}{U_e}}. \tag{10.184}$$

7.2 Referring to Fig. 7.5, the problem solution is performed through the next steps.

- The boundary conditions for the boundary layer developing over the flat plate are

  1. No slip wall

  $$v_1(0) = 0 \quad \text{for} \quad x_2 = 0\,. \tag{10.185}$$

  2. Matching condition with the outer flow field at $x_2 = \delta_0$

  $$v_1(\delta_0) = U \quad \text{for} \quad x_2 = \delta_0\,. \tag{10.186}$$

  3. Stress condition at $x_2 = \delta_0$

  $$\frac{\partial v_1}{\partial x_2} = 0 \quad \text{for} \quad x_2 = \delta_0\,. \tag{10.187}$$

- Evaluation of A, B, C.

1. Equation (10.185) implies $C = 0$.
2. Condition (10.187) imposes

$$AB\cos(Bx_2)\big|_{x_2=\delta_0} = 0 \quad \Rightarrow B = \frac{\pi}{2\delta_0}\,. \tag{10.188}$$

3. Condition (10.186) gives $A = U$. The velocity profile is therefore

$$v_1(x_2) = U\sin\left(\frac{\pi x_2}{2\delta_0}\right)\,. \tag{10.189}$$

- Computation of θ

1. Introducing the variable $s = x_2/\delta_0$, the momentum thickness becomes

$$\begin{aligned}\theta &= \delta_0\int_0^1 \sin(\frac{\pi}{2}s)\left(1-\sin(\frac{\pi}{2}s)\right)ds\\ &= \delta_0(\frac{2}{\pi}-\frac{1}{2}) = 0.1366\,\delta_0\,.\end{aligned} \tag{10.190}$$

2. Continuity over the control volume

$$-\int_0^{\delta_0}\rho U dx_2 + \int_0^{\delta_0}\rho v_1 dx_2 + \int_0^x \rho v_2'\,dx' = 0\,. \tag{10.191}$$

Note that the third integral on the left-hand side of (10.191) takes care of the mass flow rate $\Delta\dot{m}$ across the upper boundary of the control volume.
Equation (10.191) leads to the relation

$$\int_o^x \rho v_2' dx' = \int_0^{\delta_0}\rho(U-v_1)dx_2\,. \tag{10.192}$$

3. Integral momentum equation over the control volume

$$-\int_0^{\delta_0}\rho U^2 dx_2 + \int_0^{\delta_0}\rho v_1^2 dx_2 + \int_0^x \rho v_2' U dx' = -\int_0^x \tau_w(x')dx'\,. \tag{10.193}$$

Combining (10.193) with (10.192), one gets

$$-\int_0^{\delta_0}\rho(U^2-v_1^2)dx_2 + \int_0^{\delta_0}\rho U(U-v_1)dx_2 = -\int_0^x \tau_w(x')dx'\,. \tag{10.194}$$

Then

$$\int_0^{\delta_0}\rho v_1(v_1-U)dx_2 = -\int_0^x \tau_w(x')dx'\,. \tag{10.195}$$

From (10.195) we obtain

$$\tau_w = -\frac{d}{dx}\int_0^{\delta_0} \rho v_1(v_1 - U)dx_2 = \frac{d\theta}{dx}\rho U^2 \,. \tag{10.196}$$

Consequently

$$\frac{d\theta}{dx_1} = \frac{\tau_w}{\rho U^2} \,. \tag{10.197}$$

4. Computation of τ_w

$$\tau_w = \mu \frac{\partial v_1}{\partial x_2}\Big|_{x_2=0} = \frac{\mu U \pi}{2\delta_0}\cos(\frac{\pi x_2}{2\delta_0})\Big|_{x_2=0} = \frac{\mu U \pi}{2\delta_0} \,. \tag{10.198}$$

5. Computation of δ_0.
Using (10.197), (10.198) and (10.190) we have

$$\begin{aligned} \frac{d\theta}{dx_1} &= \frac{\mu\pi}{2\rho U \delta_0} \\ 0.1366\frac{d\delta_0}{dx_1} &= \frac{\mu\pi}{2\rho U \delta_0} \,. \end{aligned} \tag{10.199}$$

Integrating (10.199) one has

$$\delta_0 = 4.795\sqrt{\frac{\nu x_1}{U}} \,, \tag{10.200}$$

result that should be compared with (7.58).

7.3

- At some distance from the leading edge, the boundary layer is constant in shape and thickness. As a consequence, we have

$$\frac{\partial v_1}{\partial x_1} = 0 \,. \tag{10.201}$$

From the continuity equation and (10.201), one gets

$$\frac{\partial v_2}{\partial x_2} = 0 \quad \Rightarrow \quad v_2 = cst = V \,. \tag{10.202}$$

Prandlt's equation (7.40) with (10.202) becomes

$$V\frac{\partial v_1}{\partial x_2} = \nu \frac{\partial^2 v_1}{\partial x_2^2} \,. \tag{10.203}$$

This second-order differential equation has for solution

$$v_1 = Ae^{\frac{V}{\nu}x_2} + B \,. \tag{10.204}$$

The boundary condition at the plate imposes $v_1 = 0$ at $x_2 = 0$, giving $B = -A$. At $x_2 = \infty$, we have $v_1 = U_\infty$. Recalling that $V < 0$ one has $A = U_\infty$. Therefore the velocity profile reads

$$\frac{v_1}{U_\infty} = 1 - e^{\frac{V}{\nu}x_2} \,. \tag{10.205}$$

- The wall shear stress is

$$\tau_w = \mu \frac{\partial v_1}{\partial x_2}\Big|_{x_2=0} = -\mu(\frac{V}{\nu}U) = -\rho V U_\infty \,. \tag{10.206}$$

Observe that τ_w does not depend on the viscosity.

- The displacement thickness (7.59) with (10.204) gives

$$\delta^* = -\frac{\nu}{V} \,. \tag{10.207}$$

while the momentum thickness (7.63) becomes

$$\theta = -\frac{\nu}{2V} \,. \tag{10.208}$$

Finally the shape factor H is

$$H = \frac{\delta^*}{\theta} = 2 \,. \tag{10.209}$$

to be compared to $H = 8/3$ for the non-porous plate.

10.8 Chapter Eight

8.1 The spiral flow is the same as the helical flow solved in Sect. 3.2.3. The Couette solution (3.41) will be denoted by $V(r)$ while the axial solution (3.64) corresponding to the Poiseuille flow in the annular section is referred to as $W(r)$. The axisymmetric Navier–Stokes equations are given by (8.27)–(8.30). The stability analysis rests upon a base flow and three-dimensional axisymmetric perturbations. We have

$$\boldsymbol{v} = (u, V + v, W + w) \quad \text{and} \quad p = P + p_p \,. \tag{10.210}$$

We carry out a linearization of the governing equations discarding the second-order terms of the perturbations. We get

$$\rho\left(\frac{\partial u}{\partial t}+(W+w)\frac{\partial u}{\partial z}-\frac{(V+v)^2}{r}\right)=-\frac{\partial(P+p_p)}{\partial r}+\mu(\triangle u-\frac{u}{r^2}) \quad (10.211)$$

$$\rho\left(\frac{\partial v}{\partial t}+u\frac{dV}{dr}+(W+w)\frac{\partial v}{\partial z}+\frac{u}{r}(V+v)\right)=\mu(\triangle v-\frac{v}{r^2}) \quad (10.212)$$

$$\rho\left(\frac{\partial w}{\partial t}+u\frac{\partial(W+w)}{\partial r}+W\frac{\partial w}{\partial z}\right)=-\frac{\partial(P+p_p)}{\partial z}+\mu\Delta w \quad (10.213)$$

$$\frac{\partial u}{\partial r}+\frac{u}{r}+\frac{\partial w}{\partial z}=0\,. \quad (10.214)$$

As the base flow satisfies the Navier–Stokes equations, a further step in the linearization brings the equations

$$\rho\left(\frac{\partial u}{\partial t}+W\frac{\partial u}{\partial z}-\frac{2Vv}{r}\right)=-\frac{\partial p_p}{\partial r}+\mu(\triangle u-\frac{u}{r^2}) \quad (10.215)$$

$$\rho\left(\frac{\partial v}{\partial t}+u(\frac{V}{r}+\frac{dV}{dr})+W\frac{\partial v}{\partial z}\right)=\mu(\triangle v-\frac{v}{r^2}) \quad (10.216)$$

$$\rho\left(\frac{\partial w}{\partial t}+u\frac{dW}{dr}+W\frac{\partial w}{\partial z}\right)=-\frac{\partial p_p}{\partial z}+\mu\Delta w \quad (10.217)$$

$$\frac{\partial u}{\partial r}+\frac{u}{r}+\frac{\partial w}{\partial z}=0\,. \quad (10.218)$$

Using the normal modes (8.40) and the notation (8.41), the stability equations are

$$\sigma\hat{u}+ikW\hat{u}-\frac{2V\hat{v}}{r}=-\frac{1}{\rho}D\hat{p_p}+\nu(DD_*-k^2)\hat{u} \quad (10.219)$$

$$\sigma\hat{v}+\hat{u}D_*V+ikW\hat{v}=\nu(DD_*-k^2)\hat{v} \quad (10.220)$$

$$\sigma\hat{w}+\hat{u}\frac{dW}{dr}+ikW\hat{w}=-ik\frac{\hat{p_p}}{\rho}+\nu(D_*D-k^2)\hat{w} \quad (10.221)$$

$$D_*\hat{u}+ik\hat{w}=0\,. \quad (10.222)$$

Extracting $\hat{w}$ from Eq. (10.222) and inserting this expression in (10.221), we obtain

$$\frac{\hat{p_p}}{\rho}=\frac{1}{k^2}\left[\nu(D_*D-k^2)-\sigma-ikW\right]D_*\hat{u}+\frac{i\hat{u}}{k}\frac{dW}{dr}\,. \quad (10.223)$$

Taking the derivative D of (10.223) and using it in (10.219) we are left with the relations

$$\nu\left(DD_*-k^2\right)^2\hat{u}-2k^2\frac{V}{r}\hat{v}+ik^3\hat{u}W+\frac{i\hat{u}r}{k}\left(\frac{W'}{r}\right)'=\sigma(DD_*-k^2)\hat{u} \quad (10.224)$$

$$\nu\left(DD_*-k^2\right)\hat{v}-(D_*V)\hat{u}-ik\hat{v}W=\sigma\hat{v} \quad (10.225)$$

$$\hat{u}=\hat{v}=D\hat{u}=0 \quad \text{for} \quad r=R_1,R_2\,. \quad (10.226)$$

The interested reader may find in Ng and Turner [62] the numerical results obtained by the compound matrix method for the stability of the spiral flow under axisymmetric disturbances for the small gap approximation. This analysis sheds light on the interaction of centrifugal and shear instabilities.

8.2 **Rayleigh–Bénard instability**

The solution follows the development proposed by Chandrasekhar [18] and Drazin [26].

- The velocity of the base flow is zero $\boldsymbol{v} = 0$. The temperature profile is linear as it is solution of $d^2T_C/dx_2^2 = 0$, with the boundary conditions $T_C = T_0$ for $x_2 = 0$ and $T_C = T_1$ for $x_2 = d$. The lower index C indicates the conductive nature of the solution. Hence

$$T_C = T_0 - \frac{T_0 - T_1}{d} x_2 \,. \tag{10.227}$$

The hydrostatic pressure p_{hyd} is obtained from the Navier–Stokes equation (1.116) that yields

$$0 = -\boldsymbol{\nabla} p \; + + \rho_0((1 - \alpha(T - T_0))\boldsymbol{g} \,, \tag{10.228}$$

and consequently using (10.227)

$$p_{hyd} = p_0 - \rho g(x_2 + \alpha \frac{T_0 - T_1}{d} \frac{x_2^2}{2}) \,. \tag{10.229}$$

- For the sake of facility, the dimensionless quantities are denoted without primes in the sequel. The velocity perturbations are $\boldsymbol{v} = (u, v, w)$. Using (8.67), the linearized equations are

$$\text{div}\, \boldsymbol{v} = 0, \tag{10.230}$$

$$\frac{\partial \boldsymbol{v}}{\partial t} = -\boldsymbol{\nabla} p_p \; + \; Pr \triangle \boldsymbol{v} + Ra Pr \, T \boldsymbol{g}', \tag{10.231}$$

$$\frac{\partial T}{\partial t} - v = \triangle T. \tag{10.232}$$

- The **curl** of the velocity generates the vorticity (1.40). The dimensionless gravity vector of unit length acts in the vectorial $\boldsymbol{k}$ direction. Then we have taking (1.41) into account

$$\mathbf{curl}(T\boldsymbol{k}) = \varepsilon_{ijk} \frac{\partial T}{\partial x_j} e_k = \boldsymbol{\nabla} T \times \boldsymbol{k} \,. \tag{10.233}$$

The resulting equation reads

$$\frac{\partial \boldsymbol{\omega}}{\partial t} = Ra \; Pr \boldsymbol{\nabla} T \times \boldsymbol{e}_k + Pr \triangle \boldsymbol{\omega} \,. \tag{10.234}$$

- The application of **curl** to Eq. (10.234) leads to the relationship

$$\frac{\partial \triangle \boldsymbol{v}}{\partial t} = Ra\ Pr\left(\triangle T \boldsymbol{e}_i - \boldsymbol{\nabla}(e_j \frac{\partial T}{\partial x_j})\right) + Pr \triangle\triangle \boldsymbol{v}\ . \tag{10.235}$$

To obtain (10.235) the following computation is needed

$$\begin{aligned} \mathbf{curl}(\boldsymbol{\nabla} T \times \boldsymbol{e}_k)_i &= \varepsilon_{ijk}\varepsilon_{klm}\frac{\partial^2 T}{\partial x_l \partial x_j} e_m \\ &= (\delta_{il}\delta_{jm} - \delta_{im}\delta_{jl})\frac{\partial^2 T}{\partial x_l \partial x_j} e_m \\ &= e_j \frac{\partial^2 T}{\partial x_j \partial x_i} - e_i \triangle T\ . \end{aligned} \tag{10.236}$$

- The x_2 component of (10.235) is

$$\begin{aligned} \frac{\partial \triangle v}{\partial t} &= Ra\ Pr\left(\triangle T - \frac{\partial^2 T}{\partial x_2^2}\right) + Pr \triangle\triangle v \\ &= Ra\ Pr \triangle_H T + Pr \triangle\triangle v\ , \end{aligned} \tag{10.237}$$

where $\triangle_H = \partial^2/\partial x_1^2 + \partial^2/\partial x_3^2$ is the horizontal Laplacian.

- Let us eliminate T between (10.232) and (10.237). From (10.232) we compute

$$T = \left(\frac{\partial}{\partial t} - \triangle\right)^{-1} v\ . \tag{10.238}$$

Plugging (10.238) in (10.237) one gets

$$\left(\frac{\partial}{\partial t} - \triangle\right)\left(\frac{1}{Pr}\frac{\partial}{\partial t} - \triangle\right)\triangle v = Ra \triangle_H v\ . \tag{10.239}$$

The boundary conditions are

$$v = \frac{\partial v}{\partial x_2} = T = 0 \quad \text{for} \quad x_2 = 0 \quad \text{and} \quad x_2 = d. \tag{10.240}$$

- We choose the normal modes in horizontal Fourier space

$$T = \Theta(x_2) e^{\sigma t + i(k_1 x_1 + k_3 x_3)} \tag{10.241}$$

$$v = V(x_2) e^{\sigma t + i(k_1 x_1 + k_3 x_3)}\ . \tag{10.242}$$

Substitution of (10.241)–(10.242) in (10.232) and (10.237) produces

$$(D^2 - k^2 - \sigma)T = -W \tag{10.243}$$

$$(D^2 - k^2)(D^2 - k^2 - \frac{\sigma}{Pr})W = k^2 RaT \ , \tag{10.244}$$

with $D = d/dx_2$ and $k^2 = k_1^2 + k_3^2$.
Elimination of T between (10.243) and (10.244) yields a sixth-order differential equation

$$(D^2 - k^2)(D^2 - k^2 - \sigma)(D^2 - k^2 - \frac{\sigma}{Pr})W = -k^2 RaW \ , \tag{10.245}$$

with the boundary conditions $W = DW = T = 0$ at $x_2/d = 0, 1$.

The problem is solved numerically by a spectral method, see e.g. [23]. The critical Rayleigh number in the case of rigid conducting plates is $Ra_{crit} = 1708$ with $k_{crit} = 3.117$.

10.9 Chapter Nine

9.1 Taking the conjugate complex of (9.52) one has

$$f^*(\boldsymbol{x}) = \sum_{\boldsymbol{k}'} \hat{f}^*(\boldsymbol{k}') e^{i\boldsymbol{k}'\cdot\boldsymbol{x}} \ . \tag{10.246}$$

Setting $\boldsymbol{k}' = -\boldsymbol{k}$, one obtains

$$f^*(\boldsymbol{x}) = \sum_{\boldsymbol{k}} \hat{f}^*(-\boldsymbol{k}) e^{-i\boldsymbol{k}\cdot\boldsymbol{x}} \ . \tag{10.247}$$

As f is real, we conclude that $f^* = f$ and the relation (9.53).

9.2 With the definition (9.60), we write

$$Q_{ij}(-\boldsymbol{r}) = \overline{v_i'(\boldsymbol{x}) v_j'(\boldsymbol{x} - \boldsymbol{r})} \ . \tag{10.248}$$

If we have now $\boldsymbol{x} = \boldsymbol{x}' + \boldsymbol{r}$, the former relation yields

$$Q_{ij}(-\boldsymbol{r}) = \overline{v_i'(\boldsymbol{x}' + \boldsymbol{r}) v_j'(\boldsymbol{x}')} = Q_{ji}(\boldsymbol{r}) \ . \tag{10.249}$$

Symmetry is then proved.

9.3 The use of Eq. (9.241) requires the following algebraic expansions

$$(I_d - G)^3 = I_d - 3G + 3G^2 - G^3 \tag{10.250}$$
$$(I_d - G)^4 = I_d - 4G + 6G^2 - 4G^3 + G^4 \tag{10.251}$$
$$(I_d - G)^5 = I_d - 5G + 10G^2 - 10G^3 + 5G^4 - G^5\,. \tag{10.252}$$

Then

$$Q_3 = \sum_{n=0}^{3} (I_d - G)^n = 4I_d - 6G + 4G^2 - G^3 \tag{10.253}$$
$$Q_5 = \sum_{n=0}^{5} (I_d - G)^n = 6I_d - 15(G + G^3) + 20G^2 + 6G^4 - G^5. \tag{10.254}$$

From (10.253) and (10.254), we recover easily the relations (9.243) and (9.244).

Appendix A
Cylindrical Coordinates

We list here some differential operators as well as the principal equations for a system of cylindrical coordinates.

Shown in Fig. A.1 are the components of the stress tensor in the cylindrical coordinate system (r, θ, z).

Divergence of a vector field $\boldsymbol{v}(r, \theta, z)$

$$\operatorname{div} \boldsymbol{v} = \frac{1}{r} v_r + \frac{\partial v_r}{\partial r} + \frac{1}{r} \frac{\partial v_\theta}{\partial \theta} + \frac{\partial v_z}{\partial z} \tag{A.1}$$

or

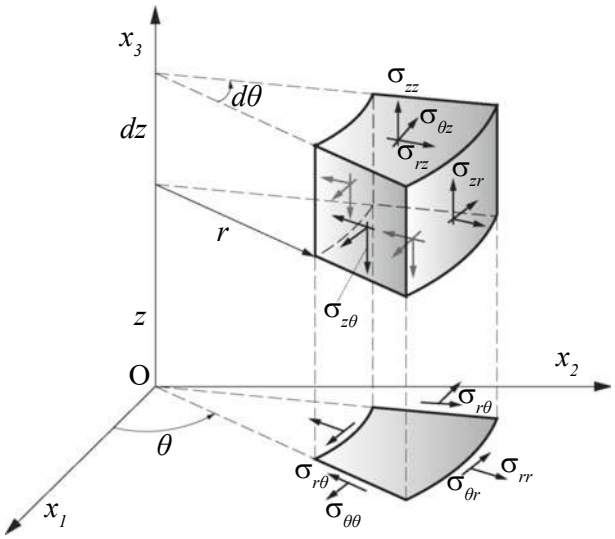

Fig. A.1 Stress tensor components in a cylindrical coordinate system

M. O. Deville, *An Introduction to the Mechanics of Incompressible Fluids*,
https://doi.org/10.1007/978-3-031-04683-4

$$\operatorname{div} \boldsymbol{v} = \frac{1}{r}\,\frac{\partial}{\partial r}\,(r v_r) + \frac{1}{r}\,\frac{\partial v_\theta}{\partial \theta} + \frac{\partial v_z}{\partial z}\,. \tag{A.2}$$

Divergence of a tensor field $\boldsymbol{\sigma}(r, \theta, z)$

$$\begin{aligned} \mathbf{div}\,\boldsymbol{\sigma} = &\left(\frac{\partial \sigma_{rr}}{\partial r} + \frac{1}{r}\,\frac{\partial \sigma_{r\theta}}{\partial \theta} + \frac{\partial \sigma_{rz}}{\partial z} + \frac{\sigma_{rr} - \sigma_{\theta\theta}}{r}\right)\boldsymbol{e}_r \\ &+ \left(\frac{\partial \sigma_{r\theta}}{\partial r} + \frac{1}{r}\,\frac{\partial \sigma_{\theta\theta}}{\partial \theta} + \frac{\partial \sigma_{\theta z}}{\partial z} + \frac{2\sigma_{r\theta}}{r}\right)\boldsymbol{e}_\theta \\ &+ \left(\frac{\partial \sigma_{rz}}{\partial r} + \frac{1}{r}\,\frac{\partial \sigma_{\theta z}}{\partial \theta} + \frac{\partial \sigma_{zz}}{\partial z} + \frac{\sigma_{rz}}{r}\right)\boldsymbol{e}_z\,. \end{aligned} \tag{A.3}$$

Gradient of a scalar field $f(r, \theta, z)$

$$\boldsymbol{\nabla} f = \frac{\partial f}{\partial r}\,\boldsymbol{e}_r + \frac{1}{r}\,\frac{\partial f}{\partial \theta}\,\boldsymbol{e}_\theta + \frac{\partial f}{\partial z}\,\boldsymbol{e}_z\,. \tag{A.4}$$

Gradient of a vector field $\boldsymbol{v}(r, \theta, z)$

$$\boldsymbol{\nabla} \boldsymbol{v} = \begin{pmatrix} \dfrac{\partial v_r}{\partial r} & \dfrac{1}{r}\,\dfrac{\partial v_r}{\partial \theta} - \dfrac{v_\theta}{r} & \dfrac{\partial v_r}{\partial z} \\[2ex] \dfrac{\partial v_\theta}{\partial r} & \dfrac{1}{r}\,\dfrac{\partial v_\theta}{\partial \theta} + \dfrac{v_r}{r} & \dfrac{\partial v_\theta}{\partial z} \\[2ex] \dfrac{\partial v_z}{\partial r} & \dfrac{1}{r}\,\dfrac{\partial v_z}{\partial \theta} & \dfrac{\partial v_z}{\partial z} \end{pmatrix}. \tag{A.5}$$

Curl of a vector field $\boldsymbol{v}(r, \theta, z)$

$$\begin{aligned} \mathbf{curl}\,\boldsymbol{v} = &\left(\frac{1}{r}\,\frac{\partial v_z}{\partial \theta} - \frac{\partial v_\theta}{\partial z}\right)\boldsymbol{e}_r + \left(\frac{\partial v_r}{\partial z} - \frac{\partial v_z}{\partial r}\right)\boldsymbol{e}_\theta \\ &+ \frac{1}{r}\left(\frac{\partial}{\partial r}\,(r v_\theta) - \frac{\partial v_r}{\partial \theta}\right)\boldsymbol{e}_z\,. \end{aligned} \tag{A.6}$$

Laplacian of a scalar field $f(r, \theta, z)$

$$\Delta f = \nabla^2 f = \frac{1}{r}\,\frac{\partial f}{\partial r} + \frac{\partial^2 f}{\partial r^2} + \frac{1}{r^2}\,\frac{\partial^2 f}{\partial \theta^2} + \frac{\partial^2 f}{\partial z^2} \tag{A.7}$$

or

$$\nabla^2 f = \frac{1}{r}\,\frac{\partial}{\partial r}\left(r\,\frac{\partial f}{\partial r}\right) + \frac{1}{r^2}\,\frac{\partial^2 f}{\partial \theta^2} + \frac{\partial^2 f}{\partial z^2}\,. \tag{A.8}$$

Laplacian of a vector field $\boldsymbol{v}(r, \theta, z)$

$$\begin{aligned}\boldsymbol{\nabla}^2\boldsymbol{v} = &\left(\nabla^2 v_r - \frac{2}{r^2}\frac{\partial v_\theta}{\partial\theta} - \frac{v_r}{r^2}\right)\boldsymbol{e}_r \\ &+ \left(\nabla^2 v_\theta + \frac{2}{r^2}\frac{\partial v_r}{\partial\theta} - \frac{v_\theta}{r^2}\right)\boldsymbol{e}_\theta \\ &+ \left(\nabla^2 v_z\right)\boldsymbol{e}_z\,.\end{aligned} \tag{A.9}$$

Material derivative of a scalar field $f(r,\theta,z)$

$$\frac{Df}{Dt} = \frac{\partial f}{\partial t} + v_r\frac{\partial f}{\partial r} + \frac{v_\theta}{r}\frac{\partial f}{\partial\theta} + v_z\frac{\partial f}{\partial z}\,. \tag{A.10}$$

Acceleration

$$\frac{Dv_r}{Dt} = \frac{\partial v_r}{\partial t} + v_r\frac{\partial v_r}{\partial r} + \frac{v_\theta}{r}\frac{\partial v_r}{\partial\theta} - \frac{v_\theta^2}{r} + v_z\frac{\partial v_r}{\partial z} \tag{A.11}$$

$$\frac{Dv_\theta}{Dt} = \frac{\partial v_\theta}{\partial t} + v_r\frac{\partial v_\theta}{\partial r} + \frac{v_\theta}{r}\frac{\partial v_\theta}{\partial\theta} + \frac{v_r v_\theta}{r} + v_z\frac{\partial v_\theta}{\partial z} \tag{A.12}$$

$$\frac{Dv_z}{Dt} = \frac{\partial v_z}{\partial t} + v_r\frac{\partial v_z}{\partial r} + \frac{v_\theta}{r}\frac{\partial v_z}{\partial\theta} + v_z\frac{\partial v_z}{\partial z}\,. \tag{A.13}$$

Motion equations

$$\begin{aligned}&\rho\left(\frac{\partial v_r}{\partial t} + v_r\frac{\partial v_r}{\partial r} + \frac{v_\theta}{r}\frac{\partial v_r}{\partial\theta} + v_z\frac{\partial v_r}{\partial z} - \frac{v_\theta^2}{r}\right) \\ &\quad = \frac{\partial\sigma_{rr}}{\partial r} + \frac{1}{r}\frac{\partial\sigma_{r\theta}}{\partial\theta} + \frac{\partial\sigma_{rz}}{\partial z} + \frac{\sigma_{rr}-\sigma_{\theta\theta}}{r} + \rho b_r\end{aligned} \tag{A.14}$$

$$\begin{aligned}&\rho\left(\frac{\partial v_\theta}{\partial t} + v_r\frac{\partial v_\theta}{\partial r} + \frac{v_\theta}{r}\frac{\partial v_\theta}{\partial\theta} + v_z\frac{\partial v_\theta}{\partial z} + \frac{v_r v_\theta}{r}\right) \\ &\quad = \frac{\partial\sigma_{r\theta}}{\partial r} + \frac{1}{r}\frac{\partial\sigma_{\theta\theta}}{\partial\theta} + \frac{\partial\sigma_{\theta z}}{\partial z} + \frac{2\sigma_{r\theta}}{r} + \rho b_\theta\end{aligned} \tag{A.15}$$

$$\begin{aligned}&\rho\left(\frac{\partial v_z}{\partial t} + v_r\frac{\partial v_z}{\partial r} + \frac{v_\theta}{r}\frac{\partial v_z}{\partial\theta} + v_z\frac{\partial v_z}{\partial z}\right) \\ &\quad = \frac{\partial\sigma_{rz}}{\partial r} + \frac{1}{r}\frac{\partial\sigma_{\theta z}}{\partial\theta} + \frac{\partial\sigma_{zz}}{\partial z} + \frac{\sigma_{rz}}{r} + \rho b_z\,.\end{aligned} \tag{A.16}$$

Components of the strain rate tensor

$$d_{rr} = \frac{\partial v_r}{\partial r} \qquad d_{\theta\theta} = \frac{v_r}{r} + \frac{1}{r}\frac{\partial v_\theta}{\partial \theta} \qquad d_{zz} = \frac{\partial v_z}{\partial z} \tag{A.17}$$

$$d_{zr} = \frac{1}{2}\left(\frac{\partial v_r}{\partial z} + \frac{\partial v_z}{\partial r}\right) \qquad d_{r\theta} = \frac{1}{2}\left(\frac{1}{r}\frac{\partial v_r}{\partial \theta} + \frac{\partial v_\theta}{\partial r} - \frac{v_\theta}{r}\right) \tag{A.18}$$

$$d_{z\theta} = \frac{1}{2}\left(\frac{1}{r}\frac{\partial v_z}{\partial \theta} + \frac{\partial v_\theta}{\partial z}\right). \tag{A.19}$$

Incompressible Navier–Stokes equations.

Conservation of mass equation

$$\frac{\partial v_r}{\partial r} + \frac{v_r}{r} + \frac{1}{r}\frac{\partial v_\theta}{\partial \theta} + \frac{\partial v_z}{\partial z} = 0\,. \tag{A.20}$$

Motion equations

$$\rho\left(\frac{\partial v_r}{\partial t} + v_r\frac{\partial v_r}{\partial r} + \frac{v_\theta}{r}\frac{\partial v_r}{\partial \theta} + v_z\frac{\partial v_r}{\partial z} - \frac{v_\theta^2}{r}\right) = -\frac{\partial p}{\partial r} + \mu\left(\triangle v_r - \frac{v_r}{r^2} - \frac{2}{r^2}\frac{\partial v_\theta}{\partial \theta}\right) + \rho b_r \tag{A.21}$$

$$\rho\left(\frac{\partial v_\theta}{\partial t} + v_r\frac{\partial v_\theta}{\partial r} + \frac{v_\theta}{r}\frac{\partial v_\theta}{\partial \theta} + v_z\frac{\partial v_\theta}{\partial z} + \frac{v_r v_\theta}{r}\right) = -\frac{1}{r}\frac{\partial p}{\partial \theta} + \mu\left(\triangle v_\theta - \frac{v_\theta}{r^2} + \frac{2}{r^2}\frac{\partial v_r}{\partial \theta}\right) + \rho b_\theta \tag{A.22}$$

$$\rho\left(\frac{\partial v_z}{\partial t} + v_r\frac{\partial v_z}{\partial r} + \frac{v_\theta}{r}\frac{\partial v_z}{\partial \theta} + v_z\frac{\partial v_z}{\partial z}\right) = -\frac{\partial p}{\partial z} + \mu\Delta v_z + \rho b_z \tag{A.23}$$

with the Laplacian operator defined by (A.7) or (A.8).

Appendix B
Spherical Coordinates

We list here some differential operators as well as the principal equations for a system of spherical coordinates. Shown in Fig. B.1 are the components of the stress tensor in the spherical coordinate system r, θ, φ.

Divergence of a vector field $\boldsymbol{v}(r, \theta, \varphi)$

$$\operatorname{div} \boldsymbol{v} = \frac{1}{r^2}\frac{\partial}{\partial r}(r^2\, v_r) + \frac{1}{r\sin\theta}\frac{\partial}{\partial \theta}(v_\theta \sin\theta) + \frac{1}{r\sin\theta}\frac{\partial v_\varphi}{\partial \varphi}\,. \tag{B.1}$$

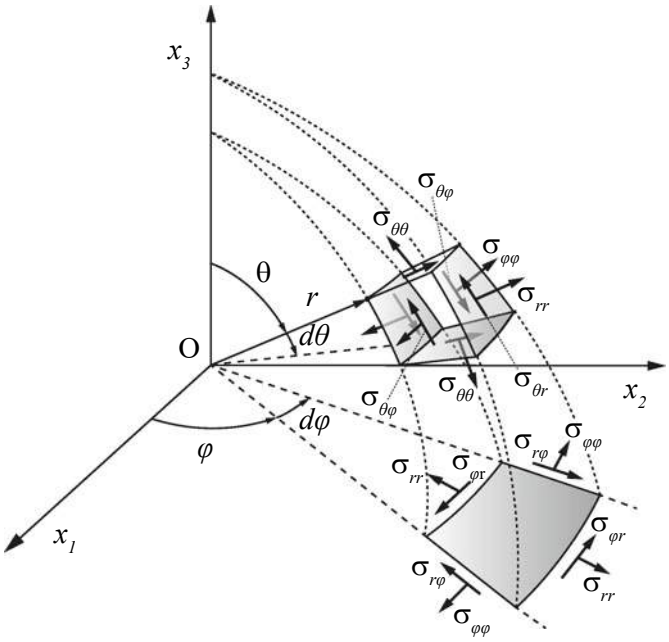

Fig. B.1 Stress tensor components in a spherical coordinate system

M. O. Deville, *An Introduction to the Mechanics of Incompressible Fluids*,
https://doi.org/10.1007/978-3-031-04683-4

Divergence of a tensor field $\boldsymbol{\sigma}(r,\theta,\varphi)$

$$\begin{aligned}\mathbf{div}\,\boldsymbol{\sigma} = &\left(\frac{\partial\sigma_{rr}}{\partial r}+\frac{1}{r}\frac{\partial\sigma_{r\theta}}{\partial\theta}+\frac{1}{r\sin\theta}\frac{\partial\sigma_{r\varphi}}{\partial\varphi}+\frac{1}{r}\left[2\sigma_{rr}-\sigma_{\theta\theta}-\sigma_{\varphi\varphi}+\sigma_{r\theta}\cot\theta\right]\right)\boldsymbol{e}_r\\ &+\left(\frac{\partial\sigma_{\theta r}}{\partial r}+\frac{1}{r}\frac{\partial\sigma_{\theta\theta}}{\partial\theta}+\frac{1}{r\sin\theta}\frac{\partial\sigma_{\theta\varphi}}{\partial\varphi}+\frac{1}{r}\left[3\sigma_{r\theta}+(\sigma_{\theta\theta}-\sigma_{\varphi\varphi})\cot\theta\right]\right)\boldsymbol{e}_\theta\\ &+\left(\frac{\partial\sigma_{\varphi r}}{\partial r}+\frac{1}{r}\frac{\partial\sigma_{\varphi\theta}}{\partial\theta}+\frac{1}{r\sin\theta}\frac{\partial\sigma_{\varphi\varphi}}{\partial\varphi}+\frac{1}{r}\left[3\sigma_{r\varphi}+2\sigma_{\theta\varphi}\cot\theta\right]\right)\boldsymbol{e}_\varphi\,.\end{aligned} \tag{B.2}$$

Gradient of a scalar field $f(r,\theta,\varphi)$

$$\boldsymbol{\nabla} f = \frac{\partial f}{\partial r}\,\boldsymbol{e}_r+\frac{1}{r}\frac{\partial f}{\partial\theta}\,\boldsymbol{e}_\theta+\frac{1}{r\sin\theta}\frac{\partial f}{\partial\varphi}\,\boldsymbol{e}_\varphi\,. \tag{B.3}$$

Gradient of a vector field $\boldsymbol{v}(r,\theta,\varphi)$

$$\boldsymbol{\nabla}\boldsymbol{v} = \begin{pmatrix}\dfrac{\partial v_r}{\partial r} & \dfrac{1}{r}\dfrac{\partial v_r}{\partial\theta}-\dfrac{v_\theta}{r} & \dfrac{1}{r\sin\theta}\dfrac{\partial v_r}{\partial\varphi}-\dfrac{v_\varphi}{r}\\ \dfrac{\partial v_\theta}{\partial r} & \dfrac{1}{r}\dfrac{\partial v_\theta}{\partial\theta}+\dfrac{v_r}{r} & \dfrac{1}{r\sin\theta}\dfrac{\partial v_\theta}{\partial\varphi}-\dfrac{v_\varphi}{r\tan\theta}\\ \dfrac{\partial v_\varphi}{\partial r} & \dfrac{1}{r}\dfrac{\partial v_\varphi}{\partial\theta} & \dfrac{1}{r\sin\theta}\left[\dfrac{\partial v_\varphi}{\partial\varphi}+v_r\sin\theta+v_\theta\cos\theta\right]\end{pmatrix}. \tag{B.4}$$

Curl of a vector field $\boldsymbol{v}(r,\theta,\varphi)$

$$\begin{aligned}\mathbf{curl}\;\boldsymbol{v} = &\frac{1}{r\sin\theta}\left(\frac{\partial(v_\varphi\sin\theta)}{\partial\theta}-\frac{\partial v_\theta}{\partial\varphi}\right)\boldsymbol{e}_r+\left(\frac{1}{r\sin\theta}\frac{\partial v_r}{\partial\varphi}-\frac{1}{r}\frac{\partial(r\,v_\varphi)}{\partial r}\right)\boldsymbol{e}_\theta\\ &+\frac{1}{r}\left(\frac{\partial(r\,v_\theta)}{\partial r}-\frac{\partial v_r}{\partial\theta}\right)\boldsymbol{e}_\varphi\,.\end{aligned} \tag{B.5}$$

Laplacian of a scalar field $f(r,\theta,\varphi)$

$$\Delta f = \nabla^2 f = \frac{1}{r^2}\frac{\partial}{\partial r}\left(r^2\frac{\partial f}{\partial r}\right)+\frac{1}{r^2\sin\theta}\frac{\partial}{\partial\theta}\left(\sin\theta\frac{\partial f}{\partial\theta}\right)+\frac{1}{r^2\sin^2\theta}\frac{\partial^2 f}{\partial\varphi^2}\,. \tag{B.6}$$

Laplacian of a vector field $\boldsymbol{v}(r,\theta,\varphi)$

$$\begin{aligned}\boldsymbol{\nabla}^2\boldsymbol{v} = &\left(\Delta v_r-\frac{2v_r}{r^2}-\frac{2}{r^2}\frac{\partial v_\theta}{\partial\theta}-\frac{2v_\theta\cot\theta}{r^2}-\frac{2}{r^2\sin\theta}\frac{\partial v_\varphi}{\partial\varphi}\right)\boldsymbol{e}_r\\ &+\left(\Delta v_\theta-\frac{v_\theta}{r^2\sin^2\theta}+\frac{2}{r^2}\frac{\partial v_r}{\partial\theta}-\frac{2\cos\theta}{r^2\sin^2\theta}\frac{\partial v_\varphi}{\partial\varphi}\right)\boldsymbol{e}_\theta\\ &+\left(\Delta v_\varphi-\frac{v_\varphi}{r^2\sin^2\theta}+\frac{2}{r^2\sin\theta}\frac{\partial v_r}{\partial\varphi}+\frac{2\cos\theta}{r^2\sin^2\theta}\frac{\partial v_\theta}{\partial\varphi}\right)\boldsymbol{e}_\varphi\,.\end{aligned} \tag{B.7}$$

Material derivative of a scalar field $f(r, \theta, \varphi)$

$$\frac{Df}{Dt} = \frac{\partial f}{\partial t} + v_r \frac{\partial f}{\partial r} + \frac{v_\theta}{r} \frac{\partial f}{\partial \theta} + \frac{v_\varphi}{r \sin\theta} \frac{\partial f}{\partial \varphi} \,. \tag{B.8}$$

Acceleration

$$a_r = \frac{Dv_r}{Dt} - \frac{v_\varphi^2 + v_\theta^2}{r} \tag{B.9}$$

$$a_\theta = \frac{Dv_\theta}{Dt} + \frac{v_r v_\theta - v_\varphi^2 \cot\theta}{r} \tag{B.10}$$

$$a_\varphi = \frac{Dv_\varphi}{Dt} + \frac{v_r v_\varphi + v_\varphi v_\theta \cot\theta}{r} \,. \tag{B.11}$$

Motion equations

$$\rho \left(\frac{Dv_r}{Dt} - \frac{v_\varphi^2 + v_\theta^2}{r} \right) = \frac{\partial \sigma_{rr}}{\partial r} + \frac{1}{r} \frac{\partial \sigma_{r\theta}}{\partial \theta} + \frac{1}{r \sin\theta} \frac{\partial \sigma_{r\varphi}}{\partial \varphi} + \frac{1}{r} (2\sigma_{rr} - \sigma_{\theta\theta} - \sigma_{\varphi\varphi} + \sigma_{r\theta} \cot\theta) + \rho\, b_r \tag{B.12}$$

$$\rho \left(\frac{Dv_\theta}{Dt} + \frac{v_r v_\theta - v_\varphi^2 \cot\theta}{r} \right) = \frac{\partial \sigma_{r\theta}}{\partial r} + \frac{1}{r} \frac{\partial \sigma_{\theta\theta}}{\partial \theta} + \frac{1}{r \sin\theta} \frac{\partial \sigma_{\theta\varphi}}{\partial \varphi} + \frac{1}{r} [\left(\sigma_{\theta\theta} - \sigma_{\varphi\varphi}\right) \cot\theta + 3\sigma_{r\theta}] + \rho\, b_\theta \tag{B.13}$$

$$\rho \left(\frac{Dv_\varphi}{Dt} + \frac{v_r v_\varphi + v_\varphi v_\theta \cot\theta}{r} \right) = \frac{\partial \sigma_{r\varphi}}{\partial r} + \frac{1}{r} \frac{\partial \sigma_{\theta\varphi}}{\partial \theta} + \frac{1}{r \sin\theta} \frac{\partial \sigma_{\varphi\varphi}}{\partial \varphi} + \frac{1}{r} (3\sigma_{r\varphi} + 2\sigma_{\theta\varphi} \cot\theta) + \rho\, b_\varphi \,. \tag{B.14}$$

Strain rate components

$$d_{rr} = \frac{\partial v_r}{\partial r}, \quad d_{\theta\theta} = \frac{1}{r} \frac{\partial v_\theta}{\partial \theta} + \frac{v_r}{r}, \tag{B.15}$$

$$d_{\varphi\varphi} = \frac{1}{r \sin\theta} \frac{\partial v_\varphi}{\partial \varphi} + \frac{v_r}{r} + \frac{v_\theta \cot\theta}{r}, \tag{B.16}$$

$$d_{\varphi\theta} = \frac{1}{2} \left(\frac{1}{r \sin\theta} \frac{\partial v_\theta}{\partial \varphi} + \frac{1}{r} \frac{\partial v_\varphi}{\partial \theta} - \frac{v_\varphi \cot\theta}{r} \right), \tag{B.17}$$

$$d_{\varphi r} = \frac{1}{2} \left(\frac{\partial v_\varphi}{\partial r} + \frac{1}{r \sin\theta} \frac{\partial v_r}{\partial \varphi} - \frac{v_\varphi}{r} \right), \tag{B.18}$$

$$d_{r\theta} = \frac{1}{2} \left(\frac{1}{r} \frac{\partial v_r}{\partial \theta} + \frac{\partial v_\theta}{\partial r} - \frac{v_\theta}{r} \right) . \tag{B.19}$$

Incompressible Navier–Stokes equations.

Conservation of mass equation

$$\frac{1}{r^2}\frac{\partial}{\partial r}(r^2\, v_r) + \frac{1}{r\sin\theta}\frac{\partial}{\partial\theta}(v_\theta \sin\theta) + \frac{1}{r\sin\theta}\frac{\partial v_\varphi}{\partial\varphi} = 0\,. \tag{B.20}$$

Motion equations

$$\begin{aligned}
&\rho\left(\frac{Dv_r}{Dt} - \frac{v_\varphi^2 + v_\theta^2}{r}\right) = -\frac{\partial p}{\partial r} \\
&+\mu\left(\Delta v_r - \frac{2v_r}{r^2} - \frac{2}{r^2}\frac{\partial v_\theta}{\partial\theta} - \frac{2v_\theta\cot\theta}{r^2} - \frac{2}{r^2\sin\theta}\frac{\partial v_\varphi}{\partial\varphi}\right) + \rho b_r
\end{aligned} \tag{B.21}$$

$$\begin{aligned}
&\rho\left(\frac{Dv_\theta}{Dt} + \frac{v_r v_\theta - v_\varphi^2\cot\theta}{r}\right) = -\frac{1}{r}\frac{\partial p}{\partial\theta} \\
&+\mu\left(\Delta v_\theta - \frac{v_\theta}{r^2\sin^2\theta} + \frac{2}{r^2}\frac{\partial v_r}{\partial\theta} - \frac{2\cos\theta}{r^2\sin^2\theta}\frac{\partial v_\varphi}{\partial\varphi}\right) + \rho b_\theta
\end{aligned} \tag{B.22}$$

$$\begin{aligned}
&\rho\left(\frac{Dv_\varphi}{Dt} + \frac{v_r v_\varphi + v_\varphi v_\theta\cot\theta}{r}\right) = -\frac{1}{r\sin\theta}\frac{\partial p}{\partial\varphi} \\
&+\mu\left(\Delta v_\varphi - \frac{v_\varphi}{r^2\sin^2\theta} + \frac{2}{r^2\sin\theta}\frac{\partial v_r}{\partial\varphi} + \frac{2\cos\theta}{r^2\sin^2\theta}\frac{\partial v_\theta}{\partial\varphi}\right) + \rho b_\varphi
\end{aligned} \tag{B.23}$$

with the Laplacian operator defined by (B.6).

Appendix C
Bessel Functions

The theory of Bessel functions is extensively described in the monograph by Watson [118]. We extract from it the necessary relations for the integration of equations expressed in cylindrical coordinates. The canonical form of Bessel equation is given by

$$\frac{d^2 f}{dz^2} + \frac{1}{z}\frac{df}{dz} + (1 - \frac{k^2}{z^2})\, f = 0\,, \tag{C.1}$$

with k a natural integer. The general solution reads

$$f = C_1 J_k(z) + C_2 Y_k(z)\,, \tag{C.2}$$

where the functions J_k and Y_k are Bessel functions of first and second kind, respectively, of order k, C_1, C_2 are arbitrary constants.

Recurrence Relations

$$\int z^{\ell+1} J_m(z) dz = z^{\ell+1} J_{m+1}(z) + (\ell - m) z^{\ell} J_m(z) - (\ell^2 - m^2) \int z^{\ell-1} J_m(z) dz \tag{C.3}$$

$$\int_{z_0}^{z} z^m J_{m-1}(z) dz = [z^m J_m(z)]_{z_0}^{z}, \tag{C.4}$$

$$z J'_m(z) = m J_m(z) - z J_{m+1}(z)\,. \tag{C.5}$$

M. O. Deville, *An Introduction to the Mechanics of Incompressible Fluids*,
https://doi.org/10.1007/978-3-031-04683-4

Appendix D
Fortran Programme for the Orr–Sommerfeld Equation

The Orr–Sommerfeld equation (8.15) subject to the boundary conditions (8.16) is solved by the Chebyshev Tau method [36, 56]. The variable φ is approximated by a series of Chebyshev polynomials with the standard notation $y = x_2$ for the sake of simplicity

$$\varphi(y) = \sum_{n=0}^{n=N} a_n \, T_n(y) \; , \tag{D.1}$$

where $T_n(y)$ is the nth degree Chebyshev polynomial defined on the interval $[-1, 1]$ such that $T_n(y) = \cos(n \arccos y)$. Therefore $T_0 = 1$, $T_1 = y$, $T_2 = 2y^2 - 1$ and the subsequent polynomials are generated by a three-term recurrence relation

$$T_{n+1} = 2yT_n - T_{n-1} \; . \tag{D.2}$$

In the appendix of Orszag [67], it is shown that the first derivative φ' is approximated by the relationship

$$\frac{d\varphi}{dy} = \sum_{n=0}^{n=N-1} a_n^{(1)} T_n(y) \quad \text{with} \quad c_n \, a_n^{(1)} = 2 \sum_{\substack{p=n+1 \\ p+n=1 \pmod 2}}^{N} p a_p \; , \tag{D.3}$$

where $c_n = 0$ for $n < 0, c_0 = 2, c_n = 1$ for $n > 0$. The notation $f = g \pmod 2$ means the $f - g$ is divisible by 2 or written more precisely, f and g are congruent modulo 2. The Eq. (D.3) is obtained via simple trigonometric relations as $T_n(\cos\theta) = \cos(n\theta)$.

Likewise the second order derivative reads

$$\frac{d^2\varphi}{dy^2} = \sum_{n=0}^{n=N-2} a_n^{(2)} T_n(y) \quad \text{with} \quad c_n \, a_n^{(2)} = 2 \sum_{\substack{p=n+2 \\ p=n \pmod 2}}^{N} p(p^2 - n^2) a_p \; . \tag{D.4}$$

M. O. Deville, *An Introduction to the Mechanics of Incompressible Fluids*,
https://doi.org/10.1007/978-3-031-04683-4

As the present computation will deal with the plane Poiseuille flow, the velocity profile taking full advantage of the Chebyshev interval is $V_1 = 1 - y^2$. Therefore we will also need the relation

$$y^2\varphi = \sum_{n=0}^{n=N} \overline{a}_n T_n(y) \ ,$$
$$\overline{a}_n = \frac{1}{4}\left(c_{n-2}a_{n-2} + (c_n + c_{n-1})a_n + a_{n+2}\right) \ . \tag{D.5}$$

In the original paper Orszag [67] gives the approximation for the fourth order derivative of the variable. Here we will not follow this approach. Instead we will use the Chebyshev matrix method described in Metcalfe's thesis [56]. From Eq. (D.1) let us define the vector $\boldsymbol{g}$

$$\boldsymbol{g} = \begin{pmatrix} a_0 \\ \vdots \\ a_N \end{pmatrix} \ . \tag{D.6}$$

Then the first order derivative $d\varphi/dy$ is associated with the vector $\boldsymbol{g}'$

$$\boldsymbol{g}' = \begin{pmatrix} a_0^{(1)} \\ \vdots \\ a_N^{(1)} \end{pmatrix} \ . \tag{D.7}$$

Through Eq. (D.3) it is easily deduced that the $a_i^{(1)}$ are linear combinations of a_i. One has

$$\boldsymbol{g}' = D\boldsymbol{g} \ , \tag{D.8}$$

where the matrix D has the coefficients

$$D = \begin{pmatrix} 0\ 1\ 0\ 3\ 0\ 5\ \ 0\ \ 7\ \ 0\ \cdots \\ 0\ 0\ 4\ 0\ 8\ \ 0\ 12\ \ 0\ 16\ \cdots \\ 0\ 0\ 0\ 6\ 0\ 10\ \ 0\ 14\ \ 0\ \cdots \\ \qquad\qquad \vdots \end{pmatrix} \tag{D.9}$$

or

$$D_{ij} = 0, \text{ if } \ i \geq j \ \text{ or } \ i + j \ \text{ even},$$
$$= \frac{2(j-1)}{c_{i-1}}, \quad \text{elsewhere} \ . \tag{D.10}$$

The matrix M corresponding to the multiplication by y^2 is such that

$$\begin{aligned} M_{ij} &= 0.75 \quad \text{for} \quad i = j = 2 \\ &= 0.5 \quad \text{for} \quad i = j = 1; i = 3, j = 1 \quad \text{and} \quad i = j, i \geq 2 \\ &= 0.25 \quad \text{for} \quad i = j + 2 \quad \text{or} \quad i = j - 2, i \geq 4 \,. \end{aligned} \tag{D.11}$$

The boundary conditions (8.16) are now

$$\phi = \frac{d\phi}{dy} = 0 \quad \text{for} \quad y = \pm 1 \,. \tag{D.12}$$

They are approximated by the relations

$$\sum_{\substack{n=0 \\ n=0 \pmod 2}}^{N} a_n = 0 \,, \qquad \sum_{\substack{n=1 \\ n=1 \pmod 2}}^{N} a_n = 0 \tag{D.13}$$

$$\sum_{\substack{n=0 \\ n=0 \pmod 2}}^{N} n^2 a_n = 0 \,, \qquad \sum_{\substack{n=1 \\ n=1 \pmod 2}}^{N} n^2 a_n = 0 \tag{D.14}$$

In the following Fortran programme, we use the truncated Chebyshev Tau method where the last governing equations are replaced by the boundary conditions. The resulting matrix equation is of the form $A + \lambda B = 0$, a generalized eigenvalue problem solved by the zggev of the Lapack library. From a historical point of view, all statements in capital letters were written in the seventies (of last century); the lowercase statements correspond to modern Fortran language.

```
PROGRAM ORRSOM
      COMPLEX*16  A(97,97),B(97,97),F(97,97),TEMP(97)
      COMPLEX*16  ATIX,Z
      complex*16 alpha(97),beta(97),lambda(97)
      complex*16 VL(97,97),VR(97,97),work(8*97)
      real*8 rwork(8*97)
      character*1 jobvl,jobvr
      Real*8 ALFA,REY,ALFAR,TALFAR,ALFA2,X
      ATIX(Z,X)=CMPLX(-X*AIMAG(Z),X*REAL(Z))
        !ATIX computes -X*Im(Z)+iX*Re(Z))
      jobvl = 'N'
!     Do not compute left eigenvectors
      jobvr = 'V'
!     Compute right eigenvectors
      lda   = 97
!     Leading dimension of matrix A (complex*16)
      ldb   = 97
!     Leading dimension of matrix B (complex*16)
      ldvl  = 97
!     Leading dimension of eigenvector matrix VL
      ldvr  = 97
!     Leading dimension of eigenvector matrix VR
      lwork = 8*97
!     Size of work array, work.
 1000  FORMAT(1H ,2(1X,1PD21.14))
      ALFA=1.D0          !ALFA=α
      REY=10000.D0       !Reynolds number
      ALFAR=ALFA*REY     !ALFAR=αR
      TALFAR=2.D0*ALFAR
      ALFA2=ALFA*ALFA    !ALFA2=α^2
      N=95
      NM2=N-2
      NP2=N+2
```

```
      DO 1 I=1,NP2
      DO 2 J=1,NP2
      A(I,J)=0.D0
   2  B(I,J)=0.D0
      A(I,I)=1.D0
 1    B(I,I)=1.D0
!     A and B are unit matrices
      CALL DERIV2(A,N,NP2)
!     A contains the matrix (D.10)
      DO 3 I=1,N
      A(I,I)=A(I,I)-CMPLX(ALFA2,0.0)    !A = D^2 - α^2 I
        DO 4 J=1,N
   4    F(I,J)=A(I,J)
   3  CONTINUE
      CALL DERIV2(A,N,NP2)          !A = D^2(D^2 - α^2 I)
      DO 5 I=1,N
      DO 5 J=1,N
 5       A(I,J)=A(I,J)-ALFA2*F(I,J)!A = (D^2 - α^2 I)^2
      DO 6 I=1,N
      DO 6 J=1,N
      B(I,J)=ATIX(F(I,J),ALFAR)    !B = iαRe(D^2 - α^2 I)
 6    A(I,J)=A(I,J)-B(I,J)
!     A = (D^2 - α^2 I)^2 - iαRe(D^2 - α^2 I)
        do 62 I=1,N
 62       A(I,I)=A(I,I)-CMPLX(0.0D0,TALFAR)
!A = (D^2 - α^2 I)^2 - iαRe(D^2 - α^2 I) - 2iαReI
      CALL MBYX2(F,N,NP2)          !F = y^2(D^2 - α^2 I)
      DO 7 I=1,N
         DO 7 J=1,N
 7         A(I,J)=A(I,J)+ATIX(F(I,J),ALFAR)
!A = (D^2 - α^2 I)^2 - iαRe(D^2 - α^2 I) + iαRe y^2(D^2 - α^2 I) - 2iαReI
       K=0    !Compute even modes
       DO 8 I=1,N,2
       K=K+1
       L=0
       DO 8 J=1,N,2
       L=L+1
       A(K,L)=A(I,J)
   8   B(K,L)=B(I,J)
       M=(N-1)/2+1
       DO 9 I=1,M
          B(M,I)=0.D0
          B(M-1,I)=0.D0
          A(M-1,I)=1.D0       !Boundary conditions
 9        A(M,I)=(2*(I-1))**2
! Solution of the generalized eigenvalue problem
       call zggev( jobvl, jobvr,M+1,A,lda,B, ldb,
     * alpha, beta,
     * vl, ldvl, vr, ldvr, work, lwork, rwork, info)
        write(6,*) info
       do i=1,M+1
            open(55,file='eigen.dat')
            lambda(i)=-(alpha(i)/beta(i))
!      NOTE: Should make sure beta .ne. 0 !
          write(6,*) i,lambda(i)
          write(55,1000)lambda(i)
       enddo
        CALL EXIT
        END
       SUBROUTINE MBYX2(A,N,NDIM)
       COMPLEX*16 A(NDIM,NDIM),B(100),C(100),D(100)
       NM1=N-1
       NM2=N-2
       DO 10 L=1,N
          B(L)=0.5D0*A(1,L)+0.25D0*A(3,L)
          C(L)=0.75D0*A(2,L)+0.25D0*A(4,L)
 10       D(L)=0.5D0*(A(1,L)+A(3,L))+0.25D0*A(5,L)
          DO 20 K=4,NM2
           DO 30 L=1,N
           A(K-3,L)=B(L)
           B(L)=C(L)
           C(L)=D(L)
 30        D(L)=0.25D0*(A(K-2,L)+A(K+2,L))+0.5D0*A(K,L)
```

```
20          CONTINUE
          DO 50 K=NM1,N
            DO 40 L=1,N
            A(K-3,L)=B(L)
            B(L)=C(L)
            C(L)=D(L)
40          D(L)=0.25D0*A(K-2,L)+0.5D0*A(K,L)
50        CONTINUE
          DO 60 L=1,N
             A(NM2,L)=B(L)
             A(NM1,L)=C(L)
60           A(N,L)=D(L)
             RETURN
             END
      SUBROUTINE DERIV2(A,N,NDIM)
      COMPLEX*16 A(NDIM,NDIM),C,DM
      C=0.5 D0
      DO 1 K=1,N
         KM1=K-1
         KP1=K+1
         DO 2 L=1,N
            A(K,L)=0.D0
            IF(KP1.GE.N) GO TO 2
            DO 3 M=KP1,N,2
               DM=FLOAT(M*(M*M-KM1*KM1))
3           A(K,L)=A(K,L)+C*DM*A(M+1,L)
2        CONTINUE
         C=1.0 D0
1     CONTINUE
      RETURN
      END
```

The Table D.1 yields the numerical results by the programme OrrSom for $Re = 10^4$, $\alpha = 1.0$. The most unstable node (the first underlined in the table) to within one part in 10^8 given by Orszag [66] is $0.23752649 + i0.00373967$ and matches what was computed with 97 Chebyshev polynomials. The next underlined eigenvalue corresponds to the first stable eigenmode. We note that in the eigenvalue spectrum computed by the truncated version of the Tau method appear many spurious values. They are generated by the replacement of the last governing discrete relations by the boundary conditions. The final word on the elimination of those spurious values is given in a paper by J. Dongarra et al. [25].

Another route to solving Orr–Sommerfeld equation by Chebyshev method rests upon the collocation (also named pseudo-spectral) approximation. L. N. Trefethen [107] describes all necessary details for such an approach. The open source software Chebfun allows the collocated solution and provides the unstable eigenvalue $0.237529564888879 + i0.003733528465259$.

Table D.1 Eigenvalues λ for the Orr–Sommerfeld equation by the Chebyshev Tau method with $Re = 10^4, \alpha = 1$

λ_R	λ_I
$-2.66604889338849D-01$	$2.87097733046296D+01$
$-2.07388966393653D+01$	$1.14507958786535D+01$
$2.00995814373983D+01$	$1.16176041920058D+01$
$-1.34153816910954D+01$	$-4.53017860171633D+00$
$1.30588426514515D+01$	$-4.17313307099387D+00$
$-5.06594705710724D+00$	$-5.68343734965716D+00$
$4.96217121533692D+00$	$-5.36249166868433D+00$
$-1.82589463534227D+00$	$-3.92946877951984D+00$
$1.91858372983250D+00$	$-3.68083840030577D+00$
$-6.72467247633158D-01$	$-2.62721293191901D+00$
$9.43057493390225D-01$	$-2.44871650295218D+00$
$-1.87295746691863D-01$	$-1.83336485394816D+00$
$6.38477362860570D-01$	$-1.71137354421215D+00$
$7.00101774478554D-02$	$-1.33606812697741D+00$
$5.67456366893795D-01$	$-1.25405760195955D+00$
$2.38275292466557D-01$	$-1.00250566539501D+00$
$5.84634559450901D-01$	$-9.46758746618285D-01$
$\underline{2.37526478603995D-01}$	$\underline{3.73966473490984D-03}$
$3.65178189628072D-01$	$-7.61290896036062D-01$
$1.90059290715517D-01$	$-1.82821928003127D-01$
$3.49106789435946D-01$	$-1.24501944643108D-01$
$6.37556269159722D-01$	$-7.22873035109884D-01$
$8.78255959767352D-01$	$-7.17897035346620D-01$
$4.69498454305100D-01$	$-5.73795473458914D-01$
$3.68501827283930D-01$	$-2.38822320021389D-01$
$\underline{9.64642518137954D-01}$	$\underline{-3.51865871548079D-02}$
$9.36351705639658D-01$	$-6.32514606659896D-02$
$8.00452914828617D-01$	$-6.13692467151395D-01$
$9.08055938470933D-01$	$-9.13136084648073D-02$
$4.74902128558263D-01$	$-2.08734187854565D-01$
$8.79759562993090D-01$	$-1.19373129743033D-01$
$7.04985247189294D-01$	$-5.43670770091760D-01$
$7.38515860155871D-01$	$-5.26317662684595D-01$
$5.60284073649713D-01$	$-4.21109286019626D-01$
$5.14647057842630D-01$	$-2.85875744904693D-01$
$8.51473802164673D-01$	$-1.47390318820456D-01$
$8.22722383407350D-01$	$-1.75532908816733D-01$
$5.77581665615992D-01$	$-3.13045387704616D-01$

(continued)

Table D.1 (continued)

λ_R	λ_I
$5.93635148629907D-01$	$-2.58744852363751D-01$
$7.32824235500709D-01$	$-4.46949652130324D-01$
$6.60620785887228D-01$	$-4.03313601464508D-01$
$7.97105849697944D-01$	$-2.03908677887358D-01$
$6.74453521799715D-01$	$-2.51228150742938D-01$
$7.58968890552879D-01$	$-2.27170016213629D-01$
$7.33092450069334D-01$	$-3.61082824563039D-01$
$7.50348291508847D-01$	$-2.57730287758630D-01$
$7.37926238726856D-01$	$-2.97800834923726D-01$

Appendix E
Figures Credits

The following figures are reproduced with the permission of the rights holders.
Figures 1.1, 1.2 from Deville-Gatski [24] with permission of Springer.
Figures 1.3 to 1.7 from Botsis-Deville [16] with permission of EPFL Press.
Figures 1.9, 3.1 to 3.8 [16] with permission of EPFL Press.
Figures 3.9, 3.10, 3.13 from Langlois-Deville [49] with permission of Springer.
Figures 4.1, 4.2 [16] with permission of EPFL Press.
Figure 4.4 [49] with permission of Springer.
Figures 5.1, 5.5 [16] with permission of EPFL Press.
Figures 5.2 to 5.4, 5.7 [49] with permission of Springer.
Figure 5.5 [102] with permission of the Physics Society of Japan.
Figure 7.3 from Ryhming [83] with permission of EPFL Press.
Figure 8.3 from Drazin and Reid [27] with permission of Cambridge University Press.
Figure 8.4 from Andereck et al. [2] with permission of Journal of Fluid Mechanics.
Figures 9.1, 9.8 [24] with permission of Springer.
Figure 9.6 from Pope [74] with permission of Cambridge University Press.
Figures 3.12, 3.13, 3.17, 4.4, 5.3, 6.26 (right), 6.27 (right), 6.28 (right), 6.29, 6.30, 7.1 were generated with the Matlab software, MATLAB and Statistics Toolbox, The MathWorks, Inc., Natick, Massachusetts, United States, 2021.

M. O. Deville, *An Introduction to the Mechanics of Incompressible Fluids*,
https://doi.org/10.1007/978-3-031-04683-4

References

1. Abramowitz M, Stegun IA (1972) Handbook of mathematical functions with formulas, graphs, and mathematical tables. Dover, New York
2. Andereck D, Liu SS, Swinney HL (1986) Flow regimes in a circular Couette system with independently rotating cylinders. J Fluid Mech 164:155–183
3. Arfken GB, Weber HG, Harris FE (2013) Mathematical methods for physicists. Elsevier, Amsterdam
4. Argyropoulos CD, Markatos NC (2015) Recent advances on the numerical modelling of turbulent flows. Appl Math Model 39:693–732
5. Aris R (1989) Vectors, tensors and the basic equations of fluid mechanics. Dover, New York
6. Atabek HB (1980) Blood flow and pulse propagation in arteries. In: Patel DJ, Vaishnav RN (eds) Basic hemodynamics and its role in disease processes. University Park Press, Baltimore, pp 255–361
7. Baldwin BS, Lomax H (1978) Thin layer approximation and algebraic model for separated turbulent flows. In: AIAA 16 aerospace sciences meeting
8. Bardina J, Ferziger JH, Reynolds WC (1989) Improved turbulence models based on large eddy simulation of homogeneous, incompressible, turbulent flows. Technical report TF-19, Thermal sciences division. Department of Mechanical Engineering, Stanford University, Stanford
9. Barenblatt GI (2003) Scaling. Cambridge University Press, Cambridge
10. Batchelor GK (1992) An introduction to fluid dynamics. Cambridge University Press, Cambridge
11. Batchelor GK (1953) The theory of homogeneous turbulence. Cambridge University Press, Cambridge
12. Batcho PF, Karniadakis GE (1994) Generalized Stokes eigenfunctions: a new trial basis for the solution of incompressible Navier-Stokes equations. J Comput Phys 115:121–146
13. Bender CM, Orszag SA (1978) Advanced methods for scientists and engineers. McGraw-Hill, New York
14. Berker R (1963) Intégration des équations du mouvement d'un fluide visqueux incompressible. Handbuch der Physik VIII/3:1–384. Springer, Berlin
15. Berselli LC, Iliescu T, Layton WJ (2006) Mathematics of large eddy simulation of turbulent flows. Springer, Berlin
16. Botsis J, Deville M (2018) Mechanics of continuous media: an introduction. EPFL Press, Lausanne
17. Boussinesq J (1877) Essai sur la théorie des eaux courantes. Mémoires présentés par divers savants à l'Académie des Sciences Paris 23(1):1–660; 24(2):1–60

M. O. Deville, *An Introduction to the Mechanics of Incompressible Fluids*,
https://doi.org/10.1007/978-3-031-04683-4

18. Chandrasekhar S (1961) Hydrodynamic and hydromagnetic stability. Clarendon, Oxford
19. Chassaing P (2000) Turbulence en mécanique des fluides. Cépaduès, Toulouse
20. Coles D (1965) Transition in circular Couette flow. J Fluid Mech 21:385–425
21. Dafalias Y (2011) Objectivity in turbulence under change of reference frame and superposed rigid body motion. J Eng Mech 137:699–707
22. Davey A (1960) The growth of Taylor vortices in flow between rotating cylinders. J Fluid Mech 14:336–368
23. Deville MO, Fischer PF, Mund EH (2002) High-order methods for incompressible fluid flows. Cambridge University Press, Cambridge
24. Deville MO, Gatski TB (2012) Mathematical modeling for complex fluids and flows. Springer, Berlin
25. Dongarra JJ, Straughan B, Walker DW (1996) Chebyshev tau-QZ algorithm for calculating spectra of hydrodynamic stability problems. Appl Numer Math 22:399–434
26. Drazin PG (2002) Introduction to hydrodynamic stability. Cambridge University Press, Cambridge
27. Drazin PG, Reid WH (1981) Hydrodynamic stability. Cambridge University Press, Cambridge
28. Drazin PG, Riley N (2006) The Navier-Stokes equations: a classification of flows and exact solutions. Cambridge University Press, Cambridge
29. Feynman RP, Leighton RB, Sands M (1964) The Feynman lectures on physics. Mainly electromagnetism and matter, vol 2. Addison-Wesley, Boston
30. Frisch U (1995) Turbulence. Cambridge University Press, Cambridge
31. Galtier S (2021) Physique de la turbulence des tourbillons aux ondes (Physics of turbulence from vortices to waves). EDP Sciences, Les Ulis
32. Gatski TB, Jongen T (2000) Nonlinear eddy viscosity and algebraic stress models for solving complex turbulent flows. Prog Aerosp Sci 36:655–682
33. Gatski TB (2004) Constitutive equations for turbulent flows. Theor Comput Fluid Dyn 18(5):345–369
34. Germano M (1986) A proposal for a redefinition of the turbulent stresses in the filtered Navier-Stokes equations. Phys Fluids 29:2323–2324
35. Germano M, Piomelli U, Moin P, Cabot WH (1991) A dynamic subgrid-scale eddy viscosity model. Phys Fluids A 3:1760–1793
36. Gottlieb D, Orszag SA (1977) Numerical analysis of spectral methods. SIAM, Philadelphia
37. Guyon E, Hulin J-P, Petit L, Mitescu CD (2015) Physical hydrodynamics, 2nd edn. Oxford University Press, Oxford
38. Hill MJM (1894) On a spherical vortex. Philos Trans R Soc A 185:213–245
39. Hornbeck RW (1975) Numerical methods. Quantum Publishers, New York
40. Jongen T, Gatski TB (1998) General explicit algebraic stress relations and best approximation for three-dimensional flows. Int J Eng Sci 36:739–763
41. Jordinson R (1970) The flat plate boundary layer. Part 1. Numerical integration of the Orr-Sommerfeld equation. J Fluid Mech 43:801–811
42. Kolmogorov AN (1941) The local structure of turbulence in incompressible viscous fluid for very large Reynolds numbers. Dokl Akad Nauk SSSR 30:301–305
43. Kolmogorov AN (1941) On degeneration of isotropic turbulence in an incompressible fluid. Dokl Akad Nauk SSSR 31:538–541
44. Koschmieder EL (1993) Bénard cells and Taylor vortices. Cambridge University Press, Cambridge
45. Kovasznay LIG (1948) Laminar flow behind a two-dimensional grid. Math Proc Camb Philos Soc 44:58–62
46. Lagrée P-Y (2019) Small *Re* flows. Teaching lecture notes. Université Pierre et Marie Curie, Paris
47. Lamb Sir H (1995) Hydrodynamics. Cambridge University Press, Cambridge
48. Landau L, Lifshitz EM (1997) Fluid mechanics. Butterworth Heinemann, Oxford
49. Langlois WE, Deville MO (2010) Slow viscous flow, 2nd edn. Springer, Berlin
50. Lesieur M (2006) Turbulence in fluids, 4th edn. Springer, Dordrecht

51. Lilly DK (1992) A proposed modification of the Germano subgrid-scale closure method. Phys Fluids A 4:633–635
52. Lumley JL (1970) Toward a turbulent constitutive relation. J Fluid Mech 41:413–434
53. Lumley JL (1978) Computational modeling of turbulent flows. Adv Appl Mech 18:123–176
54. McComb WD (2014) Homogeneous, isotropic turbulence. Phenomenology, renormalization and statistical closures. Oxford University Press, Oxford
55. Manneville P (1990) Dissipative structures and weak turbulence. Academic Press, Boston
56. Metcalfe RW (1974) Spectral methods for boundary value problems in fluid mechanics, PhD thesis, Department of Mathematics, MIT
57. Meyer RE (1971) Introduction to mathematical fluid dynamics. Dover, New York
58. Michell JH (1899) On the direct determination of stress in an elastic solid, with application to the theory of plates. Proc Lond Math Soc 31(1):100–124
59. Milne-Thomson LM (2011) Theoretical hydrodynamics, 5th edn. Dover, New York
60. Moffatt HK (1964) Viscous and resistive eddies near a sharp corner. J Fluid Mech 18:1–18
61. Morton BR (1984) The generation and decay of vorticity. Geophys Astrophys Fluid Dyn 28:277–308
62. Ng BS, Turner ER (1982) On the linear stability of spiral flow between rotating cylinders. Proc R Soc Lond A 382:83–102
63. Nore C, Abid M, Brachet ME (1997) Decaying Kolmogorov turbulence in a model of superflow. Phys Fluids 9:2644–2669
64. Ockendon H, Ockendon JR (1995) Viscous flow. Cambridge University Press, Cambridge
65. Orr WM'F (1907) The stability or instability of the steady motions of a liquid. Proc R Ir Acad A 27:69–138
66. Orszag SA (1971) Accurate solution of the Orr-Sommerfeld stability equation. J Fluid Mech 50:689–703
67. Orszag SA (1971) Numerical simulation of incompressible flows within simple boundaries. I. Galerkin (spectral) representations. Stud Appl Math 50:293–327
68. Orszag SA (1974) Numerical simulation of the Taylor-Green vortex. In: Glowinski R, Lions JL (eds) Computing methods in applied sciences and engineering part 2. Lecture notes in computer science, vol 11, pp 50–64. Springer, Berlin
69. Orszag SA, Israeli M, Deville MO (1986) Boundary conditions for incompressible flows. J Sci Comput 1:75–111
70. Oseen CW (1910) Über die Stokes'sche formel, und über eine verwandte Aufgabe in der Hydrodynamik. Arkiv för matematik, astronomi och fysik 7:1–36
71. Panton RL (2013) Incompressible flow, 4th edn. Wiley, New York
72. Piomelli U, Liu J (1994) Large-eddy simulation of rotating channel flows using localized dynamic model. Phys Fluids 7:839–848
73. Piquet J (1999) Turbulent flows: models and physics. Springer, Berlin
74. Pope SB (2000) Turbulent flows. Cambridge University Press, Cambridge
75. Proudman I, Pearson JRA (1957) Expansions at small Reynolds number for the flow past a sphere and a circular cylinder. J Fluid Mech 2:237–262
76. Rayleigh Lord JWS (1917) On the dynamics of revolving fluids. Proc R Soc Lond Ser A Contain Pap Math Phys Character 93:148–154
77. Reynolds O (1895) On the dynamical theory of incompressible viscous fluids and the determination of the criterion. Philos Trans R Soc Lond Ser A 186:123–164
78. Reynolds WC (1987) Fundamentals of turbulence for turbulence modeling and simulation. Lecture notes for the von Kármán Institute, AGARD lecture series, vol 86. NATO, New York, pp 1–66
79. Rieutord M (2015) Fluid dynamics an introduction. Springer International Publishing, Switzerland
80. Rivlin RS, Ericksen JL (1955) Stress-deformation relations for isotropic materials. Arch Ration Mech Anal 4:323–425
81. Rønquist EM (1991) Spectral element methods for the unsteady Navier-Stokes equations. Computational fluid dynamics lecture series 1991–01. von Karman Institute for Fluid Dynamics, Rhode St-Genèse

82. Rosenhead L (1988) Laminar boundary layers. Dover, New York
83. Ryhming IL (2004) Dynamique des fluides. PPUR, Lausanne
84. Sagaut P (2005) Large eddy simulation for incompressible flows: an introduction, 3rd edn. Springer, Berlin
85. Schlichting H (1960) Boundary layer theory. McGraw-Hill, New York
86. Schmid PJ, Henningson DS (2001) Stability and transition in shear flows. Springer, Berlin
87. Sengupta TK (2012) Instabilities of flows and transition to turbulence. CRC Press, Boca Raton
88. Sengupta TK (2021) Transition to turbulence a dynamical system approach to receptivity. Cambridge University Press, Cambridge
89. Sengupta TK, Singh N, Suman VK (2010) Dynamical system approach to instability of flow past a circular cylinder. J Fluid Mech 656:82–115
90. Serrin J (1959) Mathematical principles of classical fluid mechanics. In: Flügge S (ed) Handbuch der Physik, vol VIII/1. Springer, Berlin
91. Shivamoggi BK (1998) Theoretical fluid dynamics. Wiley, New York
92. Smagorinsky JS (1963) General circulation experiments with the primitive equations. Mon Weather Rev 91:99–164
93. Sommerfeld A (1908) Ein Beitrag zur hydrodynamische Erklaerung der turbulenten Fluessigkeitsbewegungen. In: Proceedings of the 4th international congress of mathematics, Rome, vol III, pp 116–124
94. Spalart PR, Allmaras SR (1994) A one-equation turbulence model for aerodynamic flows. La Recherche Aérospatiale 1:5–21
95. Speziale CG (1991) Analytical methods for the developments of Reynolds-stress closures in turbulence. Ann Rev Fluid Mech 23:107–157
96. Speziale CG, Sarkar S, Gatski TB (1991) Modelling the pressure-strain correlation of turbulence: an invariant dynamical systems approach. J Fluid Mech 227:245–272
97. Squire HB (1933) On the stability of three-dimensional disturbances of viscous flow between parallel walls. Proc R Soc Lond A 142:621–628
98. Stoltz S, Adams NA (1999) An approximate deconvolution procedure for large-eddy simulation. Phys Fluids 11:1699–1701
99. Stoltz S, Adams NA, Kleiser L (2001) An approximate deconvolution model for large-eddy simulation with application to incompressible wall-bounded flows. Phys Fluids 13:997–1015
100. Stoker JJ (1957) Water waves: the mathematical theory with applications. Wiley, New York
101. Strang G (1986) Introduction to applied mathematics. Wellesley-Cambridge Press, Wellesley
102. Taneda S (1979) Visualization of separating Stokes flows. J Phys Soc Jpn 46:1935–1942
103. Taylor GI (1923) Stability of a viscous liquid contained between two rotating cylinders. Philos Trans R Soc Lond A223:289–343
104. Taylor GI, Green AE (1937) Mechanism of the production of small eddies from large ones. Proc R Soc Lond Ser A 158:499–521
105. Tennekes H, Lumley JL (1972) A first course in turbulence. MIT Press, Cambridge
106. Tran-Cong T, Blake JR (1982) General solutions of the Stokes' flow equations. J Math Anal Appl 90:72–84
107. Trefethen LN (2000) Spectral methods in Matlab. SIAM, Philadelphia
108. Tritton DJ (1988) Physical fluid dynamics, 2nd edn. Van Nostrand Reinhold, New York
109. Truesdell C (1952) The mechanical foundation of elasticity and fluid dynamics. J Ration Mech Anal 1:125–300
110. Truesdell C (1954) The kinematics of vorticity. Indiana University Press, Bloomington
111. Truesdell C, Rajagopal KR (2000) An introduction to the mechanics of fluids. Birkhäuser, Boston
112. Uchida S (1956) The pulsating viscous flow superposed on the steady laminar motion of incompressible fluid in a circular pipe. Zeit Angewand Math Phys 7:403–422
113. Van Cittert PH (1931) Zum Einfluss der Spaltbreite auf die Intensitätsverteilung in Spektrallinien. II. Zeitschrift für Physik 69:298–308
114. Van Dyke M (1983) An album of fluid motion. Parabolic Press, Stanford
115. von Mises R (2004) Mathematical theory of compressible fluid flow. Dover, New York

116. von Mises R, Friedrichs KO (1971) Fluid dynamics. Springer, New York
117. Walsh O (1992) Eddy solutions of the Navier-Stokes equations. In: Heywood JG, Masuda K, Rautmann R, Solonnikov SA (eds) The Navier-Stokes equations II- theory and numerical methods. Lecture notes in mathematics, vol 1530. Springer, Berlin, pp 306–309
118. Watson GH (1966) Theory of Bessel functions. Cambridge University Press, Cambridge
119. Wilcox DC (1988) Multiscale model for turbulent flows. AIAA J 26:1311–1320
120. Wilcox DC (2008) Formulation of the $k - \omega$ turbulence model revisited. AIAA J 46:2823–2838
121. Williamson CHK (1996) Vortex dynamics in cylinder wake. Annu Rev Fluid Mech 28:477–539
122. Womersley JR (1955) Method for the calculation of velocity, rate flow, and viscous drag in arteries when the pressure gradient is known. J Physiol 127:553–563
123. Yakhot V, Orszag SA (1986) Renormalisation group analysis of turbulence. I. Basic theory. J Sci Comput 1:3–51
124. Yakhot V, Orszag SA, Thangam S, Gatski TB, Speziale CG (1992) Development of turbulence models for shear flows by a double expansion technique. Phys Fluids A 4:1510–1520
125. Yih C-S (1969) Fluid mechanics. McGraw-Hill, New York
126. Zang Y, Street RL, Koseff JR (1993) A dynamic mixed subgrid-scale model and its application to turbulent recirculating flows. Phys Fluids A 5:3186–3196
127. Zamir M (2000) The physics of pulsatile flow. Springer, New York

Index

M. O. Deville, *An Introduction to the Mechanics of Incompressible Fluids*,
https://doi.org/10.1007/978-3-031-04683-4